OPTIMISATION OF WAISTED TENSILE TEST SPECIMEN GEOMETRY AND DETERMINATION OF TENSILE ENERGY WELDING FACTORS FOR DIFFERENT POLYETHYLENE PIPE WALL THICKNESSES

A thesis submitted in partial fulfilment of the requirements for the degree of

Doctor of Philosophy

MOHAMMAD TAGHIPOURFARD
College of Engineering, Design and Physical Sciences

Abstract

High-density polyethylene (HDPE) pipes are employed in a wide range of industries such as water, gas, nuclear and energy. HDPE pipes have steadily replaced clay, copper, asbestos-cement, aluminium, iron and concrete pipes in various applications. Butt fusion welding is one of the most commonly used techniques to weld HDPE pipes. There are many test methods available for assessing the short-term performance of butt fusion welded joints in HDPE pipes. Recent research publications have shown that waisted tensile test specimen is the most discriminating short-term examination in a tensile test, such as those described in ISO 13953, EN 12814-2, EN 12814-7 and WIS 4-32-08.

The current challenge of using the abovementioned standards is to quantify the quality of welds since the same waisted geometry is used for any pipe size diameter with any thickness. As the thickness of the specimen increases, the degree of ductility reduces significantly in both welded and unwelded specimens. Therefore, a new specimen geometry that can be used for specimens with all thicknesses must be defined to allow a more accurate measurement of weld quality.

In order to simplify the aforementioned problem, specimens using an unwelded flat sheet made from HDPE were used to investigate the geometry parameters, which believed to have the most influence on the fracture of the specimen. The effects of parameters such as width and radius of the waisted section, diameter and distance of loading holes, and overall width of the specimen were investigated through various experimental procedures, tensile tests, and Central Composite Design (CCD) optimisation.

After understanding the effect of geometry parameters, Finite Element Analysis (FEA) techniques using constitutive equations are used to confirm experimental findings. FEA modelling also covered a wide range of specimen geometries, where the experimental investigation was not feasible due to machining and testing limitations of specimens with large thicknesses (e.g., 20-100mm).

The final contribution of this thesis is to propose a modified geometry, which could be used for all pipe sizes and demonstrate its advantages over the standard geometry specimen. This task was carried out on pipes with Outer Diameter (OD) of 140, 160, 250, 280, 500 and 630mm. Improvements on 140, 160 and 250mm with a thickness of less than 20mm, are providing more considerable elongation using parent pipe material and necking starting at earlier stages of the tensile test. Improvements on 280, 500 and 630mm OD with a thickness of over 20mm, are having the specimen fail in a ductile manner with ductility in welded and unwelded specimen whereas, no ductility could be observed when standard geometry was used. X-ray photography was taken to verify the types of failures accrued in specimens. The outcome of the research conducted in this thesis, which proposed a modified geometry for tensile tests, paves the way to enhance reliability in the examination of HDPE weld qualities.

Table of Contents

List of Figures

List of Tables

List of Abbreviations

ANN	Artificial Neural Network
ANOVA	Analysis of Variance
ASTM	American Society for Testing and Materials
AWS	American Welding Society
AWWA	American Water Works associations
BS EN	British Standard European Norm
CCD	Central Composite Design
CSA	Cross Sectional Area
CSA	Canadian Standards Association
CTOD	Crack Tip Opening Displacement
DIC	Digital Image Correlation
DOE	Design of Experiment
DP	Degree of Polymerization
ESCR	Environmental Stress Crack Resistance
EWF	Essential Work of Fracture
FE	Finite Element
FEA	Finite Element Analysis
FPZ	Fracture Process Zone
HDPE	High-Density Polyethylene
ISO	International Organization for Standardization
LB	Larger Better
LEFM	Linear Elastic Fracture Mechanic

MS	Mean Square
MW	Molecular Weight
NB	Nominal Better
NLEFM	Non-Linear Elastic Fracture Mechanic
OD	Outer Diameter
PE	Polyethylene
RSM	Response Surface Methodology
SB	Smaller Better
SCG	Slow Crack Growth
SDR	Ratio of Diameter to wall Thickness
SS	Sum of Square
WIS	water Industry Specification

List of Symbols

A	Area
B	Thickness
D	Composite Desirability Function
E	Young's Modulus
$\bar{E}_r$	arithmetic mean of the energy to break values of test specimens cut from the parent pipe
$\bar{E}_w$	arithmetic mean of the energy to break values of the welded test specimens
f_e	Tensile energy welding factor
F	Factor
I	Second Order Unit Tensor
K	Stress Concentration Factor
K_I	Elastic Stress Intensity
L	Lower limit of the Response
L_0	Initial Length
P	Pressure
r_p	Radius of the Plastic Zone
T	Target of the Response
t_0	Initial Specimen Thickness
T_g	Glass Transition Temperature
T_m	Crystalline Melting Temperature
U	Upper Limit
W_e	Work for Formation of Fracture Surface

w_f	Total Work of Fracture
W_p	Work for Plastic Deformation
X	Vector of the designed Variables
y	Response
αf	Final Angle
β	Shape Factor
σ	Average Stress
σ_r	Radial Stress
σ_t	Transverse Stress
σ_1	First Principal Stress
σ_2	Second Principal Stress
σ_3	Third Principal Stress
σ_{eqv}	Von-Mises Equivalent Stress
σ_h	Hydrostatic Pressure Stress
$\overline{M_n}$	Number average
$\overline{M_w}$	Weight Average
n_i	Number of Molecules
W_i	Weight
K_{IC}	Plane-Strain Fracture Toughness
σ_y	Yield Stress
$\sigma*$	Stress Triaxiality

Statement of original Authorship

The work contained in this thesis has not been previously submitted to the requirement for an award at this or any other higher education institution. To the best of my knowledge and belief, the thesis contains no material previously published or written by another person except where due reference is made.

Signature:

Date:

Acknowledgments

I would like to take this opportunity to thank everyone who helped me in different ways to achieve this valuable milestone in my life.

First of all, I would like to thank my family, especially my younger brother *Amir*, for their love and support throughout my life. Without you, I could have never got to this stage.

Special praise should be reserved for my industrial supervisor, *Dr. Mike Troughton.* Not only I have gained technical knowledge from him throughout my PhD programme, I have learned how approach and solve challenging problems. *Mike*, your contribution to this work cannot be overstated.

I would like to offer special thanks to *Dr. Amir Khamsehnezhad* and *Steve Willis* for their constant care, guidance and supervision. They have always given me assurance and believed in the integrity of my research work. I am also grateful to *Prof. Jim Song, Dr. Bin Wang* and *Prof. Luis Wrobel* for their continuous support throughout the research.

I gratefully acknowledge my friends and colleagues within TWI and Brunel University London, especially *Dr. Sina Fateri* for giving me guidance and motivation to finish this work and *Dr. Mario Kostan* for making my life in Cambridge more enjoyable.

Finally I would like to thank the Engineering and Physical Sciences research Board (EPSRC), Brunel University London and TWI for providing the funding for this research.

Chapter 1. Introduction

The first plastic pipes were installed in the mid-1930s, with their usage increasing rapidly in the 1950s. Plastics have steadily replaced clay, copper, asbestos-cement, aluminium, iron and concrete pipes in various applications. Polyethylene (PE) is employed in about 20% of plastic pipe applications [1, 2]. High-density polyethylene (HDPE) pipes are used extensively for the transportation and distribution of natural gas, with over 80% of the new piping installations using HDPE.

There are many tests available for assessing the short-term performance of butt fusion welded joints in HDPE pipes. Previous work [3, 4] has shown that the most discriminating short-term test is a tensile test using waisted test specimen (Figure 1-1), such as those described in ISO 13953, EN 12814-2, EN12814-7 and WIS 4-32-08.

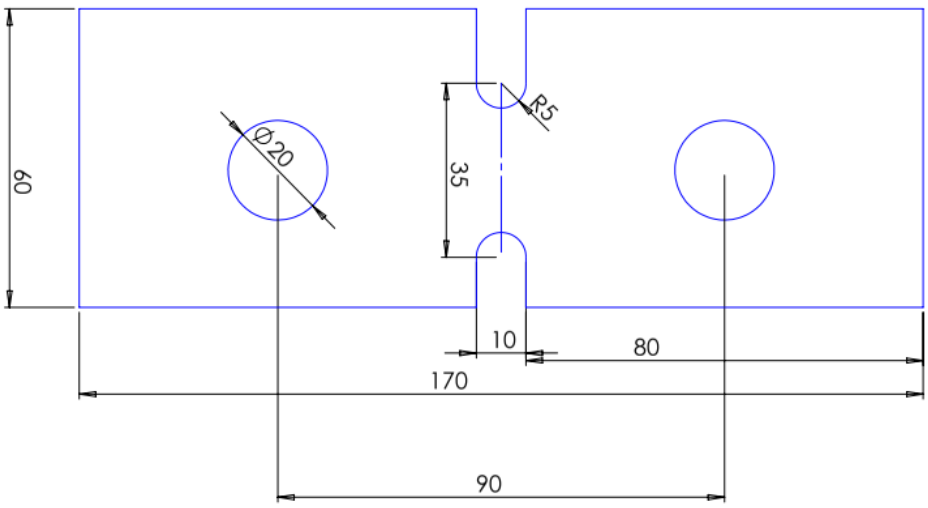

Figure 1-1, Waisted tensile test specimen (EN12814-7)

This type of test is therefore specified in some standards relating to the qualification of butt fusion welding procedures and welding operators for PE pipes (EN 13067, AWS B2.4).

In tensile tests using a waisted specimen [4], it is shown that the most discriminating test parameter is the energy to break the specimen. Standards such as ISO 13953, EN 12814-2, EN 12814-6 and EN 12814-7 describe tensile tests on butt fusion welds in PE pipes where the Cross-Sectional Area (CSA) is at minimum at the weld interface. Most of these tests specify that the tensile strength of the welded specimen is determined and compared to that of a specimen cut from the parent pipe. However, Chipperfield & Troughton [4] showed that tensile strength is a poor discriminator of weld quality. ISO 13953 specifies that the fracture surfaces of the tested specimen should be examined and categorised as either ductile (large-scale deformation and yielding of material at the weld interface) or brittle (little or no large-scale deformation of material at the weld interface). However, as can be seen in Figure 1-2 this categorisation is subjective, qualitative and the degree of ductility reduces significantly with wall thickness [5].

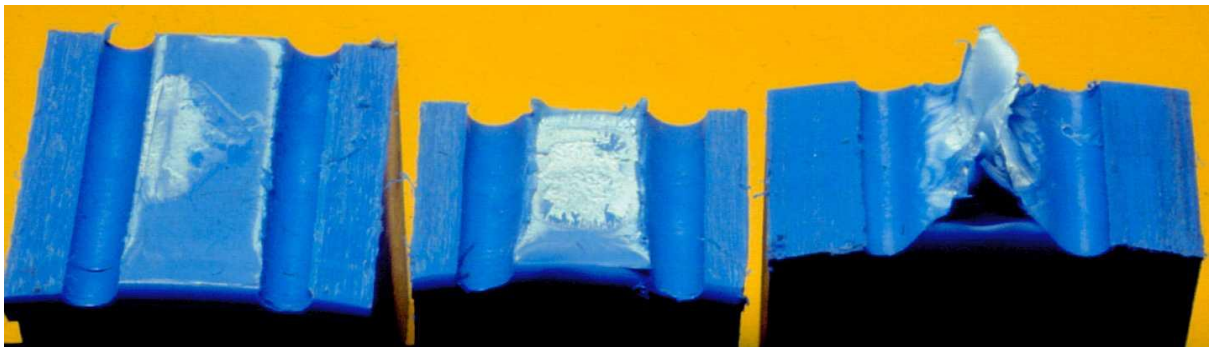

Figure 1-2, Three different types of failures in a waisted tensile test. From left; brittle, mixed and ductile failure

EN 12814-7 does specify measuring the energy to break of the specimen and determining a tensile energy welding factor, f_e, defined as:

$$f_e = \frac{\bar{E}_w}{\bar{E}_r} \quad \text{Equation 1-1}$$

Where $\bar{E}_w$ is the arithmetic mean of the energy to break values of the welded test specimens and $\bar{E}_r$ is the arithmetic mean of the energy to break values of test specimens cut from the parent pipe.

The values of energy to break have been shown to be dependent on wall thickness [6] and specimen geometry [7] and may also be dependent on PE resin and butt fusion welding procedure.

1.1 Industrial needs

HDPE pipes are employed in a wide range of industries such as water, gas, nuclear, and energy. A government review of the UK's electrical energy requirements for 2025 has indicated that 60 GW of net new capacity will be required to meet demand. This need comes from new nuclear fission installations, which require joining of HDPE pipes. The implementation of these pipes in nuclear power plants with strict policies, regulations, and inspection practices require a vote of confidence for structural integrity and accurate prediction of welds' lifetime. Currently, standard BS EN 12814-7 is used to quantify between different qualities of welds. This standard fails to provide accurate discrimination among different weld qualities, especially for pipes with large thicknesses (25mm and above). Therefore, an updated specimen geometry is required to provide accurate testing methods for the abovementioned industries.

1.2 Aim and Objectives

This research aims to investigate and improve the current standard geometry in quantifying the quality of welds in HDPE pipes. Specific objectives of this research are:

- To investigate the current standard specimen geometry and identify factors indicating the quality of the welds.
- To investigate the effect of geometry parameters on the value of the tensile energy to break of welds experimentally.
- To determine the effect of specimen thickness on the failure of the waisted specimen via Finite Element Analysis (FEA).
- To propose the most appropriate specimen geometry for tensile tests using waisted specimens, which provides the most discrimination between different weld qualities.
- To provide a quantitative comparison between energy to break values of the standard and proposed/improved geometry for pipes with different wall thicknesses and dimensions.

1.3 Thesis Structure

A combination of laboratory experiments, optimisation modelling, and FEA analysis are employed to evaluate the effect of geometry parameters on specimen failure. This led to four distinct contributions to knowledge which are listed below:

- The effect of the width of waisted section specimen on waisted geometry at 15 and 25mm thickness using different test techniques are investigated. Total energy to break value of specimen has been considered in recent literature as an indication of ductility in a specimen. Therefore, specimen tensile tests have been compared against energy to break values. During the observation of tensile tests, elongation around the loading hole could be observed; therefore, in this research, different regions for the energy consumed are defined as the area of interest (waisted area). Thus, Region 3 (energy consumed in necking of the specimen) is proposed to be used as an indication of ductility in the waisted region. The most suitable width of the waisted section, for a particular thickness, was found to have an aspect ratio of 1 to the thickness.

- Optimisation modelling technique is employed to investigate five different parameters of waisted specimen geometry to understand their effects on responses. Parameters used for this investigation are:

    - Width and radius of the waisted section.
    - Diameter and distance between loading holes.
    - The overall width of the specimen.
    - Responses of total energy to break value.

- Region 3 energy to break value and elongation in loading holes of the specimen.

For each response, a mathematical model has been found, including a combination of factors with great significance. As a result of this optimisation modelling, the most suitable specimen geometry is proposed for 15mm thickness specimens.

- Different FEA modelling methods in combination with constitutive equations are performed to model the waisted tensile test (made of polyethylene), which can undergo large deformations. The triaxiality factor is used to compare different models investigating the effect of thickness, radius and width of the waisted section. Different modes of failure are identified, which have been found to be related to triaxiality factors used in FEA. These two modes of failure, ductile and micro ductile, are verified using X-ray photography.

- Three different specimen geometries are proposed based on studies summarised above. According to best of author's knowledge, this investigation has not been undertaken in the field prior. Welding of different pipe diameters has been carried out, and standard geometry (offered by BSEN1284) has been compared to the proposed modified geometry for each case. Fully ductile failure has taken place on all specimen with modified geometry in all thicknesses whereas, failure mode using standard geometry on the specimen with thickness over 20mm have been challenging, even on parent material. On welded specimen, the proposed geometry provided ductility on all thicknesses, unlike standard geometry where any thickness above 20mm, the fracture surface is entirely flat, which provides no useful information on the quality of welds.

Chapter 2. Background Theory

2.1 Chapter Overview

In this chapter, a brief background theory of polymers and their categorisation is explained. PE pipes, their application, classifications and manufacturing techniques used are also explained in this section. Towards the end of this chapter, welding theory is described, and a review of current test methods is provided.

2.1.1 Introduction to Polymers

High molecular weight materials which have a variety of applications are called polymers. Unlike low molecular weight compounds, polymers do not follow a uniform structure and are combinations of macromolecules of different length and different structural arrangements. The average molecular weight of these macromolecules can vary from 10,000 to more than 100,000g/mol, which is produced by joining many mers through chemical bonding.

2.1.2 Polymer Types

Polymers get classified in different ways, but the most common ones are classified based on their reaction to heat and their molecular structure.

To classify polymers based on their response to heat, the polymers are divided into two types, namely, thermoplastics and thermosets. When the polymer is softened upon heating and solidifies on cooling and ability to repeat this cycle without affecting the property of the material, the polymer is classified as thermoplastics.

One of the reasons that thermoplastics can melt and flow refers to their linear structure, comprising chains of repeated chemical units called monomers which, when linked together end to end, form linear chain-like polymer molecules [8].

Thermosets are from large numbers of repeated chemical units with the difference that instead of linking together in linear chains, same for thermoplastics, thermosets cross-link to form a covalently bonded network. The reason that thermosets will not melt or flow refers to their cross-linked nature, which does not follow this behaviour [9].

Another classification of polymers is based on their molecular structure, which divides the polymers into three sections of linear, Branched and cross-linked-chain polymers.

For monomers to be able to form polymers, they must have a reactive functional group or double or triple bonds. The number of these functional groups is the factor for defining the functionality of these monomers. Double bonds are equivalent to the functionality of two, whereas a triple bond has the functionality of four (Figure 2-1).

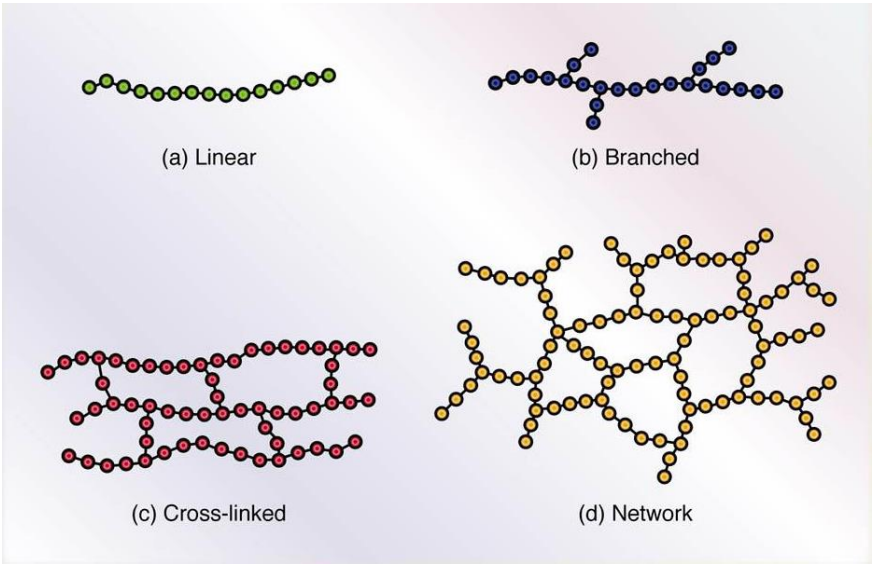

Figure 2-1, Schematic diagram of the polymer structure [9]

2.1.3 Polymerisation

When a product molecule can grow indefinitely in size as long as reactants are supplied in a chemical reaction, it is called polymerisation. The functionality of the monomers plays a significant role in polymerisation as monomers involved in polymerisation should have proper functionalities.

Polymerisation divides into two different mechanisms, based on reaction kinetics or the mechanism by which the chain grows. Polymerisation reactions are step and chain polymerisation.

In chain polymerisation, which is represented by the addition polymerisation, the reaction takes place by successive addition of monomer molecules to reactive end of a growing polymer chain. During the chain polymerisation at the beginning, the long chain appears, and steadily monomers are added to these long chains and slowly disappear during the process. During this process, molecules with high molecular weights can be obtained (10^5 to 2×10^6). The continuation of polymerisation increases only the conversion length, not the chain length [10].

The polymerisation of Vinyl monomers such as ethane, propane, styrene and vinylchloride is one of the main groups of chain-growth polymerisation. To start a chain-growth reaction, an initiator or a catalyst is required.

$$nCH2 = CHX \rightarrow -(CH2 - CHX)n - \ in\ which\ X = H, CH3, C5H6, or\ Cl \qquad \text{Equation 2-1}$$

The process in step-growth polymerisation is different from chain polymerisation, in which in step-growth, the reaction is between the functional groups of any two molecules. At the beginning of the process as mention dimers, trimers and tetramers are formed from the reacting pairs of opposing functional groups which also causes the monomers to disappear at the beginning.

As monomers were disappearing slowly during the process of chain polymerisation, in step polymerisation, monomers disappear at the early stages of the process. During this process, molecules with low to medium molecular weights can be obtained. For this process, continuation of polymerisation increases both the conversion length and the chain length (Figure 2-2) [11].

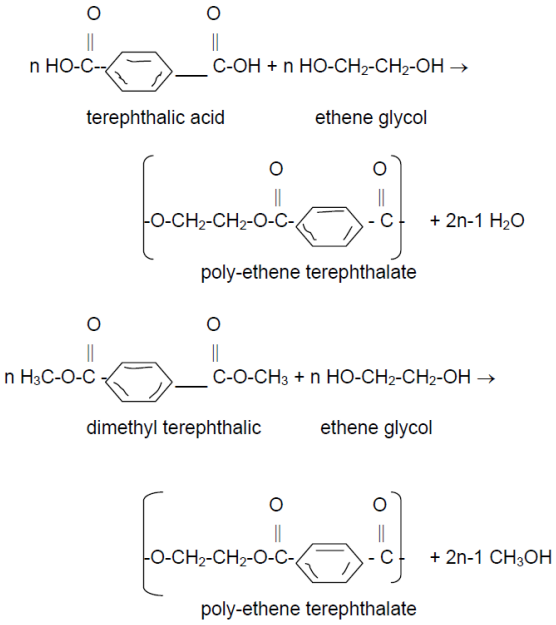

Figure 2-2, Reactions to the productions of polyethylene terephthalate [11]

2.1.4 Amorphous and Semi-Crystalline Thermoplastics

The thermoplastic group divides into groups of materials based on their structure which are crystalline (ordered) and amorphous (random). It is impossible to have a completely crystalline structure for a moulded plastic, and it is mainly because of its complex physical nature of the molecular chain [12].

In more details, when a linear thermoplastic follows a regular pattern within repeated units with the least or no chain branching, then it can be said that it is in crystalline form.

In amorphous thermoplastics, there is no order on the repeat units, which is the main reason for producing long chain macromolecule, which is called short-range order.

Plastics such as polyethylene and nylon can have a high degree of crystallinity, but as it is not entirely crystalline, it is described as partially crystalline or semi-crystalline. Plastics such as polystyrene and acrylic are always amorphous because of their structure.

2.1.5 Polymer Molecular weight

Mechanical properties and processing behaviour of solid thermoplastics at certain temperature depend strongly on the average size and the distribution of sizes of macromolecules in the sample. It is the main reason that there are different grades for each polymer on the plastic market [13].

For a substance to be called polymer, there is an exact molecular weight required, there are arguments about this number, but often polymer scientists put the number at about 25,000 g/mol. To have excellent physical and mechanical properties minimum molecular weight of 25,000 g/mol is required for many vital polymers [14]. There are chains of different lengths so only the average molecular weight can be determined. To have full characterization, the width of the molecular weight distribution is required [12].

The number of repeating units (mers) defines the chain length of the polymer. In polymer science, this term is called the degree of polymerisation (DP). To calculate the molecular weight (*MW*) of the polymer, the DP is multiplied by the molecular weight of the repeating units.

There are different mathematical averaging methods, but for this case, number average, $\overline{M_n}$and weight average, $\overline{M_w}$ methods have been used.

$$\overline{M_n} = \frac{n_1M_1+n_2M_2+\ldots+n_nM_n}{n_1+n_2+\ldots+n_N} = \frac{\sum n_iM_i}{\sum n_i} = \frac{\sum W_i}{\sum \frac{W_i}{M_i}}$$ Equation 2-2

$$n_i = number\ of\ molecules$$

$$\overline{M_w} = \frac{W_1M_1+W_2M_2+\ldots+W_nM_n}{W_1+W_2+\ldots+W_N} = \frac{\sum W_iM_i}{\sum W_i} = \frac{\sum n_iW_i^2}{\sum n_iM_i}$$ Equation 2-3

$$W_i = weight\ of\ a\ chain\ that\ has\ MW = M_i$$

The relation between weight $W_i$and the number of chains n_i is as follows: W_i=n_iM_i . It can be proven that by definition, $\overline{M_w} > \overline{M_n}$ and therefore the ratio $\overline{M_w}/\overline{M_n}$ can be taken to measure the breath of the distribution.

2.1.6 Polyethylene

Polyethylene is a polymer with one of the most straightforward molecular structure ($[CH_2CH_2]_n$). The largest tonnage plastics material was first produced in 1939, and it was mainly used for electric insulations. To name a few advantages of polyethylene which reason was to be an attractive material were the excellent insulation properties over a wide range of frequencies, good chemical resistance, easy processability, toughness, flexibility and easy transparency [15].

There are some difficulties over the agreed name of this polymer; despite it is one of the simplest molecular structures of all polymers but still, it does not have a complete agreed name. As it is a polymer of ethylene therefore in most scientific publications, it is called polyethylene. The word ethylene does not accord with the terminology for alkenes (olefins) adopted by the international union of pure and applied chemistry and which would indicate the word ethane, therefore mainly, for this reason, polyethene is sometimes and more likely to be used in chemistry compared to industry [15].

2.2 PE Pipes and Applications

PE plastic has become one of the world's widely used thermoplastic materials since its discovery in 1933 [16]. Due to the unique properties of this material, there is a broad range of application for which this material is used. It is also used as a substitute for rubber in electrical insulations during World War II which was one of the first applications for PE materials.

The new and unique properties of polyethylene pipe provided an alternative to traditional material like steel and copper and in non-pressure applications where clay and fibre cement pipes are used. One of the first industrial applications of PE pipes in North America was for these pipes used for rural water and oil field production, where a flexible, robust and lightweight piping product was required for the rapidly growing oil and gas production industry.

Natural gas distribution industry which requires coilable, corrosion-free piping material that can assure a leak-free method, has also used PE piping. As the installation of this PE pipe in different critical applications been successful, it has led to being the material of choice for the natural gas distribution industry. Other properties of PE pipes, such as impact resistance and resistance to abrasion, have turned PE pipes to be a good choice in mining and industrial markets.

PE pipes also provide reliable, long-term service durability and cost-effectiveness properties which are the main factors for designers, owners and contractors while selecting a piping material. There are also some specific benefits of PE pipe which are as follows; Life cycle cost savings, Leak-free, fully restrained Joints, corrosion and chemical resistance, Fatigue resistance and flexibility, ductility and visco-elasticity behaviour.

2.2.1 PE Pipe Manufacturing

The main steps of PE pipe and fitting production are to melt and convey the material into shape and hold that shape during the cooling process.

Different diameters of solid wall PE pipe extrude through an annular die. For large diameter profile PE pipes, the outline is spirally wound onto a mandrel and heat-fusion sealed along the seams. The range of substantial wall PE pipe diameter under production is currently from ½ inch to 63 inches in diameter. Spirally wound profile pipe could be made up to 10 feet in diameter or more.

Industry standards and specifications such as ASTM (American Society for Testing and Materials) and AWWA (American Water Works Associations) are usually used to produce solid wall type and the profile wall type PE pipes, which are due to the different requirements of each industry. ASTM standards are also used to produce PE fittings used with solid wall PE pipe.

The primary standards for solid wall and profile pipe manufacturing processes are as follows;

- *ASTM D2239 Standard Specification for Polyethylene (PE) plastic pipe (SIDR_PR) Based on Controlled Inside Diameter*
- *ASTM D2447 Standard Specification for Polyethylene (PE) plastic pipe, Schedules 40 and 80, Based on Outside Diameter*
- *ASTM D2513 Standard Specification for Thermoplastic Gas Pressure Pipe, Tubing, and Fittings*
- *ASTM D3035 Standard Specification for Polyethylene (PE) Plastic Pipe (SDR-PR) Based on controlled outside Diameter*
- *ASTM F714 Standard Specification for Polyethylene (PE) Plastic Pipe (SDR-PR) Based on Outside Diameter*

- *ASTM F894 Standard Specification for Polyethylene (PE) Large Diameter Profile Wall Sewer and Drain Pipe*
- *AWWA C906 AWWA Standard for Polyethylene (PE) Pressure Pipe and Fittings*

Injection or compression mouldings are methods usually used for thermoplastic fittings, fabricated using sections of pipe, or machined from moulded plates.

2.2.2 Pipe Extrusion

The main aspects of a solid wall PE pipe manufacturing facility are shown in Figure 2-3. The steps which form the production of solid wall pipe are raw material handling, extrusion, sizing, cooling, printing, and cutting through finished product handling.

A battery of tests is used at the resin manufacturing site to ensure that the resin is of prime quality. Important physical properties of resins such as melt index, density, ESCR (environmental stress crack resistance), SCG (slow crack growth) and stabiliser tests are usually sent to the pipe and fitting manufacturer.

The raw material, which is known as PE compound, is supplied to the producer as non-pigmented pellets. Heat and UV protection are the two factors in which PE pellets are used to stabilise them. The two common colours used are black and yellow, which are dependent on the application of the pipe. For water, industrial, sewer and above ground uses, carbon black is the most common pigment used, whereas yellow is mainly for natural gas applications.

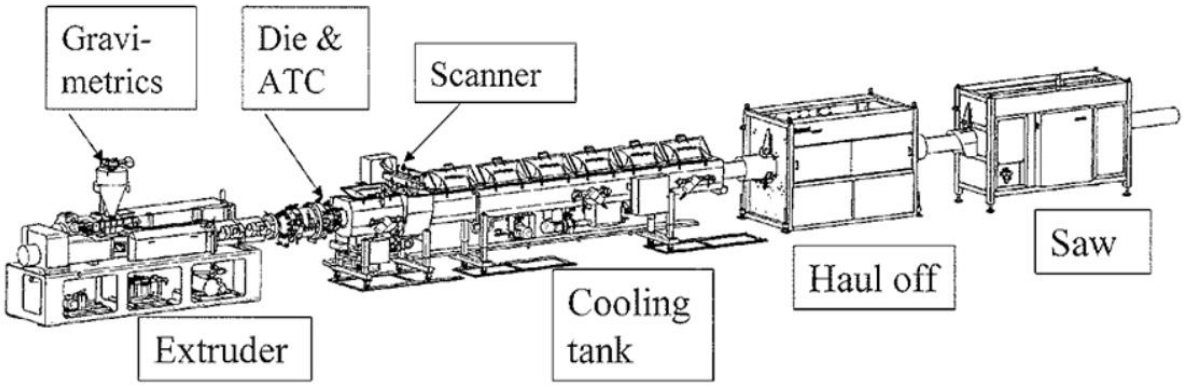

Figure 2-3, Typical Extrusion Line [17]

After the resins are delivered to the pipe manufacturer, some quality control testing is applied against specification requirements. The parameters could be, melt flow rate, density, moisture content and checks for contamination.

As mentioned, one of the methods of processing plastics is *extrusion* using a screw inside a barrel, as shown in Figure 2-4.

The main principles of the extruder are based on heat, melt, mix, and convey the material to the die, which then it is shaped into a pipe [18]. An extruder is divided into three different parts of the feed zone, Compression zone and metering zone.

In producing a homogeneous mix and high-quality pipe, extruder screw design has a big factor; therefore, it is an essential section of the extruder which requires good design.

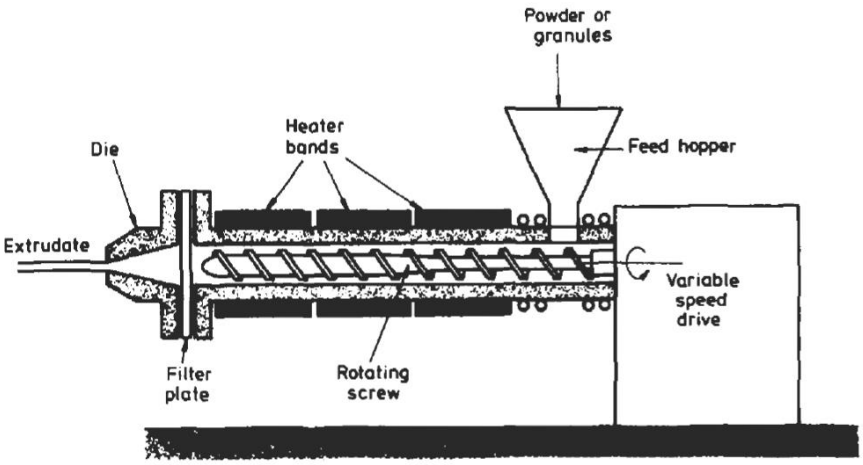

Figure 2-4 Single-Screw Extruder [18]

The function of the feed zone is to heat the plastic and carry it to the subsequent zones. Supplying enough material to the metering zone is very important as supplying less or more material to the metering zone it should not be starved or overrun.

In the compression zone, the screw depth decreases slowly to compact the plastic. Apart from compacting the plastic, in this zone, when the plastic is squeezed, the trapped air pockets back into the feed zone and also improve the heat transfer through the reduced thickness of the material.

In the metering zone, the depth is also constant but less than the feed zone. In this zone, as the supply rate is constant and the material has a uniform temperature and pressure, therefore, the melt is homogenised.

During the sizing and cooling operation of the pipe, the dimensions and tolerances are usually determined. During the sizing operation, the pipe is being held in its required dimensions during the cooling of the molten material. There are two types of sizing which are vacuum and pressure sizing technique, but in both techniques, the pipe must be cold enough, so it finds its rigidity before it exits the cooling tank.

2.2.3 Classification

Different standard specifications which are issued by different organisations such as; ASTM, AWWA, and Canadian Standards Association (CSA) have been set up to have the correct design and use of PE piping.

As there is a wide range of property variations that has applications in piping, ASTM has issued standard D3350, “Standard Specification for Polyethylene Plastic Pipe and fitting Materials”. This standard has introduced six properties that have the most effects on in manufacturing of PE piping, heat fusion joining and defining the long-term performance of the pipe. Each of these properties is assigned into a “cell” which each cell includes some numbers indicated a wide range of the large overall range that is covered by a property “cell”. Table 2-1 shows the D3350 property cells and classes.

Table 2-1, Cell Classification System from ASTM D 3350-06 [19]

Property	Test Method	0	1	2	3	4	5	6	7	8
Density, g/cm³	D1505	Un-specified	0.925 or lower	>0.925-0.940	>0.940-0.957	>0.947-0.955	>0.955	-	Specify value	-
Melt Index	D1238	Un-specified	1.0	1.0 to 0.4	<0.4 to 0.15	<0.15	A	-	Specify value	-
Flexural Modules, MPa	D790	Un-specified	<138	138-<246	276-<552	552-<758	758-<1103	>1103	Specify value	-
Tensile Strength, MPa	D638	Un-specified	<15	15-<18	18-<21	21-<24	24-<28	>28	Specify value	-
Slow Crack Growth. ESCR	D1693	Un-specified								
a. Test Conditions **b. Test duration, hours** **c. Failure, max, %**			A 48 50	B 24 50	C 192 20	C 600 20	- - -	- - -	- - -	Specify value
Slow Crack Growth Resistance, Pent	F-1473	Un-specified	-	-	-	10	30	100	500	Specify value
Hydraulic Strength 1. Hydrostatic design basis, MPa	D2837	NPR	5.52	6.89	8.62	11.03	-	-	-	-

Hydraulic Strength 2. Minimum required strength, MPa	ISO 12162	-	-	-	-	-	8	10	-	-

To identify if the material contains a colourant and the nature of the stabiliser that has been added to the material to have protection against damaging effects such as sunlight, code letters are produced and used in D3350, which is shown in Table 2-2.

Table 2-2 Code letter presentation (D3350)

Code Letter	Colour and UV Stabilizer
A	Natural
B	Coloured
C	Black with 2% minimum carbon black
D	Natural with UV stabilizer
E	Coloured with UV stabilizer

As mentioned before, the cell number for each cell property is identified for defining each material following ASTM D 3350. The same order as shown in table 1 which is then followed by an appropriate code letter has also been used.

2.3 Welding of Thermoplastics

Thermal welding of thermoplastic is based on the temperature of thermoplastics, where it must be above T_g for amorphous thermoplastics and above T_m for semi-crystalline thermoplastics. The temperature region in which the amorphous thermoplastics changes from a viscous or rubbery condition above this temperature to a hard and brittle material below it is called glass transition temperature T_g.

As discussed in section one, semi-crystalline thermoplastics are made up both from crystalline regions and amorphous regions. For flow to occur in semi-crystalline thermoplastics, all the crystalline regions must be disappeared which happens when the temperature is above the crystalline melting point T_m [19]. In semi-crystalline thermoplastics, as there are also amorphous regions, there is T_g related to that. It must be considered that viscous flow in semi-crystalline thermoplastics only happens above T_m.

There are other possible techniques of welding thermoplastics apart from thermal welding. One of these techniques is solvent welding which is described as when the joint is formed with self-bond between two polymeric components with the presence of a solvent [20].

The principle for solvent welding is that the surfaced of the thermoplastic is breached by the solvent which causes the thermoplastic to have a swelling and plasticization surface. Amorphous polymers can be welded using this technique while the material is in the glassy state and below T_g without thermal activation.

Thermal welding divides into three different techniques. The differences between these groups are the way heat is applied. In some techniques, heat is generated by an external movement of the components to be joint, an external source generates some heat, and this source heats the joint by thermal conduction and the last group uses electromagnetism directly [21].

1. Techniques where heat is generated by mechanical movement

- Spin welding
- Vibration welding
- Ultrasonic welding
- Orbital welding
- Friction Stir Welding

2. Techniques employing an external heat source

- Hot Plate welding
- Hot bar welding
- Impulse welding
- Hot gas welding
- Extrusion welding
- Forced Mixed extrusion welding
- Flash-free (BCF) welding

3. Techniques that directly employ electromagnetism

- Resistive implant welding
- Induction welding
- EMA weld
- Dielectric welding
- Microwave welding
- Infrared welding
- Laser welding

The most common techniques in thermoplastic welding are techniques employing an external heat source. One of the main factors which have enabled these techniques to be applied extensively is the thermal conductivity of thermoplastics.

Low coefficients of thermal conductivity for thermoplastics cause the temperature gradient normal to the surface to be high when the heat is applied. This heat can be used to soften or melt the surface of the thermoplastic without causing a high-temperature increase in the rest of the thermoplastic.

Several welding techniques where heated metal plates or heated gas is used are based on this principle. The high melt viscosity of thermoplastics does also help the welding procedure by preventing the hot area following away, and the weld area does not need support.

2.3.1 Welding theory

A joint can be made between two pieces of uncross-linked natural rubber when these two pieces are brought together under enough pressure to guarantee intimate contact at the interface. Molecular theories to explain this phenomenon based on the concept of diffusion [22].

As mentioned in thermoplastics, the weld is formed when two pieces of thermoplastics above their glass transition temperature or melting point are brought together under enough pressure to ensure intimate contact at the joint interface, and after some time at temperature, a weld is formed.

When some polymers pass their glass transition temperature, the polymer possesses a characteristic called tack. Tack is defined as 'the property of an adhesive that enables it to form a bond of measurable strength immediately after adhesive and adherend are brought into contact under low pressure'. This phenomenon has many uses in the field of adhesive bonding as well as welding.

One of the most significant advances in the theory of thermoplastics is from the development of reputation theory. It was first coined by de Gennes [23], to explain the motion of polymer chains under certain circumstances. He described the movement of a linear chain as the movement of sneak inside a strongly cross-linked polymer gel. The gel provided a regular array of fixed obstacles through which the chain could not pass. Instead, the linear chain had to wriggle between the obstacles. The reason for this approach was that theories for the motion of polymer molecules in their molten state could not be made to agree with the experimental observations of viscosity and self-diffusion.

2.3.2 Hot Plate Welding

Hot plate welding or heated tool welding is one of the most straightforward techniques for thermoplastics. The parts to be welded are held in fixtures and then against a heated tool. The heating usually happens in two steps. The first step is when the heated tool melts the thermoplastic surfaces and material is placed against the tool so that full contact with the heater plate is obtained.

The parts continue to be heated until they are softening some distance away from them. The next step is when the fixtures are open, the heated tools are withdrawn, and the fixture forces the parts together. Pressure controllers in the device are usually used to control the pressure applied to the parts during the welding process. The parts are usually held together during this stage of the welding process.

The heat in this process is usually applied electrically by resistance heaters or by the use of hot gas or gas burners. PTFE is used to cover the surface of the hot plate to prevent the adherence of molten plastic. To produce a consistent weld, the temperature across the surface of the hot plate should not vary more than $5^{o}C$.

The parameters which are critical in this process are the temperature of the hot plate, the heating time, the welding pressure, the plate removal time and the welding time. The tolerances to variations in the welding conditions are different from material to material.

Hot plate welding is being used to manufacture hydraulic reservoirs and battery cases in the automotive industry and welding plasticised PVC door and window frames for the building industry. The most critical application for hot plate welding is the welding of thermoplastic pipes for gas and water distribution. The needs to weld pipes of diameter up to 1500mm with high integrity have made hot plate welding one of the best options for this process.

2.4 The integrity of Plastic Joints

2.4.1 Safety-critical applications

An industry example of PE pipe installation in a safety-critical application is the service water pipe replacement by Duke Energy at Catawba. The main reason for using PE pipes for this application was the general corrosion and microbiologically influenced corrosion (MIC) which had plagued carbon steel piping in-service water systems in operating reactors. This has brought the industry to believe that the use of plastic piping, like that used in water, sewer, petrochemical and natural gas distribution applications, is quite viable for nuclear applications because of its resistance to general corrosion, bacteria, fungi and microbiological corrosion.

Due to excellent operating experience, Duke Energy plans to submit a relief request (license amendment) to replace safety relate portions of the Catawba Nuclear Station low-pressure service water system with polyethylene piping. Duke has proposed criteria for the production, design, material specifications, installation and inspection of the polyethylene piping.

2.4.2 Different types of Defects

There are different sources of defects in butt fusion welds of polyethylene pipes. These sources are as follows:

2.4.2.1 Weld beads

During the process of butt fusion welds, weld bead appears, which rolls towards the pipe surface. The interface of the rolling bead and the pipe surface creates a notch. This notch is the site of crack initiation [24, 25]. It is also shown that in fatigue tests, the removal of the bead has relocated the failure away from the welded joints in fatigue test [25].

2.4.2.2 Cold Weld

During the butt fusion welding process, crystallising the surfaces of the pipe ends before they come to contact must be avoided; otherwise, a 'cold' weld would occur. Such welds tend to fail in a brittle manner at the weld interface in internal pressure tests.

2.4.2.3 Contamination at the weld interface

The welding of PE pipes is frequently carried out on construction sites. Welding takes place in all weathers with no protection for equipment during the welding operation, which is not an ideal environment and in addition to that standard joining procedures may not be followed. There is, therefore, the possibility that wind or other external factors may introduce contaminants such as dust, soil water and grease to the welding surfaces of the pipe and the heater plate.

As part of the standard joining procedure, cleaning the welding surfaces just before the heating step and the use of a clean heated plate is essential (ASTM D 2657-97). However, it is impractical to clean the surfaces of the heater plate manually while they are hot working temperature. It has been recommended for preventing contamination, which might be present on the heater plate, to make a dummy weld (or two dummy welds for pipe walls thicker than 20mm) before production welding [26].

2.4.3 Modes of Failure

The failure modes for butt fusion welding joints can generally be divided into three modes of fracture behaviour mode, fatigue behaviour mode and stress rupture behaviour mode.

2.4.3.1 Fracture Behaviour

Different types of empirical test have been developed which are suitable to measure the impact strength of welds in polymers [27].

Polymers exhibit a transition from robust ductile behaviour to low energy brittle failure as either increase in strain rate or decrease in temperature. Ductile fracture is usually associated with extensive shear yielding, a process which is tough to arise from crystalline regions in the polymer undergoing processes such as slip or twinning [28].

Crazing is the predominant initiating mechanism for brittle fracture, which is a cavitation process in which micro voids are nucleated under applied tensile stress but do not coalesce to form a crack because they are bridged by fibrils spanning the craze [28]. By rupture of these fibrils the crack propagation occurs. Crazing does not follow a metallic failure mode analogue; polymeric materials do not possess a failure mode analogous to cleavage. The failure mechanism and toughness are also being affected by a critical factor called the chemical environment.

There has been a need to develop a quantitative relationship between tolerable flaw size and applied stress which Charpy testing does not allow that, despite it is suitable for comparing the toughness of weld joints in plastics.

2.4.3.2 Fatigue behaviour

Stress range is the critical variable controlling fatigue behaviour, but for polymers, there are numbers of factors that are essential in polymers but are insignificant in metals. These factors could be the environment and ambient temperature cyclic frequency, which all strongly influences behaviour. The main reason that these factors do have significant effects on polymers is the viscoelastic nature of them. The viscoelastic behaviour exhibits mechanical hysteresis even at low strains.

It must be considered that under cycling loading, energy dissipates as heat, which causes an increase in specimen temperature, which can rise significantly above ambient. This does influence the fatigue

performance; therefore, to obtain appropriate fatigue data, the test conditions and the cycling frequency must closely parallel the service conditions.

2.4.3.3 Stress rupture Behaviour

When a welded PE specimen is under stress, depending on the stress, it will fail after a certain length of time, and a log-log graph of stress versus time to failure can be produced.

When the stress is high in a short period, the failure occurs by local, large-scale deformation. This can be called a 'ductile' failure and is due to shear yielding.

When the stress is low in a more significant period, the failure occurs as a 'brittle' failure and is due to a crazing process known as 'slow crack growth' (SCG), which is a phenomenon based on the initiation of a crack from defect in the specimen which eventually propagates through the thickness.

At lower stresses with longer times, the specimen will fail due to degradation of PE. This type of failure becomes important at only high service temperatures or environments which accelerate degradation.

Maximum local stress and its position determine the lifetime of a PE pipe system in service and whether it will have a ductile or brittle failure.

2.5 Mechanical Testing

2.5.1 Bend Tests

There are three different cases for the bend test using BS EN 12814-1, which are; asymmetrical welds, symmetrical welds and side bend test (Figure 2-5).

In cases where the weld thickness is equal to or above 30mm, the side bend can be used, or the thickness of the test specimen can be reduced to less than 30 mm by machining from the side in contact with the ram end.

The test consists of subjecting a test specimen to deformation by bending at a constant speed without reversing the direction of bending during the test. The bend angle (ram displacement) and fracture appearance provide a guide to the ductility of a welded joint and hence the weld quality.

The final angle, α f, (final ram position), is recorded when the fracture occurs, a crack is visible with the naked eye, or a maximum load is reached. If no crack occurs, the test is terminated at either a bend angle of 160° or at a ram displacement given in Figure 2-5.

Table 2-3 Ram displacement corresponding to the bend angle of 160°

Thickness of Test Specimens	Ram Displacement (mm)
3 < a ≤ 5	60
5 < a ≤ 15	70
15 < a ≤ 20	85
20 < a ≤ 25	170
25 < a ≤ 30	150

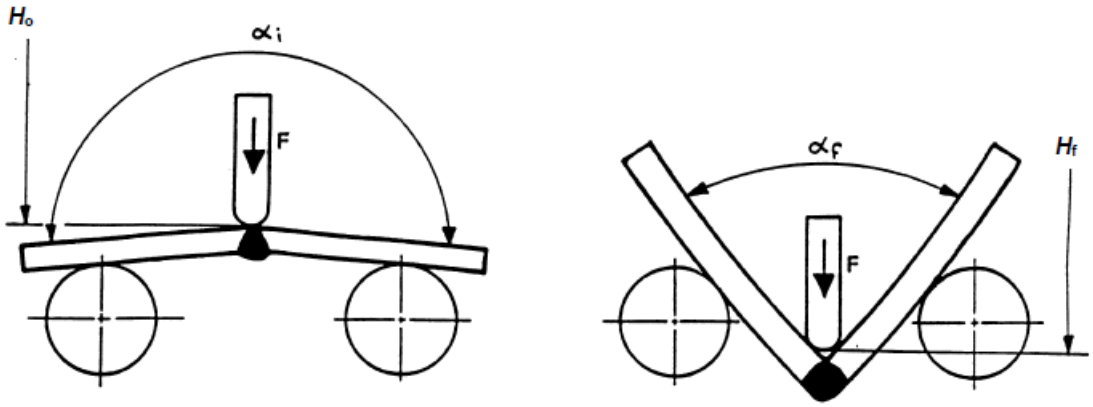

Figure 2-5, Determination of bend angle and the ram displacement (BS EN 12814-1)

2.5.2 Short-Term Testing

Among the short-term testing methods, the tensile test is one of the popular tests applied to the routine evaluation of the weld because the sample preparation is straight forward to carry out, the test is inexpensive, and analysis of the results is not time-consuming process.

In a butt fused pipe, the samples are taken in the longitudinal direction from the weld such that the weld is in the middle of the test specimen. In order to compare the tensile properties of the weld with parent material and assess the quality of the joint. The results obtained from these tests then can be compared with the tensile results obtained from testing of the parent material. A welding factor related to yield strength can be defined as can be seen below:

$$f = \frac{Yield\ strength\ of\ welded\ material}{Yield\ strength\ of\ parent\ material}$$ Equation 2-4

The tensile tests have been used previously to evaluate the optimum welding conditions and parameters by Atkinson et al. [29, 30, 31, 32, 33]. In the studies carried out by Atkinson et al., the results were reported concerning the welding factor, and the change in welding factor observed within the range of the welding conditions examined was negligible. The highest variation observed in welding factor was found to vary between 0.89 and 0.95 for the welding temperature variation of 150 to 250°C.

Malguarnera reported tensile test results regarding yield strength, where a significant decrease in yield strength observed for specimens welded under the following conditions:

a) Very low (204°C) and very high (370°C) welding temperature

b) Low heating time

c) Low heating pressure

d) Low fusion pressure

Tensile test is not the preferred testing method as suggested by several investigators [34, 35, 36, 37, 38] as the results obtained from tensile tests vary only slightly, as exemplified by Atkinson [29, 30] and Malguarnera [33] work. This method overestimates the weld strength, welding factor of 0.95 to 1, and it is only capable of detecting a weld with inferior quality.

Also, it is known that the mechanical properties of thermoplastic materials are time-dependent; bearing in mind that pipe systems are usually designed for 50 years, the tensile test provides, at its very best, only a limited guide to the long-term behaviour. Furthermore, the failure obtained under a tensile test is not like service failures.

Although Potente et al. [39, 40] disagree with the use of the tensile test, they agree with two modified short-term testing procedures proposed by Herfort, Hessel [41, 42, 43] and Menges and co-workers.

Herfort proposed using the low temperature bending test, and Menges and co-workers proposal [43, 44] involves the tensile test to be carried with a hole notch at the butt weld to concentrate the stress on the joint and also use the breaking strain rather than yield stress for the evaluation.

Currently, there are several test methods which are suggested by available butt fusion joining standards to be used for qualifying the butt fusion joints. These tests are summarised below.

2.5.3 Tensile test using dumb-bell specimens

To use tensile test using dumb-bell specimens for butt fusion joints, the European standard BS EN 12814-2 should be used (Figure 2-6).

Specimens are cut perpendicular to the welded joint and also from the parent pipe away from the joint. The minimum width of the parallel section can be 6mm with a tolerance of ±1mm. Where the

weld beads are left intact in service, they shall remain intact for testing, and if the beads are going to be removed in service, they shall be removed before the test.

The distance between the grips shall be approximately 220mm, and the specimens shall be tested at room temperature with a crosshead speed of 50mm/min. The tensile strain at break, as defined in BS EN ISO 527-1 [45], and the energy to break value can be determined by calculating the area under the curve for the force-displacement curve.

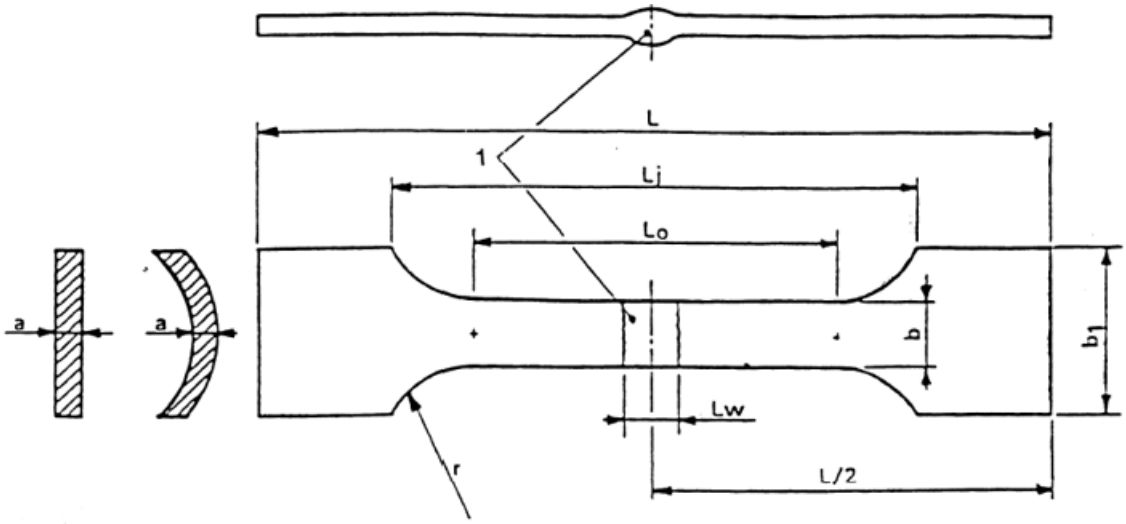

D_n or a_n	b	min. b_1	L_0	L	r
$20 \leq D_n < 50$	$a_n + \frac{D_n}{10}$	$b + 10$	80	≥ 120	60
$50 \leq D_n < 100$	$a_n + \frac{D_n}{10}$	$b + 10$	120	≥ 170	60
$D_n \geq 100$ or flat assemblies :					
$a_n \leq 10$	10	20	120	≥ 170	60
$10 < a_n \leq 20$	30	40	120	≥ 300	60
$a_n > 20$	$1{,}5a_n$	80	200	≥ 400	60

Figure 2-6, Type 2 specimen geometry and dimensions (mm) (EN-12814-2)

2.5.4 Tensile test using waisted specimen

This method, as outlined in BS EN 12814-7, includes measurement of the energy to break as well as a visual assessment of the fracture surface. Specimen geometry of this test is illustrated in Figure 2-7.

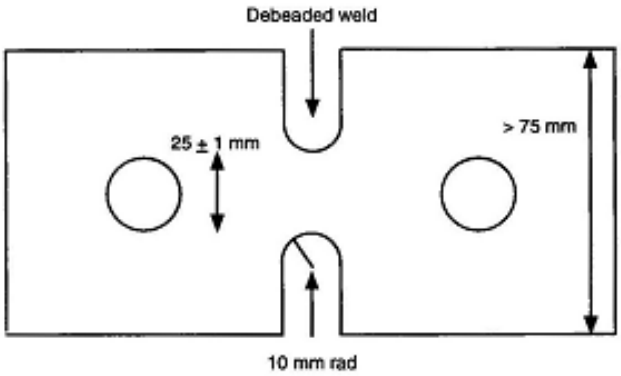

Figure 2-7, Recommended Waisted tensile test specimen by WIS standard [46]

Energy to break values obtained from this test is dependent on CSA of the waist and aspect ratio of width to thickness of the waist, as reported by Hill et al. [43, 47]. Based on this, data obtained for energy to break at any aspect ratio can be corrected for the effects of thickness by dividing the energy to break values by aspect ratio to allow comparison of the results in samples with different thicknesses. The test is carried out at a speed of 5 mm/min at 23°C.

The tests shall be carried out at room temperature. The specimen geometry and dimensions of the notched tensile test specimen are shown in Figure 2-8.

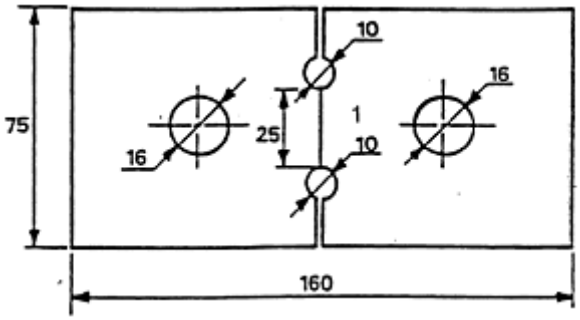

Figure 2-8 Notched tensile specimen geometry and dimensions [45]

Two more tensile test specimens with similar geometry to waisted tensile test specimen are defined in ISO 13953. This test can only be performed on pipes with an outside diameter greater than 90mm. The specimen types, A or B, are defined by the thickness of the pipe wall.

The failure mode and tensile strength are used as criteria for the evaluation of the butt-fused joint. The specimen geometry for type A and B with dimensions given in Figure 2-9, Figure 2-10 and Table 2-4, respectively.

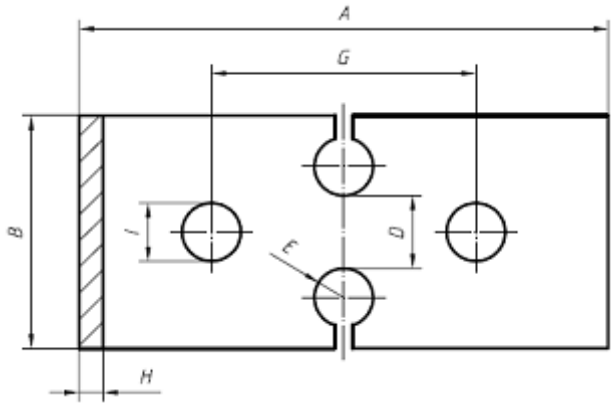

Figure 2-9, Type A tensile test specimen for wall thickness less than 25mm (ISO 13953)

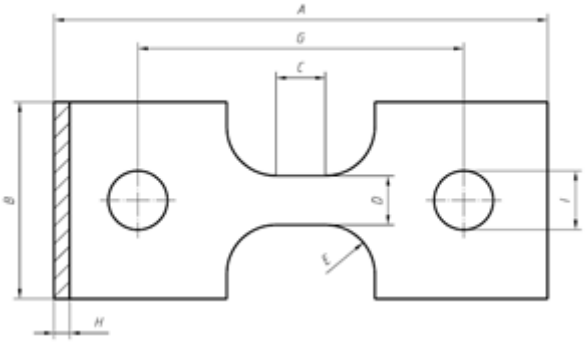

Figure 2-10, Type B tensile test specimen for wall thickness greater than 25mm (ISO 13953)

Table 2-4, Dimensions of the tensile test specimens in ISO 13953

Symbol	Description	Dimensions of type A test piece		Dimensions of type B test piece
A	Overall Length(min)	180	180	
B	Width at ends	60 ± 3	80 ± 3	250
C	Length of narrow parallel-sided portion	Not applicable	Not applicable	25 ± 1
D	Width of narrow portion	25 ± 1	25 ± 1	25 ± 1
E	Radius	5 ± 0.5		25 ± 1
G	Initial distance between grips	90 ± 5	90 ± 5	165 ± 5
H	Thickness	Full wall thickness	Full wall thickness	Full wall thickness
I	Diameter of the traction holes	20 ± 5	20 ± 5	30 ± 5

2.5.5 Tensile Impact tests

Impact tests are not mainly well developed. The results are strongly dependent on the specimen geometry and strain rate of the test. Potential variability of the results may lead to a change of behaviour and a misleading result.

The current standard that is being used for testing butt fusion joints in tensile impact mode is defined in ASTM F2634. The test can be carried out on pipes with an outer diameter larger than 60.3 mm and wall thicknesses not smaller than 6.3 mm. The specimen shall conform to the geometry and dimensions given in Figure 2-11.

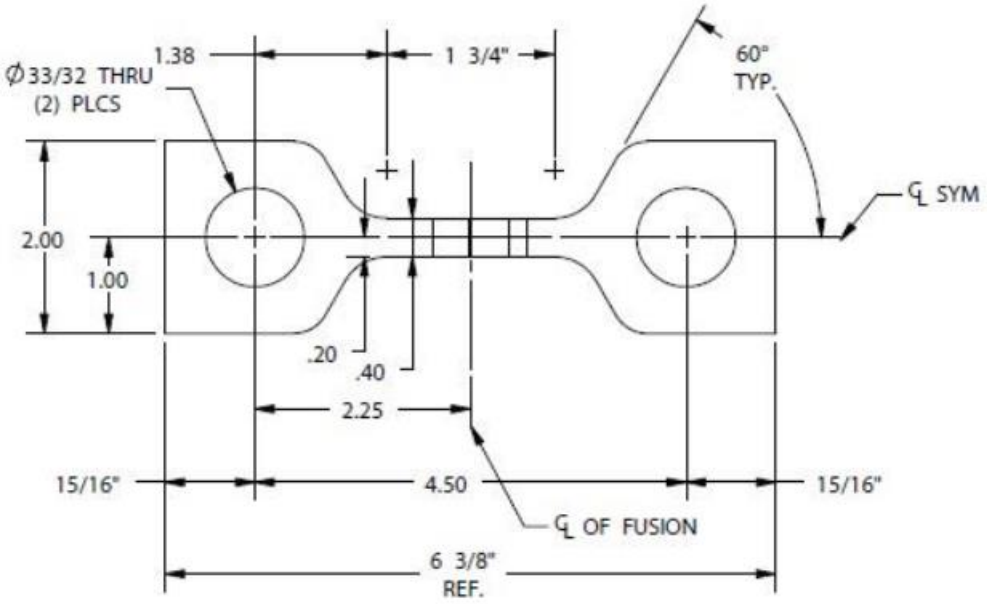

Figure 2-11, Tensile impact test specimen (all dimensions are in inches) (ASTM F2634)

The speed of the test shall be decided based on Young's modulus of the material being tested and the wall thickness of the pipe. The speed of testing for wall thicknesses smaller than 32mm is 152mm/s, and for wall thicknesses greater than 32mm, the speed of testing shall be adjusted to 102mm/s. Specimens shall be tested to failure, and the energy to yield and to failure shall be calculated and along with failure mode (ductile or brittle) shall be compared with results obtained from parent pipe.

2.5.6 Hydrostatic pressure test

The extruded pipe, joints and fittings are the components that form the integrity of pressure pipeline systems. To take into account the possible difference between the performance of the pipe and the components, the industry merely tends to increase the safety factor. It can be understood that there is a need to assess the long-term performance of joints in order to define a safety that is not overestimated.

The primary test for ensuring a 50 years lifetime for PE pipe systems is the internal hydrostatic pressure test which is stated in BS 4728:1971 and ISO 1167:1973, where the length of the pipe sample is typically higher than three times the outside diameter. These pipe samples are fitted with end caps designed to make a pressure-tight connection between the pipe sample and pressuring equipment. These samples are then filled with water and immersed unconstrained in a water bath, which is maintained at a constant temperature, and after a conditioning period (usually an hour), the hydrostatic pressure is applied and the time to failure measured.

The hydrostatic pressure test also forms the basis of quality control and type test, which are generally performed at a temperature of 80 and for the period between 120 and 1000 hours, depending on the hydrostatic test pressure used.

It has to be taken into account that these tests cannot be regarded as adequate methods for assessing the performance of butt fusion welds since joints are more vulnerable to stress in the axial direction. In the hydrostatic pressure tests, the axial stress in the pipe wall, due to pressure against the end caps, is only half the hoop stress and therefore, except in the case of very poor-quality welds, failure always occurs in the pipe wall first. It can be seen these tests suggest that the weld is as strong as the pipe, but in reality, the only real information they give is that the weld has a strength higher than 50% of that of the pipe. Therefore, it can be said that as in service, a pressure pipe has to withstand additional axial stress due to bending, thermal contraction, misalignment, etc.

2.6 Mechanics of Materials

2.6.1 Introduction

Mechanical behaviour refers to the response of materials to forces. Different factors cause a material to deform or break under load. The factors that influence the material's resistance to deform are entirely different from the factors that affect the resistance to fracture.

2.6.2 Stress Distribution at the Neck

A complex triaxle state of stress is usually produced by the formation of a neck in the tensile specimen. A notch under tension produces radial stress (σ_r) and transverse stress (σ_t). These stresses raise the value of longitudinal stress and would cause the plastic flow. It can be understood that the true stress at the neck, which is determined by dividing the axial tensile load by the minimum CSA of the specimen at the neck, is higher than the stress that would be required to cause flow in simple tension.

2.6.3 Fracture in High-Density Polyethylene

Since engineering plastics have begun to be used in critical structural applications, the fracture behaviour of polymeric materials has become a significant concern for engineers. It must be considered that in some products from polymers, the fracture may not be an essential safety issue (. e.g., toys, garbage bags, ice chests, etc.), but when the fracture comes to critical applications such as plastic, natural gas piping systems or aircraft wings, however, can have dire consequences.

Fracture and yielding are the primary failure mechanisms in metals. As it has been mentioned before, in cases where yielding is difficult, the failure tends towards brittle fracture. In ductile metals, the material experiences an extensive plastic deformation before the reach the fracture step. Low

temperature, high strain rates, and triaxial tensile stresses tend to suppress yielding and favour brittle fracture.

Polymers do not contain crystallographic planes, dislocations and grain boundaries; instead, they consist of long molecular chains. Therefore the microscopic details of yielding and fracture in plastics are different from metals. One of the main reasons for this difference refers to the two types of bonds in polymers: the covalent bond between carbon atoms and the secondary van der waals forces between molecule segments.

ASTM E 399 is the standard test method used to evaluate the toughness of materials by fracture toughness testing. Standard test methods and specimen geometries have been defined in this standard for measuring the critical stress intensity factor for metals. Similar standards have not yet been produced for plastics, but it has been recommended that the test procedures for metals used in ASTM E 399 are equally worthwhile for plastics, except the ductile nature and low yield strength of plastics causes problems in specimen size.

For applying ASTM E 399 in fracture toughness testing of polymers, the sample size can be reduced as long as all dimensions of the laboratory specimen are much larger than the plastic zone size. According to ASTM E 399, the thickness, B, must be:

$$B \geq 2.5\left(\frac{K_{IC}}{\sigma_y}\right)^2 \approx 16 r_p \qquad \text{equation 2-5}$$

Where K_{IC} is the plane-strain fracture toughness, σ_y is the yield stress, and r_p is the radius of the plastic zone, which is given by:

$$r_p = \frac{1}{2}\left(\frac{K_{IC}}{\sigma_y}\right)^2$$ Equation 2-6

By applying these conditions, the thickness would be much more significant than the yield zone size (at least 16 times larger), which causes the specimen to be in the state of everyday strain. This is mainly because of the hydrostatic stresses that develop a crack tip under plain-strain a condition, yielding is suppressed, and a minimum value for fracture toughness is obtained.

HDPE often fractures in a ductile manner if it is under uniaxial tension. The ductile fracture involves great drawing, which is believed to occur in the plane-stress condition. However, for large-scale HDPE products like polyethylene pipe, a crack might overgrow in a brittle manner. This type of fracture, which happens in a brittle manner, is known to be in the plane-strain condition (no drawing in the failure), which has much lower toughness than that in the plane-stress condition [48].

When the fracture resistance of very ductile materials is under investigation, usually a large plastic zone is produced; therefore, it can be seen that the energy dissipation is no longer confined to a small region around the crack tip. The J-integral has been the traditional method to quantify the toughness. The values from J integral method for ductile materials present a coupled contribution from plastic deformation and crack formation [49, 50]. To extract the specific energy needed for the crack formation, a different approach which was firstly proposed by Broberg [50], known as essential work of fracture (EWF), was developed to extract the specific energy needed for the crack formation by separating it from the non-essential work for the plastic deformation. As the EWF concept has also been investigated by many researchers, therefore it is now a popular concept to be used for determining the fracture toughness of ductile materials. To be able to apply the EWF concept to double-edge-notched tensile (DENT) specimens, two conditions are required. The first one is that the ligament between two edge cracks, L_0 in Figure 2-12, should yield completely before the fracture commences, and the second one is that the plastic deformation should occur only in the region around

the ligament. When these conditions are followed, the energy absorbed during the test, after normalised by the original ligament area, is known to be a linear function of the ligament length.

By using the concept above, work provided to fracture the specimen can mainly be divided into two sections. The first section is the work for plastically deforming the region around the ligament, which is expected to be proportional to the volume of the plastic deformation zone. If we assume that the plastic deformation is completely developed before the crack growth commences, then it can be said that the width of the plastic deformation zone, d in is then proportional to the initial ligament length, L_0, and the total work for plastic deformation, W_p, is proportional to $L_0^2 \times t_0$.

The second part is the essential work used for the formation of the fracture surface, W_e, which is proportional to the CSA of the ligament $L_0 \times t_0$. By adding these two parts, it can be said that the total work of fracture, W_f is;

$$Wf = We + Wp = weL0t0 + \beta wpL20t0 \qquad \text{Equation 2-7}$$

Where t_0 is the initial specimen thickness, w_e the specific EWF, W_p the average plastic work density, and β the shape factor for the plastic deformation zone. By measuring the total work of fracture for specimens of different ligament lengths, and dividing W_f by the ligament CSA $L_0 \times t_0$, to the specific work of fracture, w_f can be expressed as;

$$Wf = we\beta wpL0 \qquad \text{Equation 2-8}$$

The specific EWF, w_e, can then be determined by extrapolating w_f to zero ligament length.

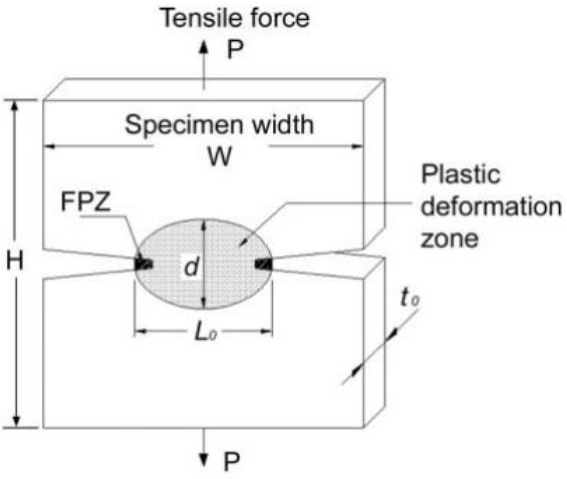

Figure 2-12, Dent Specimen with FPZ zone shown

2.6.4 Fracture toughness range in high-density polyethylene

As polyethylene is one the most ductile materials, therefore its fracture at room temperature is usually higher than 100%. As the fracture of polyethylene involves extensive necking, therefore it is categorised to have ductile fracture; however, a pressurised polyethylene pipe can fail in a brittle manner without any sign of necking. These kinds of failures are known as rapid crack propagation.

Different factors, such as high crack growth speed (sometimes exceeding the sound speed), low ambient temperature, deformation constraint, etc. [50, 48, 51, 52]are known to prohibit neck formation, resulting in brittle fracture behaviour. These are usually called plane-strain fracture, which is opposite the plane-stress fracture that involves extensive necking. The toughness of polyethylene in the two fracture modes is expected to be significantly different in the plane-stress fracture; the toughness of polyethylene was reported to be above 30 kJ/m2. Some types of high-density polyethylene (HDPE) were reported to show toughness around 35 kJ/m [53, 48]. The main reason it must be considered that these values are measured in the plane-stress condition, with the

involvement of necking in the fracture process. These values are much higher than the steady-state dynamic fracture toughness (G_d) of polyethylene pipe, estimated to be around 6 kJ/m^2 [49].

2.6.5 Triaxiality

The stress triaxiality is usually represented as the dimensionless stress triaxiality ratio σ^*. The definition of stress triaxiality was shown by Hancock and Mackenzie [54].

$$\sigma^* = \frac{I_1}{3\sqrt{3J_2}} \qquad \text{Equation 2-9}$$

First stress invariant, $I_1 = tr\sigma$, second stress invariant $J_2 = \frac{1}{2}\sigma^{dev}:\sigma^{dev}$, $where\ \sigma$ is the Cauchy stress tensor, $\sigma^{dev} = \sigma - \frac{1}{3}tr(\sigma)I\ is\ the\ deviatoric\ stress\ tensor$ and I is the second-order unit tensor. Based on the above definition, it can be said that a uniaxial stress state in tension gives σ^*=1/3 whereas a complete hydrostatic stress state in tension produces an infinity high-stress triaxiality ratio.

The triaxiality factor can also be defined as the ratio of hydrostatic pressure stress, or mean stress, σ_h, to the Von-Mises equivalent stress, σ_{eqv}. The formula for the triaxiality factor is given below, where σ_1, σ_2, and σ_3 are the first, second and third principal stresses, respectively.

$$\frac{\sigma_h}{\sigma_{eqv}} = \frac{\frac{1}{3}(\sigma_1+\sigma_2+\sigma_3)}{\frac{1}{\sqrt{2}}\sqrt{(\sigma_1-\sigma_2)^2+(\sigma_2-\sigma_3)^2+(\sigma_3-\sigma_1)^2}} \qquad \text{Equation 2-10}$$

The influence of stress triaxiality on the failure mechanism of polymers has been investigated by researchers recently. It has been found that an increase in stress triaxiality would accelerate void growth, which is one main form of polymer failures, especially at higher thicknesses. It has also been found that different triaxiality rate would not have an effect on the yield load but influences the yielding of the failure directly. As yielding of a specimen (more yield means energy to break the specimen) is an indication for the failure therefore, triaxiality would be an important factor in this research [55] [56].

In chapter 5, the application of triaxiality in this study is demonstrated, and it is shown how triaxiality could affect the failure behaviour of plastics.

2.7 Summary

In summary, in this section, different types of mechanical testing used for quantifying the quality of butt fusion welding and HDPE are explained. Current methods of investigating the fracture toughness of plastic materials, including their advantages and disadvantages, are also explained. The testing geometry selected to be optimised and the factors such as energy to break which is a similar approach as EWF concept, are selected and are fully described in the sections which they have been used.

Chapter 3. Effect of the width of the waisted section on the properties of the waisted tensile test specimen

3.1 Chapter overview

As mentioned in Chapter 1, the energy to break value of the specimen is the primary parameter which the geometry of the specimen is to be optimised. Waisted tensile test specimen made of polyethylene follows different failure mechanisms; therefore, accurate finite element modelling of such scenario can be challenging.

In this chapter, the main work involves experimental investigations. To simplify the problem and to understand more about the behaviour of the material, unwelded flat sheets have been used. Experimental work in this chapter could also support validating the attempts for modelling as well as the limitation to optimise the geometry based on energy to break values.

3.2 Literature review

Wilson carried out tensile tests using a waisted specimen on 500mm SDR (Standard Dimension Ratio) 11 HDPE pipe where he varied the width of the waisted section [57]. This work suggested that when the ratio of the width of the waisted section to the thickness is 1, the energy to break value per CSA is maximised. There are two limitations to this work. The first is that the width of the waisted section is limited to be equal to or smaller than the thickness. Thus no attention is given where the width of the waisted section is larger than the thickness. The second limitation is that it is not clear that the increase

in the energy to break per CSA is only from the extension in the middle of the specimen and not the elongation in holes.

One of the methods which have been used widely to determine the fracture toughness of the polymers is linear elastic fracture mechanics (LEFM), which uses the K_{IC} and G_{IC} parameters in the brittle region of polymers [58, 59]. The brittle region of polymers is usually at a high strain rate or low-temperature testing condition. When polymer behaviour is in the region of ductile behaviour, the linear elastic stress intensity factor K_I cannot be used to describe the stress condition in this type of failure, and different methodology which is a non-linear elastic fracture mechanic methodology (NLEFM) by using either CTOD or J integral [60, 61, 62].

When investigating the fracture behaviour of polymers in the ductile-to-brittle region is neither completely brittle nor entirely ductile [63, 64, 64, 65]. Load-displacement data for polymers are always non-linear, and consequently, LEFM presents difficulties when used within the transition region. While using these techniques for polymers, operating in the ductile and the ductile-brittle transition region present doubt about their toughness value. The abovementioned methods, regardless of covering the linear and nonlinear behaviour of polymers are mainly based on a small plastic zone around the crack tip. However, the values found from techniques such as J-integral presents coupled contribution from plastic deformation and crack formation [66].

As a result of these complications to quantify the toughness of polymers, a different approach was proposed by Broberg [50] known as essential work of fracture (EWF), which was developed to identify the specific energy needed for the crack formation by separating it from the non-essential work for the plastic deformation.

Different researchers investigated and applied this technique to quantify the toughness characterisation of ductile materials. To apply the EWF concept correctly, there are some

requirements. The first requirement is to have the ligament between two edges crack and yield completely before the fracture takes place. The other requirement is to have all the plastic deformation to be around the ligament. When these procedures and requirements are met, the energy used to deform the specimen, after getting normalised by the ligament area, will be a function of the ligament length (Figure 3-1).

The specific EWF contains energy for mainly two deformations. The first one is the energy for necking inside the fracture process zone (FPZ), which is the circle around the ligament or width of the waisted section. The second one is the energy for generating a new fracture surface [52]. As mentioned previously, some polymers especially high-density polyethylene, undergoes a high strain-hardening behaviour in large deformation, which usually produces a stable neck development. The techniques to measure the fracture toughness of polymers as mentioned above have mostly been tested on thin sheets of polymer (maximum 6mm) [48] and have investigated transition of plane strain to plane stress by adjusting the ligament length. The ability of the polymeric material to undergo a stable neck development before it fails or fractures is essential for HDPE in applications such as pipeline or pressure vessels that are used to distribute oil and gas. However, despite extensive research [67, 68, 69, 70] and its importance in industries, the mechanism involved in necking and its criteria requires more investigations due to a lack of quantitative investigations.

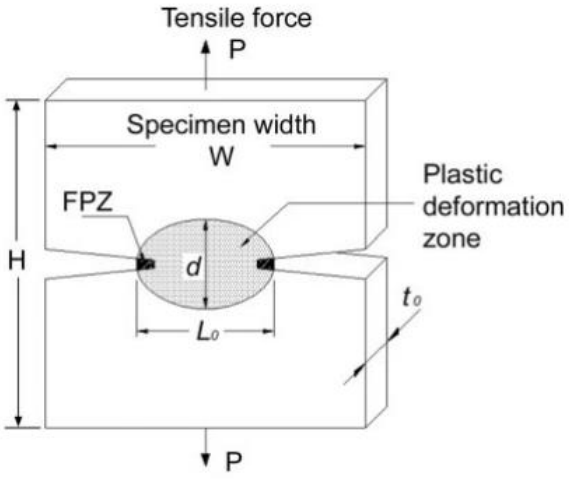

Figure 3-1. Dent Specimen with FPZ zone shown [48]

The previous studies on necking behaviour or the fracture of polymers such as HDPE were mainly on strain rate, temperature and initial imperfection size and less on geometry effect of the specimens. Thus, the objective of this part of this chapter is to understand the geometry influence, especially the width of the waisted section or ligament on different thicknesses (15 and 25mm) and aspect ratio (width of the waisted section to thickness) of the specimen.

3.3 Problem definition and research methodology

The specimen which is under investigation in this chapter is waisted tensile test specimen used in ISO 13953, EN 12814-2, EN12814-7 and WIS 4-32-08 and is used to quantify the quality of butt fusion welds. Regardless of the thickness of the pipe, many of these standards use similar geometries to quantify the quality of the weld. The examination is usually by tensile testing and by examining the fracture surface quality for acceptance of the weld quality. As mentioned in Chapter 1. , the work carried out by Chipperfield [71] has shown that as well as fracture surface quantification, energy to break the specimen per CSA could be a suitable indication to quantify the quality of the weld. The visual assessment of butt fusion weld sample in WIS 4-32-08 is shown below.

In WIS4-32-08 different fracture surface modes is shown in Figure 3-2, and from the left, it has been called Ductile, Mixed and brittle failure. When investigating the waisted specimen geometry experimentally, it should be tested and cut from a welded pipe, but HDPE failure behaviour in normal conditions performs a complex behaviour with different uncertainty and still with difficulties to predict its failure behaviour. Having specimens from welded pipes adds two parameters into our problem equation with no data on how they will affect the failure mode of the specimen:

- The first parameter is the curved geometry which will lead the specimen to be bending perpendicular to the loading axis

- The other parameter has welded specimen, which will have a polymer with slightly different material property in our waited area as well as some difference in thickness due to the weld around the specimen.

3.4 Experimental setup

In order to focus on the effect of the width of the waisted section, unwelded flat sheet HDPE has been used. The sheets had thicknesses of 15mm and 25mm. All the specimens in this work have been cut and tested in the extrusion direction. The first sets of experiments are designed to fully understand the effect of the width of the waisted section in thickness of 15mm. The thickness of 15mm has been chosen to assure all the specimen fail in a complete ductile manner. As unwelded flat sheets are used to only study the effect of the width of the waisted section, side plates have also been used to limit the movement and extension of the specimen to be only around the waisted area (Figure 3-3).

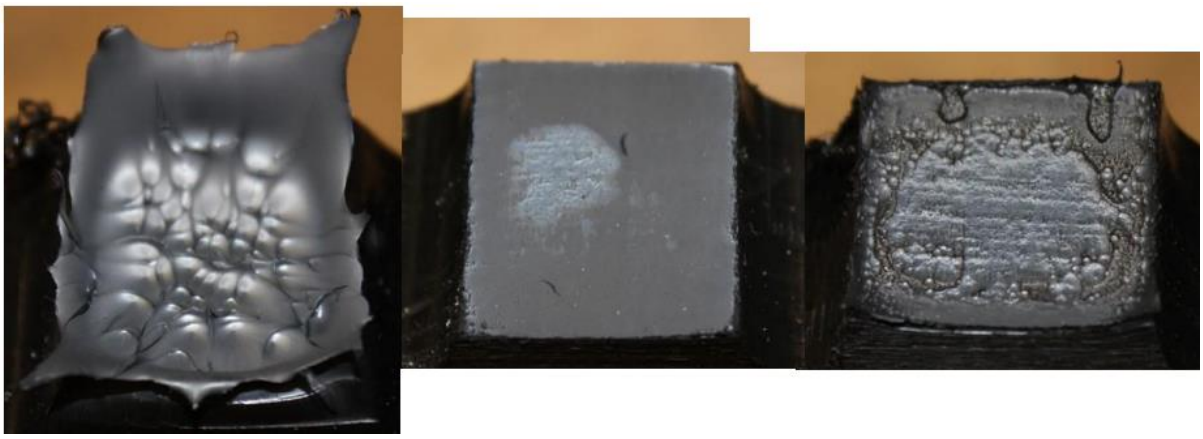

Figure 3-2, from left ductile, brittle and mixed failure mode according to WIS 4-32-08

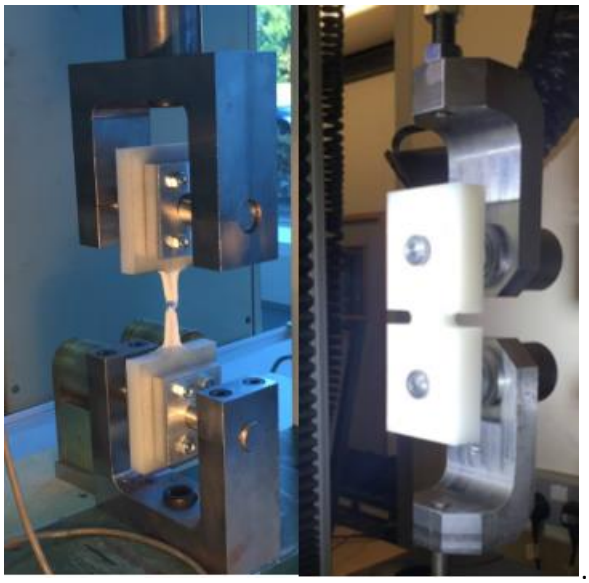

Figure 3-3, from left tensile testing with and without side plates

There are mainly four experiments carried out in this chapter. The first experiment is carried out on 15mm thickness with side plates, and the width of the waisted section varied from 3 to 35mm. Having the width of the waisted section to be varied from 3 to 35mm will give an aspect ratio of 0.2 to 2.3 for the width to thickness of the specimen.

The second experiment is carried out on 25mm thickness using side plates, and the width of the waisted section is varied from 5 to 45mm, which produces an aspect ratio ranging from 0.2 to 1.8.

Experiments 3 and 4 are designed after the results from the first two experiments are investigated, which will be described fully in the result and discussion section.

Table 3-1, Set of Experiments carried out to investigate the effect of the waisted section

Experiment no	Specimens	Thickness (mm)	Width (mm)	Side plate	Welded	Flat
1	11	15	3 to 35	Yes	No	Yes
2	10	25	5 to 45	Yes	No	Yes
3	6	15	12.5 to 22.5	No	No	Yes
4	6	25	15 to 27.5	No	No	Yes

3.5 Results and discussion

For each specimen, the force-deformation curve is recorded, which total energy to break of the specimen per CSA calculated from force-deformation data. Before tensile testing, each specimen is measured accurately to know the exact CSA. This CSA is the initial CSA before the test takes place, and the CSA is not updated or calculated during deformation; therefore, the energy to break over the CSA is based on a constant value for the CSA.

Figure 3-4 shows the total energy per CSA against the width of the waisted section for experiment 1. As mentioned before, for these specimens, all the geometric parameters have been kept constant (same value as stated in BS EN 12814-7 standard), which means 20mm for loading hole diameter, 90mm for the distance between loading holes, 60mm for width of the specimen, 5mm for radius of the waisted section and 170mm for total length of the specimen. It is evident that, by increasing the width of the waisted section, the energy to break per CSA increases, except from 20mm to 25mm. From the overall result by comparing total energy to break against the width of the waisted section, it

could be concluded that more investigation regarding this type of comparison and measurement must take place.

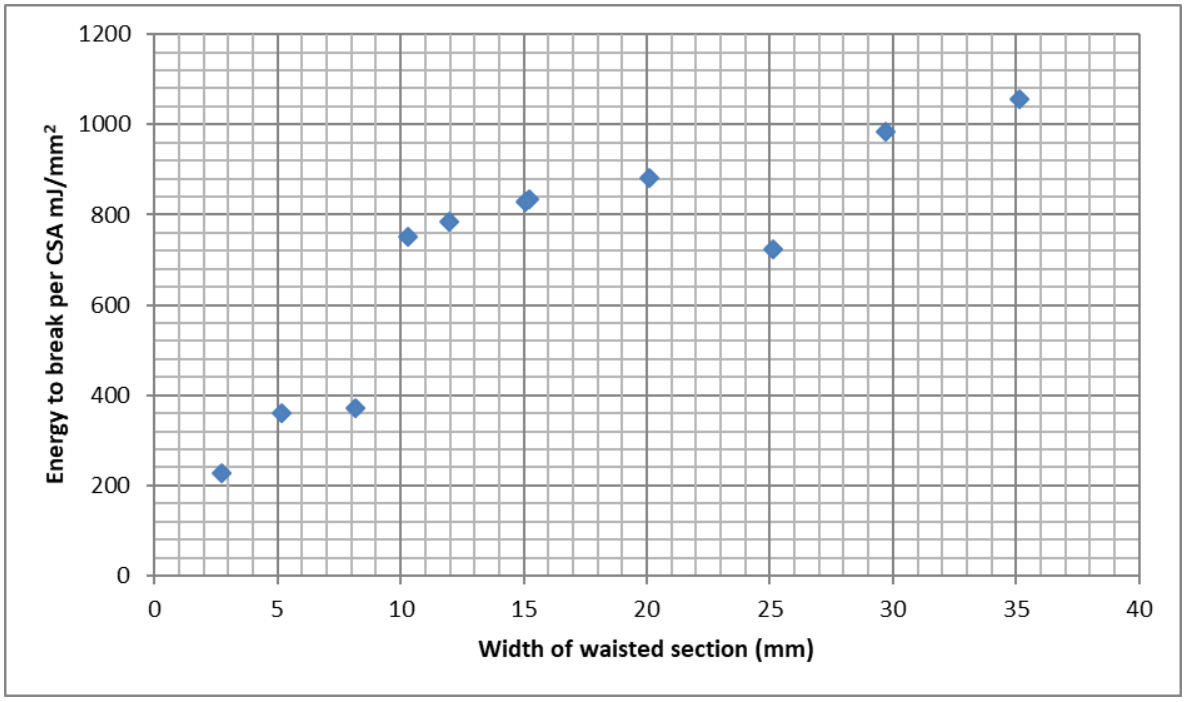

Figure 3-4, Graph shows the total energy to break value per CSA against the width of the waisted section for 15mm sheet thickness with side plates (Experiment 1)

Since the necking of the specimen is in the area of interest, the first step for in-depth investigation is to quantify the amount of total energy to break that has been consumed for the necking of the specimen. This is shown in Figure 3-5, where the force-displacement curve is divided into four different regions:

- Region one is from the beginning of the test till the beginning of necking.
- Region two is from the beginning of the necking to the start of the cold drawing, and this can also be called the neck formation region.
- Region three is mainly a cold drawing region.
- Region four is the tearing section.

The method used to distinguish these regions is that the differentiation of the data, which is energy per CSA, is taken, and on the step or the moment, the differentiation value reached zero (means a complete change in gradient of the curve) is assumed to be the moment where the different region in these fractures has started.

As shown in Figure 3-6, Regions 1, 2 and 3 indicate that when the width of the waisted section increases, the energy to break value per CSA also increases accordingly. Region three is the cold drawing region with the highest energy per CSA.

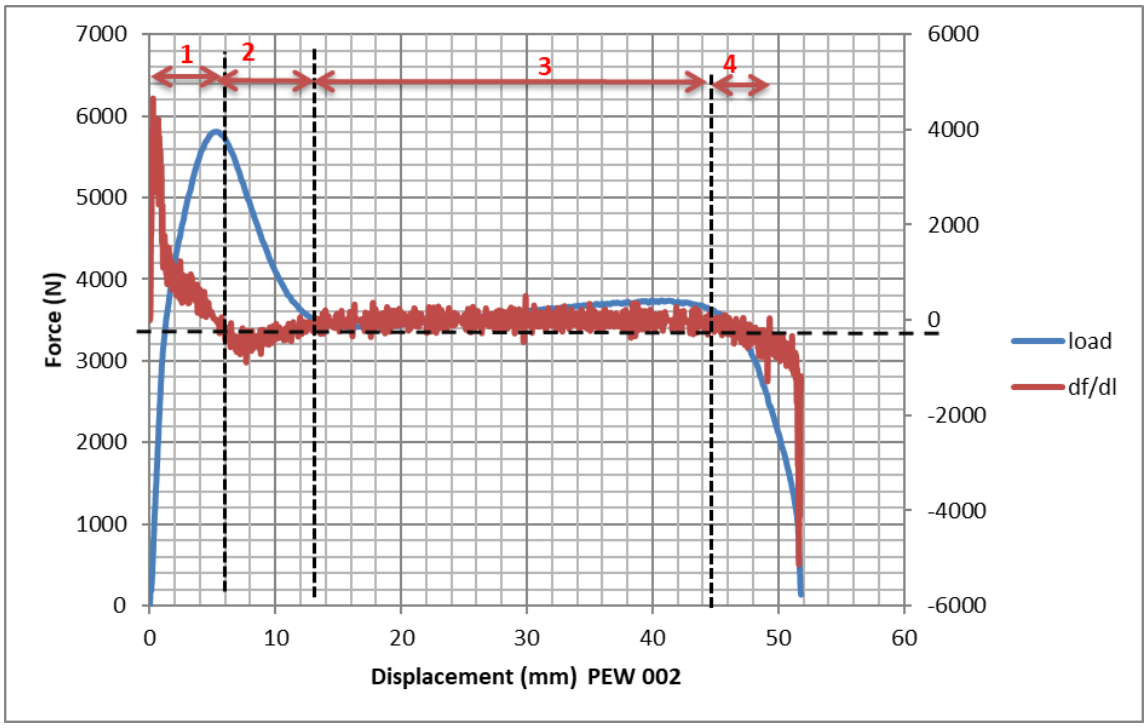

Figure 3-5, Graph shows the force-displacement curve for specimen no PEW02, divided into four regions

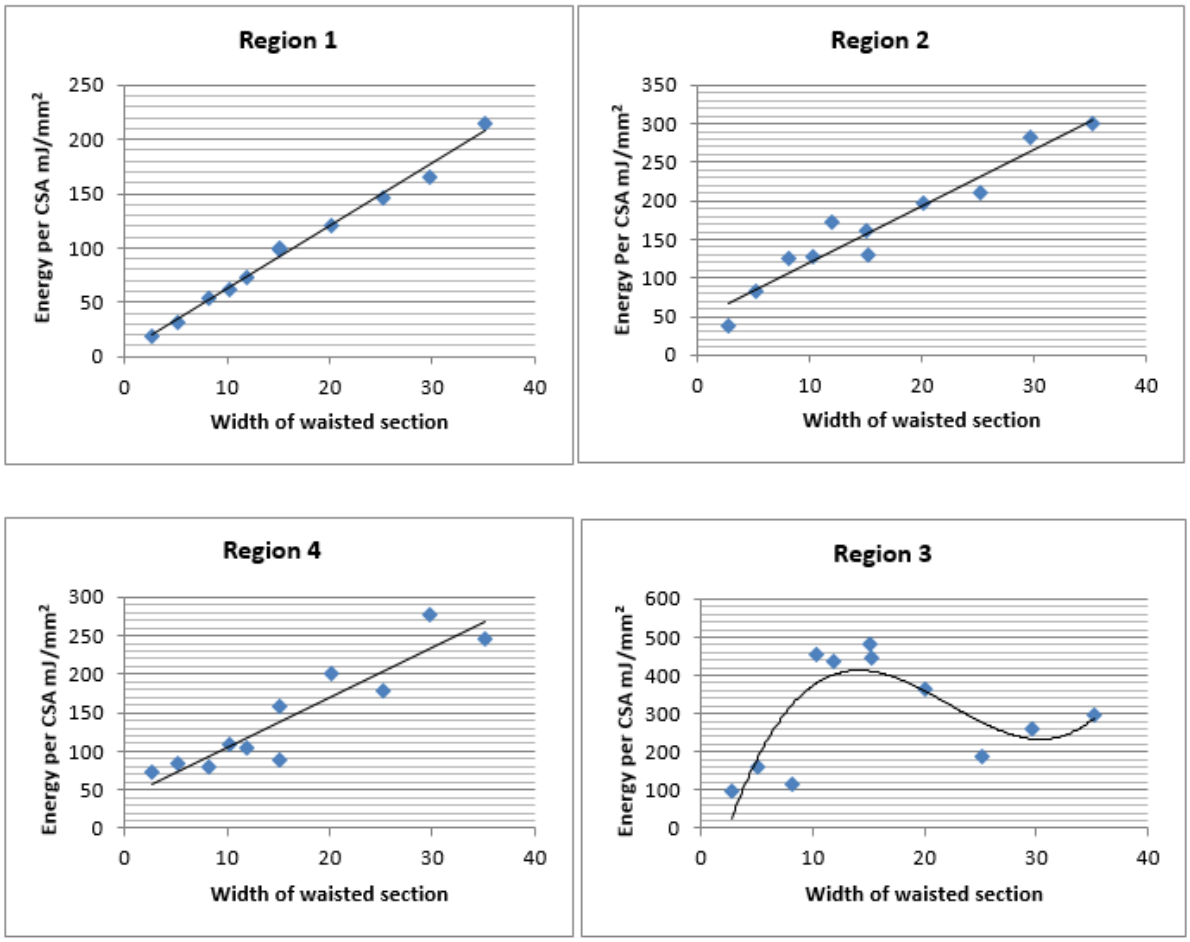

Figure 3-6, Energy to break values of different regions against the width of the waisted section for the first experiment

Experiment 2 is also designed to investigate the effect of the width of the waisted section. The specimen numbers with the dimension can be seen in Appendix A. By investigating the force-displacement curves Figure 3-7 it can be seen that region three is non-existent for this experiment. When the width of the waisted section just reached 25mm, Region 3 seems to be appearing again, which could be mainly due to two reasons. First is mainly because it is becoming closer to the thickness value (it would have a more uniform cross-section and reduces the triaxiality factor), the second reason is that the pin diameter is 20mm, and as the width is becoming larger than the loading hole

diameter, it causes more deformation throughout the specimen; therefore the specimen consumes more energy to break.

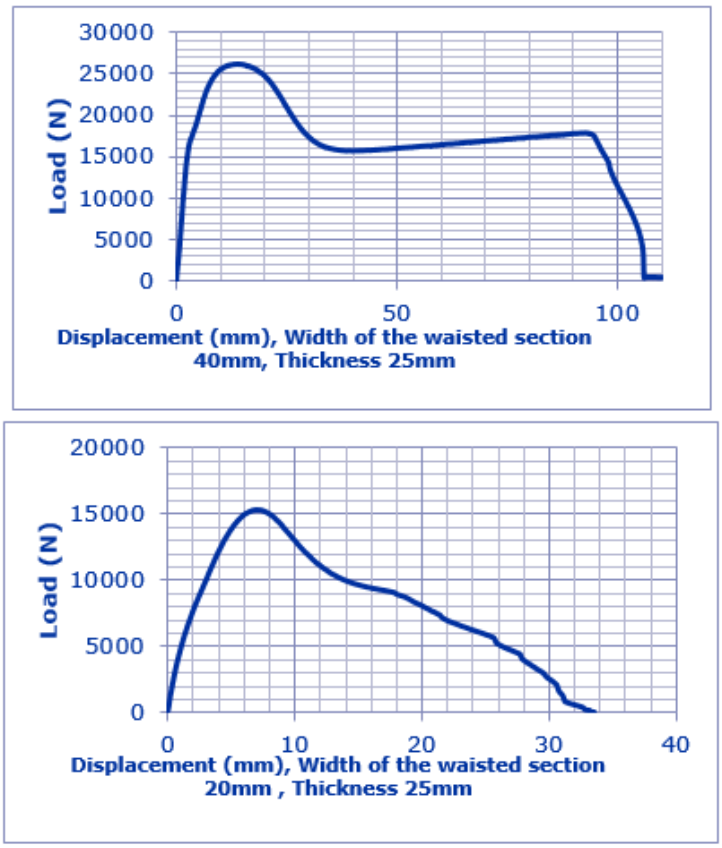

Figure 3-7, Load-displacement for 20mm and 40mm width of the waisted section

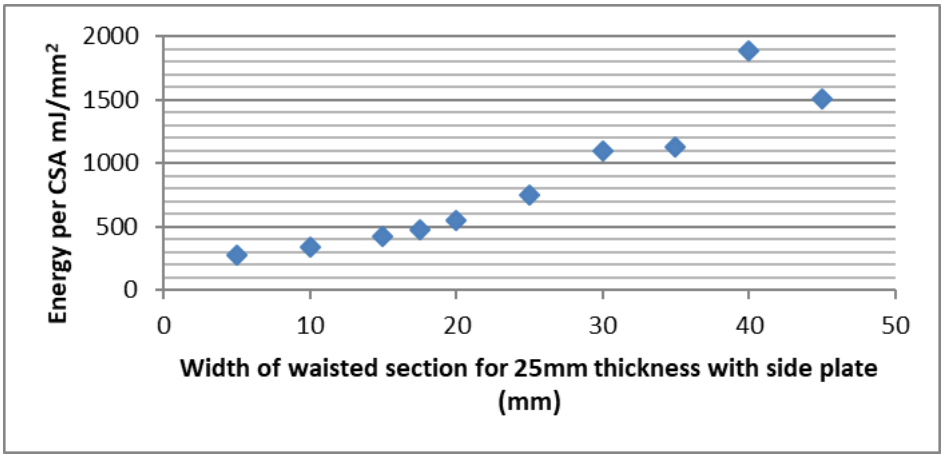

Figure 3-8, Total energy to break value per CSA against the width of the waisted section for 25mm sheet thickness with side plates (experiment 2)

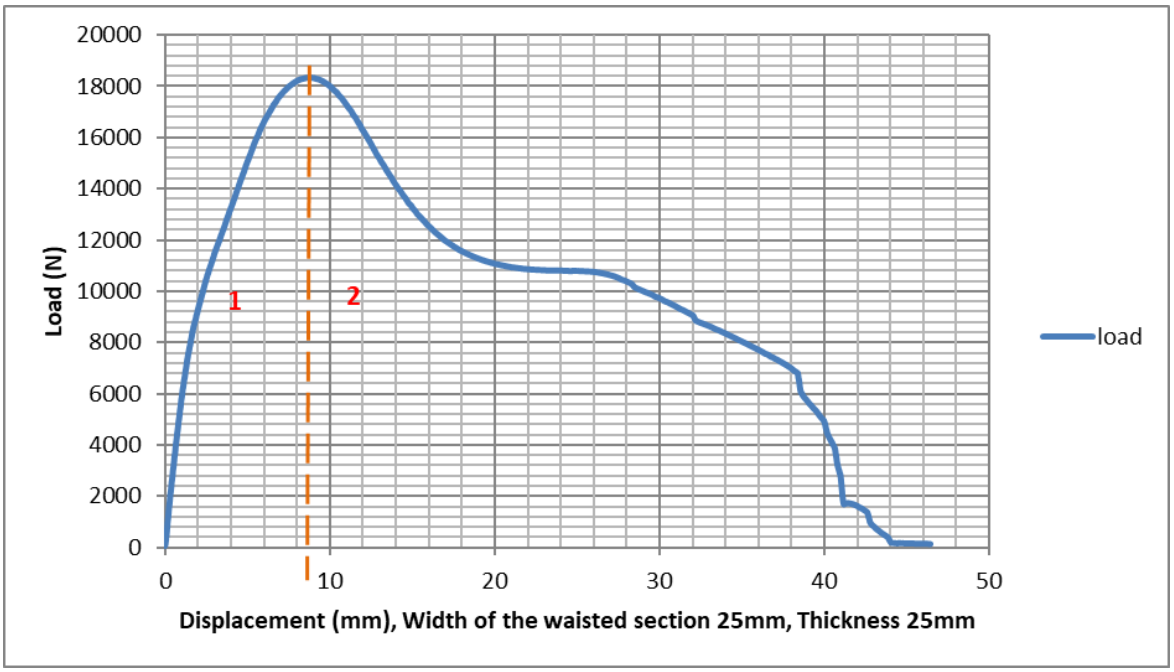

Figure 3-9, Force-displacement curve divided into two regions

As can be seen in Figure 3-8, by increasing the width of the waisted section, the energy per CSA also increases. One of the key reasons to have more considerable energy consumption is for having a width of waisted section larger than both thicknesses of the specimen as well loading hole diameter, which causes deformation throughout the whole specimen instead of extension in the waisted region, which

is our area of interest. To eliminate other factors (energy consumed to elongate the hole), the force-displacement graph is divided into two sections (Figure 3-9), and energy per CSA against the width of the specimen is displayed Figure 3-10. It can be concluded from both regions that increase in the width of the waisted section gives rise to an increase in the energy content of region one as well as the energy in after the yield section. This experiment could not be conclusive as most of the failures are not ductile, and if they are ductile, they failed due to void growth. The few specimens that failed in a ductile manner had substantial deformation in loading pin diameters which shows a significant error in the test result. This is also including the energy consumed for the deformation of the areas which are not in our area of interest (the waisted area).

Side plates are used to limit the deformation on the waisted area and eliminate deformation over the specimen as well as understand its effect on the failure behaviour. However, in standards used to quantify the quality of welds, specimens that are cut from welded pipes are tested without side plates. It is notable that using side plates can have some disadvantages not only from time and cost, which would require side plates for every pipe size but also as it fully limits the deformation of the specimen to the waisted region, it does not allow a uniform stress distribution in the waisted section. Due to the factors mentioned above, the next few experiments are designed without having side plates in the test.

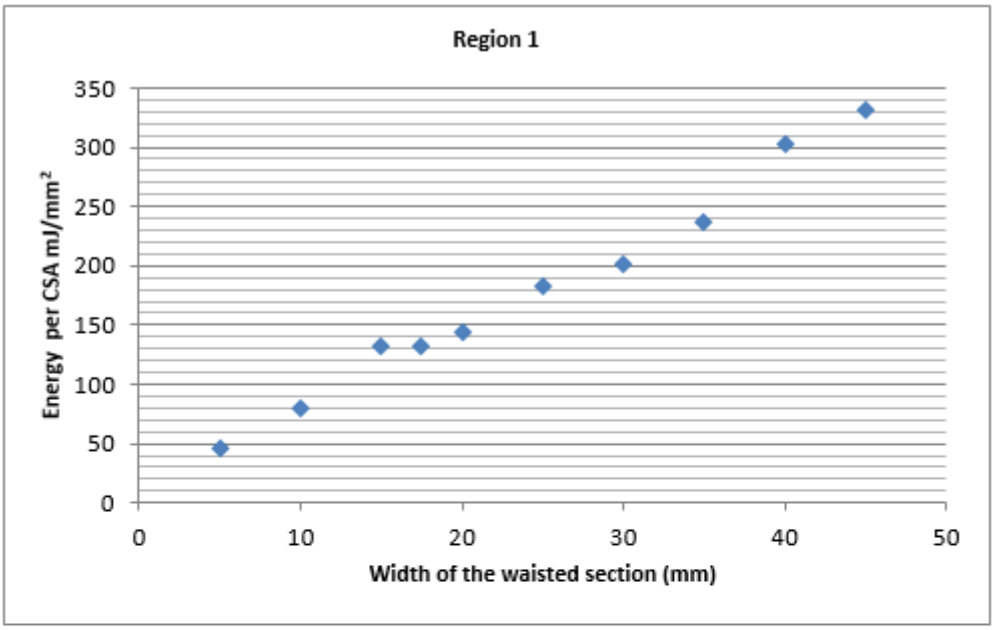

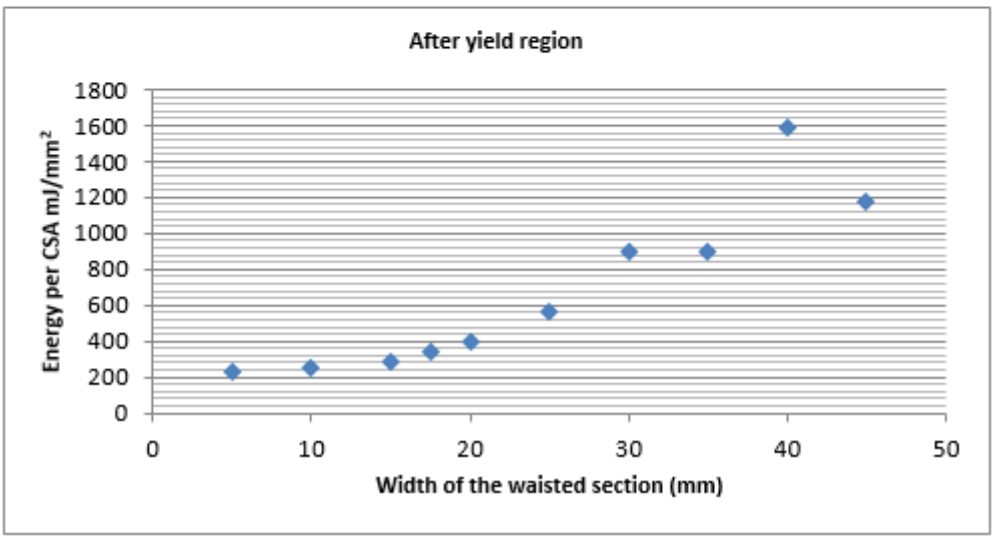

Figure 3-10, Total energy to break value per CSA against the width of the waisted section for 25mm sheet thickness with side plates (experiment 2)

Experiment 3 is on 15 mm HDPE sheet but without using side plates. The results from this experiment have been compared with the first experiment against energy consumption per CSA for each of the four mentioned regions. As can be seen in Figure 3-11, energy per cross-section area increased with an increase in width of the waisted section, which shows a similar trend for both experiments, which

are carried out with or without side plates. As described briefly earlier, the energy consumed in Region one is used to take the specimen up to the yield point. As the width of the waisted section increases, regardless of any other parameter, it would increase the energy consumed to yield the waisted region.

In the case of specimens without side plates, there has been higher energy used compared to the condition with the side plate on larger width of the waisted section. This is due to the ability of larger width, which has caused more deformation through the specimen compared to the condition with the side plate; the deformation is limited in the waisted area. As the distance between the centre of the specimen (waisted area) to the loading point is higher on the cases without side plates, more material (plastics) is used to transfer the loads to the waisted area. This transformation of the load, which is a larger area on specimens with no side plates would use energy to elongate and transfer the deformation, which would affect the energy consumed and explains why there is more consumed on the cases with no side plates. As the specimen with 25mm width was not following the trend, it was repeated, and therefore, two sets of data points are available 25mm width with side plates.

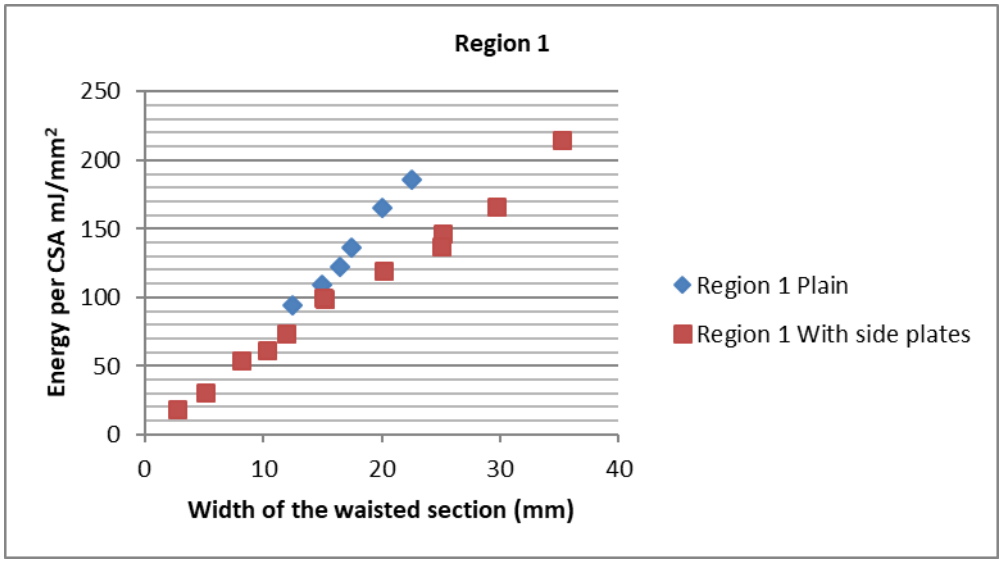

Figure 3-11, Energy per CSA against the width of the waisted section on 15mm thick specimen with and without side plates for Region 1

Energy used in Region 2 is an indication of energy used to bring the specimen from the necking or yield point to the start of cold drawing. The energy consumed in this part does not provide any discriminative information for experiments in both cases with or without side plates (Figure 3-12).

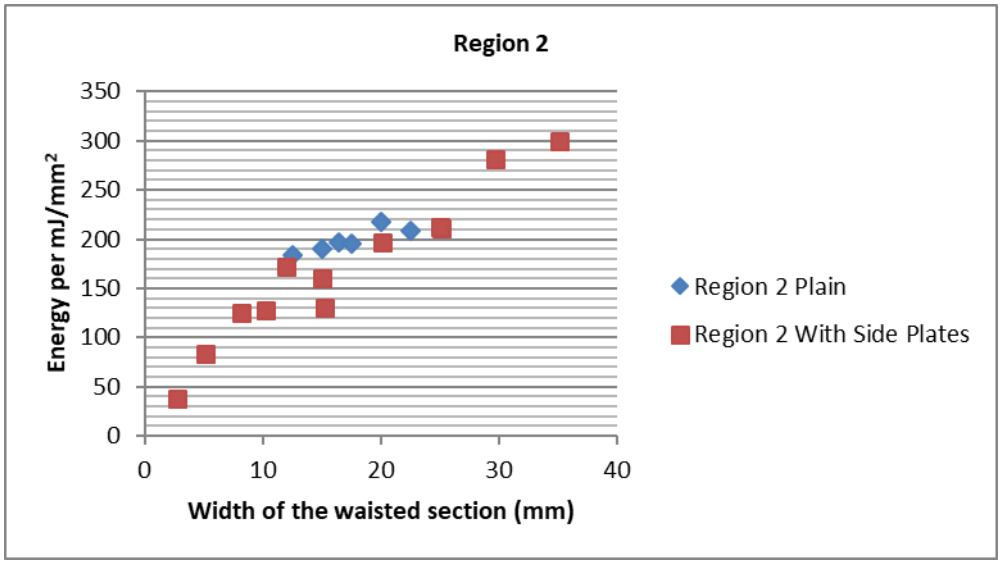

Figure 3-12, Energy per CSA against the width of the waisted section on 15mm thick specimen with and without side plates for Region 2

The comparison for Region 3 cold drawing and the main indication of ductility in a specimen provides useful discriminative information. The average total energy used for specimens without side plates is higher than the set of experiments using side plates. This is due to limiting the deformation in the surface area of the specimen except for the waisted area while using the side plates, therefore transferring all the strain rate directly to the waisted area. When the specimen is tested without side plates, there are deformations throughout the whole specimen. Also, the strain rates applied from loading holes are much lower in the middle of the specimen. This makes the tensile testing without side plates more reliable.

The other finding from this analysis is that in both cases (with and without side plates) when the width of the waisted section is equal to the thickness (both 15mm) the energy to break per CSA for Region

3 is maximised. One of the reasons is having a square CSA and therefore, more normal and axial stresses (Figure 3-13).

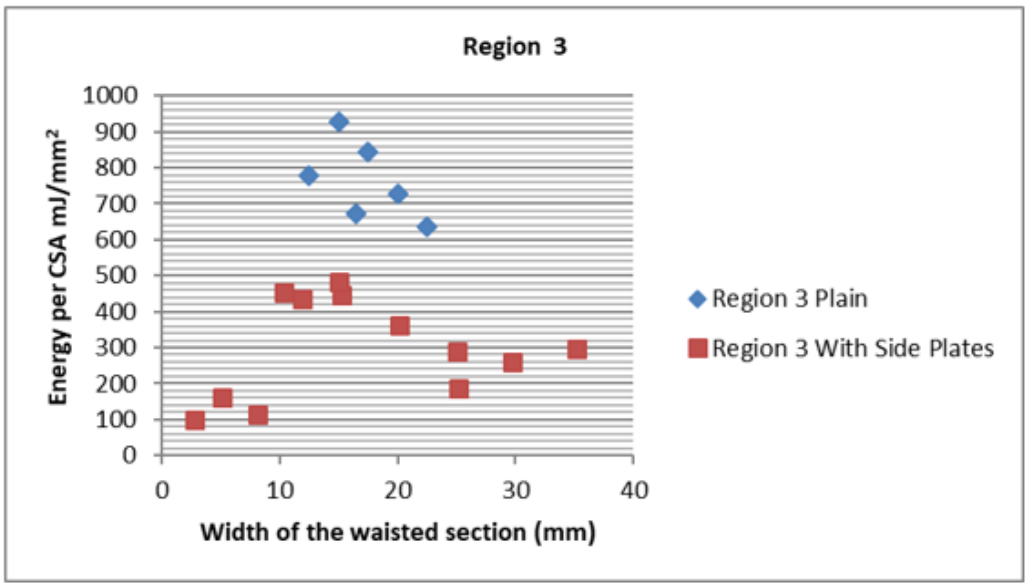

Figure 3-13, Energy per CSA against the width of the waisted section on 15mm thick specimen with and without side plates for Region 3

Region 4 did not provide useful information, as it is an indication of tearing, and it is the step after the cold drawing (Figure 3-14). To check and understand the effect of side plates on tensile tests, two specimens, one from each set of experiment is selected. Load-displacement data is shown in Figure 3-15. The geometry factor for both specimens is the same, and the width of the waisted section for the specimen is set to be 15mm. The behaviour of both specimens is similar throughout most of the test except in the necking section. The necking points are the same as well as the stress for necking the specimen. This comparison suggests that using side plates produces limitation to the test and decreases the ductility in the specimen.

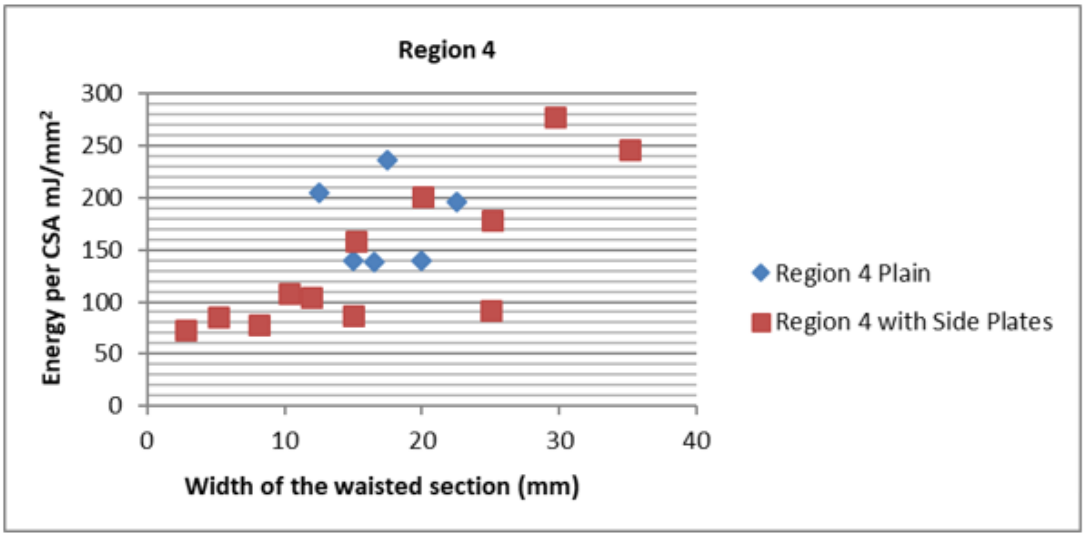

Figure 3-14, Energy per CSA against the width of the waisted section on 15mm thick specimen with and without side plates for Region 4

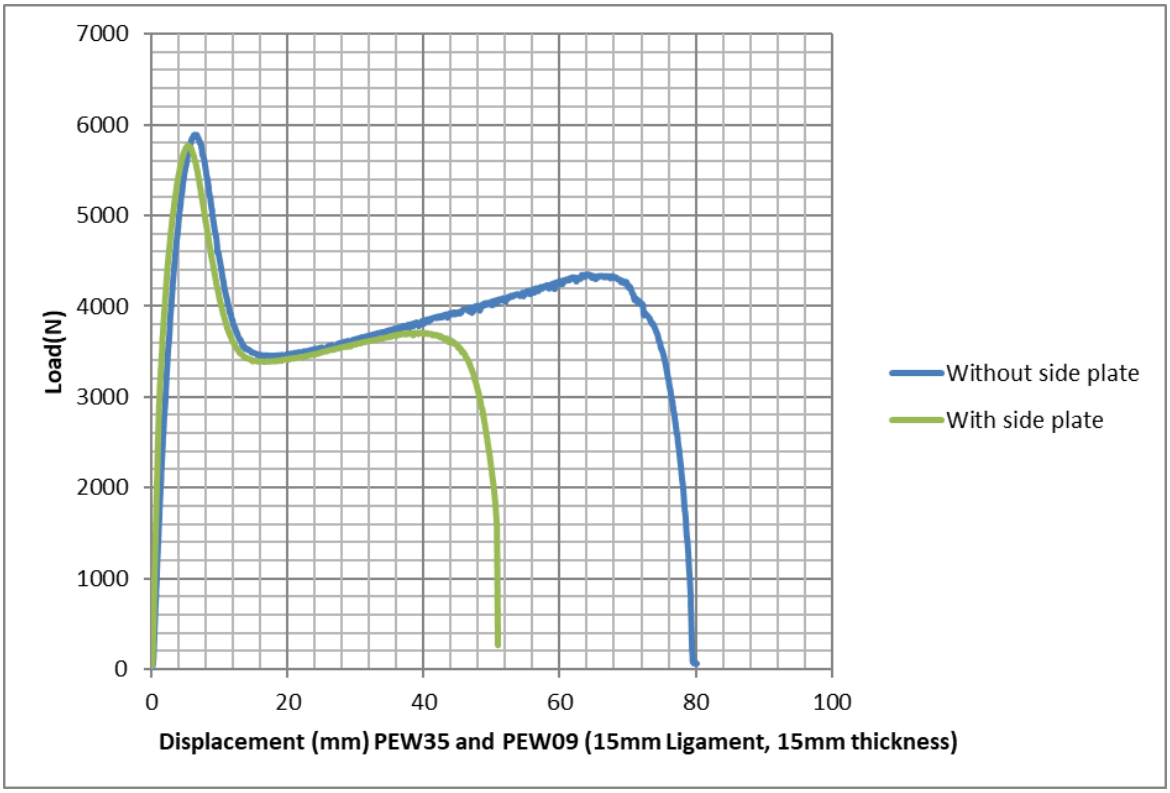

Figure 3-15, Load vs displacement for 15mm thick specimen with and without side plates

After understanding the effect of side plates and the width of the waisted section, the next experiment is carried out without side plates using specimens with 25mm thickness. The width of the waisted section for this set of experiment is varied from 15mm to 27.5 mm (Figure 3-16).

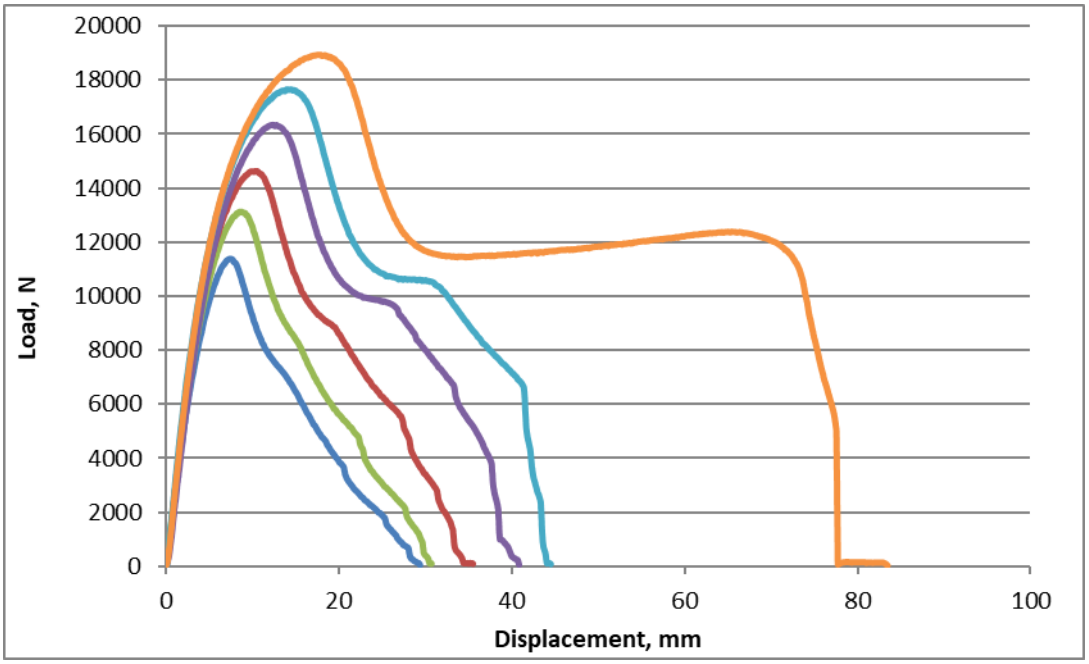

Figure 3-16, Load-Displacement curve for 25mm thickness with 15mm to 27.5mm in width of the waisted section (in order, from the smallest to largest graph, where 15mm is the smallest and 27.5 is the largest)

In this set of experiment, most of the specimens failed in a manner that no cold drawing occurred in most of the specimens. The only specimen where Region 3 (cold drawing region) appeared is the specimen with 27.5mm width of the waisted section. Since the thickness of the specimen is 25mm, large elongation in loading pinholes appeared during the tensile test. The fracture surface of a specimen from this experiment is the right specimen in Figure 5-25 which has a width of the waisted section of 27.5mm.

3.6 Summary

Experimental investigations carried out in this chapter resulted in useful information as to how the parent material fails using waisted specimen geometry, specifically 25mm thickness specimens. This shows the gap in the knowledge and confirms the need to solve this substantial industrial problem in assessing the quality of butt fusion welds.

Experiments were carried out on a non-welded, flat sheet of specimens without any particle (Carbon Black). Despite these simplifications, there was yet no possibility of ductile failure in specimens with 25mm thickness as they failed from void growth. This indicates the lack of appropriate procedure and an acceptable standard to quantify the quality of welds at this thickness or above.

The other conclusion is the effect of the side plates which reduces the ductility of the specimen. Also, the effect of the width of the waisted section has shown to be at maximum energy to break when it has an aspect ratio of one to the thickness. This finding is further investigated using FEA analysis to confirm this phenomenon.

It can also be hypothesised that, as the thickness of the material exceeds a specific value, the fracture behaviour of the specimen completely changes. This means, if any optimisation is carried out on these specimens, the first step is expected to involve making sure that all specimens fail in the same manner (ideally ductile with elongations) so that the effect of each parameter can be observed and recorded accordingly. This investigation is covered in the next chapter.

Chapter 4. Effect of different parameters of waisted tensile test specimen using DOE optimisation

4.1 Chapter Overview

This chapter investigates the geometry effect of the waisted tensile test specimen (Figure 4-1) on the energy to break value using CCD (Central Composite Design) optimisation technique. This technique which is one of the design of experiments (DOE) optimisation methods combined with response surface methodology, is explained in the literature section of this chapter and used in this chapter. CCD applied to understand the effect of geometry factors such as; width of the waisted section, the radius of the waisted section, loading hole diameter, distance between the loading holes and width of the specimen independently and dependently against different responses. Responses used in this study are;

- Total Energy to Break value of the specimen
- Energy consumed in the cold drawing stage
- Elongation of the loading hole

Justifications for selecting the named factors and responses are explained in depth in this chapter. Experimental methodology, as well as the findings in the forms of graphs and equations, are presented in this chapter. At the end of this chapter new optimised geometry with different dimensions for the thickness of 15mm is proposed.

4.2 Literature review

As mentioned in the overview section, to optimise the specimen geometry, the following parameters are investigated; width of the waisted section, the radius of the waisted section, loading holes, the distance between loading hole diameter and width of the specimen.

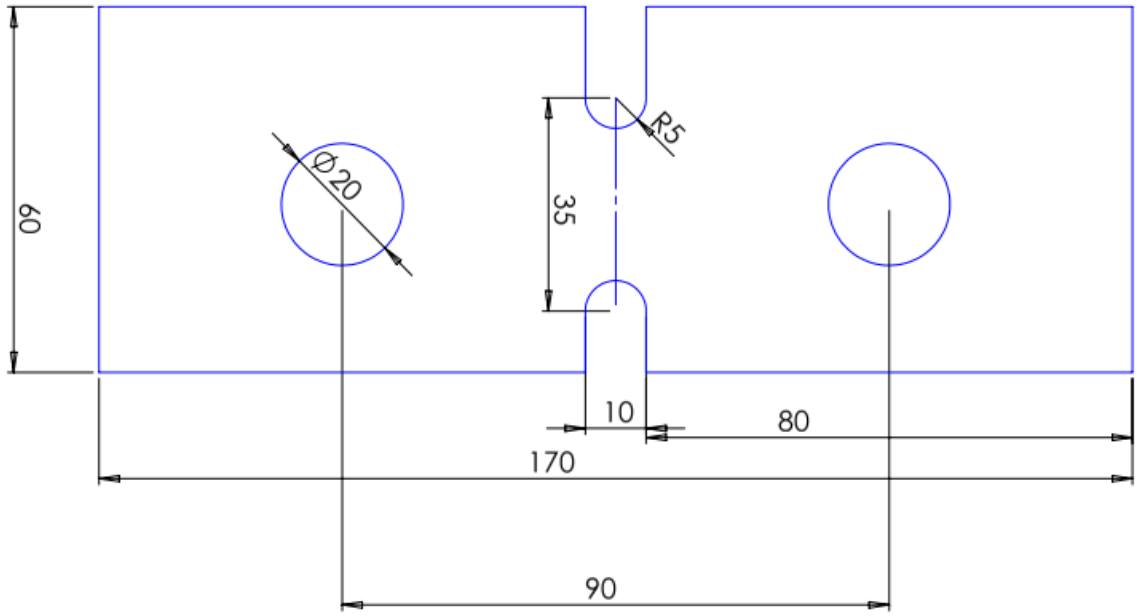

Figure 4-1, Waisted tensile test specimen (EN 12814-7) (dimensions in mm)

To investigate the effect of these parameters, a set of experiments had to be designed. Previously, experiments were carried out by changing one-factor at-a-time; however, this type of approach is expensive and time-consuming due to the many tests required. Another disadvantage of changing the factors one-at-a-time is that the factor interactions cannot be identified. Therefore, techniques that can provide better solutions with a lower number of experiments, such as the design of experiments (DOE), Artificial Neural Network (ANN) etc., are preferable [72, 73].

The design of experiments is a statistical technique that is used for multi factors system optimisation. As mentioned earlier design of experiments will be used to carry out a lower number of experiments rather than experimenting with every combination. Based on the number of factors and the number of experiments we can carry out, there are different optimisation types within DOE that could be selected to design the experiments. Central Composite Design (CCD) and Box-Behnken Design (BBD) are two common types where more than three factors are being optimised [74].

A review study carried out by Benyonis and Olabi [75] on different techniques of optimisation for mechanical properties of different welding techniques suggested that a response surface methodology (RSM) performs better than other techniques, especially when a large number of tests cannot be carried out. The main benefit of applying the RSM technique is its ability to indicate each factor's effect on different responses from coefficients in the regression model. This advantage can be used in identifying the insignificant factors main effect, insignificant interactions and insignificant quadratic terms in the model, which means that those factors can be removed, which helps in reducing the complexity of the model. The most popular methods within the RSM techniques are CCD and BBD. RSM technique generally is widely used in mathematics, and statistics is a known tool for modelling, which eases the process of optimisation when the effect of factors are interactions are required. This will also allow having a great estimate on a condition where the actual test has not taken place [76]. To be able to apply the RSM technique to optimisation, the factorial design of the experiment must include centre points in the experimental space plus edge centre points or face centre points. These multilevel experimental points allow fitting the responses to quadratic or cubic equations. CCD is one the best methods which would be suitable for RSM due to being a two-level factorial design with additional points to be outside the range of the factors, points between the axes (star points) and repeated points at the centre. Depends on the application where CCD is used, the start points at the face may extend, but in most cases, it is located on the plane with other coordinates. Below is the experimental space for a three-factor CCD [77, 78].

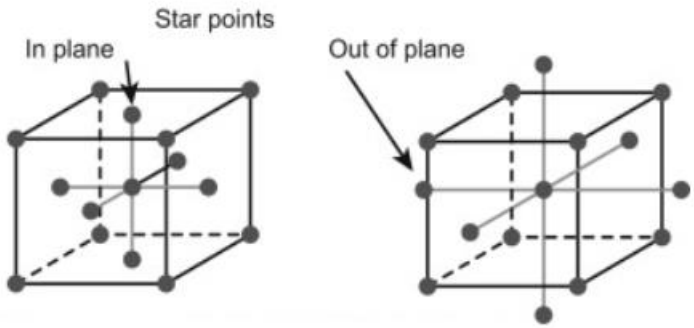

Figure 4-2, Central Composite Design (CCD) experimental space [77]

If optimisation is carried using any of DOE techniques, it can still be processed without RSM, but only the result of the carried out tests from the experiments could be seen, and the results for the interaction of factors would be unknown.

In summary, CCD, a method of DOE, is used just to design the experiment and RSM is used to analyse the data and the output of the experiment.

For this study, the CCD technique is applied to have the minimum number of runs and get the full information regarding the effect of each factor and factor interactions effect.

4.3 Experiment

4.3.1 The material, sample preparation, and testing

A commercial extruded HDPE sheet of 15mm supplied by Amari Plastics (UK) was used for this study. The tensile yield strength of the material is 22MPa with a modulus of elasticity of 900MPa. The specimens were prepared and machined using an Isel CNC machine and were conditioned for a minimum of 24 hours before performing the tensile test. The tensile tests were carried out according to EN12814-7 condition (not the geometry dimensions) with a speed rate of 5mm/min. The tensile

test machine used to carry out this experiment is a Hounsfield servo-electric tensile machine with a maximum tensile capacity of 50kN.

4.3.2 Design of experiment and characterisation

Design expert software (stat-ease) is used to design a 5-factorial CCD. As the objective of this study is to investigate the effect of each parameter in the geometry, the effect of specimen thickness is not investigated in this study because increasing thickness changes the failure mode from ductile to brittle, making the DOE invalid as it will not allow the specimen to fail in the same manner.

The initial test matrix consisted of 50 test specimens, and the limits of each parameter are based on the specimen dimensions given in the current standard. To set the limits for the width of the waisted section, 25 mm is set for the high limit, and 15 mm is set for the low limit. The high limit is the value given in BS EN 12814-7, and the low limit is selected as 15 as previous work carried by Wilson et al. [7] suggests that a ratio between the specimen thickness and the width of the waisted section of one to one produces the highest energy to break per unit area.

The low limit of the radius of the waisted section, 5mm, is therefore defined in BS EN 12814-7 since an increase in radius will reduce the stress concentration. The high limit of this parameter is selected as 10mm. The other three parameters' effect is not apparent, so the standard dimensions given in BS EN are set to be at the middle of the design. The table below shows the values and limits of the design.

Table 4-1, Variables used in the central composite design

Parameters	***Levels used***		
	Low (-1)	**Middle (0)**	**High (+1)**
The width of the waisted section, mm	15	20	25
The radius of the waisted section, mm	5	7.5	10
Loading hole diameter, mm	15	20	25
The distance between the loading hole, mm	80	90	100
The width of the specimen, mm	60	70	80

The different regions of a typical force-displacement graph for HDPE are shown in (Figure 4-3). Like any other optimisation design, the optimum solution is based on having an optimum response. The primary response and characterization used in this study is the total energy to break value per unit cross-sectioned area at the waisted section, i.e., the area under the force-displacement curve divided by the CSA of the waisted section. Indicating Region 3 is mainly an indication of energy being used for the cold drawing region. The cold drawing or necking region starts when the neck is fully developed and ends just before tearing (completed shear yielding) of the specimen.

The other response that is investigated is the Region 3 energy per unit CSA. The final response is the deformation in the loading holes. When the energy to break the specimen is calculated from the area under the curve of force vs displacement of the loading pins, any deformation of the loading pin holes introduces energy since the measured energy will consist of the energy to break the specimen as well as the energy to elongate the loading pin holes.

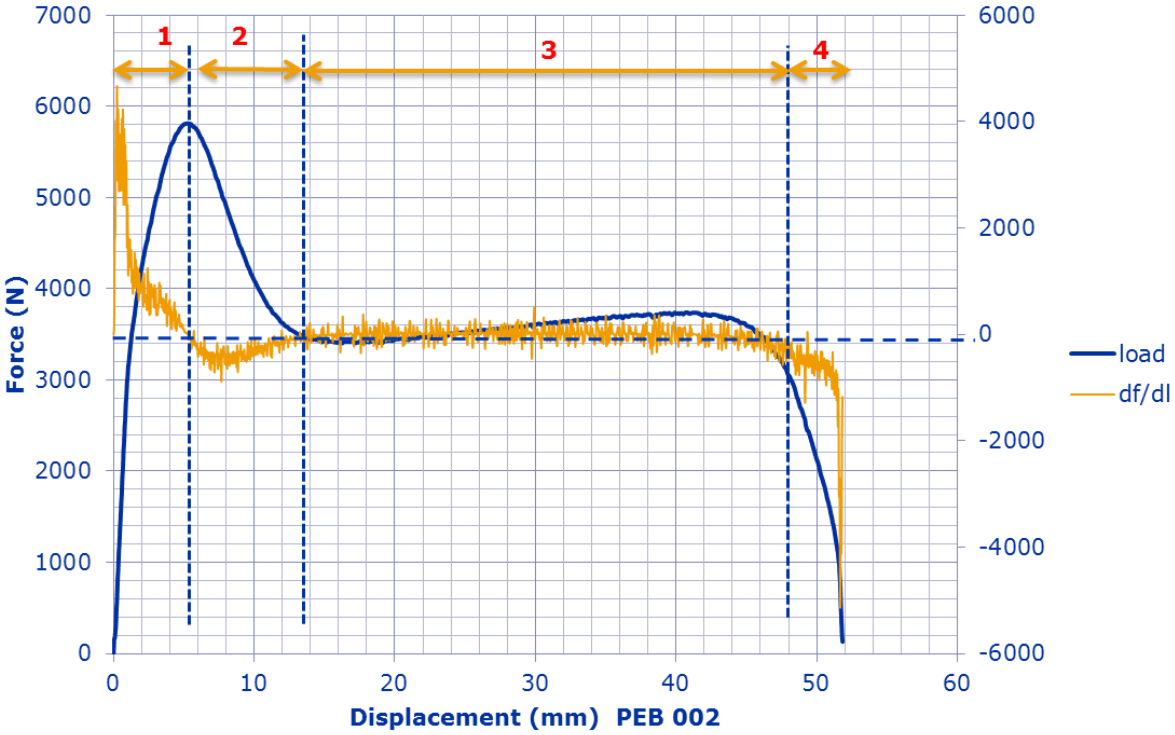

Figure 4-3, Example of a typical Force-Deformation graph

4.4 Results and Discussions

To understand the effect of each parameter on a particular response, a model is fitted for each response. All three responses are analysed statistically using analysis of variance (ANOVA) in order to determine the effect of the five specimen geometry parameters (width of the waisted section, the radius of the waisted section, the diameter of loading holes, the distance between loading holes and width of the specimen). Complete tensile tested specimens for this study are shown in Figure 4-4.

Figure 4-4, Tensile tested specimens for the DOE experiment

4.4.1 Optimisation of Total Energy Factor

Table 8-5 in the Appendix shows the results of the ANOVA analysis for the total energy to break value. The ANOVA table shows the sum of the squares (SS) and means square (MS) of each parameter where the P-value and F-ratio are defined as the ratio of respective mean square effect and the mean square error. To consider a constant, any confidence level can be used considering how vital the parameter is to the design, but for a 95% confidence level, an effect is called significant when the P-value is less than 0.05. By investigating the P-values in Table 8-5, the whole model, which consists of 18 terms, is a significant model with P-value of <0.0001. The three parameters that show the most significant are the width of the waisted section, the radius of the waisted section and distance between the loading holes with P-values of 0.0009, 0.0002 and 0.0043 respectively. The diameter of loading holes and width of the specimen which in order had P-values of 0.3466 and 0.3495 despite having a lower

significance but as they have about 65% confidence level, it is decided to consider them for analysis. As shown in Table 8-5 interaction effects of *AE*, *BD*, C^2 and A^2 also are also statistically significant.

To be able to model this optimisation for one response, an equation is produced by the stat ease software, which works based on principle curve fitting similar to finding an equation of a line used in excel. The line is the equation of the experiments carried out, and it must be as close to experimental values as possible. This line could be 1st order or curved of the 2nd order or 3rd order with some constants and coefficients as listed in equation 4-1 as an example. The target is to find this equation so we can discover the values of areas (factor combinations) where we did not carry out experiments, but they are interesting areas. To have a more accurate curve fitting technique or equation, the coefficient of combination of factors are checked, and they are used as constants in the equation, which represents how significant their effects are on the response. As mentioned, if these coefficients are large, then they will be used in the equation, and if they are small, it means the effect of the interaction for these factors are small, and they should be removed. As equations 4-1, 4-2, 4-3 are a multiple dimension equation, graphically, it is not possible to show the curve fitting image.

Before finalising the ANOVA table, many model types with a different number of terms are studied, but after investigating the significance of the terms and comparing the predictions with the actual values, this model, which is a modified quadratic model, is chosen. The total energy to break (per unit CSA) value can be calculated using the equation below.

$$Total\ Energy = 1678.75 + 41.80A + 402.33B + 45.34C + 151.01D + 5.04E - 108.98AE + 102.21BD + 62.99CD - 69.47\ A^2 - 235.98\ C^2 + 44.14\ D^2 - 51.05\ E^2$$ Equation 4-1

In Equations 4-1, 4-2 and 4-3, A stands for width of waisted section, B for radius of the waisted section, C for diameter of loading hole, D for distance between loading holes and E for width of the specimen.

Equation 4-1 includes a large number of terms. Some terms with low coefficient could be removed from the equation, but then it would reduce the model's accuracy. A graph to analyse the model's adequacy by showing the relationship between the actual and predicted values of total energy to break is shown in Figure 4-5. Figure 4-5 is produced to show the quality of the fitting process. The points (each point is a combination of factors) near the diagonal line indicate a better model as they have a value closer to the actual value, therefore if a combination is selected with conditions close to these points, there would be more confident in the accuracy of the results.

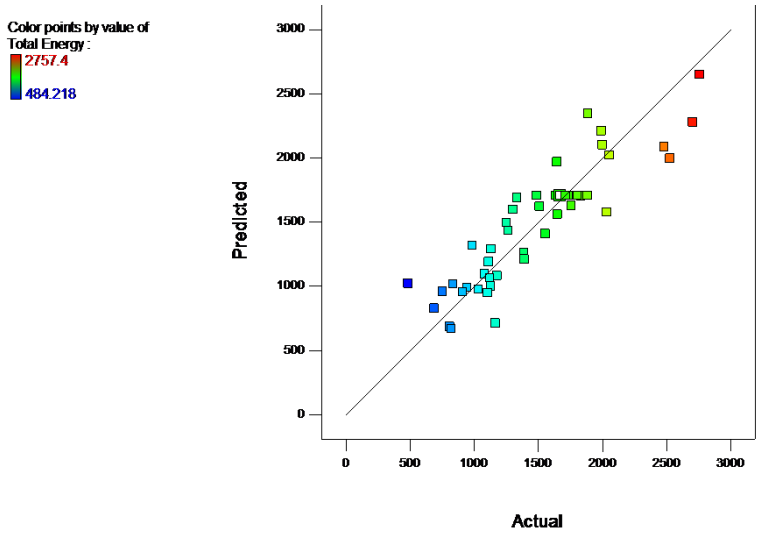

Figure 4-5, Total energy to break values per unit CSA

This figure indicates that the overall developed model is adequate. This is because residuals of many terms in predictions of each response are minimal since the residuals tend to be close to the diagonal line. The main effects and surface plots are generated to represent the results of the polynomial model analysis. The main effects of each parameter on the total energy to break value response is presented in Figure 4-6. This figure is a direct output of the software.

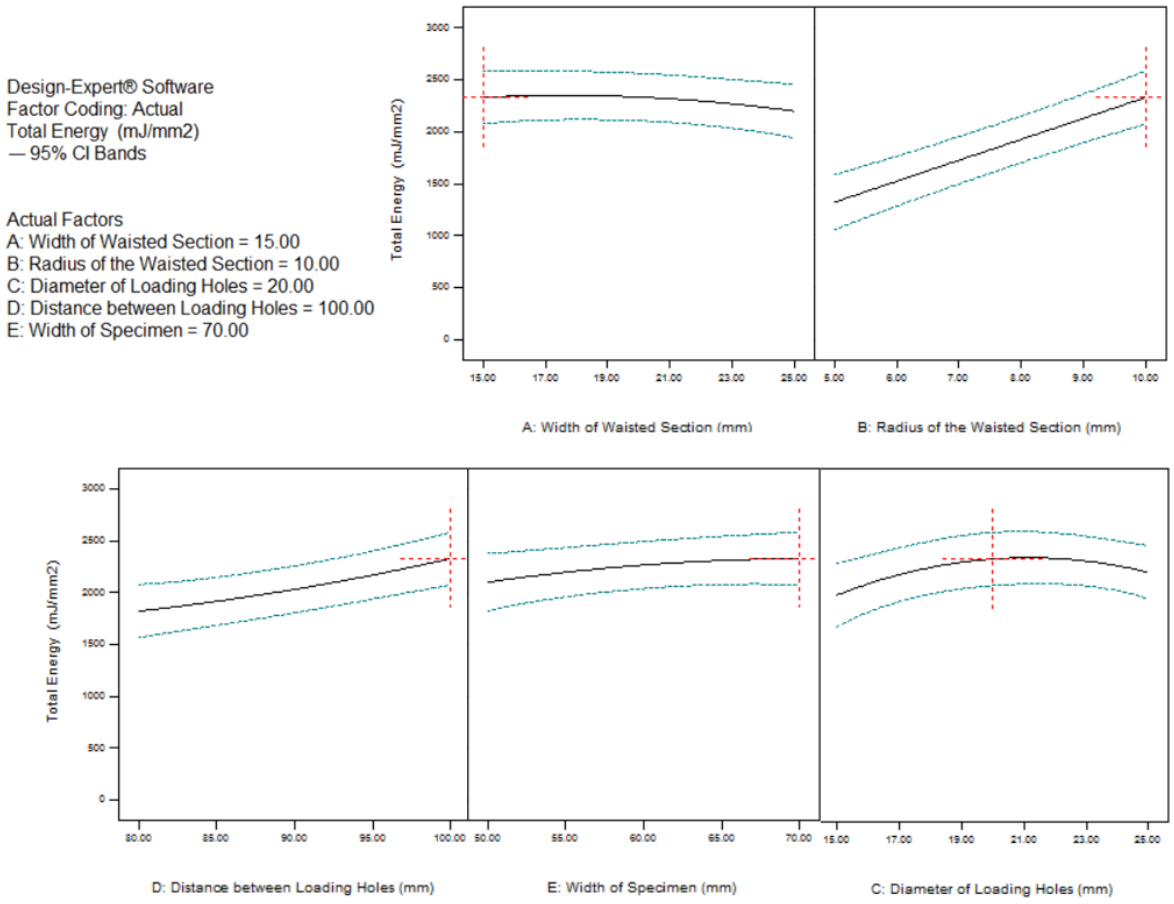

Figure 4-6, Main effect plot for total energy to break per unit CSA value for specific terms

There are two facts to be considered when investigating graphs in Figure 4-6. The first fact is understanding the graph indicates the main effects, which show the deviation of the average between high and low levels for each parameter. The second important fact is that the effect of each parameter on a specific graph is only valid for the stated value of the other factor; these factors interact with each other, and when investigating one of the parameters, the other four parameters are kept constant. If these constants changes, these factors would have a different effect on the total energy to break per CSA value.

From Figure 4-6, it can be seen that increasing the width of the specimen, the distance between the loading holes and the radius of the waisted section increases the total energy to break values. There

are several reasons for this increase. Increasing the distance between the loading holes or width of the specimen increases the volume of material between the loading pin holes, which causes more loads to be allowed due to the larger amount of material, which leads to higher total energy to break values. The increase in distance between loading holes and the radius of the waisted section also causes the stress distribution to be more uniform in the waisted section, which will help the specimen to have a longer necking stage.

Increasing the radius of the waisted section will also reduce the stress concentration in the waisted section. Despite calculating the energy to break values based on CSA to eliminate the effect of the volume of material in the waisted section, but the effects still can easily be seen due to the behaviour and characteristics of the material. This can also be explained with the mechanism polymers handle the load, which to transfer load on each particle, the material could undergo elastic and hyper-elastic deformation before transforming the load.

The increase in diameter of the loading hole leads to a decrease in total energy to break value in the specimen. This could be because of the larger contact surface of the loading pin to the specimen hole's which causes a more significant stress distribution around the pin and the specimen. The optimum value for the width of the waisted section is around 17mm, which then reduces when the width of the waisted is increased.

4.4.2 Optimisation of Region 3 Energy Factor

Table 8-6 shows the results of the ANOVA analysis for the Region 3 of the force-displacement curve as indicated in Figure 4-3. From the P-value in Table 8-6, it can be seen that the width of the waisted section, the radius of the waisted section and the distance between the loading holes and their interactions are statistically significant. The diameter of the loading hole and width of the specimen have large P-values, but they have been included in the analyses because they are two of the main

parameters in the analysis and some of their interactions with other parameters are also statistically significant. After considering the significance of the parameters and analysing the predicted vs actual values, the model in coded units is found. The total Region 3 energy to break value based on coded levels can be calculated using Equation 4-2.

$$Region\ 3\ Energy = +1166.83 - 42.73A\ + 390.03B\ + 76.69C\ + 144.69D + 32.12E\ - 88.11AE\ + 123.18BD\ - 49.12A^2 - 257.90C^2\ + 41.13D^2\ - 73.52E^2$$

Equation 4-2

From the coefficients of The total Region 3 energy to break value based on coded levels can be calculated using Equation 4-2, the distance between the loading holes has the most significant effects on the Region 3 energy, followed by the radius of the waisted section and width of the waisted section. Figure 4-7, shows the plot of actual versus predicted values for Region 3 energy per unit area. It shows the adequacy of the model is certain small points and there few points with low Region 3 energy and very high Region 3 energy which have large adequacy.

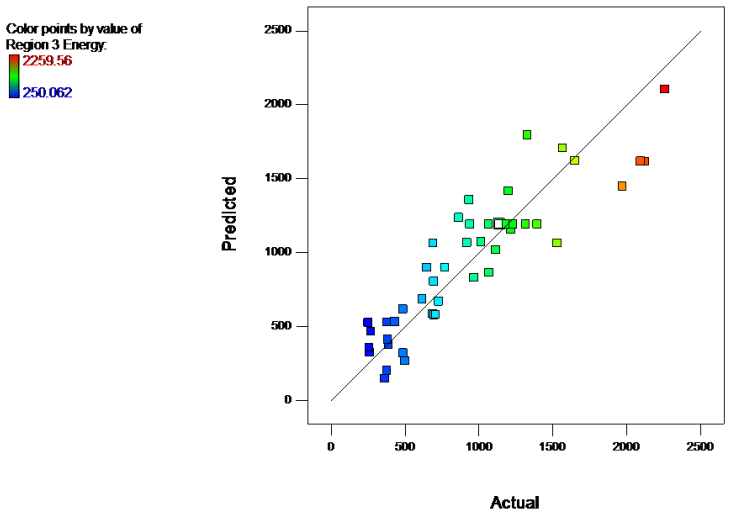

Figure 4-7, Region 3 energy to break values per unit CSA

The main effects of each parameter on the Region 3 energy are shown in Figure 4-8, which shows the increase in the radius of waisted section and distance between the loading holes increases the Region 3 energy. Figure 4-8 also shows that the width of the waisted section increases the Region 3 energy when it is in the range of 15 to 17mm. Other two parameters, which are the width of the specimen and diameter of the loading holes, do not seem to have much effect on Region 3 energy.

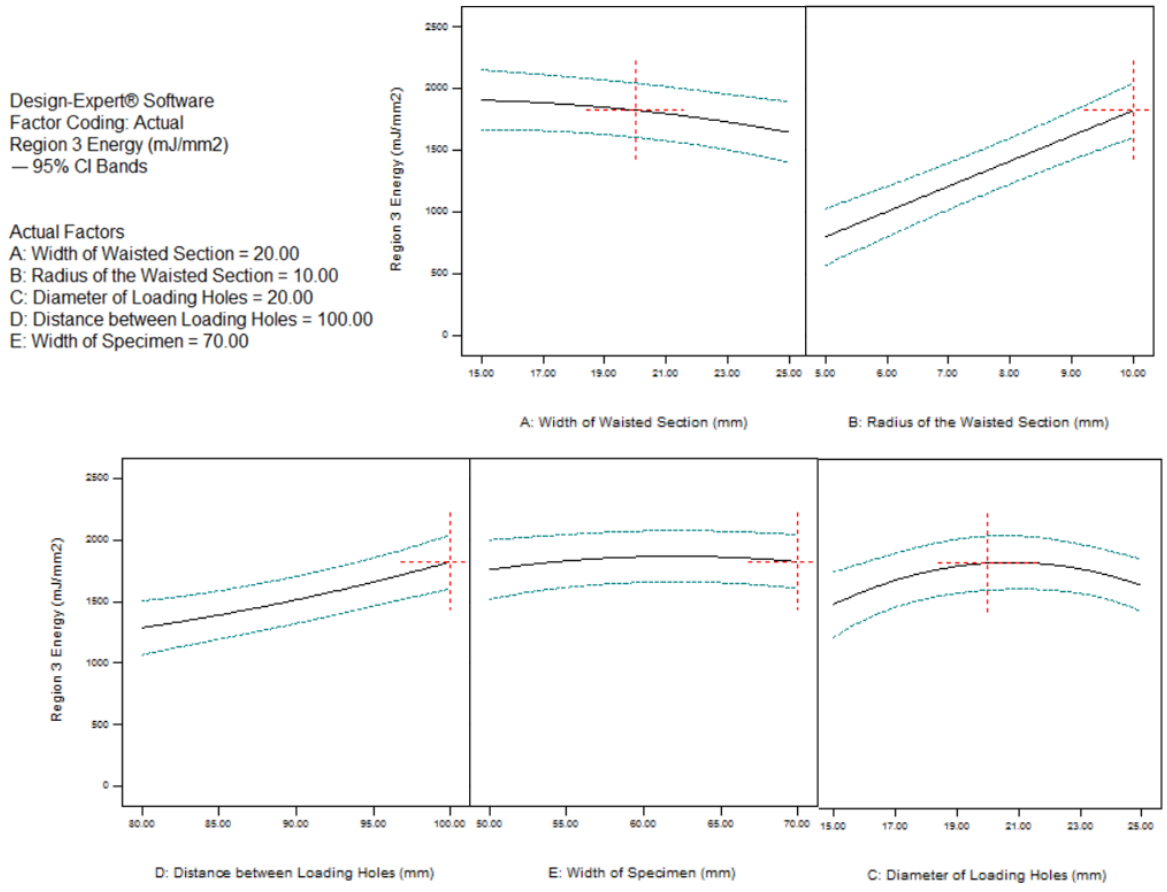

Figure 4-8, Main effect plot for Region 3 energy

When performing the tensile test on the standard geometry of waisted tensile test geometry, the deformation applied to the specimen does not always fully deforms the waisted section but deforms the loading hole pin and the materials between the loading holes as well as the waisted section. As the weld line is in the waisted section and energy used to deformed the specimen is the indication of the quality of the weld; therefore, it is important to have most of the deformation in the waisted

section. One way to make sure the deformation has taken place in the waisted section is to check the elongation in the loading pin diameter. For example, if the loading hole diameter is 20mm before performing the tensile test, and the loading hole diameter after the specimen's failure is 20.2 mm, the loading hole has gone through more considerable deformation. After recovering the elastic deformations, the permanent plastic deformation in the hole is about 0.2mm. The permanent elongation in the loading pinhole has been taken as one of the minimise responses for this analysis.

4.4.3 Optimisation for Loading Pin Holes Factor

The ANOVA analysis results for elongation in the loading pinhole is shown in Table 8-7.

As can be seen from P-value in Table 8-7, the width of the waisted section and the width of the specimen are statically significant. The distance between the loading hole and the radius of the listed section does not seem to have any effect; therefore, they have not been included in the ANOVA table. The obtained model is coded units are presented in Equation 4-3 as;

$$Deformation\ at\ loading\ pin\ hole\ (mm) = +0.38 + 0.30A - 4.709E - 003B - 0.063C - 0.051D - 0.098E$$ Equation 4-3

From the coefficients in Equation 4-3, it can be seen that two parameters are missing due to their low effect and the diameter of loading holes have a slightly lower coefficient compared to the width of the waisted section and width of the specimen. Figure 4-9 shows the plot of actual versus predicted values for the elongation in the loading pinhole. As a linear model is fitted for this analysis, the difference between the predicted and actual values are not perfectly aligned due to the simple modelling of this response. The line is fitted as an estimate to have an equation to predict the actual values using the stat ease software. This is similar to excel when a line (with equation) is fitted to a graph, and it can become more accurate by increasing the order of the equation.

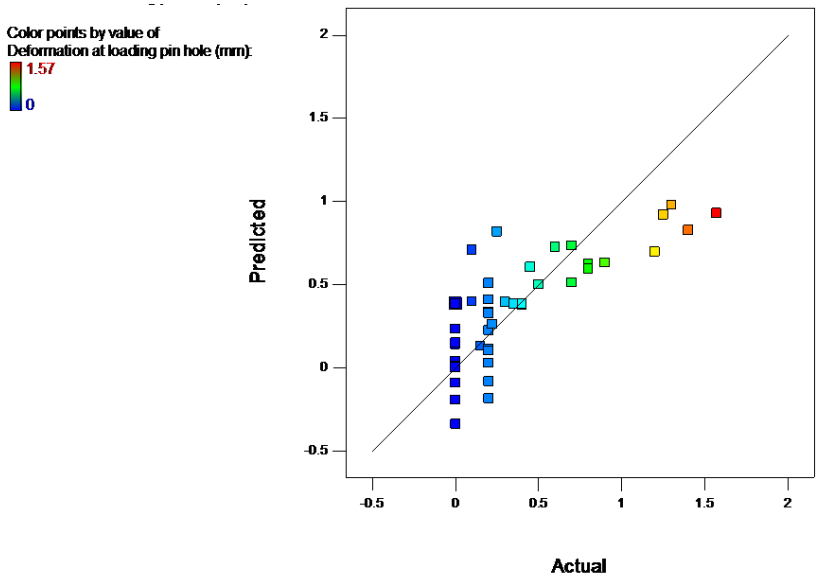

Figure 4-9, Elongation in the loading pinhole

The main effect of each parameter on the elongation in the loading pinhole is shown in Figure 4-10. From Figure 4-10, the increase in width of the waisted section leads to an increase in deformation at the loading pinhole. This is mainly due to increasing the cross-sectional area of the waisted section, which is also the area of interest to perform the necking. By increasing the cross-sectional area, the force to neck that region is increased, which would require the whole specimen to undergo a more considerable amount of force that leads to elongation in the loading pinhole. Increasing the diameter of the loading hole leads to a decrease in deformation at the loading pinhole. This could mainly be due to the increase in the top surface area of the loading pin, which helps to transfer the load required to neck the material to more regions of the specimen without elongating the hole. The increase in the total width of the specimen also leads to a decrease in deformation at a loading pinhole. This could be due to the increase in the material on the sides of the loading pin hole, which reduces deformation on regions around the loading hole by holding the materials together.

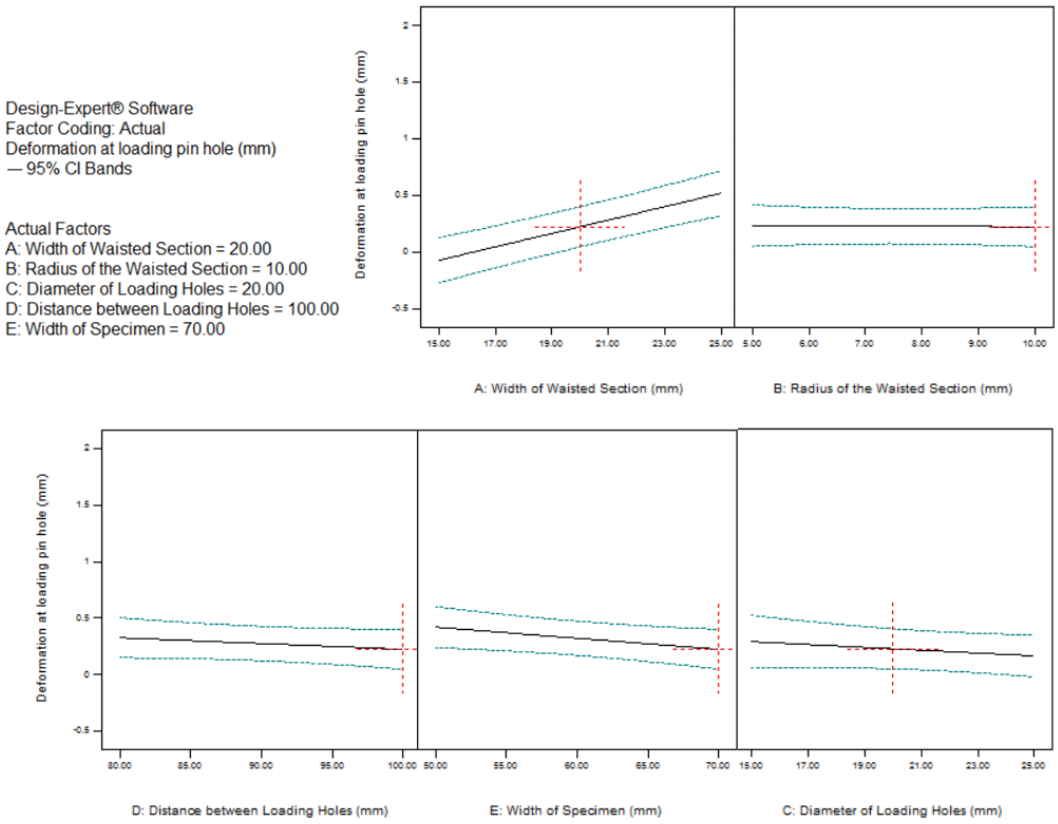

Figure 4-10, Main effect plot for elongation in the loading pinhole.

4.5 Maximisation and minimisation of the responses

For this optimisation study, three energy responses are required to get maximised simultaneously, and one response which is the deformation in the loading pinhole is required to get minimised. One of the methods to solve multiple response optimisation problems is to use the desirability function which is a useful approach to cut the dimensionality of a simultaneous optimisation problem to just one. In this technique, each response equation is first transformed to an individual desirability function (d) that varies over the range $0 \leq d \leq 1$. Based on the need of the response there are, three forms of a desirability function can be set to which are [79] :

- Larger better (LB) – for an object function of the response to be maximum;

- Smaller better (SB) – for an object function of the response to be minimized;
- and nominal better (NB) – for an object function of the response to attaining a specific goal.

In this study, three responses desirability function is the larger better (LB), and one response which is the elongation in the loading hole is the smaller better (SB). The desirability function LB can be written in an overall form shown in;

$$d = \begin{cases} 0 & y < L \\ (\frac{Y-L}{T-L})^r & L \leq y \leq T \\ 1 & y > T \end{cases}$$

Equation 4-4

Where y can be called as the response, L would be the lower limit of the response, T is the target of the response, and r is the weight factor. The desirability function of the smaller better (SB) where U would be the upper limit and the function can also be written as in the form of [79];

$$d = \begin{cases} 0 & y > U \\ (\frac{Y-L}{T-L})^r & U \geq y \geq T \\ 1 & y < T \end{cases}$$

Equation 4-5

In this study, the desirability (d) for each response is a unity that makes the composite desirability (D) also unity. The composite desirability function (D) used in this study can be calculated as Equation 4-6.

$$D = \sqrt[3]{d1(Total\ Energy(X)) \times d2(Region\ 3\ Energy(X)) \times d3(Elongation\ in\ the\ pin(X))}$$

Equation 4-6

In the equation above, as mentioned before, D is the composite desirability function, X is the vector of the designed variables (coded values), d_1 is the individual desirability function corresponding to the first response (i.e., total energy), d_2 is the individual desirability function corresponding to the second response (i.e., energy in Region 3) and d_3 is the individual desirability function corresponding to the

third response. The desirability of all response and composite desirability have all been calculated using STATE EASE software with the weight factor of r = 0.5. The result of the total desirability function analysis is given in Figure 4-11. From Figure 4-11, it can also be seen that the desirability changes by varying the value of the parameters. The least desired are shown by gree, and most desired are shown by the orange, the colouring in between is the transition.

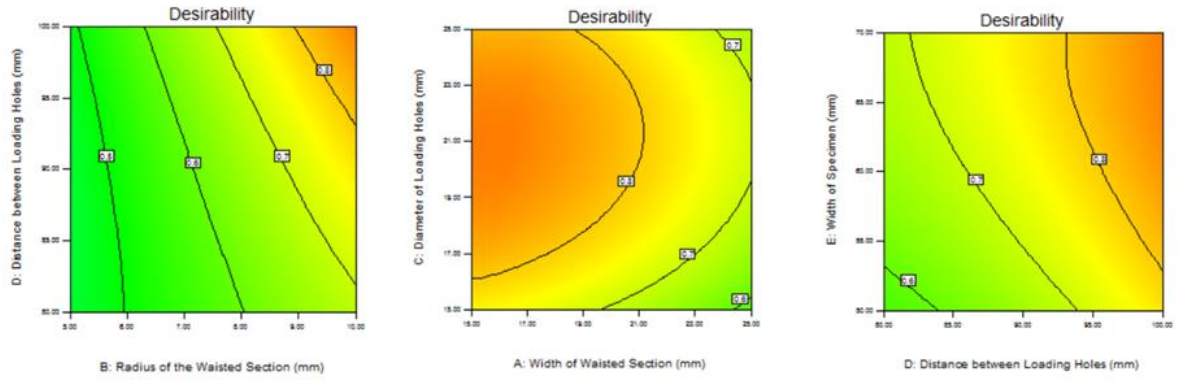

Figure 4-11, Desirability and parameters

The optimum solution suggested by the model had a combined desirability of 0.87 and individual desirability of 0.822 for total energy, 0.825 for Region 3 energy and 1 for loading pinhole response. The optimum solution, which considers all the responses, suggested 16mm in width of the waisted section, 10mm for the radius of the waisted section, 20.8mm for the diameter of loading holes, 100mm for the distance between the loading holes and 68mm for the width of the waisted section. To select the optimum geometry, these values have been rounded for ease of machining and have been tested against BS-EN 12814-7 standard geometry, and the results can be seen in the figure below.

Table 4-2, Optimisation results for predicted vs actual values

Parameters	12814-7 Geometry	Improved Geometry
The width of Waisted Section (mm)	25	15
The radius of Waisted Section (mm)	5	10
The diameter of Loading Hole (mm)	20	20
Distance Between Loading Hole (mm)	90	100
Width of Specimen (mm)	60	70
Predicted/Actual Total Energy (mJ/mm^2)	1250/1252	2330/2145
Predicted/Actual Region 3 Energy (mJ/mm^2)	688/666	1906/1800
Predicted/Actual Elongation in Pin Hole (mJ/mm^2)	0.67/0.6	0/0

In Table 4-2, parameter values for standard and improved geometries are shown. In addition to parameters dimensions, predicted versus the actual values for three responses have been shown in Table 4-2. The primary response, which is the total energy, has been improved from 1250 mJ/mm^2 to 2140$mJ/mm^{2,}$ which is around 70% improvement. The Region 3 response, which is the cold drawing region, had around 170% improve which shows a significant improvement. The elongation in the pin has been reduced to 0, which is ideal and could not be improved in a better way.

4.6 Conclusion

The result of the ANOVA for total energy response and Region 3 response analysis shows that the radius of the waisted section and distance between the loading holes were two of the most influenced parameters which had the lowest P value. Despite some parameters such as the width of the waisted

section and width of the specimen, had larger P values in the first two responses (total energy and Region 3), but these two parameters were two of the most influential in the elongation in the loading pin response. The increase of parameters such as the width of the specimen, the distance between loading holes and the radius of the waisted section has led to improving the total energy and Region 3 energy responses. Based on desirability function, the best combination for waisted geometry on total energy, Region 3, and elongation in the pin response is 15mm for the width of the waisted section, 70mm for the width of the specimen, 10mm for the radius of the waisted section, 20mm for the diameter of the loading holes, and 100mm for the distance between the loading holes. Finally, all the responses have been improved significantly with 70% of total energy, 170% for Region 3 energy and zero elongation in loading pinholes and this trend can be used for larger thickness specimen.

Chapter 5. Modelling of necking in HDPE specimen and effect of triaxiality factor

5.1 Chapter overview

This chapter investigates the effect of geometry parameters on the deformation of the waisted tensile test specimen made of HDPE and the triaxiality in the middle section. The mechanical behaviour under various stress triaxialities induced by different specimen thickness, notch radius, and width of the cross-section of the specimen is investigated. The capacities of a constitutive model based on macro deformation of polymers to model this material are also studied.

5.2 Literature Review

Plastic dilation and energy to break the specimen are the critical response parameters to evaluate the ductility of the specimen and the flow potential of the constitutive model. It is found that plastic dilatation and energy to break the specimen are highly sensitive to stress triaxiality [80].

The two key elements which perform an essential role in obtaining different failure modes are different thicknesses of the pipes as well as the radius of the notch at the welded area of the specimen. These are the two main reasons which can cause more production of the tension-dominated triaxial stress state.

The geometry shown in Figure 4-1 is known to introduce transverse components to the stress tensor, which produces a large triaxial stress state. The larger the thickness and smaller the radius of the waisted section, the higher the stress triaxiality would be.

In a previous study [81] on a bar specimen made of HDPE, where the tension and compression are equal, the plastic dilation in a uniaxial stress state is minor, whereas micro holes started to grow in the centre of the HDPE specimens subjected to biaxial tension. This study shows that higher stress triaxialities may trigger a damage mechanism that leads to micro ductile failure.

To investigate the triaxial stress state as well as experimental trials, modelling of HDPE with the suitable material's behaviour must be carried out. The problem in modelling polymers such as high-density Polyethylene is their complex behaviour such as, strain localisation (Necking) which takes place from large deformation. The ability to model and predict necking in polymers have crucial industrial applications, where polyethylene is used, such as pipelines and pressure vessels.

There have been several approaches to propose a stress-strain relationship for polymer deformation. One of those approaches is known as slip-link or tube links [82] which offers minor improvements from rubber elasticity, taking into account chain entanglements in the molecular network for the mechanical response during the deformation. This approach is known as Edward-vilgis theory [83].

Another approach that was carried out by drozdov and Christiansen [84] considered the interactions at the molecular level to relate the molecular interactions with macroscopic deformation behaviour. This approach mimics plastic and visco-plastic deformation in semi-crystalline polymers.

Phenomenological models was developed mainly by taking into account the deformation at the macroscopic scale. Research works which employs this technique is based on elastic-plastic deformation [85, 86, 87, 88, 89, 67, 90, 91, 92, 93] and [94].

The technique used in this chapter is using the phenomenological modelling approach that uses finite element (FE) technique to mimic the deformation while the neck develops.

In this section, the technique and constants used by Muhammad [95] were used as the same material,

HDPE, was used for his study and had access to equipment where it was able to measure the strains in both directions.

Despite applying advanced material properties to model HDPE specimens, the failure mechanisms cannot be modelled due to different types of failure mechanisms such as shear yielding or micro ductile failure from void growth [96].

Some of the trials which had been carried on waisted tensile test specimen using parent material with larger thicknesses has shown significant evidence of failure due to void growth which has caused micro ductile failures.

Parent specimens which were in a lower thickness range (around 15mm) failed in a ductile manner which is also called failure from shear yielding.

In this chapter, validation of the model has been carried out by comparing Force-Deformation graph from experiment to the modelling, and different sets of modelling have been used to understand the geometry effect of the specimen on triaxiality stress state. Some practical experiments have also been carried on the parent material to understand the effect of thickness as well as other parameters (such as the width of the waisted section) on the failure mechanism (Practical experiments are from Chapter3).

5.3 Materials and experimental method

5.3.1 Materials

Natural PE100 extruded HDPE sheet of 15 and 25mm thickness supplied by Amari Plastics (UK) is used in this study (the same material used in experiments for chapter 3). As Moura et al. [97] found a direction dependency about the mechanical behaviour when pipes are tested, they are in the

extrusion direction. Therefore, it was asked by the provider to mark the extrusion direction, and all specimens were cut in the extrusion direction. The quoted tensile yield strength of the material is ~22MPa with the modulus of elasticity being ~900 MPa.

5.4 Numerical Study

FE modelling is carried out using ABAQUS Standard Explicit model. To model HDPE material in this study, (C3D20R) 3-dimensional 20 node quadratic brick elements are used. This element was particularly used because of its reduced integration properties, allowing large deformations and yielding without causing hourglass issues. Initially, when this element was not used, the hourglass was one of the modelling challenges which was solved using this element.

Equation 5-1 is the stress-strain relationship employed to carry out the current modelling. The equation contains four equations for elastic and plastic deformation.

$$Y(\varepsilon) = \begin{cases} E\varepsilon & (\varepsilon \leq \varepsilon_y)\ (a) \\ d[a(\varepsilon+b)^{c-1} - a(\varepsilon+b)^{-c}] + e & (\varepsilon_y \leq \varepsilon \leq \varepsilon_n)\ (b) \\ \alpha k \varepsilon^N & (\varepsilon_n \leq \varepsilon \leq \varepsilon_t)\ (c) \\ K\ exp(M\varepsilon^{\beta}) & (\varepsilon \geq \varepsilon_t)\ (d) \end{cases} \quad \text{Equation 5-1}$$

In Equation 5-1 σ is the effective stress in MPa, ε is the equivalent strain, ε_y is the critical strain for the transition from linear to nonlinear deformation, ε_n is the strain for the onset of necking, ε_t is the transitional strain for strain hardening, E is Young's modulus, and the rest of the parameters (a, b, c, d, e, α, k, B, M, A, n, m and β) are user-defined constants. The constants used for this study are from work carried out by S.Muhammad [95]. The corresponding graph for the above equation is shown in Figure 5-1.

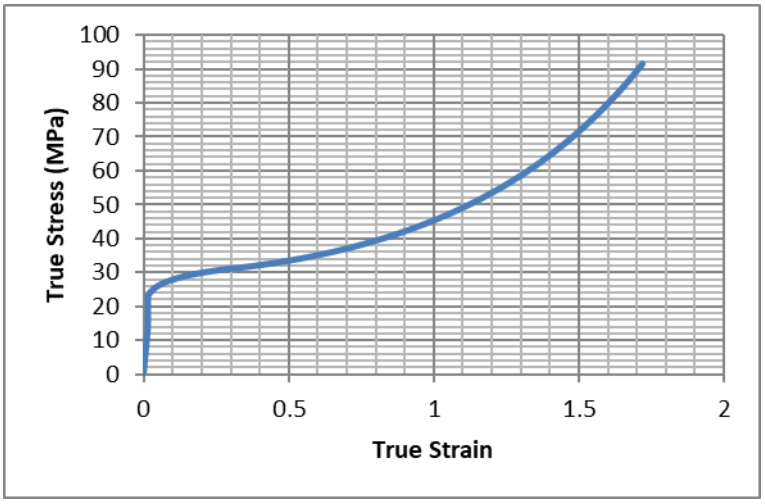

Figure 5-1, True stress-true strain graph for HDPE

It has to be noted that the graph shown in Figure 5-1, is implemented into the FEA model using more than 2000 discrete points in data format. Using a large number of data points allows minor adjustment to satisfy continuity in the stress-strain relationship. The number of data points in use and their increments investigated by running an enormous number of FEA models starting from simple geometry with a minimum number of boundary conditions. Having an element to follow a specific stress/strain curve is not sufficient to run this model computing waisted geometry. The real challenge appeared when the model was unable to perform necking, and the hourglass (massive distortion) appeared in models just after few millimetres of elongation in the specimen. This was another indication for starting the modelling with a simple geometry which is the dumbbell test specimen.

Challenges of performing large deformation in specimen raised mainly from large distortion in elements and difficulties to perform necking in the specimen. To overcome these challenges, different steps and techniques are applied, which are mainly mesh sizing, pattern, and correct use of boundary conditions. Necking is first performed on the dumbbell test specimen, and similar pattern and data points are transferred to other geometries.

Different time steps for dumbbell test specimen from the beginning to the final stage is also presented to show how the necking develops on this material and geometry.

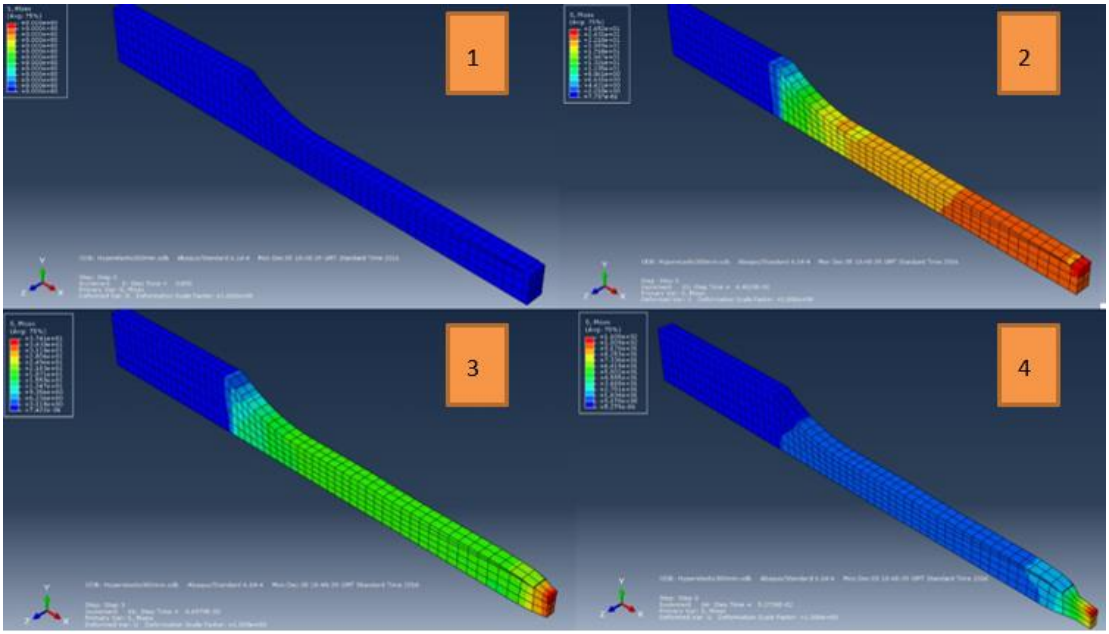

Figure 5-2, Necking steps in the dumbbell test specimen

5.4.1 FEA Validation

To validate FEA findings, validation is carried out by comparing the load-displacement graph generated for a specimen geometry with 15mm thickness and 17.5mm in width of the waisted section. In order to validate the model, the predicted load-displacement curve from the FEA is compared with the experimental curve using the same specimen geometry (Figure 5-3).

Mesh configuration of the specimen (PEW36) used in this validation is shown in Figure 8-2 and Figure 8-3. Different increments of the modelling for this specimen are also shown in Figure 8-4 and Figure 8-5 with a more clear pattern of the necking inFigure 8-6. Boundary conditions used for this numerical modelling is same as conditions used in section 5.5.4.

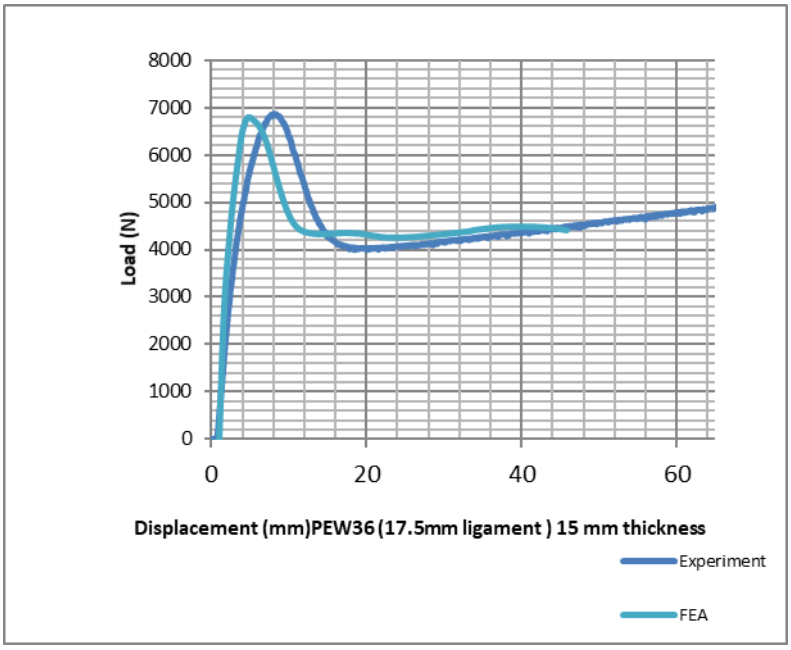

Figure 5-3, Validation of the FEA model on a particular specimen with a thickness of 15mm, the Loading hole diameter of 20mm and width of the waisted section of 17.5mm (refer to Figure 8-2 to Figure 8-6 for the necking of the specimen)

As shown in Figure 5-3, although it is not possible to model the specimen's fracture, there are trends and correlations between the FEA model and experimental results displacement values up to 60mm, particularly the essential features of the load at yield and the cold drawing load. The main reasons for the differences in displacement at yield are due to having different constants in Equation 5-1 for different HDPE resins, strain rates or specimen geometry that are used for the experimental trials. However, this will not have a significant effect on the FEA results.

Another challenge to model the reduced section tensile test is to define the failure mechanism. Unlike metals, the failure mechanism for polymers cannot be solely based on von Mises stresses; HDPE in large thicknesses using waisted geometry often fractures due to the growth of cavitation during deformation, resulting in a micro-ductile failure.

FEA modelling of cavitation growth in polymers during deformation is yet an open topic for research. However, recent research publications explain the cause of void formation in polymers [80], which as

the triaxiality of the stress state to be an influential factor, this is also known as to have a great influence on the amount of plastic strain that a material can undergo before ductile failure occurs.

As mentioned in chapter 2, the triaxiality factor is defined as the ratio of hydrostatic pressure stress, or mean stress, $\sigma_{h,}$ to the Von-Mises equivalent stress, σ_{eqv}. The formula for the triaxiality factor is given below, where σ_1, $\sigma_{2,}$ and σ_3 are the first, second and third principal stresses, respectively.

$$\frac{\sigma_h}{\sigma_{eqv}} = \frac{\frac{1}{3}(\sigma_1+\sigma_2+\sigma_3)}{\frac{1}{\sqrt{2}}\sqrt{(\sigma_1-\sigma_2)^2+(\sigma_2-\sigma_3)^2+(\sigma_3-\sigma_1)^2}} \qquad \text{Equation 5-2}$$

The average triaxiality is calculated at the minimum waisted section versus displacement during the tensile test. As a result, the maximum average triaxiality during the test is recorded.

The geometry used for sections 5.5.1 to 5.5.3 is shown in Figure 5-4, and the triaxiality measurement point are shown in Figure 5-5. the displacement value at which the average triaxiality is at maximum, the variation of the triaxiality factor is then calculated along the line at the mid-wall thickness (Figure 5-5).

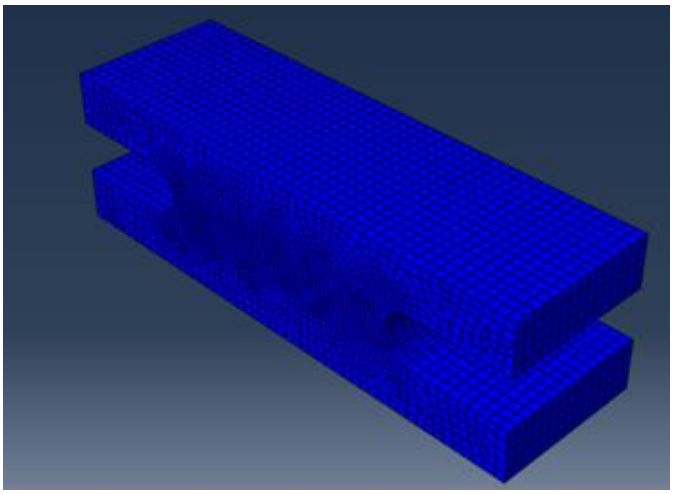

Figure 5-4, Geometry configuration for determining the geometry effects on triaxiality

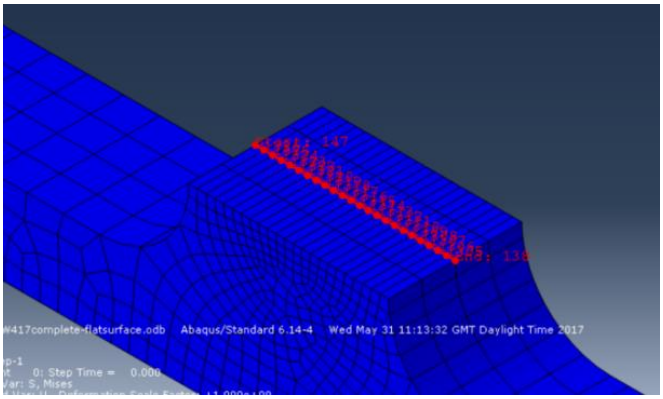

Figure 5-5, Triaxiality measurement point locations in the specimens

The boundary condition for this set is to have the top surface subjected to 100mm displacement to the top and the bottom surface to be fixed points (Figure 5-6). No symmetry condition was used on this set as the recording data was from the middle of the specimen, and preferred not to have readings close the edges subjected to constraints.

The mesh configuration for sections 5.5.1 to 5.5.3 is shown in Figure 5-7, where the specimen is sectioned from the middle to seed the middle of the specimen for more detailed analyses. All the edges of the specimen are seeded and designed to be denser in essential areas.

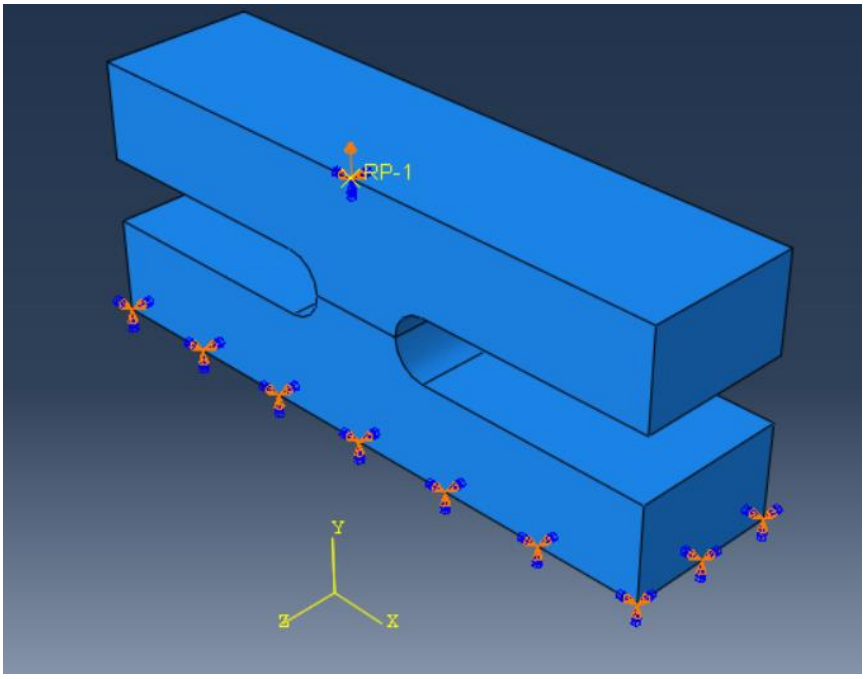

Figure 5-6, Boundary conditions and fixed point for the geometry used

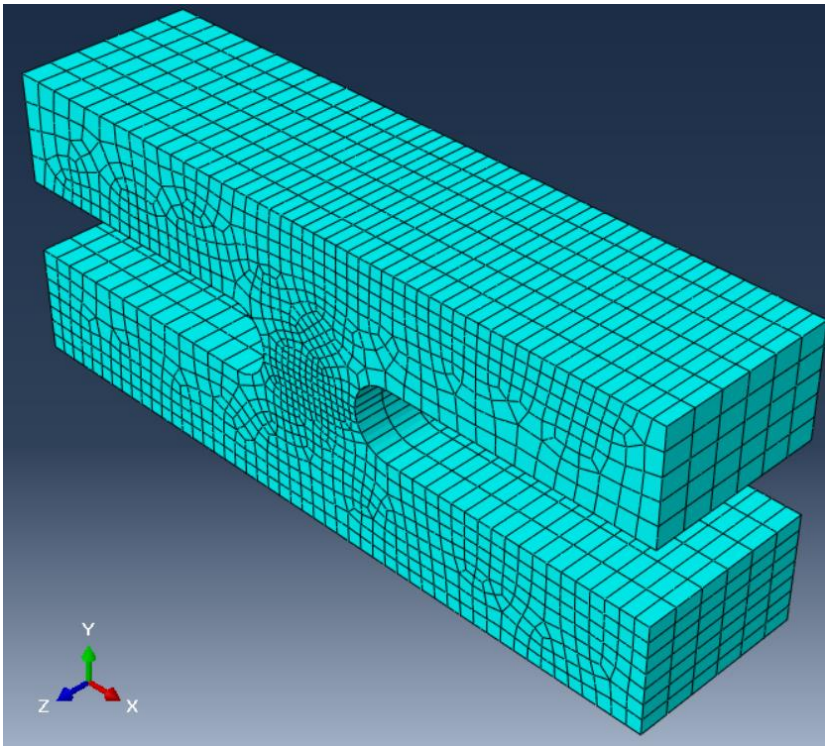

Figure 5-7, Mesh setting for the geometry used

5.5 Results

5.5.1 Effect of Specimen thickness

To understand the effect of thickness on triaxiality, six specimens ranging from 15 to 100mm thickness was modelled bases on conditions described in the previous section. Two increments from one of the samples using this geometry are presented below to show the neck development modelling for this study. Figure 5-8 shows an early increment of the samples used in this study where the necking has just started to occur. Figure 5-9 is a later increment where the necking has already taken place, and a reduction in the waisted area is evident in the middle of the specimen.

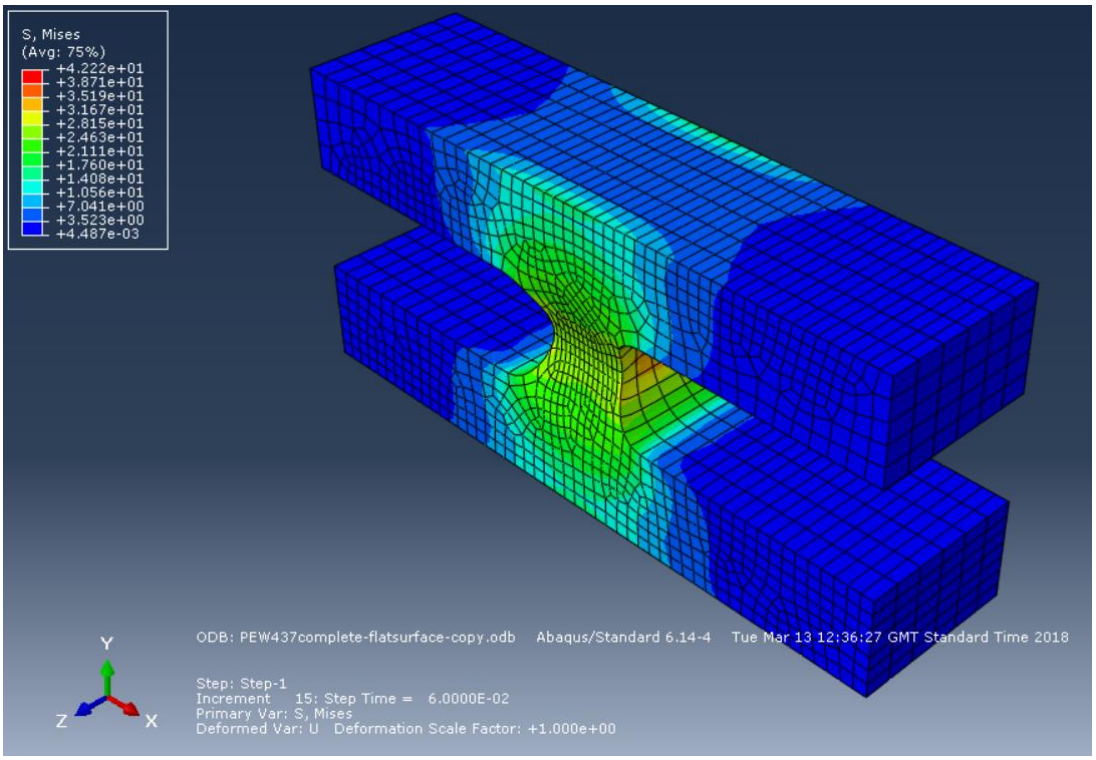

Figure 5-8, Early increment of neck development modelling

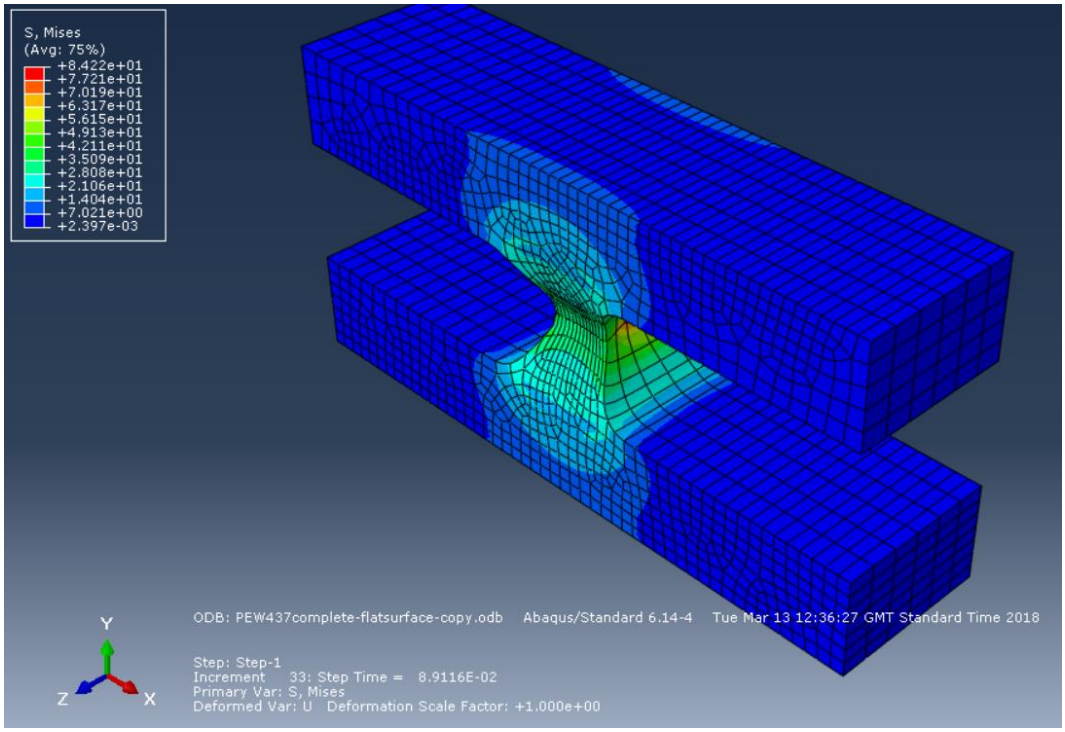

Figure 5-9, later increment of neck development modelling

Figure 5-10 shows the triaxiality across the width of the waisted section at the deformation where the average triaxiality is the highest for different specimen thicknesses; increasing the thickness of the specimen increases the maximum triaxiality. Triaxiality values greater than one tends to cause void formation in the specimen, resulting in micro-ductile fracture and little elongation [83]. Figure 5-10 suggests that it is not possible to generate a ductile failure, even in the parent material, for thicknesses greater than 30mm. For this reason, it is recommended that the maximum specimen thickness used for the reduced section tensile test is 30mm. For pipe thicknesses larger than 30mm, it is recommended that the specimens are cut equally into two or more layers such that the maximum thickness of any specimen is 30mm. This approach has also been adopted in the new version of WIS-4-32-08.

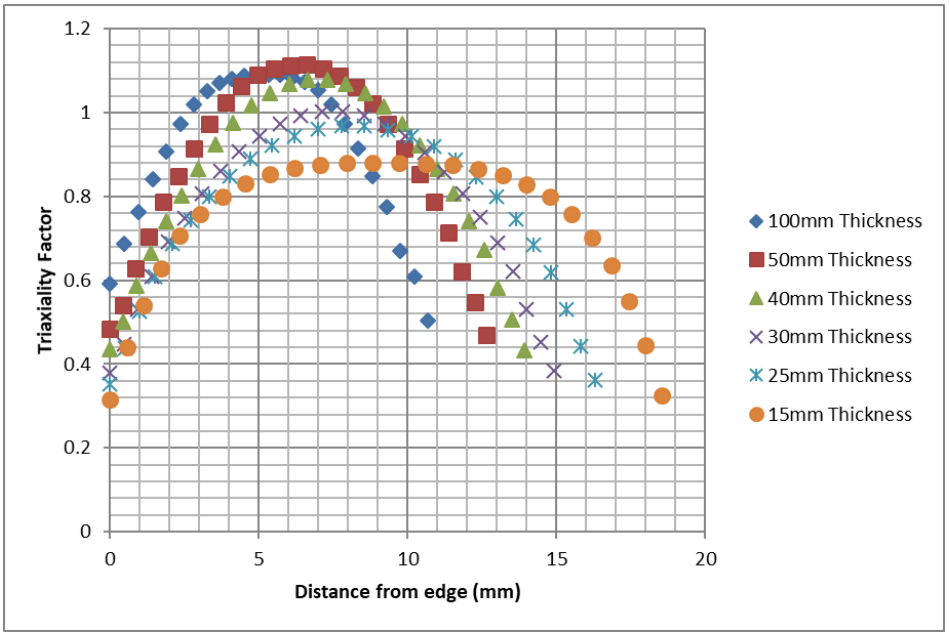

Figure 5-10, Variation of triaxiality across the width of the waisted section for specimens with different thicknesses (width of the waisted section 25mm and radius of the waisted section 10mm)

The experimental tests to indicate the thickness effect were carried on 15 and 25mm thickness (from Chapter 3). The Force-Deformation graphs for these two specimens are shown in Figure 5-11. The dimensions used in these specimens are from BE EN 12814-7, which is shown in Figure 1-1.

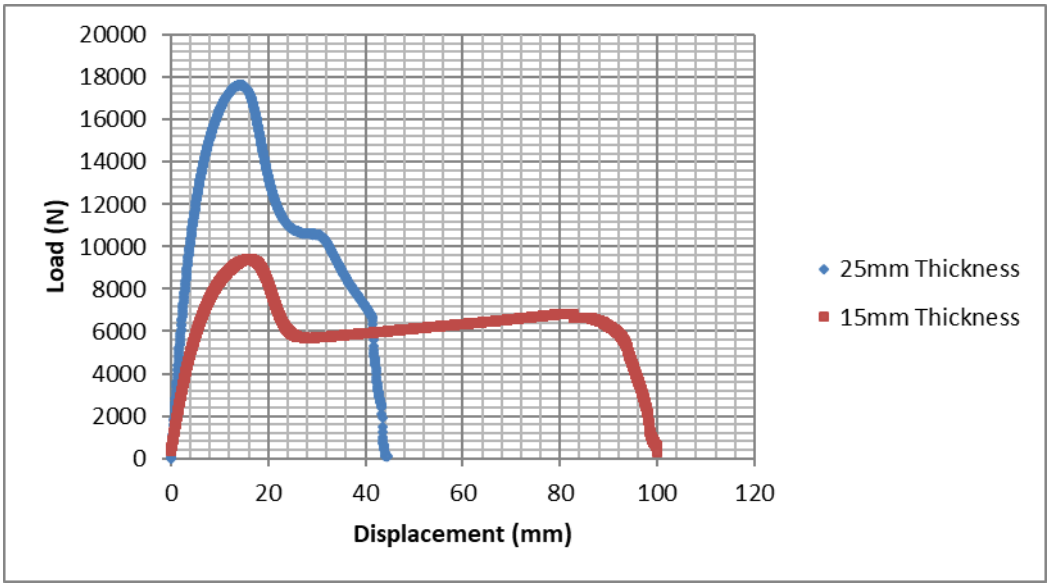

Figure 5-11, Experimental Load-Displacement for 15 and 25mm thickness

In Figure 5-11, it can be seen that the yield point for 25mm thickness is higher than 15mm thick specimen which is due to the larger CSA in the specimen. The cold drawing region in 15mm thick specimen provides a long elongation which shows a high ductility in the specimen. The 25mm thick specimen has failed to undergo cold drawing region and has started to fail from micro voiding growth. Photos from the fracture surface of these two specimens are shown in Figure 5-25.

5.5.2 Effect of the width of the waisted section on triaxiality

To determine the effect of the width of the waisted section on triaxiality the same geometry configuration as given in Figure 5-4 is used; however, the specimen thickness is kept constant at 25mm. This was selected purposely to have the failure due to void growth, which is from triaxiality. The radius of the waisted section is kept constant at 5mm, and the width of the waisted section is varied between 15 and 27.5mm.

This set of experiment is also carried out empirically by varying the width of the waisted section and keeping other parameters constant.

The distance between loading holes also has some effects, but in this study, it has been considered to have it close to its initial value and increase the amount that would be lost from an increase in loading hole diameter. Loading hole diameter is adjusted to be equal to the width of the waisted section to avoid elongation of the loading pinhole.

Figure 5-12 shows the variation of triaxiality factor across the width of the waisted section at the displacement value where the average triaxiality is the highest for a 5mm radius of the waisted section. From this figure, it can also be seen that for a 25mm thick specimen, the larger the width of the waisted section is the lower the maximum triaxiality point is.

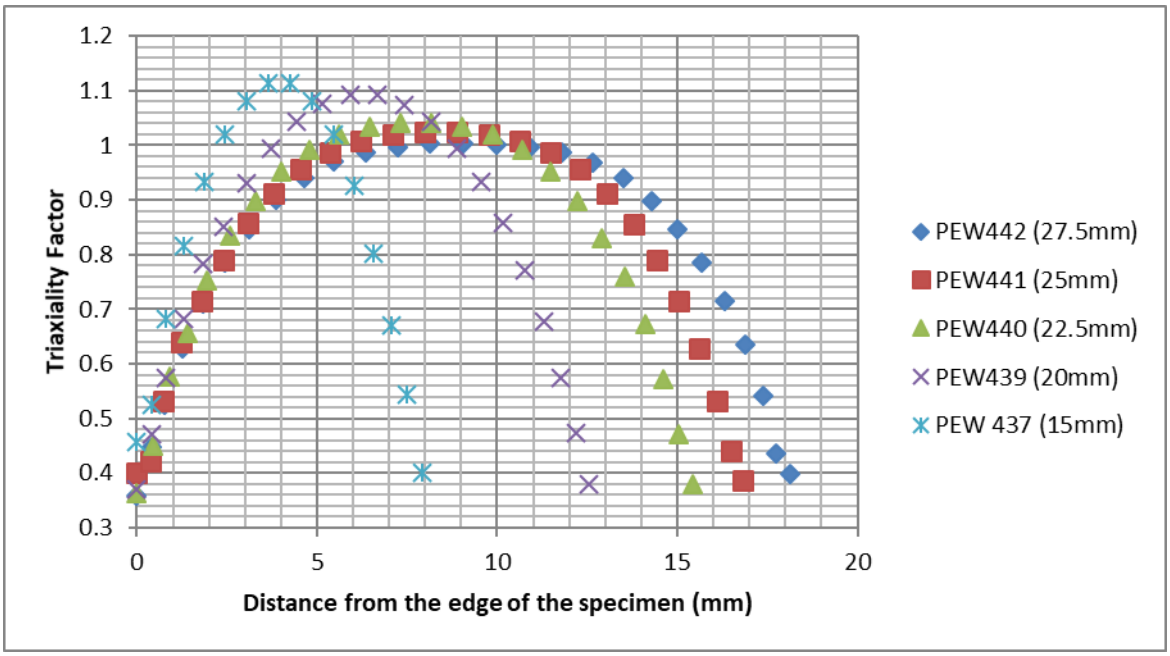

Figure 5-12, Validation of across the width of the waisted section for specimens with different widths of the waisted section (wall thickness 25mm, the radius of the waisted section 5mm)

Recording the highest triaxiality point on the specimen during the tensile testing is essential as it is the main factor to trigger the void formation. Void formation in the specimen would trigger the failure and stops the cold drawing to take place.

In Figure 5-12, it can also be seen that the specimen with a 15mm width of the waisted section had the most substantial triaxiality factor value. From 15mm to 27.5mm width of the waisted section, all specimens have triaxiality values of over one except 27.5mm, where the maximum triaxiality point reaches one and have the lowest triaxiality value across other specimens.

Figure 5-13 shows experimental tensile test specimen load-displacement curves for 25mm thick specimens with different width of the waisted section specimens. 5 out of 6 specimens in this experiment failed due to void growth. One specimen, which is PEW45 with 27.5mm width of the waisted section is failed after going through a long cold drawing and failed from tearing.

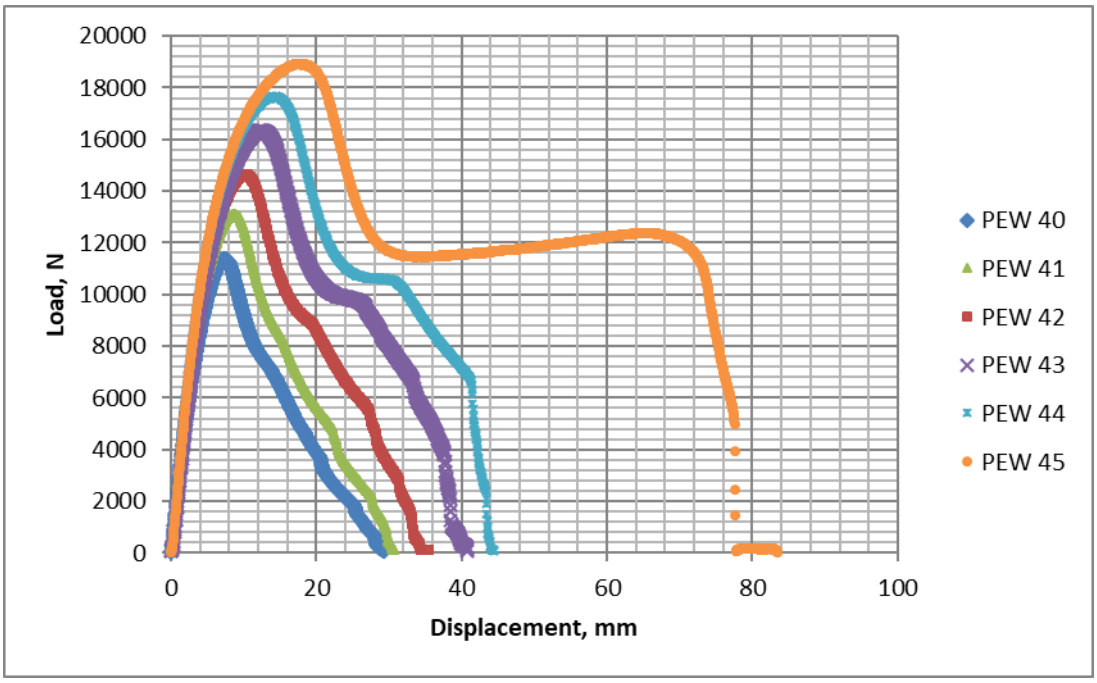

Figure 5-13, Load-displacement curves on 25mm thick specimens varying the width of the waisted section

The experimental results shown in Figure 5-13 provides sufficient evidence for the effect of the triaxiality on the failure of HDPE due to geometric effects.

The primary purpose of performing these modellings and experiments is to propose a new specimen geometry for the geometry shown in Figure 1-1. The other parameter which would be used for the investigation of triaxiality is the radius of the waisted section, which can be seen in the next section.

5.5.3 Effect of the radius of the waisted section on triaxiality

Effects of the thickness and width of the waisted section of the specimen are investigated in the last two parts of this chapter. Taking into account the trends seen in the effect of the thickness and effect of the width of the waisted section on failure behaviour, a similar analysis is carried on the radius of the waisted section. To investigate the effect of the radius, four types of assessments are carried out using radiuses of 5mm, 7.5mm, 10mm and 12.5mm accordingly. The result of this analysis is shown in Figure 5-14, where the triaxiality factor for each point across the width of the waisted section is recorded.

From Figure 5-14, it can be seen that the increase in the radius of the waisted section reduces the maximum triaxiality during the test. Therefore, adjusting the radius is one of the geometry parameters that can prevent failures occurring due to void growth in this scenario, the specimen with a radius of 5mm has the maximum triaxiality of 1.07, whereas the specimen with a radius of 12.5mm has a triaxiality of 0.97.

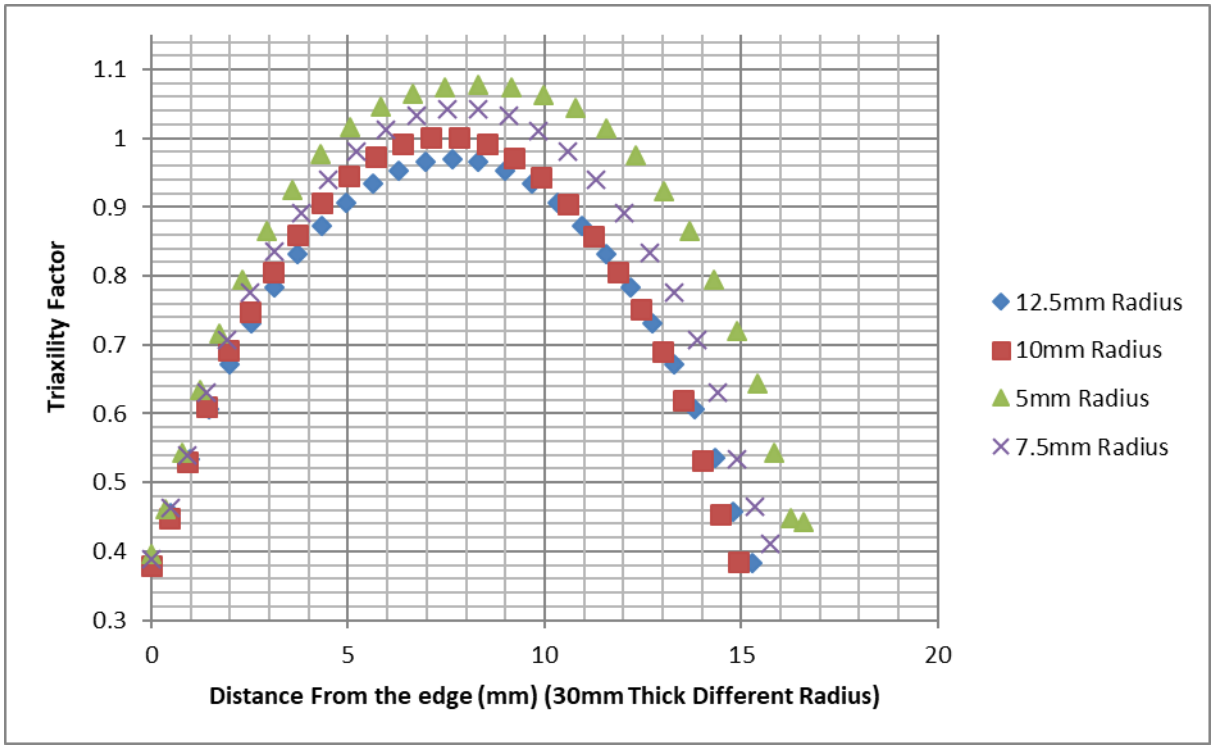

Figure 5-14, Variation of triaxiality across the width of the waisted section for specimens with a different radius of the waisted section (width of the waisted section 25mm)

It can be noted that specimens have the highest stress triaxiality at the centre of the specimen. This is the location where the void grows and initiates the failure of the specimen. However, in a situation where the thickness is larger or the width of the waisted section larger (than 30mm), then the areas where the maximum triaxiality is high (over 1) is not only localised in the centre of the specimen, it is also localised throughout the fracture surface. In this situation, the failure is not only due to one void growth but also many other points on the fracture surface.

5.5.4 Effect of the width of the waisted section and loading hole diameter on elongation in the loading hole

As the effect of the loading hole is being investigated from this study, changes were made to the geometry. Figure 5-15 shows the boundary conditions and meshing for the geometry used in this study; the Left figure shows the geometry configuration and the areas where partition has taken place.

As this geometry is 1/8th of the actual geometry, symmetric boundary conditions have been applied on the surfaces and edges where the yellow dots indicate their separations. The top quarter of the hole has been taken as the pin effect where displacement is used to pull the specimen. Overall meshed geometry is on the right side of Figure 5-15 where partitions are used to produce a more dense mesh area on the areas of interest. As the mesh is very dense on the waisted area it is shown separately in Figure 5-16.

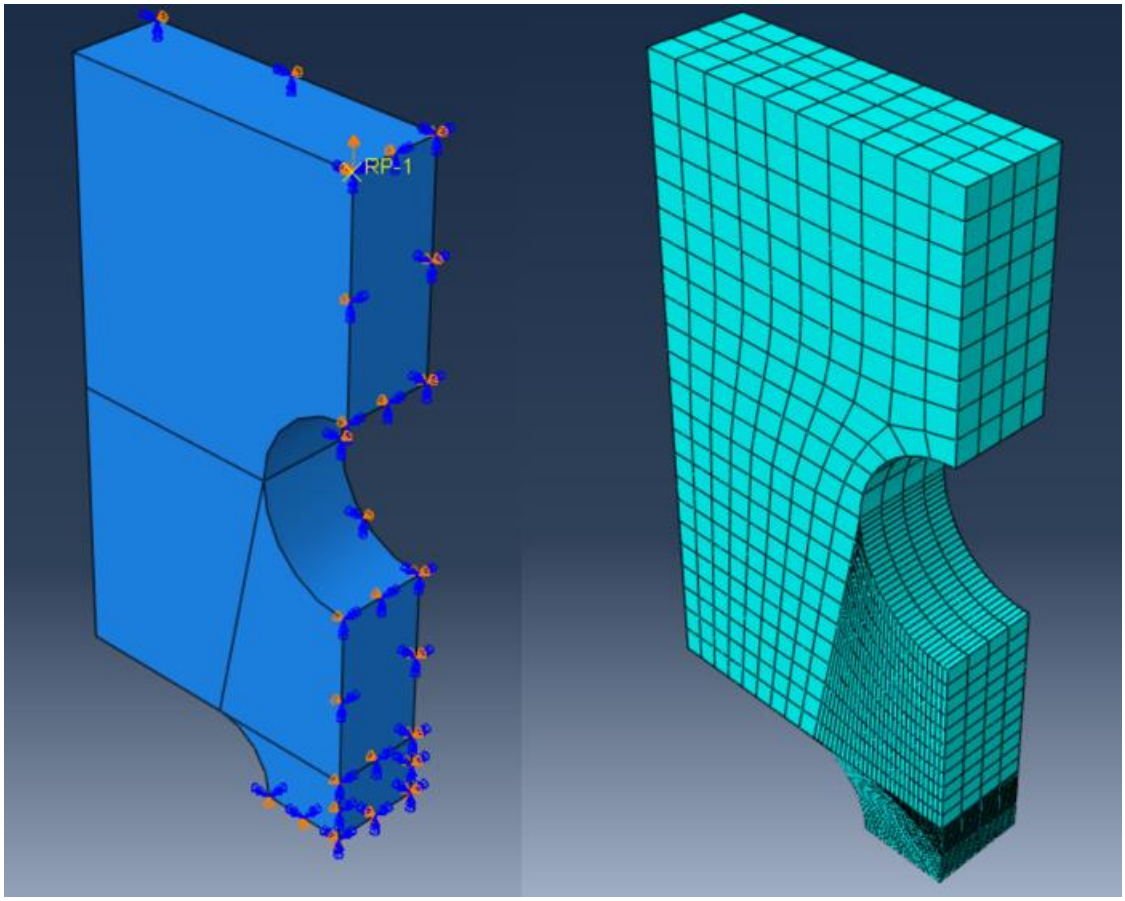

Figure 5-15, Boundary conditions and meshing used for determining the effect of the width of the waisted section on elongation in the loading hole diameter

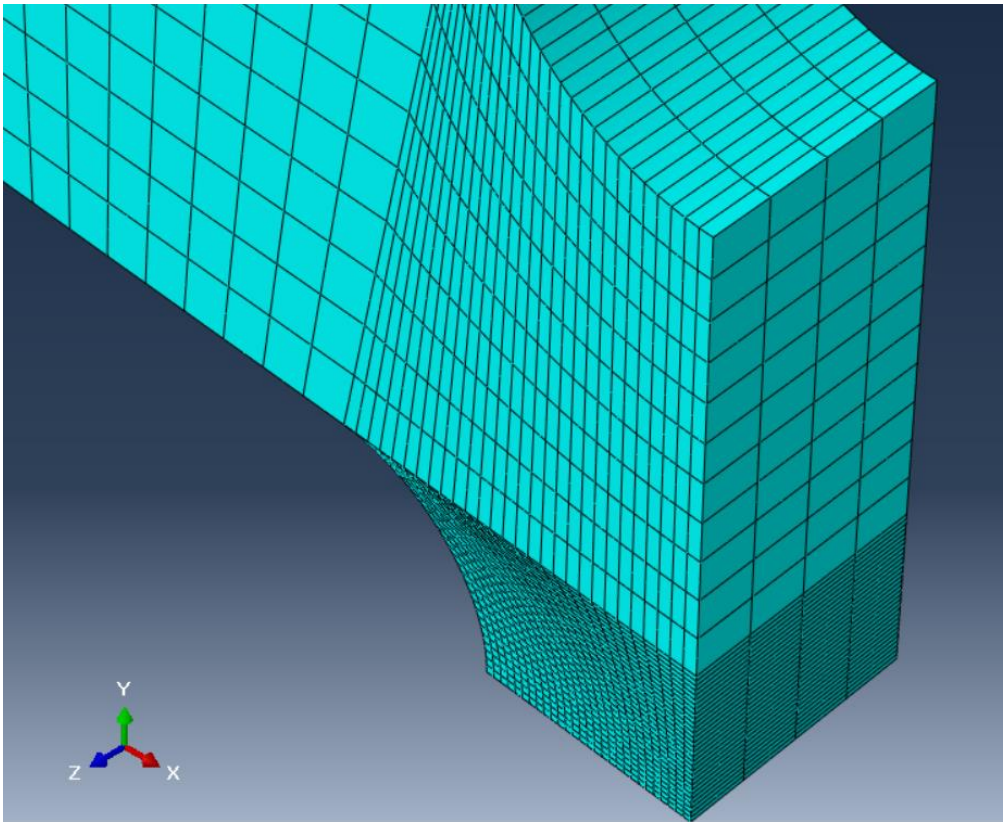

Figure 5-16, Detailed mesh configuration at the waisted area

To present the necking that occurred in these specimens, two geometries from early and later increments of the modelling is presented in Figure 5-17 and Figure 5-18. This clearly shows the neck development in the symmetric configuration used. This geometry and conditions are used in this study to investigate the effect of wasited section on the elongation in loading hole for two cases. One is when the pin is a constant value and the second case is when the pin diameter is changed with the size of the waisted section.

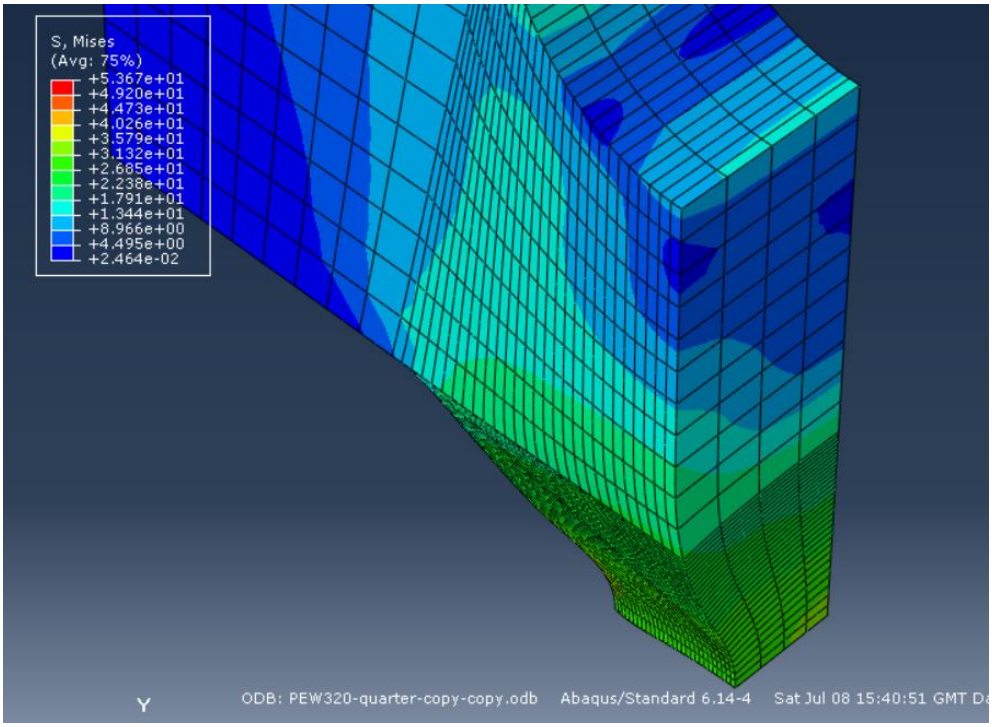

Figure 5-17, Early increment of neck modelling using symmetry geometry

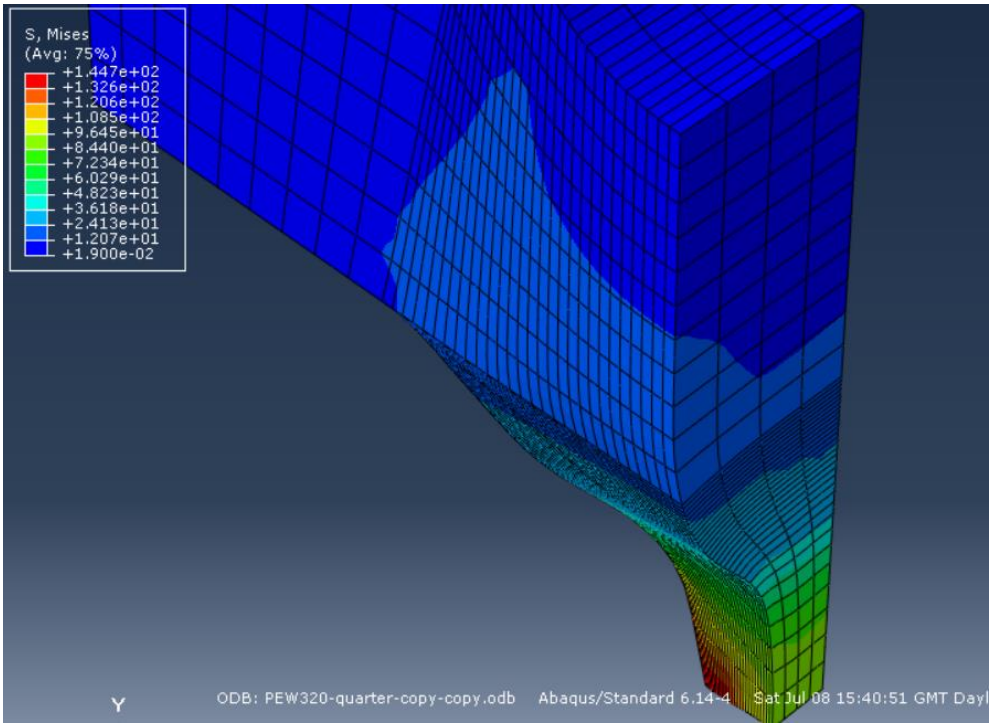

Figure 5-18, Later increment of neck modelling using symmetry geometry

The elongation in the loading hole versus overall deformation of the specimen, for different values of the width of the specimen, is shown in Figure 5-19, which indicates that reducing the width of the waisted section reduces the elongation in the loading hole. It is therefore suggested that to keep the elongation of the loading hole low, the loading hole diameter and width of the waisted section is recommended to be equal.

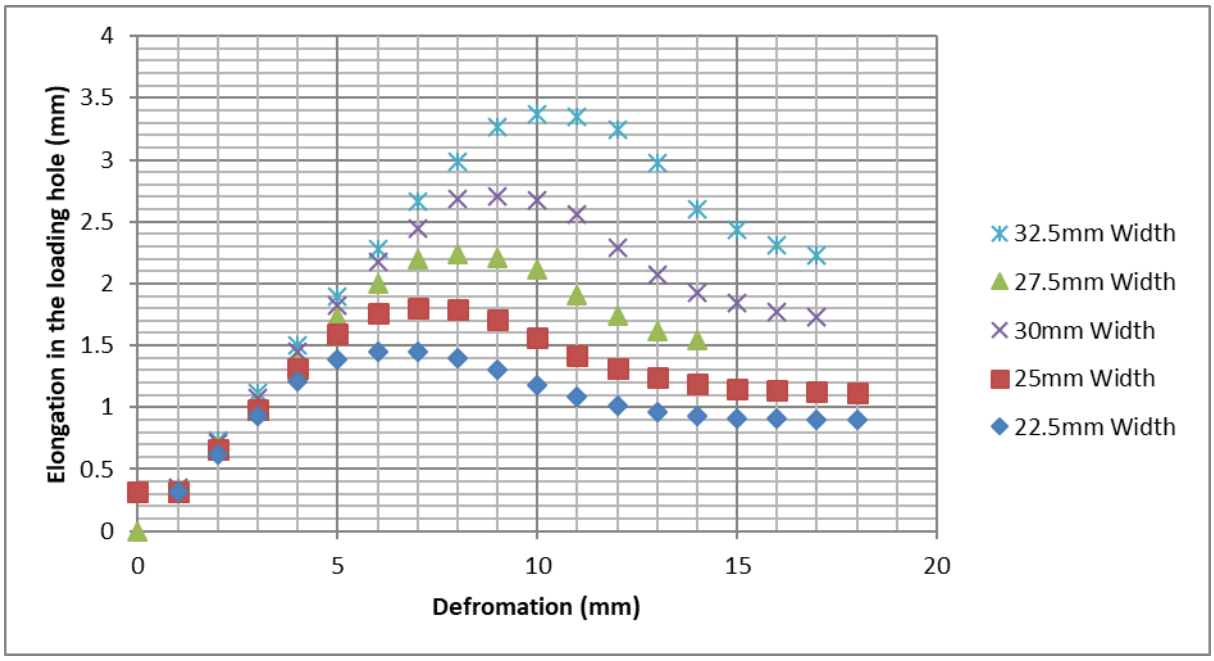

Figure 5-19, Elongation of the loading hole versus the deformation in the specimen for different widths of the waisted section and constant loading hole diameter of 20mm (wall thickness 30mm, the radius of waisted section 5mm)

The elongation in the loading hole versus the overall deformation of the specimen is shown in Figure 5-20. For this analysis, the diameter of the loading hole has been selected to be equal to the width of the waisted section. From the data shown in this figure, it can be concluded that the increase in width of the waisted section would increase the elongation of the loading hole.

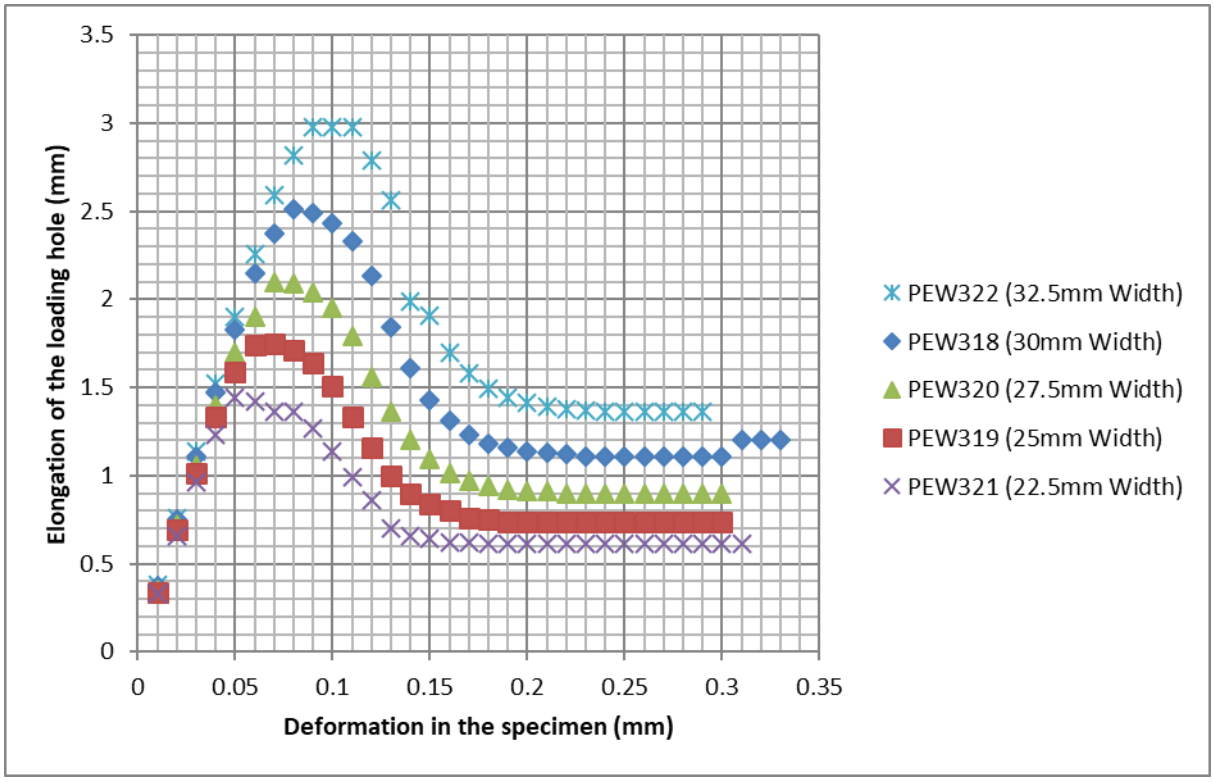

Figure 5-20, Elongation of the loading hole versus deformation of the specimen for different widths of the waisted section (wall thickness 30mm, the radius of waisted section 5mm, loading hole diameter same as the width of the waisted section)

5.5.5 Ductile and micro-ductile failure

As shown in Figure 5-21, an X-ray computed tomography (XCT) is used to observe the fracture surfaces for PEW42&37 specimens. The motive behind applying XCT method is being able to scan and investigate the fracture surface in 3 dimensions. To investigate the fracture surfaces of specimens using XCT, unlike many other techniques, the surface is not required to be flat.

The XCT system used to obtain XCT scans during this study is an HMX 225 originally supplied by Metrix X-Tek Ltd. The source, manipulator, detector and XCT data acquisition are controlled by X-Tek InspectX software which digitizes the radiographic images to 16-bit format. One of the specimens in this observation is PEW42 with the thickness of 25mm and width of the waisted section of 20mm with failures from void growth in the centre of the specimen.

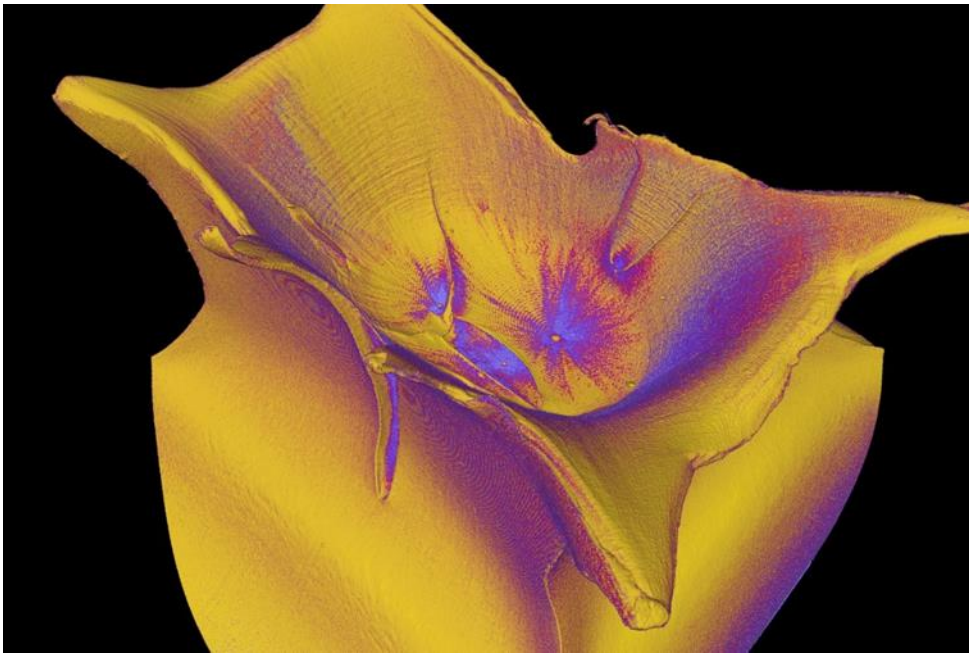

Figure 5-21, Xray photography of micro ductile failure for specimen number 42

The initial observation and analysis of the fracture surface show that the failure is due to one void, but more in-depth visualisation lead through x-ray photography lead to the discovery of three central voids mostly in the centre of the fracture surface. By zooming at the images found from X-Ray, at the surface of the fracture surface in Figure 5-22, a large number of small circles (voids which have not grown) could be seen, but most are in small dimensions which can be said that they have not been triggered. This phenomenon and creation of these circles could be due to reaching a certain amount of triaxiality, but few are triggered, which caused the failure, and the rest are not triggered entirely due to the reduction of triaxiality value after the failure starts to happen.

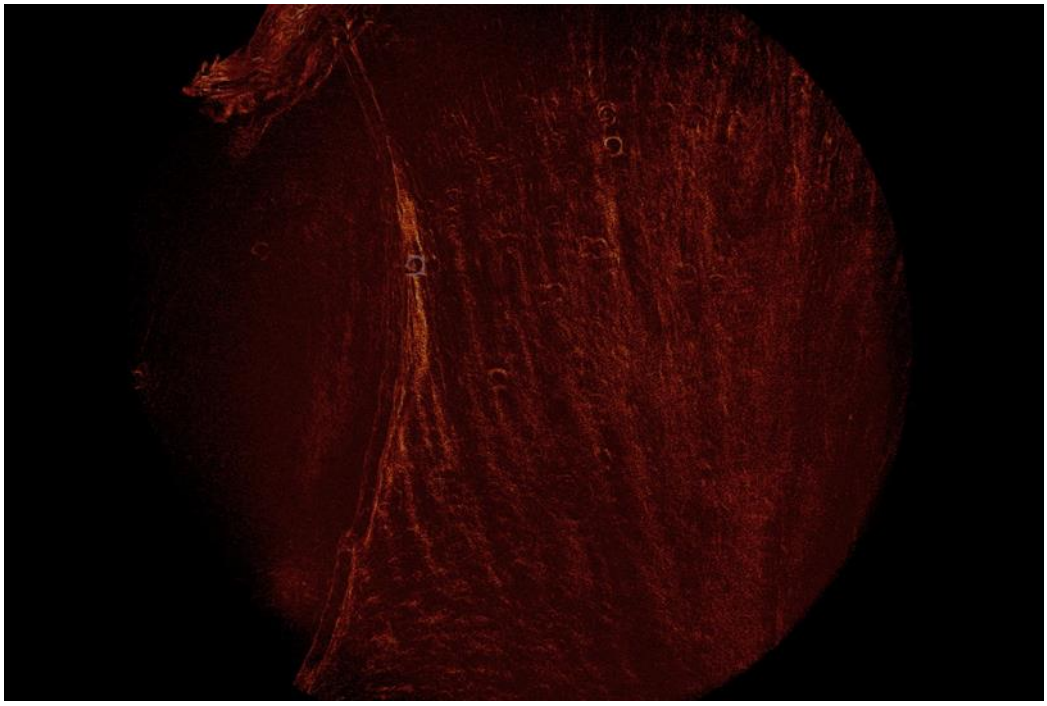

Figure 5-22, X-Ray Photography of micro ductile failure for specimen number 42

The other type of failure mode occurs on specimens with different thicknesses (usually lower), and different geometry configuration is the ductile failure, where the failure happens after the specimen has gone through large deformation. The X-Ray photography of ductile failure can be seen in Figure 5-23 and Figure 5-24.

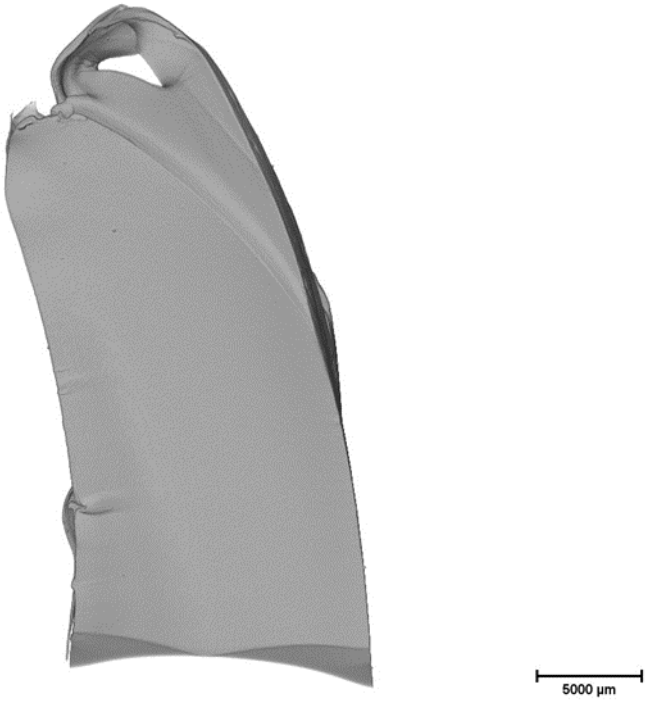

Figure 5-23, X-Ray photography of ductile failure for specimen no 37

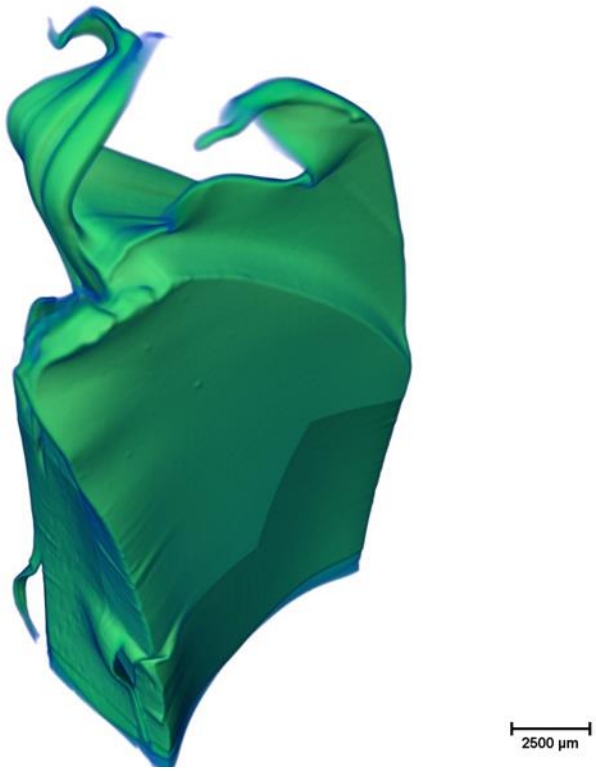

Figure 5-24, X-Ray photography of ductile failure for specimen no 37

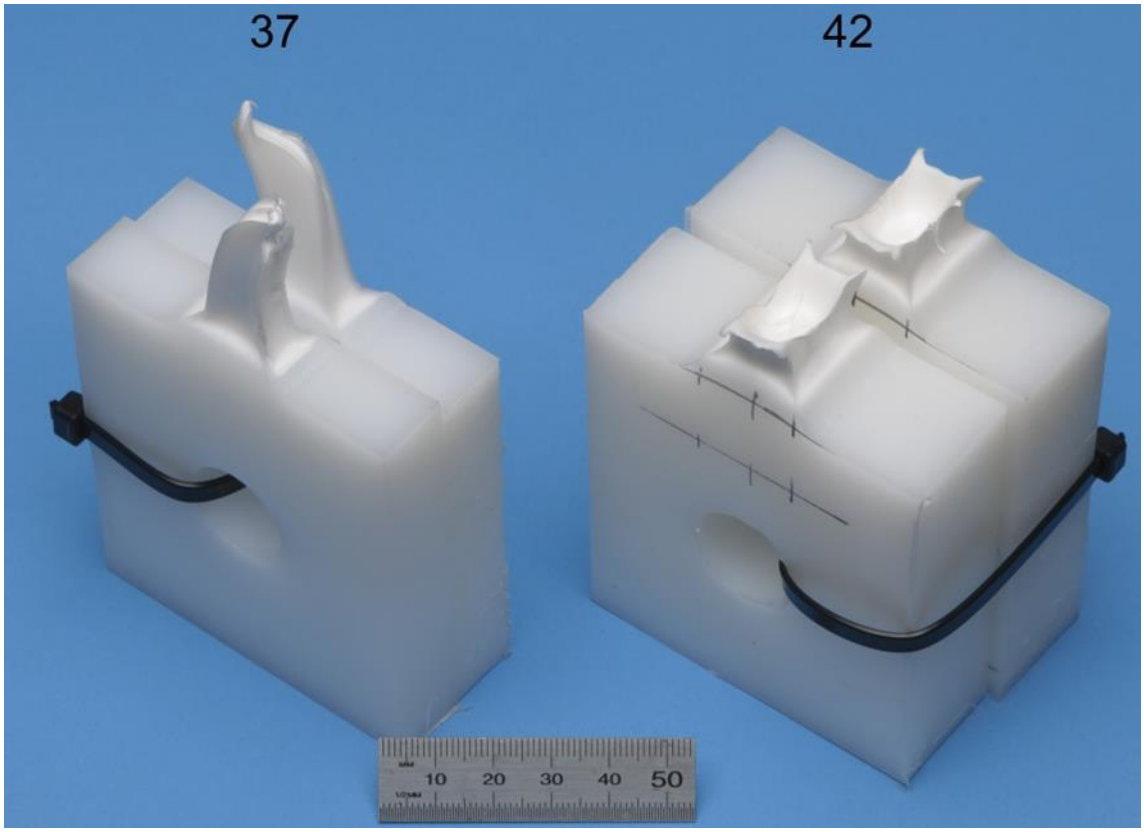

Figure 5-25, from left, fully ductile and micro ductile failure

The specimens used to carry out X-Ray for the demonstration of fully ductile and micro ductile failure are shown in Figure 5-25. The difference between the fracture surfaces of these specimens is also visible by visual inspections.

5.6 Conclusion

In this chapter, a summary of the techniques used to model polymers is compared and explained. The constitutive model used in this study is explained with constants used in the equation revealed. A step by step methodology is explained as to how the numerical modelling is set up and what criteria are used for measurements in modelling.

Despite the possibility of modelling necking in the specimen, failure of the specimen could not be modelled due to different challenges and complex failure mechanism of polymers. To be able to

compare the experiments in modelling, the triaxiality factor, which is an indication of the state of the stress at a certain point, is used. As the maximum triaxiality is the point where it triggers the voids in the specimen, triaxiality points at increments and locations with the highest triaxiality value are used.

Two types of failures seen in parent material specimens, ductile and micro ductile, are displayed from experimental work carried out in previous chapter 3 and are related to triaxiality values found using FE analysis. Two types of ductile failure modes are exposed and explained with in-depth X-Ray photography, which explains these failures' reasons.

Using numerical modelling techniques, comparison against thickness, width and radius of the waisted section of the specimen are carried out and compared with their triaxiality stress state in the middle of the specimen. Elongation in the loading hole diameter against the width of the waisted section and loading hole diameter is also investigated.

This part of the research suggests that for specimens with a thickness of over 30mm, the triaxiality factor would be around the value of one, which means any specimen with a thickness of over 30mm would have a high chance of failing from void growth in the specimen. An increase in width and radius both reduces the triaxiality factor, but the study suggests there should be a limit to the increase as this would affect the elongation in the loading hole as well as where the failure in the specimen takes place.

Chapter 6. Proposed specimen geometry and its application on welded and unwelded HDPE pipes

6.1 Chapter overview

In this chapter, an enhanced geometry is proposed, experimentally tested, and been applied to different pipes with different thicknesses having welded and unwelded conditions. This chapter also clarifies the motives for selecting specific pipe sizes. Welding parameters, as well as the location of each sample on the pipe, is also explained.

6.2 Introduction

In previous chapters, the effect of different parameters on waisted tensile geometry was investigated both experimentally and using FEA analysis techniques. The principal reason to conduct this research is to identify a geometry that can be utilised to quantify the quality of butt fusion joints for different thicknesses and provides useful quantitative information to allow discrimination among different weld qualities. Standard geometry using a flat sheet for the thickness of 25mm is tested in Chapter 3, which showed that a fully ductile failure could not be achieved, and the specimens with 25mm thickness failed from void growths. The benefits of the proposed modified geometry are confirmed after the comparison provided against the standard geometry.

For each condition (each weld and pipe size), few samples (4-5-6) using standard and proposed modified geometry have been machined and tested at different angles of the pipe to investigate all factors which could affect the results.

Finally, the results are compared, and the effect of different pipe sizes will also be investigated using both current standard geometry (BS-EN 12814-7) as well as the proposed enhanced geometry.

6.3 Designed geometry for different thicknesses

FEA results revealed the challenges of generating a ductile fracture in a reduced section specimen for specimen thicknesses greater than 30mm. This challenge is present for both flat specimens and specimens cut from the parent pipe. This means that for thicknesses greater than 30mm, it can be difficult to differentiate between good and bad welds using this test method.

Since all specimens fail in a brittle (micro ductile) manner, it is therefore suggested that, for pipe wall thicknesses greater than 30mm, the specimens are cut equally into two or more layers such that the maximum thickness of the specimen is 30mm.

Based on the DOE study (provided in chapter 4), increasing the radius of the waisted section increases the energy to break the specimen. This means, the triaxiality factor reduces as the radius increases and also it is highly likely that failures occur outside of the weld region in a welded specimen. Therefore, it is recommended to use a radius of 10mm for the waisted section in different scenarios.

The DOE study, as well as the work carried out in chapter three, suggested that for a specimen with 15mm thickness, the width of the waisted section should be equal to the specimen's thickness in order to achieve higher energy to break value (specifically Region 3 energy). The FEA study suggested that for a specimen with 30mm thickness, the width of the waisted section should not be less than the specimen thickness in order to achieve a low triaxiality factor. However, increasing the width of the waisted section also increases the elongation in the loading hole. Therefore, it is suggested that the width of the waisted section of 30mm should be used for 30mm thick specimen.

The DoE study on 15mm thick specimens suggests that a loading hole diameter of 20mm will give the highest energy to break. However, for 30mm thick specimens, the FEA suggests that, in order to reduce the elongation in the loading hole, it is better to keep the loading hole diameter equal to the width of the waisted section, i.e. 30mm.

The DoE study on 15mm thick specimens suggests that the energy to break increases as the distance between the loading hole increases. This is due to the decrease in strain rate at the waisted region. The suggested distance between the loading holes for a 15mm thick specimen with a diameter of 20mm is 100mm. Therefore, the suggested distance between the loading holes for a 30mm thick specimen, with a diameter of 30mm is 110mm, to compensate for the larger diameter.

From the DoE study on 15mm thick specimens, the energy to break increases as the overall width of the specimen increases. There have to be limits on how much the width can be increased. This limit is set not to have the specimen being failed or elongated from the side of the specimen. Therefore, the proposed overall width for specimens with thickness of lower than 20mm, between 20 to 25mm and between 25 to 30mm are 70, 80 and 80mm, respectively.

Based on these results, the proposed optimised geometry of 30mm thick reduced section specimens is given in Table 6-1, where it is compared with the geometry specified in WIS 4-32-08-2017.

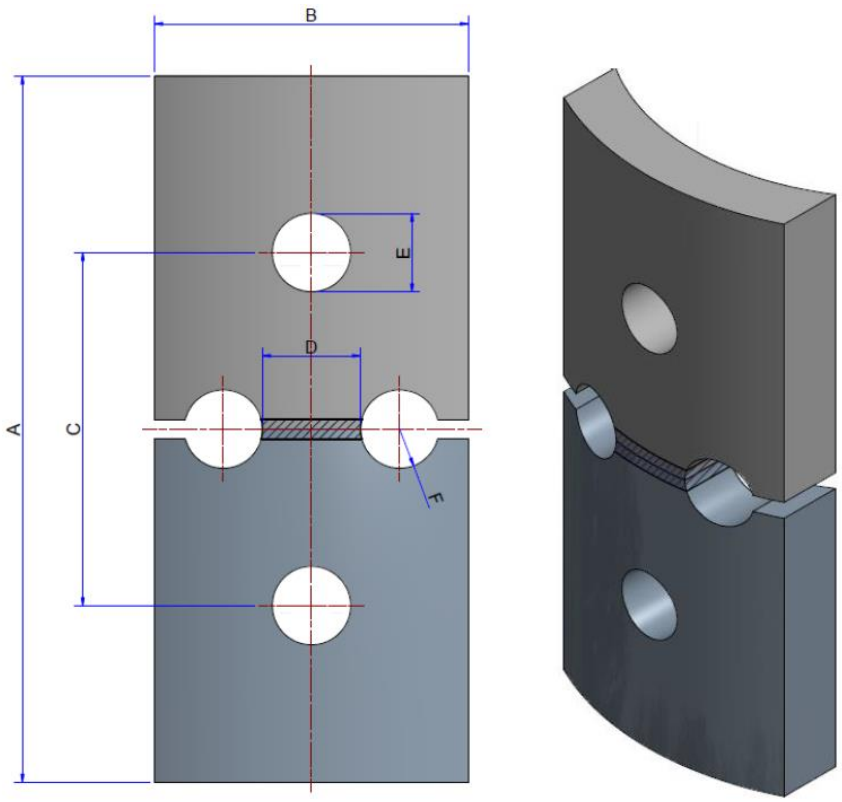

Figure 6-1, reduced section specimen related to the table below

Table 6-1, Dimensions for reduced section specimen geometry given in WIS 4-32-08:2-17 and the proposed optimised geometry from this study

Symbol	**Description**	**WIS 4-32-08**	**Enhanced Geometry (For 30mm Thickness)**
A	Overall length (mm)	≥180	210
B	Overall width (mm)	80	80
C	The distance between loading holes (mm)	90	110
D	Width of waisted section (mm)	25	30
E	The diameter of loading holes (mm)	20	30
F	The radius of the waisted section (mm)	10	10

In Table 6-1, the proposed overall length of the enhanced geometry specimen is 210mm. The overall length of the test specimen should not have a significant effect on the energy to break. It is essential that there is sufficient material between the loading hole and the end of the specimen to prevent the loading pin from pulling out of the hole. In the specimen defined in WIS-4-32-08, the distance between the top of the loading hole and the end of the specimen is 35mm. If this distance is measured in the enhanced specimen geometry, then the proposed overall length of the specimen will be 210mm.

As the thickness does have a direct effect on the deformation, the proposed dimensions for each thickness band is shown in Table 6-2.

Table 6-2, Dimensions for BS EN 12814-7 standard and improved geometry

Parameters	**12814-7 Geometry (Any Thickness)**	**Improved Geometry T<20**	**Improved Geometry 20<T<25**	**Improved Geometry 25<T<30**
Width of Waisted Section (mm)	25	15	25	30
Radius of Waisted Section (mm)	5	10	10	10
Diameter of Loading Hole (mm)	20	20	25	30
Distance Between Loading Hole (mm)	90	100	105	110
Width of Specimen (mm)	60	70	80	80

6.4 Pipe Sizes

To compare the modified geometry with the current standard's geometry using welded specimens, pipes with different dimensions had to be prepared. The requests on quotations were to have all the pipes from the same resin batch and the length to be around 2 meters. Suppliers informed to have resins from one batch is not possible, and the minimum order quantity is 5 meters for each pipe size requested. The main task after finding the right manufacturer was to start the selection process with the least number of pipes and have the maximum combination for different factors. The main factor in this study is the thickness of the pipe, and therefore while selecting the pipe sizes, it is assumed to have a full range of thicknesses. The other factor is to understand the effect of curvature for the pipe, and that is shown with the standard dimension ratio SDR (ratio of the outside diameter to the wall thickness of the pipe) of the pipe.

The pipe dimensions selected for this study are shown in Table 6-3. The thicknesses selected starts from 12.7mm to 57.3mm with an outer diameter of 140mm to 630mm. Pipe sizes with an outer diameter of 160mm and 250mm were explicitly used to have a similar thickness (closest thickness among available pipe sizes) to precisely compare the SDR of the pipe. The other pipe sizes were mainly to check the effect of the thickness except for 140 and 160mm, which provide the closest outer diameter but different thicknesses.

Table 6-3, Pipes used for this study with their dimensions and welding machines used

Outer Diameter (mm)	SDR	Thickness (mm)	No of Welds	Welding Machine
140	11	12.7	4	BF315
160	11	14.5	4	BF315
250	17	14.7	2	BF315
280	11	25.5	2	BF315
500	11	45.5	2	Mc1236
630	11	57.3	2	Mc1236

6.5 Butt Fusion Welding

As mentioned in the literature review section, the principle of the fusion welding technique is to melt two pipe surfaces sufficiently so that molecular segments can diffuse across the contact surface and form bonds in which extend to provide a joint with comparable strength to the parent component. For joining pipes with an outer diameter of lower than 250mm, butt fusion and electrofusion techniques could be used. For PE pipes with an outer diameter greater than 250mm, butt fusion welding is the primary technique, and it is the only technique available for pipes greater than 500mm outer diameter.

The steps for butt fusion welding is shown below in Figure 6-2, Schematic diagram of the pressure cycle during the butt fusion welding process with a few steps before starting this welding procedure. The first step of the welding procedure is placing pipes into the clamp of the butt fusion machine and check for alignment. The next step is trimming the pipe ends to ensure they are flat and square. After these two steps, the primary procedure starts by applying the heater plate and increasing the pressure to reach the bead-up pressure, where the schematic diagram of the pressure cycle is shown in Figure 6-2.

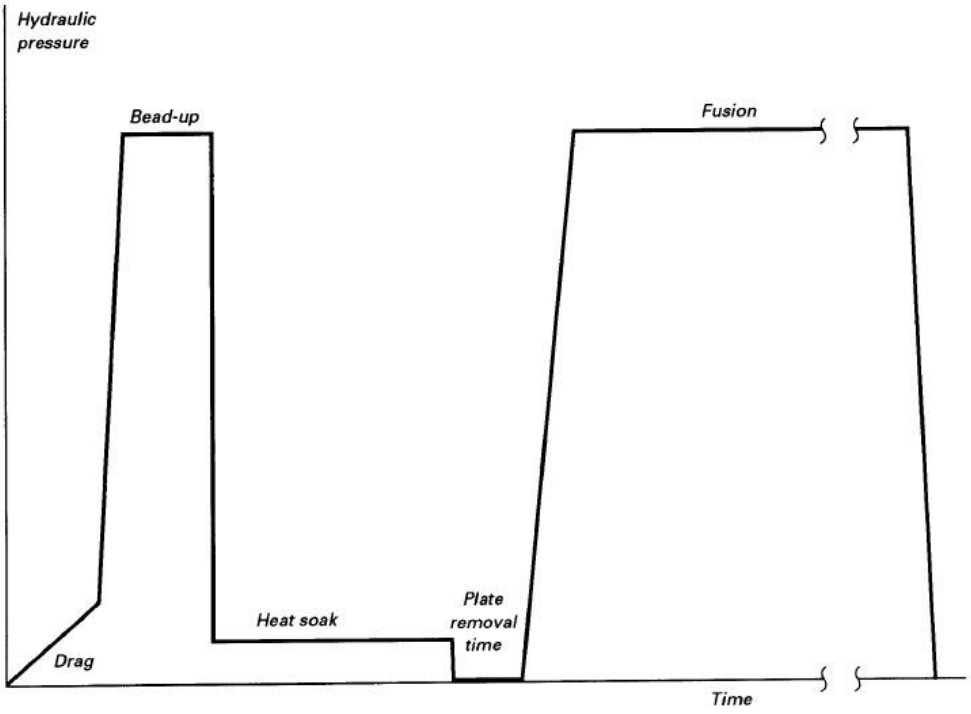

Figure 6-2, Schematic diagram of the pressure cycle during the butt fusion welding process)

To carry out a butt fusion welding, similar welding machine procedures and welding processes apply to pipes with different outer diameter and thicknesses, but the factors such as time, hydraulic pressure and temperature of the heater plate are entirely based on the dimensions and thickness of the pipe.

The standard followed to carry out the welding for this research is DVS 2207-1. As mentioned in the introduction section and shown in the diagram above, the process after alignment and trimming is divided into bead-up, heat soak, changeover and finally joining or fusion.

The bead-up step starts with pressing the pipe surfaces to the heated tool, and it is carried out to make sure all angles and surface area of the pipe is pressing the heated tool. This process is carried out by measuring the bead height. When the bead height has reached an absolute value (0.5mm for pipes up to 355mm and 1mm for pipes with an outside diameter of 400 and 630mm according to DVS-2207-01, Table 8-15), it is an indication that the joining areas are all in contact with the heated tools.

The heat-soak or heating-up stage takes place after the confirmation of full contact between the joining area and the heater plate. The pressure for this process is reduced to zero and the time varies based on the thickness of the pipe.

After completing the heating-up stage, the heated tool should be withdrawn from the welding machine without causing any damage or contamination to the heated joining zones. The changeover stage must take place as quick as possible. Otherwise, the plasticised area will be cooled down. The quality of the weld will be highly be influenced if this procedure is not carried out on the targeted time given in Table 6-4.

Table 6-4, Recommended values for the heated tool butt welding of pipes (DVS-2207-01)

1 Nominal wall thickness s	2 Alignment	3 Heating-up	4 Changeover	5 Joining	
	Heated tool temperature see figure 2		Changeover time (Maximum time)	Joining pressure build-up time	Cooling time under joining pressure (minimum values) $p = 0{,}15\ N/mm^2 \pm 0{,}01$
	Bead height on heated tool on the end of the alignment time (alignment $p = 0{,}15\ N/mm^2$)	Heating-up time =10 x wall thickness $p = \leq 0{,}01\ N/mm^2$)			
mm	mm	s	s	s	min
up to 4,5	0,5	up to 45	5	5	6
4,5 ... 7	1,0	45 ... 70	5 ... 6	5 ... 6	6 ...10
7 ... 12	1,5	70 ... 120	6 ... 8	6 ... 8	10 ...16
12 ... 19	2,0	120 ... 190	8 ... 10	8 ... 11	16 ... 24
19 ... 26	2,5	190 ... 260	10 ... 12	11 ... 14	24 ... 32
26 ... 37	3,0	260 ... 370	12 ... 16	14 ... 19	32 ... 45
37 ... 50	3,5	370 ... 500	16 ... 20	19 ... 25	45 ... 60
50 ... 70	4,0	500 ... 700	20 ... 25	25 ... 35	60 ... 80

The joining or fusion stage takes place when the joining area is pressed together, starting with very low pressure and once reached each other; the pressure increases linearly to 0.15N/mm^2. The joining pressure must be constant during the cooling time (mentioned in Table 6-4). After the cooling time, the pressure can be released, and the pipe with the joint can be removed from the welding machine only if very slight loads applies to the weld.

Welding reports have been prepared for each well and are available for each pipe diameter.

6.6 Pipe with 140mm outer diameter

The first set of experiments were carried out using pipes with 140mm outer diameter. The welding was carried out using a BF315 welding machine, where the welding machine has different advantages and disadvantages.

An advantage of the machine is its automatic feature, where after placing the pipes and selecting welding standard with the right pipe diameter, the welding process can be carried out automatically. However, this automatic feature has a drawback, where each weld is required to be fully completed before starting a new weld. This made the process of dummy welds (used to clean contamination from a hot plate) time-consuming. The only manual works required for this machine is to replace the trimmer with a heater over the welding machine, and the rest of the welding process is carried out automatically.

The primary purpose of these experiments is to compare the standard geometry with the enhanced geometry for welded pipes as well as parent material cut from the pipes. To assure the reliability of the data, for every pipe size, a minimum of 5 repeated specimens for every condition is tested. For every weld or parent pipe, the experiment is designed to cut the modified and standard geometry at adjacent positions. For this case, as the outer diameter is 140mm, a maximum of four specimens could be taken from each weld or parent pipe. The position of each specimen with specimen numbers is provided in Appendix part D (Table 8-9).

The standard and modified geometry dimensions for this set of the experiment are shown in Figure 6-3.

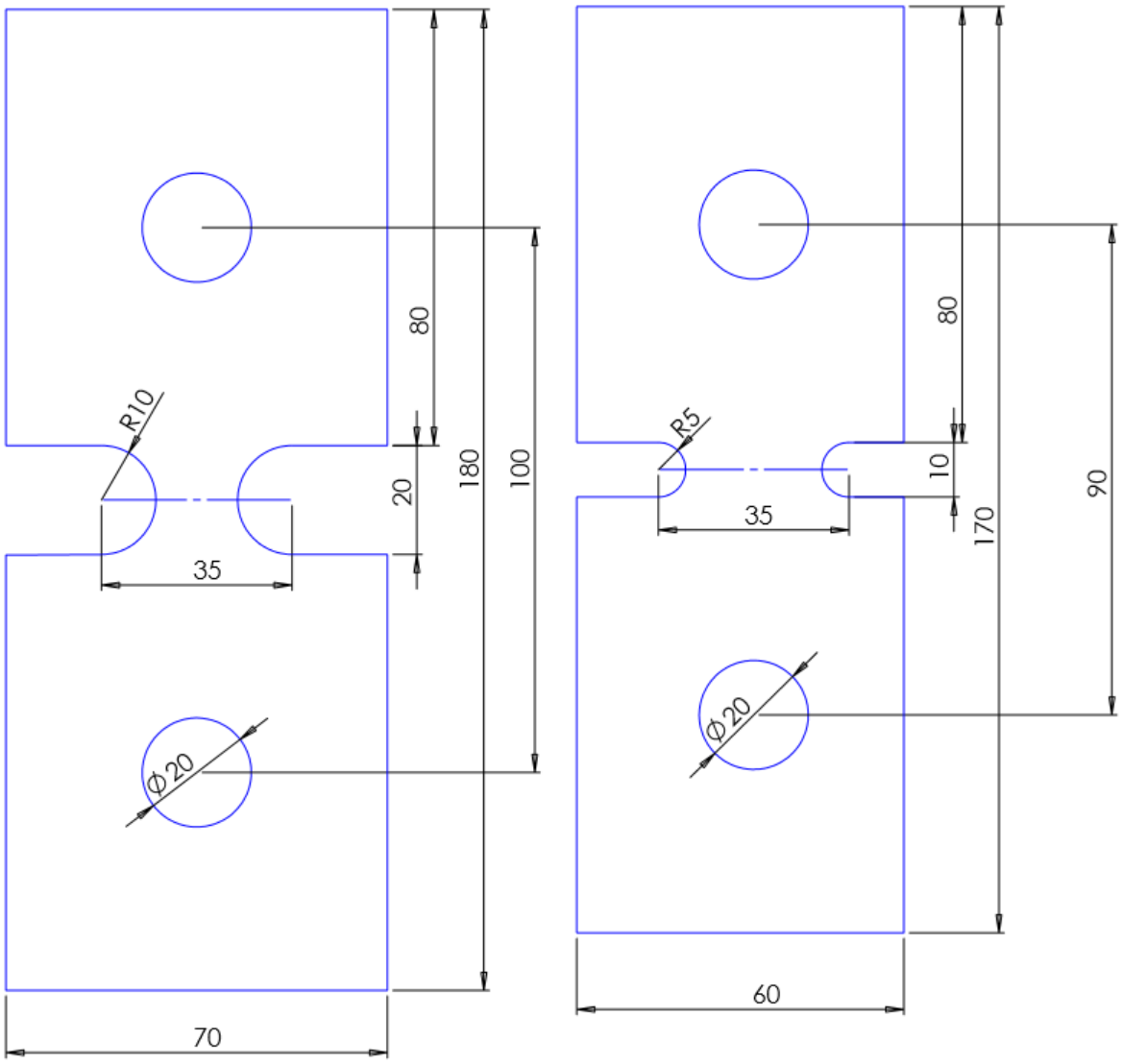

Figure 6-3, Modified geometry on the left used for thicknesses less than 20mm vs standard 12814-7 geometry on the right

The comparison of 140mm pipe for a specimen that is cut from parent pipe material, using standard and modified geometry is shown in Figure 6-4. The graph shows the force-deformation data for both specimens. As the CSA of specimens is different, there is a significant difference in the maximum loads of specimens. The cold drawing region in the modified specimen is much higher than the standard specimen. This proves higher ductility for unwelded modified geometry specimen compared to unwelded standard geometry specimen. The other advantage of the modified specimen geometry is the necking at earlier stages of the test, compared to the standard geometry. When the necking occurs

in earlier stages of the deformation, it is an indication of lower elongation throughout the specimen surface (lower elongations in loading hole diameter), and deformations are likely taking place in the waisted area of the specimen. The fracture surfaces of these two specimens are shown in Figure 6-5, which shows longer elongation for the modified specimen geometry. As discussed in previous chapters, longer elongation is desirable in this application due to providing a suitable condition for the welded area to be assessed.

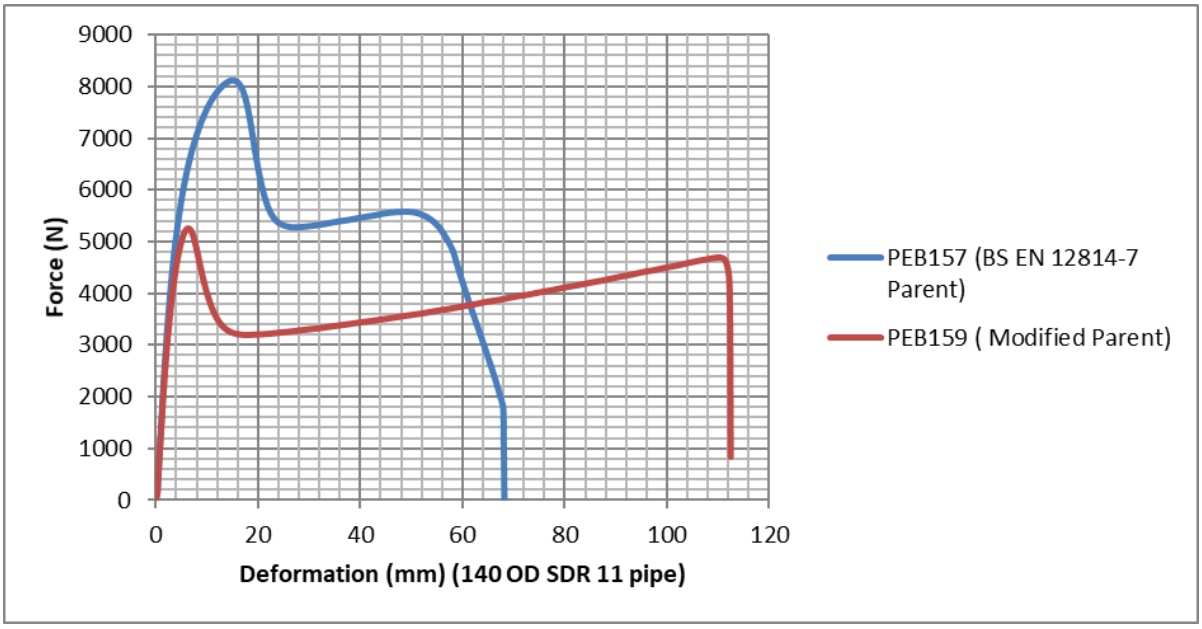

Figure 6-4, Force-Deformation graph for modified and standard geometry on unwelded 140mm OD pipe

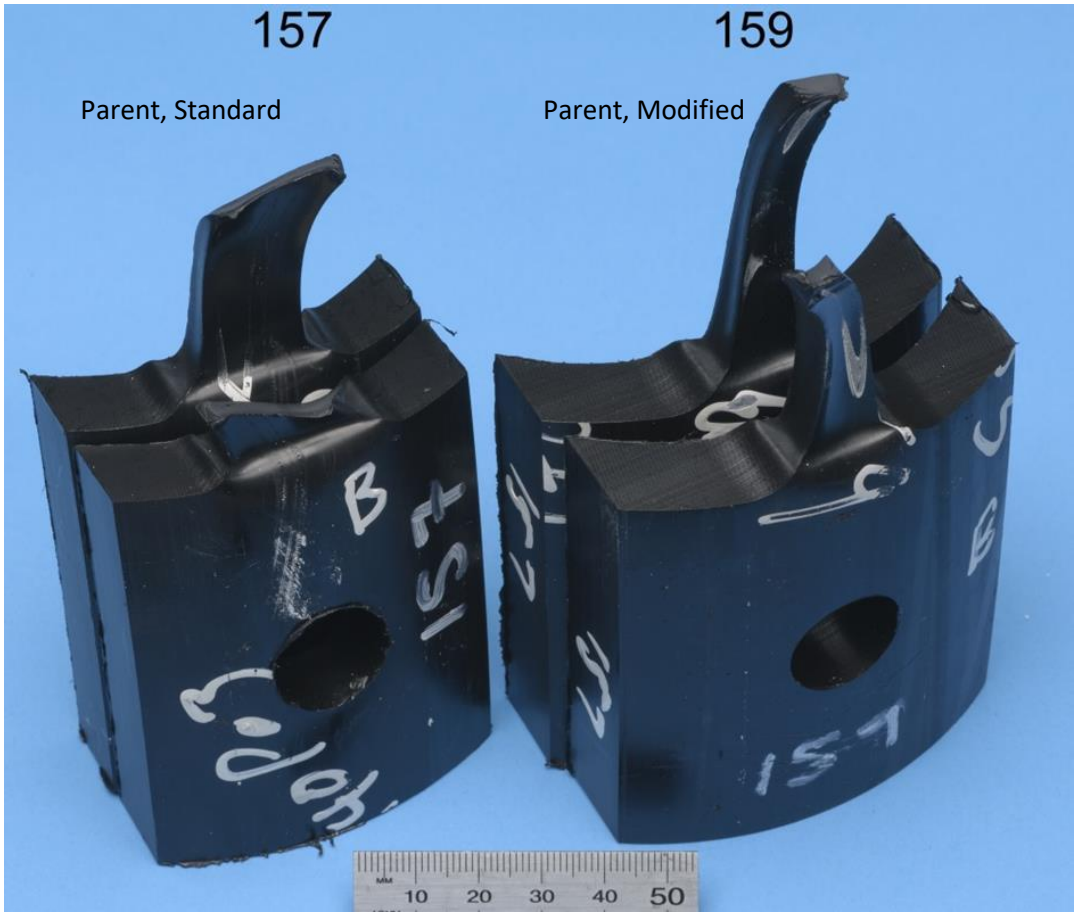

Figure 6-5, Fracture surface of the parent standard on the left and parent modified geometry on the right from 140mm OD pipe

As the CSA is different for the mentioned specimens, the force is divided by the CSA to provide nominal stress and allow a uniform comparison condition (Figure 6-6). In this figure, it is shown how the modified geometry has improved the deformation in the specimen comparing to the standard geometry. Necking also starts at an earlier stage which is a great indication of lower elongation in holes.

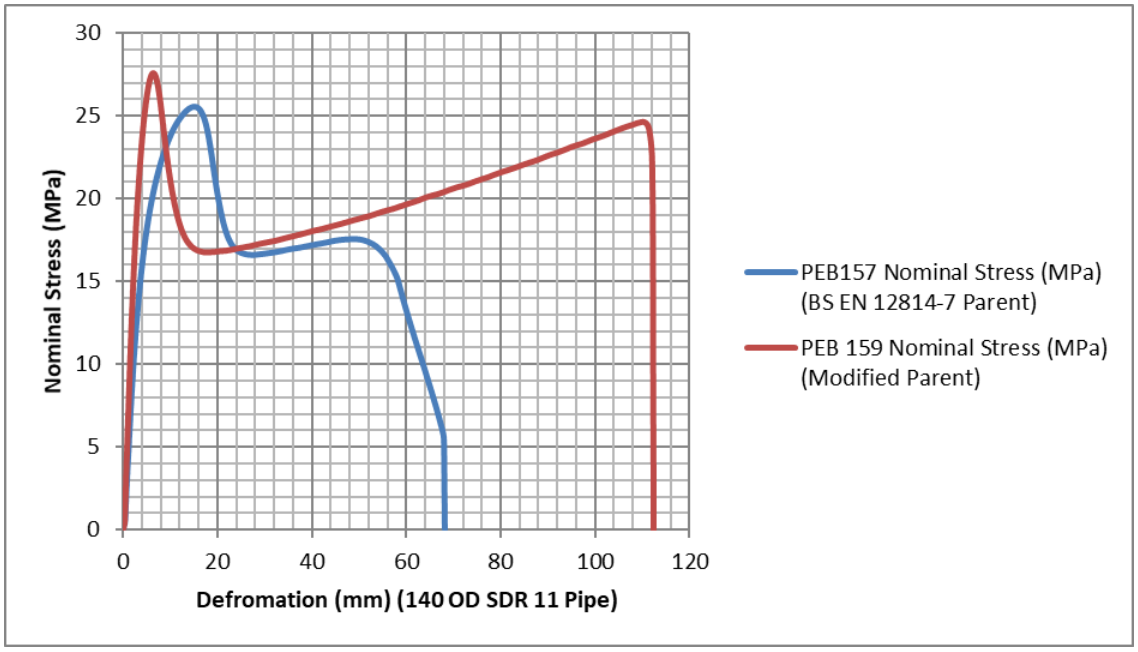

Figure 6-6, Nominal stress-Deformation graph for modified and standard geometry on unwelded 140mm OD pipe

The next set of comparison shows the two specimens (modified and standard) from welded pipes. Their positions are adjacent to each other on the pipe to minimise uncertainties affecting the result of the tensile tests introduced by heater plate or extrusion machines. In both specimens, cold drawing region has disappeared, which is due to having an additional material with different material property (weld) as well as the effect of the shape produces by the beads (Figure 6-7).

The fracture surfaces shown in Figure 6-8 indicate ductility for both modified and standard geometry with elongations in both cases. Specimens that have formed one of the welded pipes, including two modified and two standard geometry, are shown in Figure 6-9, and ductility can be confirmed in all cases.

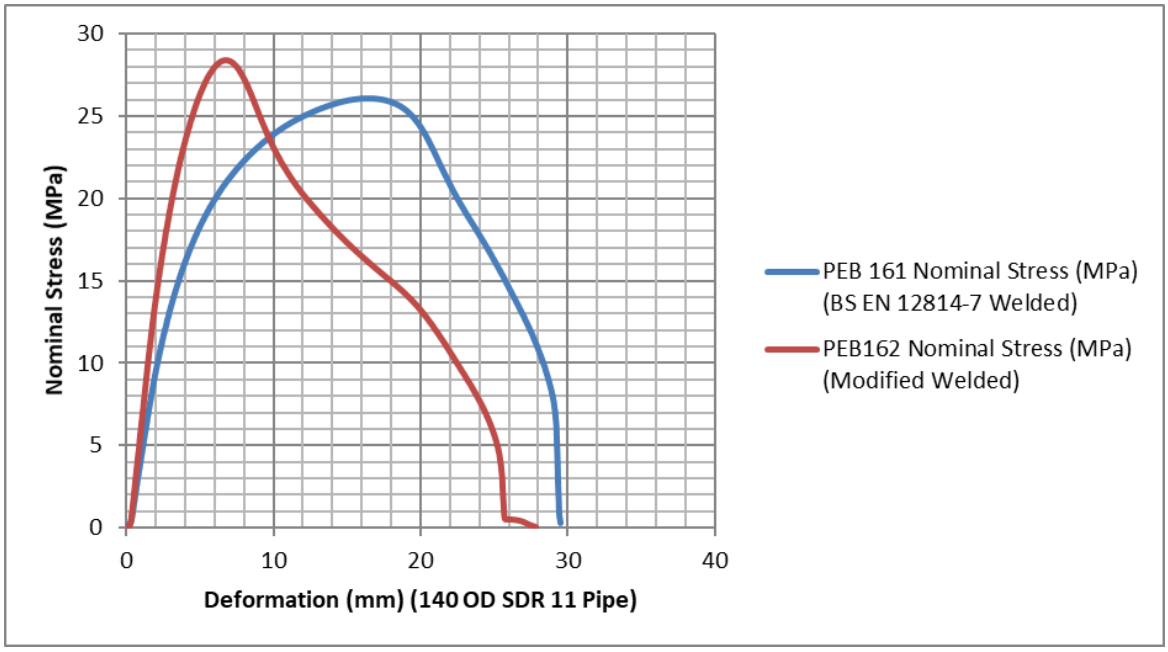

Figure 6-7, Nominal stress-Deformation graph for modified and standard geometry on welded 140mm OD pipe

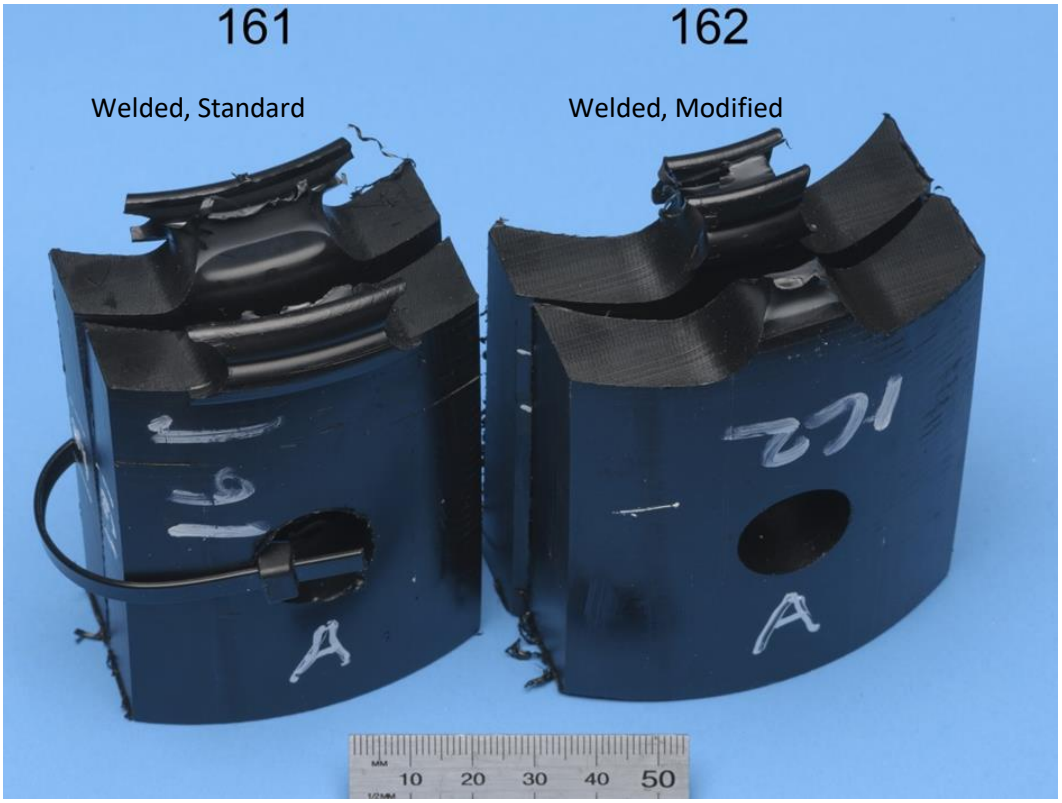

Figure 6-8, Fracture surface of the welded standard specimen on the left and welded modified specimen geometry on the right from 140mm OD pipe

Figure 6-9, From Left, the fracture surface of standard, modified, standard and modified specimen geometry from 140mm OD welded pipe

For 140mm OD welded pipe, one experiment is carried out where the weld beads are removed internally and externally. The comparison graph for modified and standard geometry specimens from welded pipes without beads are shown in Figure 6-10. Cold drawing region can be observed in the graph, which confirms the effect of the beads on the specimen. Taking beads off from the welded pipes has led to more elongation in both specimens using both standard and modified geometry. The fracture surfaces for these specimens are shown in Figure 6-11. Comparison of these fracture surfaces indicates a longer elongation in the welded area for modified specimen geometry, despite a more extended deformation in the tensile test for the whole standard geometry.

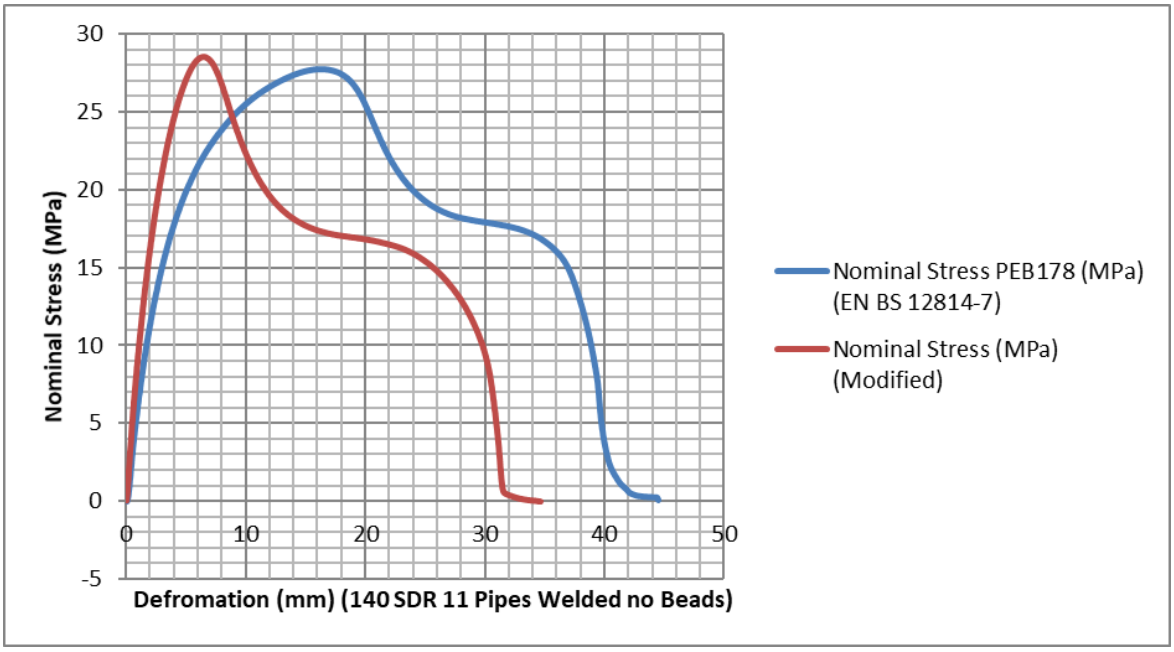

Figure 6-10, Nominal stress-Deformation graph for modified and standard geometry on welded with beads off on 140mm OD pipe

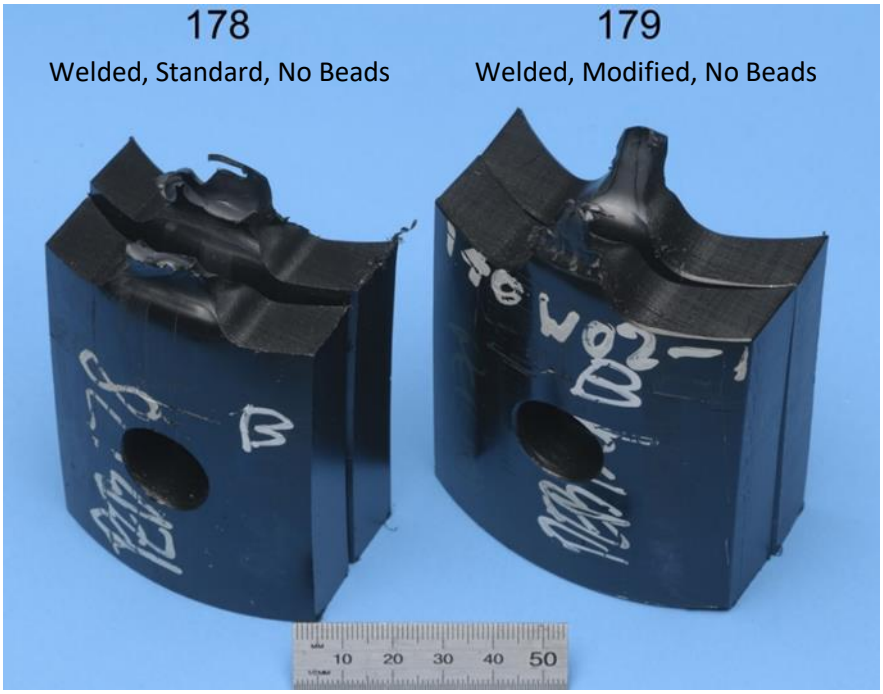

Figure 6-11, Fracture surface of the welded standard specimen on the left and welded modified specimen geometry on the right from 140mm OD beads off pipe

Total energy per CSA for different conditions of 140mm OD SDR 11 pipe is shown in Figure 6-12. The conditions shown are; standard and modified specimen using the unwelded welded and welded pipes with no beads. Each bar represents the average of five samples, with error lines representing the standard deviation for the five repeated experiments carried out for 140mm OD pipes.

From Figure 6-12, it can be seen that the modified specimen using unwelded pipe provides the maximum total energy per CSA. When comparing the specimens with the welded condition, the modified geometry did not provide higher total energy compared to the standard geometry specimen. However, as can be seen in the graph, the energy indicated in the modified geometry test is a better indication of the energy consumed in the waisted area of the specimen. On conditions where beads are taken off, the total energy is higher compared to the welded with beads, despite removing the extra material from around the welded area. This can be due to a more uniform cross-sectional area of the specimen, which allows longer necking.

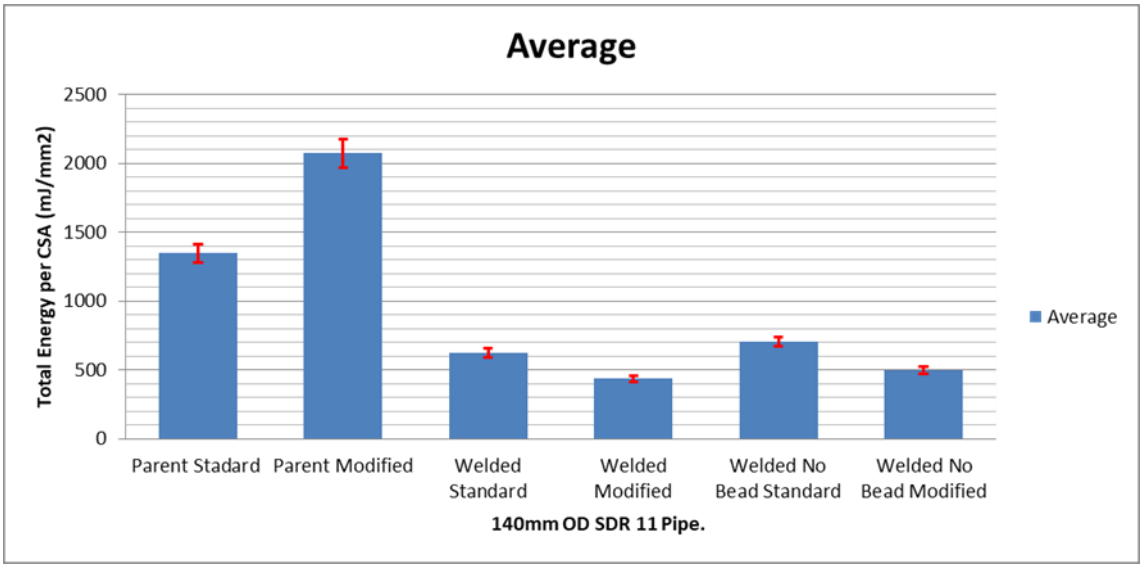

Figure 6-12, Total Energy per CSA for different scenarios on 140mm OD SDR 11 pipe

6.7 Pipe with 160mm outer diameter

Similar to 140mm OD pipes, welding is carried using a BF315 welding machine. The modified geometry for lower than 20mm is the geometry used for specimens with a thickness of lower than 20mm.

The first comparison is provided for a standard against modified geometry using unwelded pipe specimens (Figure 6-13). The specimen with modified geometry provides a much larger elongation compared to standard geometry, which is more desirable in this application.

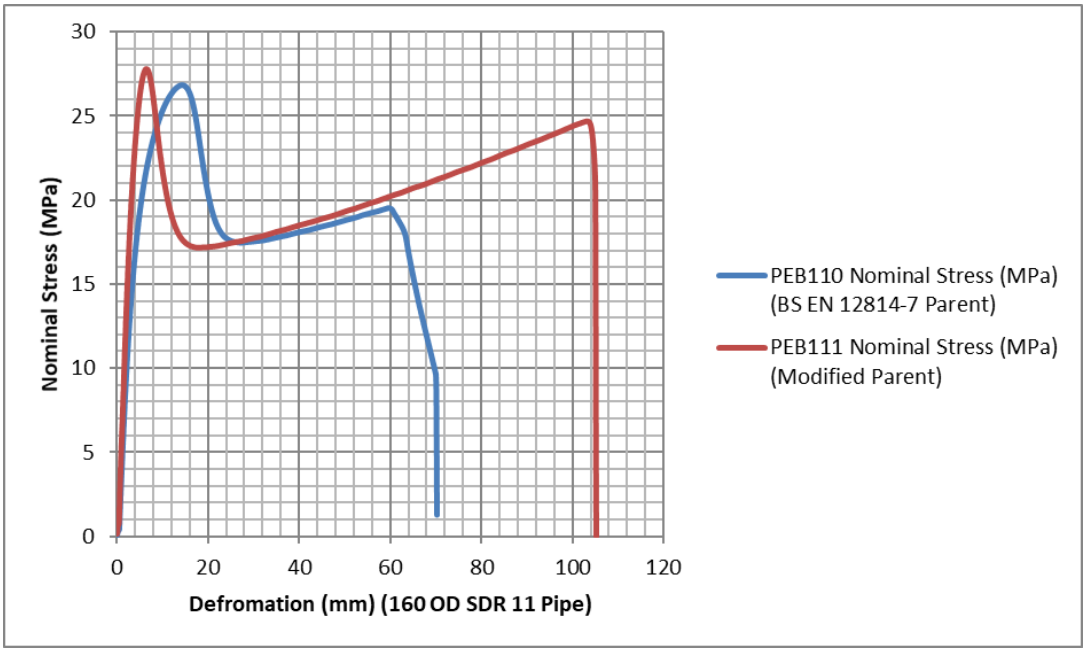

Figure 6-13, Nominal stress-Deformation graph for modified and standard geometry on parent 160mm OD pipe

The next comparison is provided for modified and standard specimen geometry for 160mm OD welded pipes. From the graph in Figure 6-14, necking starts after ~ 7.5mm deformation on the modified specimen, whereas the necking starts after about 16mm deformation on the standard geometry. This suggests that, despite the larger area under the curve (energy consumption) for

standard geometry, the data in modified geometry represent the energy consumed are mainly in the area of interest (waisted region of the specimen).

The fracture surfaces for standard and modified geometry of 160mm OD welded pipe is shown in Figure 6-16. For four cases of parent and welded specimen using standard and modified geometry, comparison of the average energy per CSA for these different conditions are shown in Figure 6-15. Modified specimen provided the largest energy to break value, and welded modified specimen provided lower total energy compared to the standard geometry. However, it is a better indication of energy consumed in the welded area due to necking initiating at earlier stages of the tensile test.

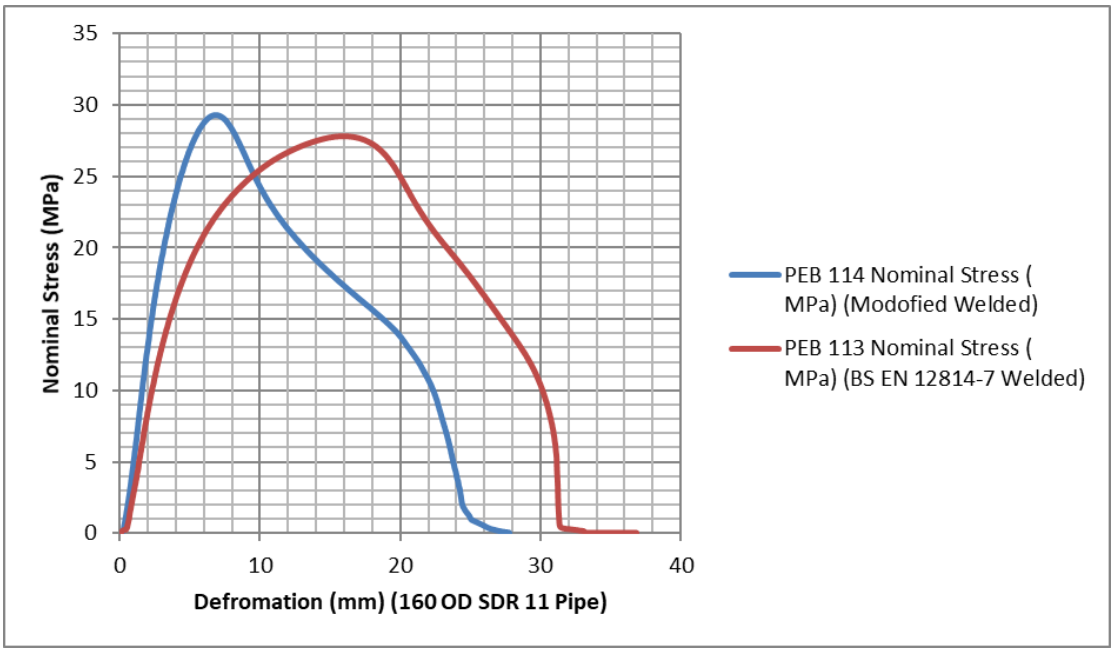

Figure 6-14, Nominal Stress-Deformation graph for modified and standard geometry on welded 160mm OD pipe

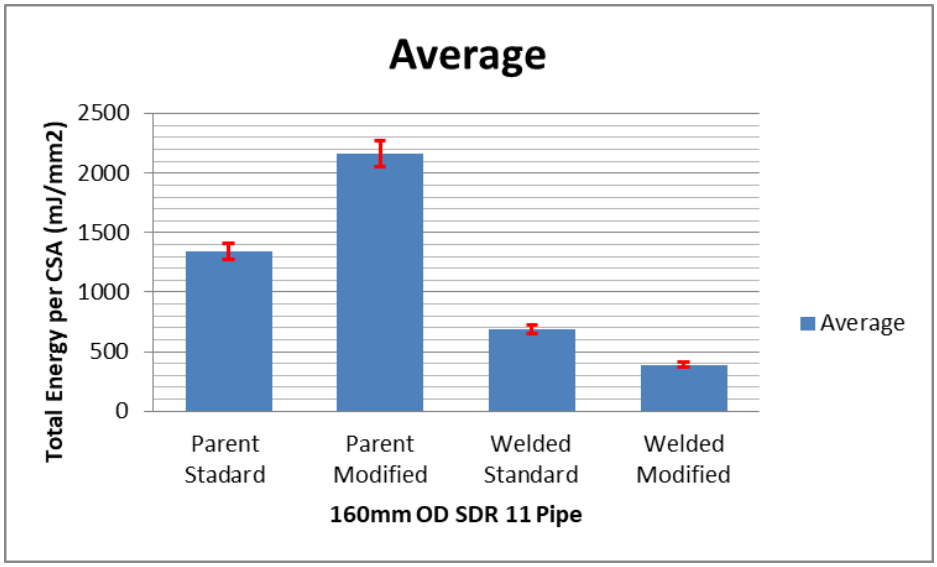

Figure 6-15, Total Energy per CSA (mJ/mm^2) for different scenarios on 160mm OD SDR 11 pipe

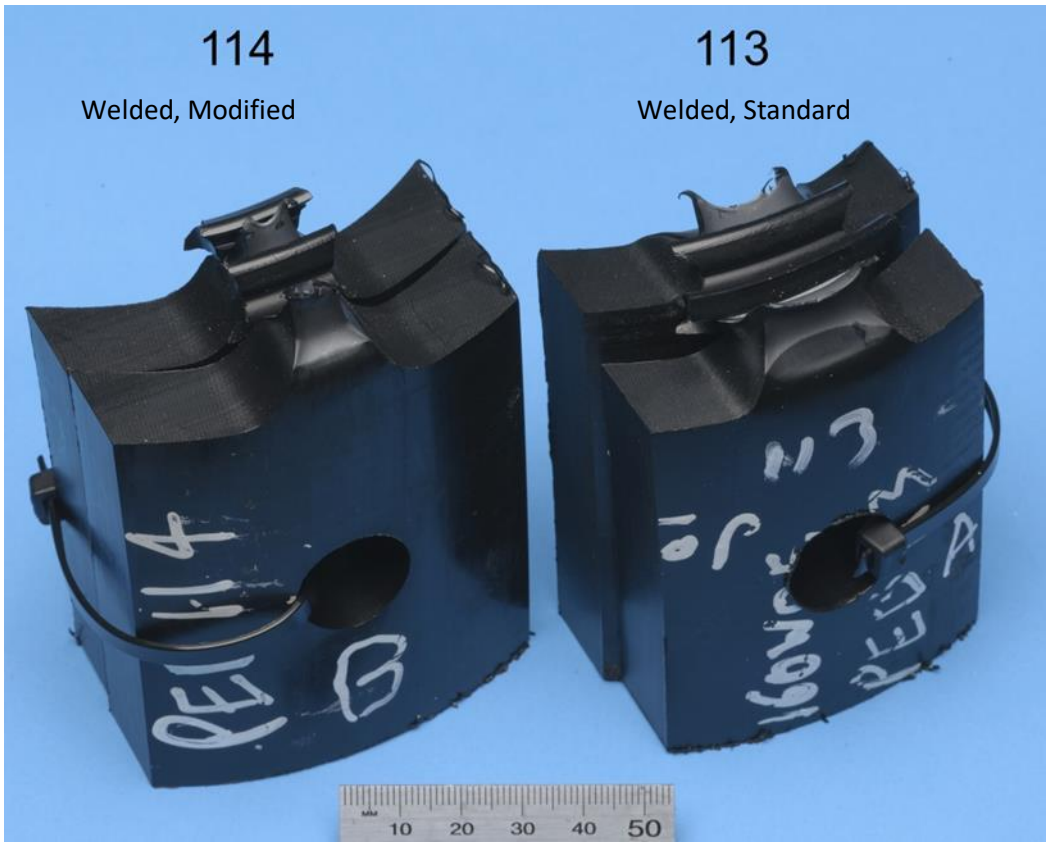

Figure 6-16, Fracture surface of the welded modified specimen on the left and welded standard specimen geometry on the right from 160mm OD pipe

6.8 Pipe with 250mm outer diameter

This experiment is carried out on 250mm SDR 17 pipes which are the only pipes with SDR 17 in this study, whereas the other pipes are SDR11. Similar to 140mm and 160mm OD pipes, the geometry for specimens with a thickness of less than 20mm is used against the standard geometry. The experiment is carried out on both the unwelded and welded pipes. Welding is carried out using the BF315 machine. The result for the unwelded specimen is similar to 140mm and 160mm OD pipe cases. The modified geometry has larger elongation and earlier necking stage compared to the standard geometry (Figure 6-17).

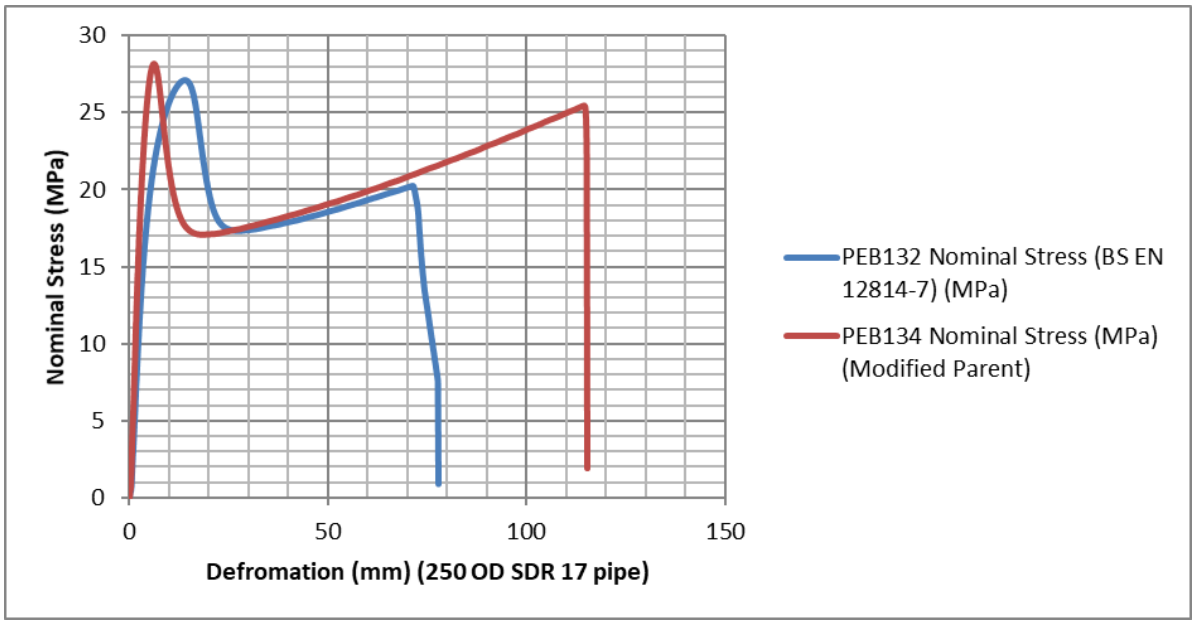

Figure 6-17, Nominal stress-Deformation graph for modified and standard geometry on parent 250mm OD pipe

Figure 6-18, which confirm longer elongation in modified geometry. For welded case, similar to 140mm and 160mm pipes, the necking started in much earlier stages compared to the standard geometry, which means again, the energy for the modified geometry is mainly consumed to elongate the waisted area (Figure 6-19). Fracture surfaces of these conditions are shown in Figure 6-21, in which

all fracture surfaces pass the welding criteria and count as ductile failure. Figure 6-20 shows the comparison of energy to break values for different cases with more considerable value for parent modified condition, which is approximately twice as the standard parent material. The standard deviation value is at its highest for parent modified, which indicates the differences between energy to break the value of specimens.

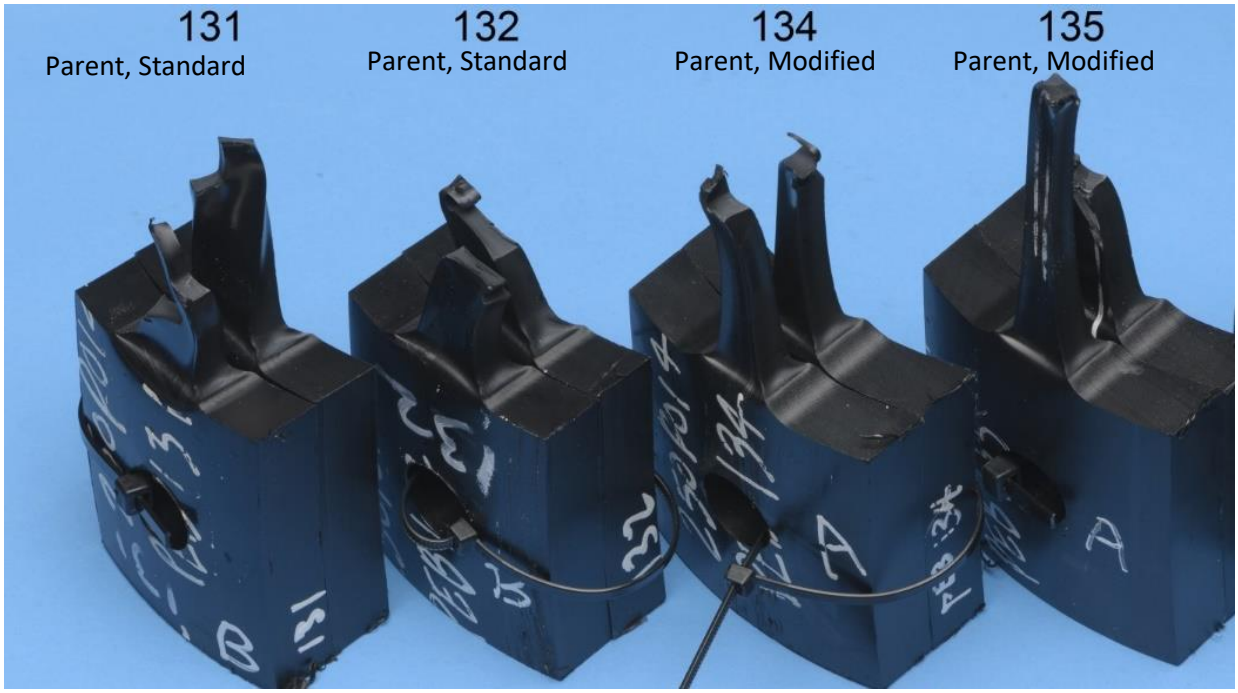

Figure 6-18, From left, fracture surface of standard, standard, modified and modified specimen geometry on 250mm OD parent pipe

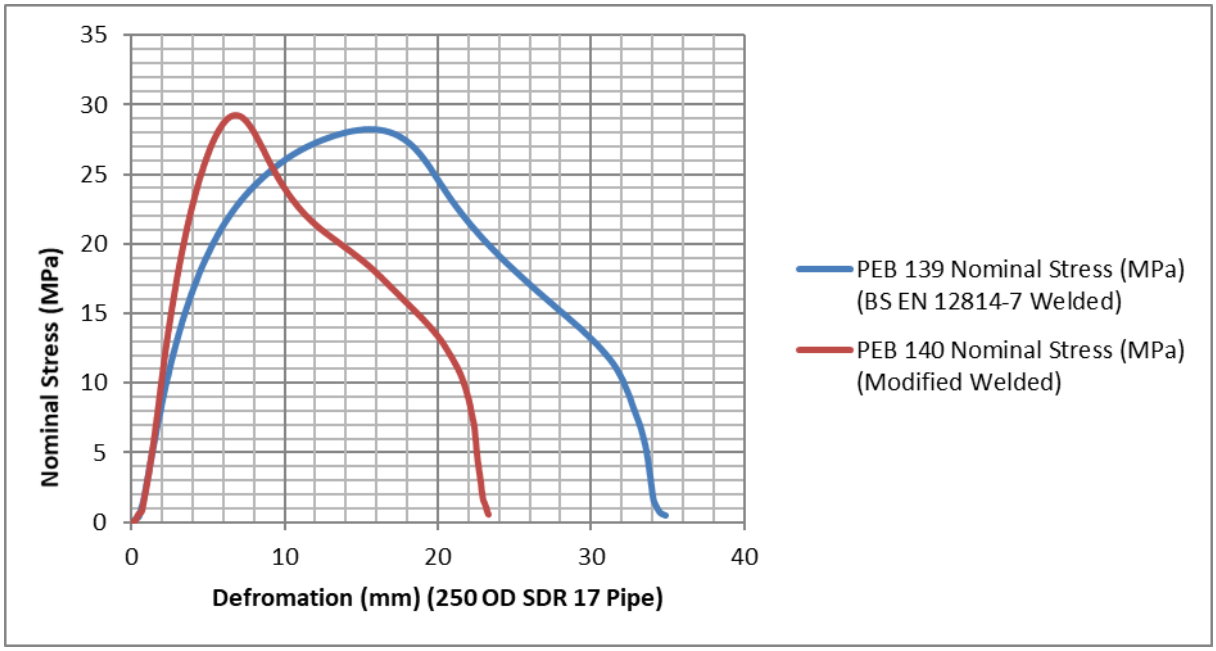

Figure 6-19, Nominal stress-Deformation graph for modified and standard geometry on welded 250mm OD pipe

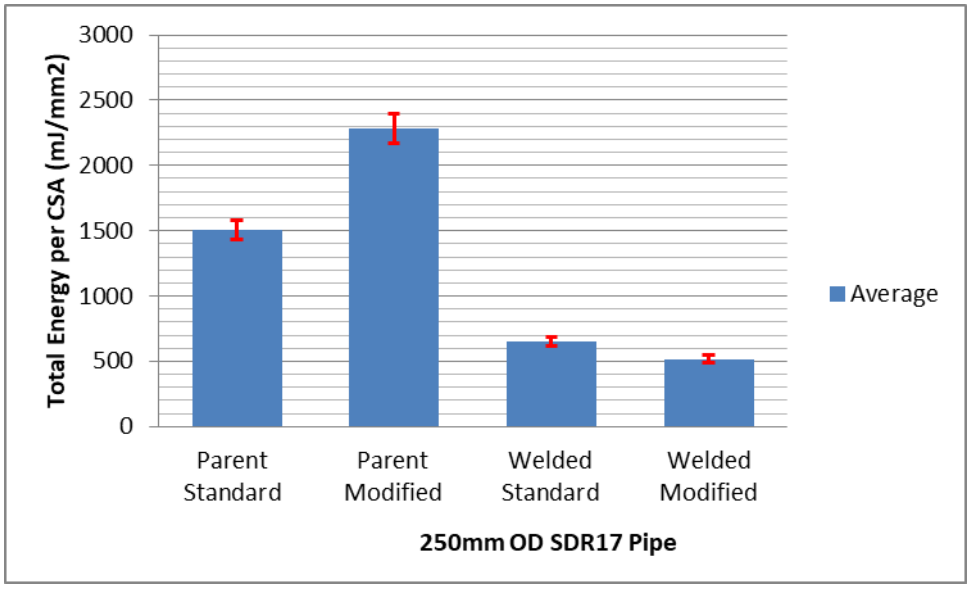

Figure 6-20, Total Energy per CSA (mJ/mm^2) for different scenarios on 250mm OD SDR 17 pipe

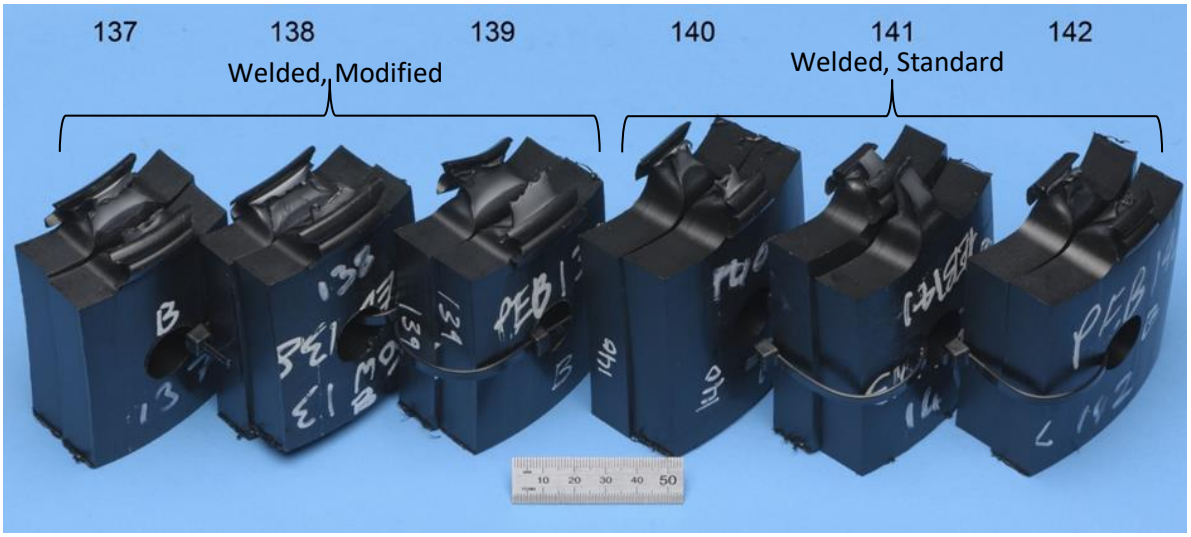

Figure 6-21, From left, fracture surface of modified, modified, modified, standard, standard and standard specimen geometry on 250mm OD welded pipe

6.9 Pipe with 280mm outer diameter

For 280mm OD pipe, the wall thickness is ~ 25.5mm. Therefore the modified geometry for a specimen with a wall thickness of between 25mm to 30mm is used. The standard geometry next to the modified geometry used for this set of the experiment can be seen in Figure 6-22. As it was mentioned in previous chapters, thickness is one of the main factors affecting the failure modes of the specimen.

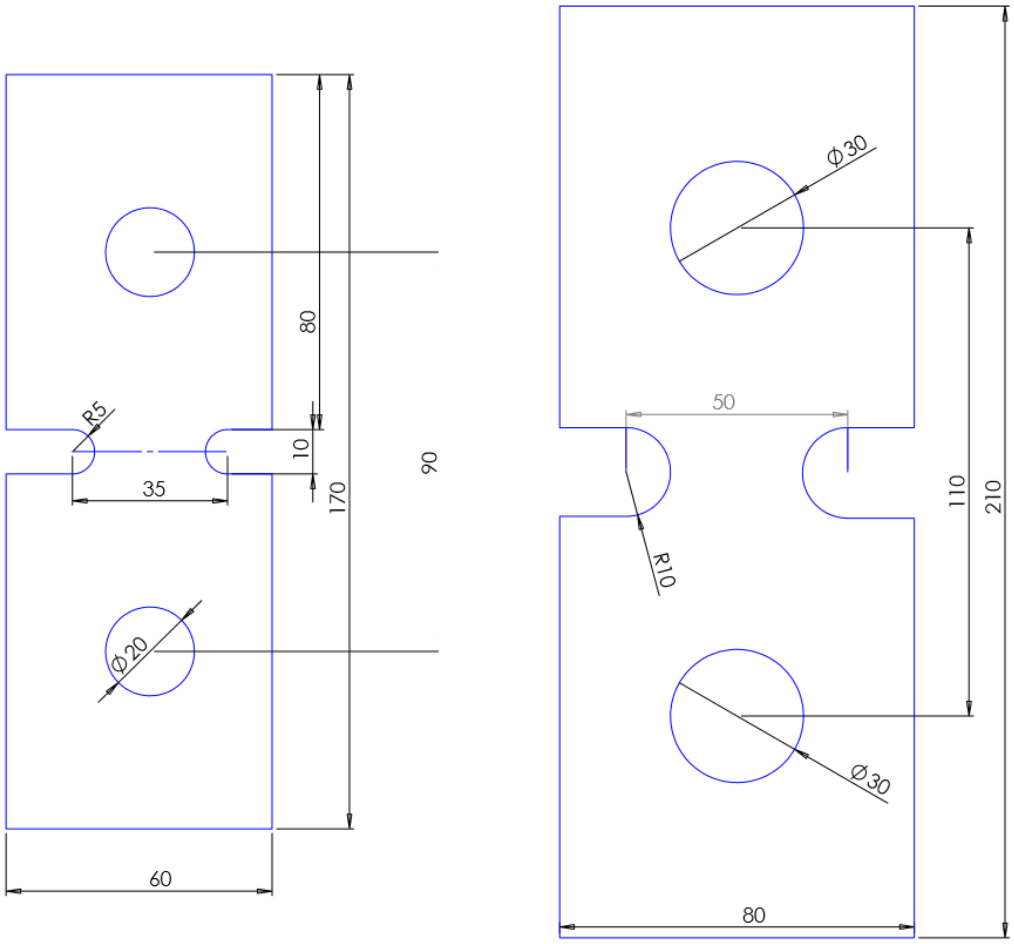

Figure 6-22, from left to right, standard and modified geometry used for thickness in between 25mm and 30mm

When the tensile test is applied to the standard specimen on the unwelded pipe situation, the specimen did not experience any elongation or cold drawing and resulted in a rapid failure after necking. In opposite, the modified geometry did go through a complete cold drawing region and failed from tearing (shear yielding) at the end of the test (Figure 6-23). This highlights the standard geometry challenges where ductile failures do not occur despite using unwelded parent material. As discussed in the introduction, this standard has been used in industrial applications for a long time; however, this geometry is not necessarily providing useful information about the weld's quality. Our proposed modified geometry overcomes this challenge by providing desirable ductile failures in all parent pipe specimens.

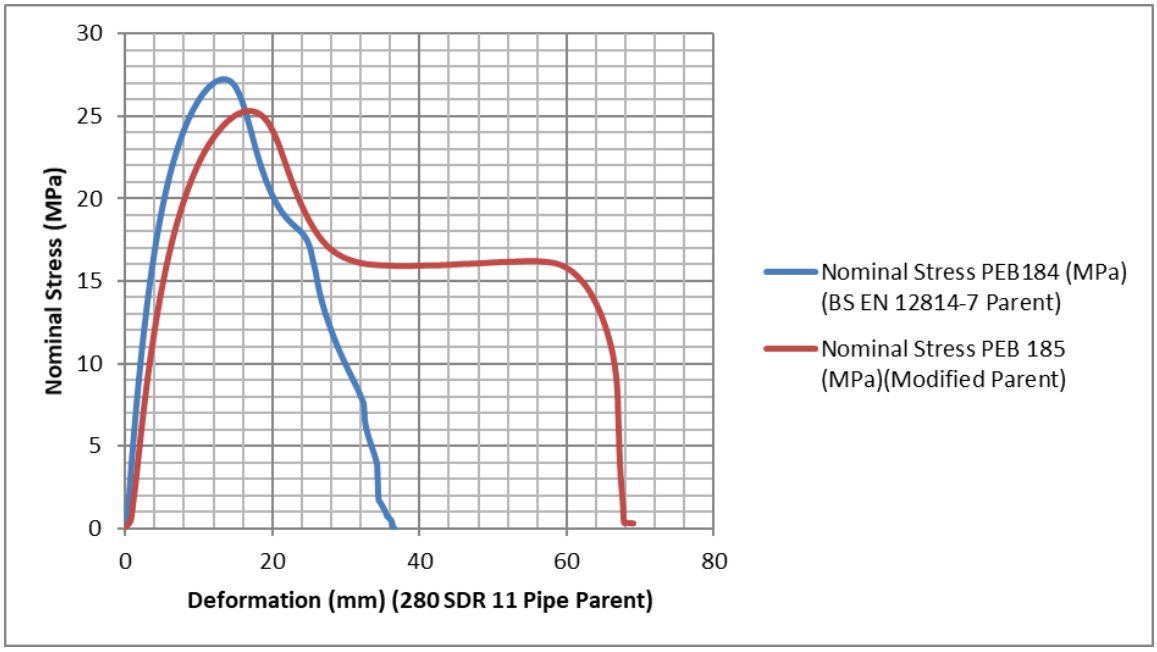

Figure 6-23, Nominal stress-Deformation graph for modified and standard geometry on parent 280mm OD pipe

The same geometries are applied to the welded specimen, where the comparison is shown in Figure 6-24. As expected in welded condition, the specimen with standard geometry failed just after the necking point, whereas the modified geometry had more drawing before the failure. The fracture surface for this condition is shown in Figure 6-25, where more ductility can be seen on the modified geometry. From the fracture surface of these specimen in Figure 6-25, the fracture surface of the specimen using standard geometry does not contain any yielding or drawing in its surface and contains large number dots, which have been the points of failure for this specimen geometry. By checking these two fracture surfaces, it is clear that the failure mechanism for these specimens is different. Two more specimens from the same pipe and weld are shown for 280mm pipes which are Figure 6-28 and Figure 6-29.

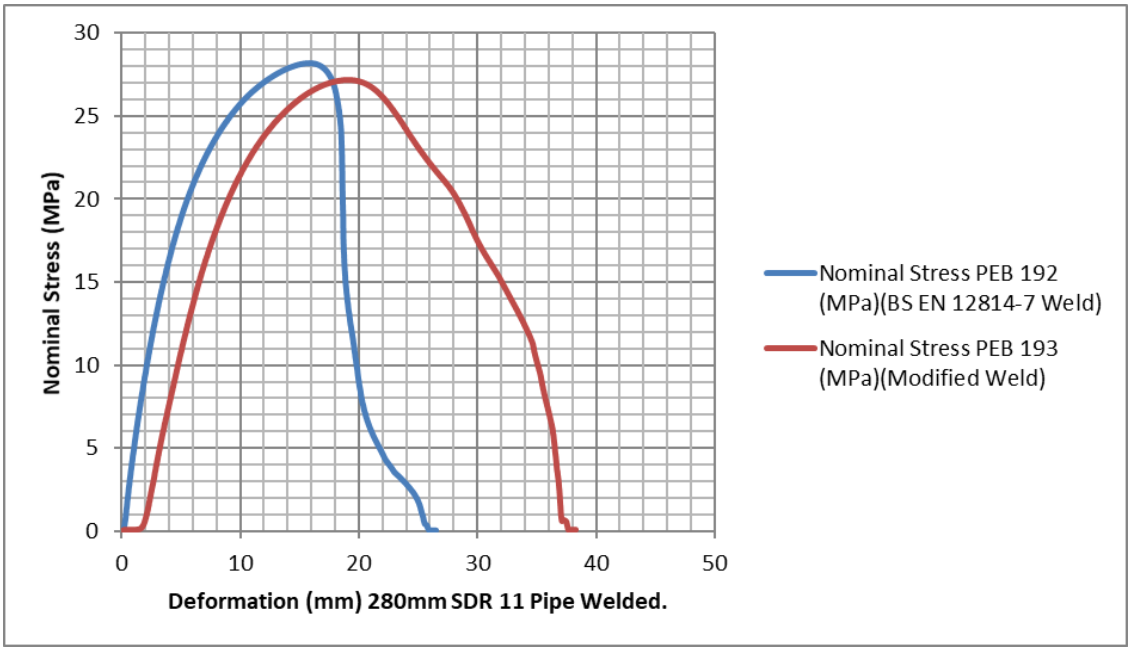

Figure 6-24, Nominal stress-Deformation graph for modified and standard geometry on welded 280mm OD

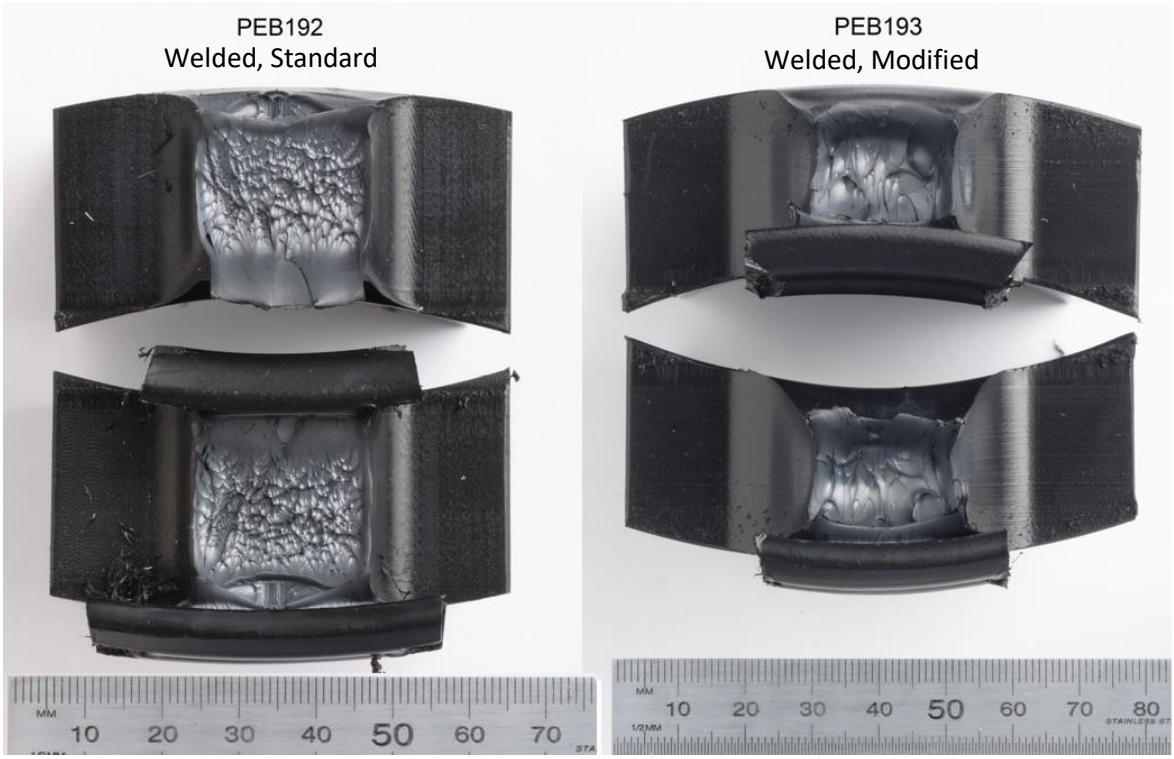

Figure 6-25, Fracture surface of the welded standard specimen on the left and modified welded geometry on the right from welded 280mm OD pipe

For both conditions of the welded and unwelded specimen, five samples are selected for each geometry. The chart given in Figure 6-26 shows that the modified geometry for both conditions has higher energy to break values compared to the standard geometry. Unwelded condition using modified geometry provided the most substantial energy to break value, which is approximately twice as the energy to break for standard geometry on unwelded parent pipe. As expected, the welded specimen using the standard geometry has the lowest energy to break value which can be seen in the graph provided as well as their fracture surfaces.

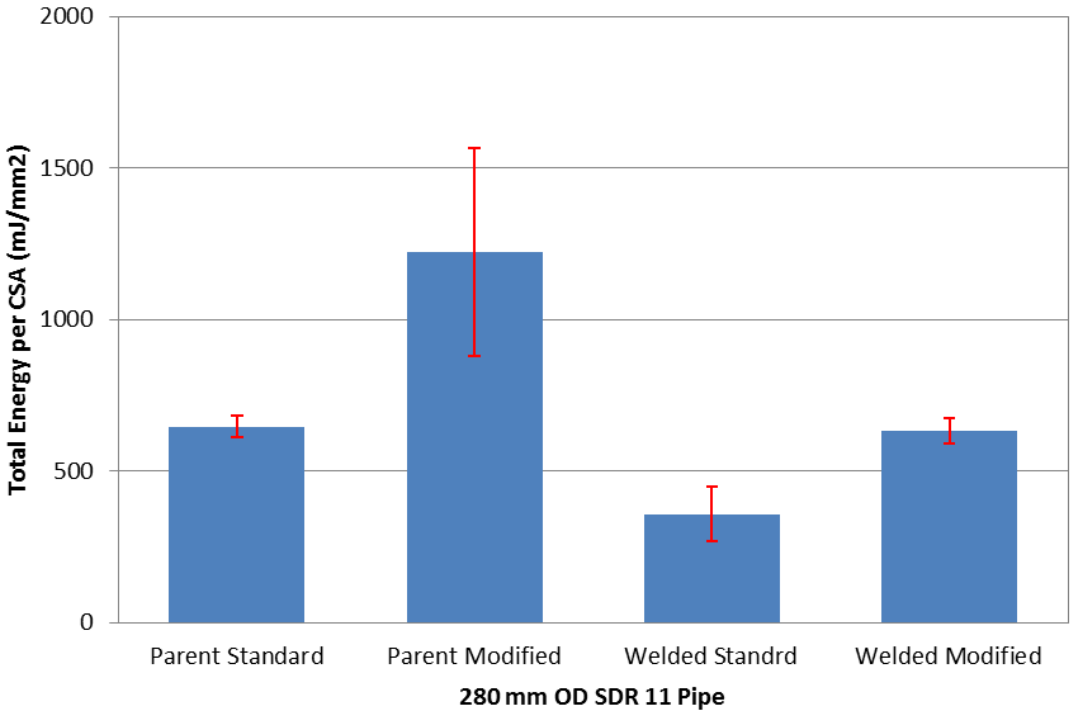

Figure 6-26, Total Energy per CSA (mJ/mm^2) for different cases on 280mm OD SDR 11 pipe

Fracture surfaces for welded 280mm OD pipes are shown in Figure 6-27. As mentioned earlier, the position for each specimen is selected to have the standard and modified geometries adjacent to each other in a particular weld or pipe. As can be seen in Figure 6-27, the specimen with wider widths are the specimens with modified geometries, which indicates more elongation at their fracture surfaces compared to the standard geometry (Figure 6-28).

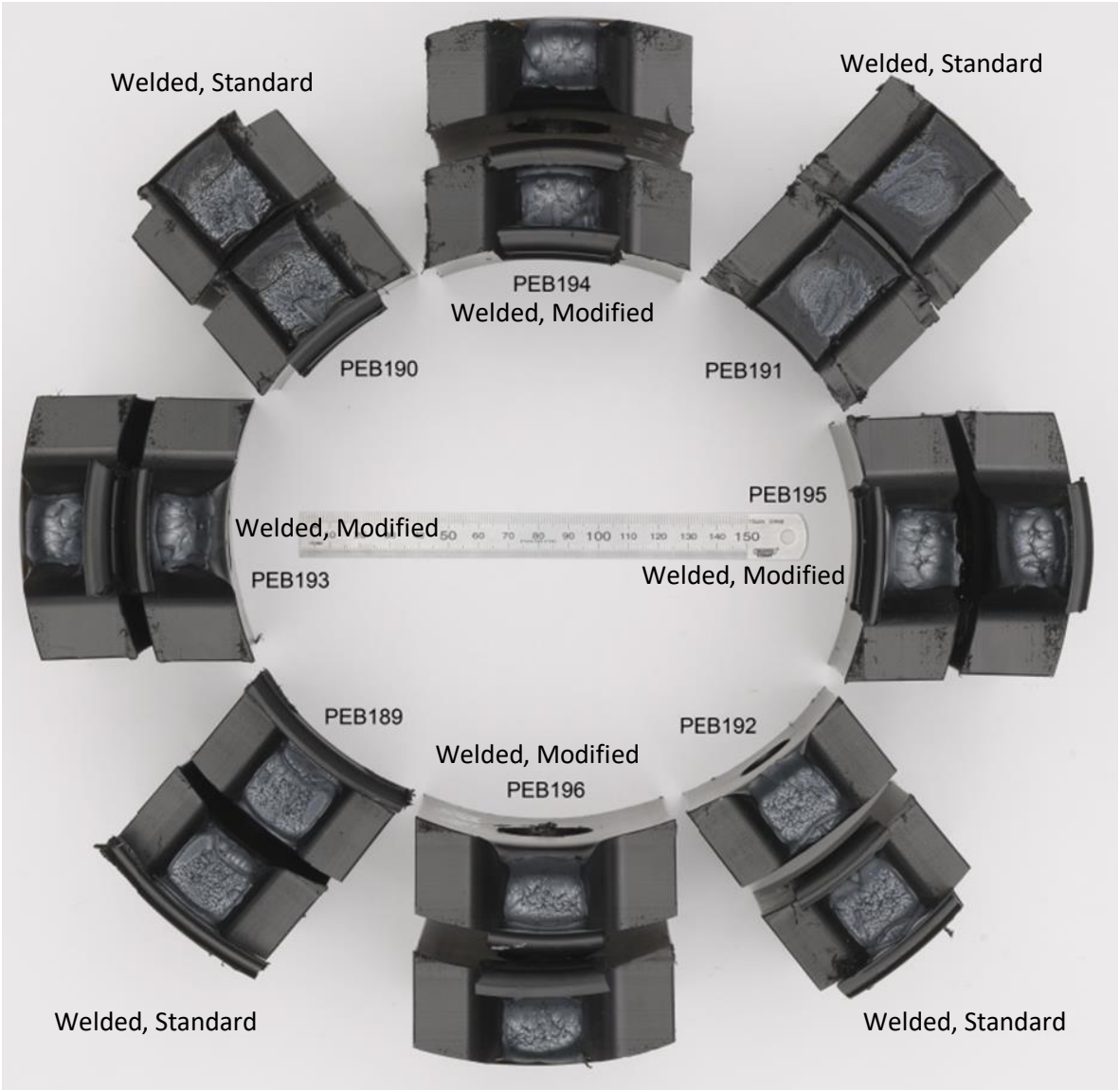

Figure 6-27, Fracture surface for welded 280mm OD pipe using standard and modified geometry

Figure 6-28, Fracture surface of modified welded specimen from 280mm pipe (PEB195)

Looking at the specimen (PEB 191) at one o'clock position shown in Figure 6-27, which is a standard (BS EN 12814-7) geometry, it can be seen that the specimen did not experience any elongation and the fracture surface is entirely flat. This brittle fracture surface does not repeat for the neighbouring specimens (PEB 194 &195), as modified specimen geometries are used. This also proves that the fracture surface of (PEB 191, Figure 6-29) exhibits poor/flat condition, which is not representing the quality of the weld, as changing the specimen geometry (modified geometry) has fully transformed the fracture surface of the specimens from the same weld.

Figure 6-29, Fracture surface of standard welded specimen from 280mm pipe (PEB191)

6.10 Pipe with 500mm outer diameter

For 500mm OD pipes different welding machine, called MC1236, is used. Welding for 500 and 630mm pipes was one of the most challenging tasks in this research. Operating the machine required extensive training by McElroy Manufacturing. Pipes were placed and removed from the welding machine using a 5-ton overhead crane. Some of the welding steps using this machine are shown in Figure 6-30.

Figure 6-30, From top left clockwise, Trimming, pipe position in the machine, heater plate in place, final weld

Each weld for 500mm and 630mm pipe diameters provide enough number of specimens for the experiment (more than 10), but for assurance, two welds are produced for each pipe size. Welding reports with corresponding graphs are available in Appendix D.

Thickness for 500mm OD Pipe is 45.5mm, therefore as WIS-32-04-08 standard suggested and findings presented in chapter 5 recommended, the modified geometries for this experiment are cut to half from the middle. It is also discussed in chapter 5 that specimen with a large thickness (over 20mm)

under tensile stress, undergo a large stress triaxiality states which do not allow ductile failure to take place.

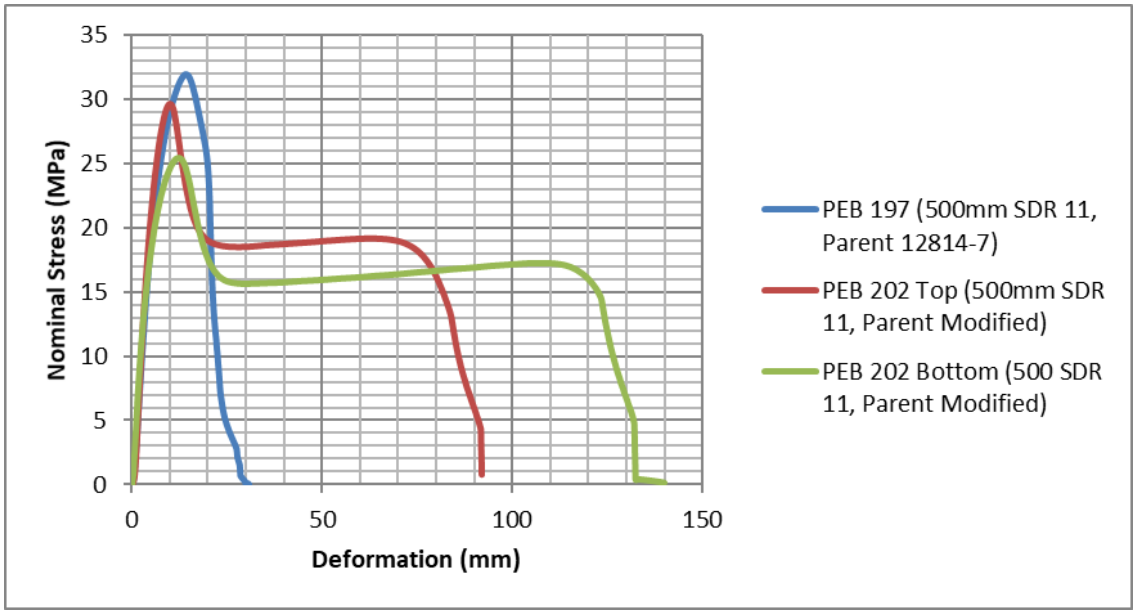

Figure 6-31, Nominal Stress-Deformation graph for modified and standard geometry on parent 500mm OD SDR 11 pipe

Two specimens from the parent pipe are tested, one using standard geometry (BS EN 12814-7) and one using modified geometry. The modified specimen geometry specimens were cut from the middle, and the nominal stress-deformation graph for these specimens are shown in Figure 6-31. From the same figure, it could be seen that the standard geometry hardly goes under any deformation, whereas the modified ones provide desirable elongations.

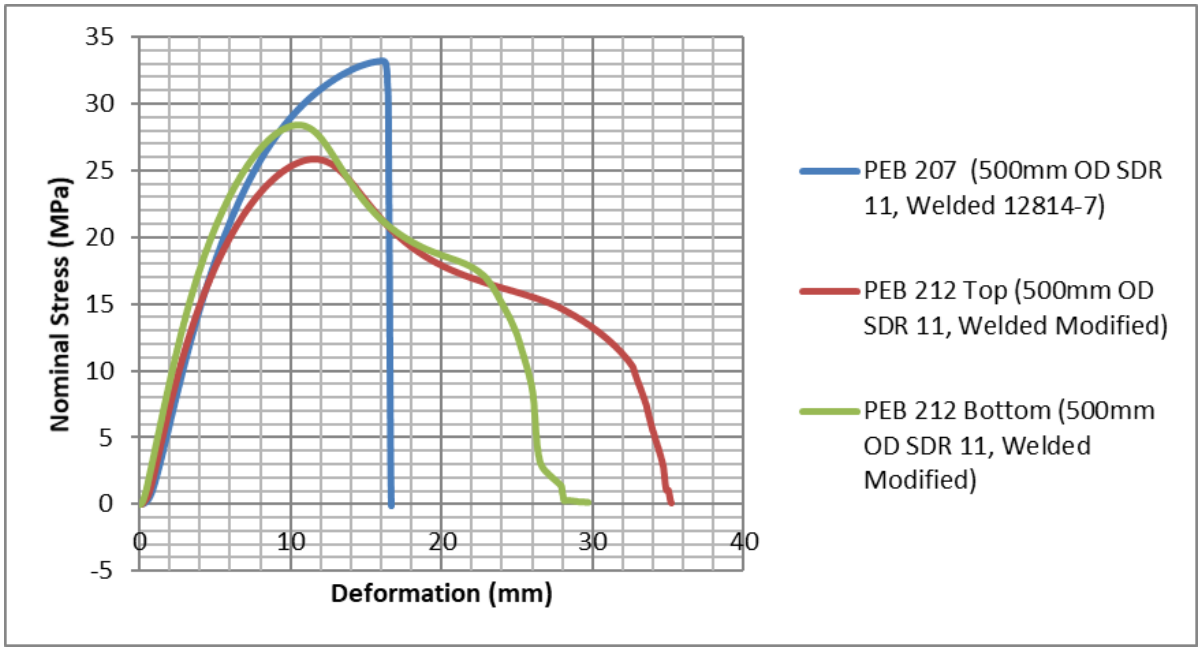

Figure 6-32, Nominal stress-Deformation graph for modified and standard geometry on welded 500mm OD

A similar procedure and specimen geometries are used for welded pipes. The nominal stress-deformation graph for these two specimens is shown in Figure 6-32, which exhibit little elongation for the standard geometry with a sharp drop in force absorbed by the specimen. The modified geometries provide some elongation which can be confirmed using fracture surface photos provided later in this chapter (Figure 6-36).

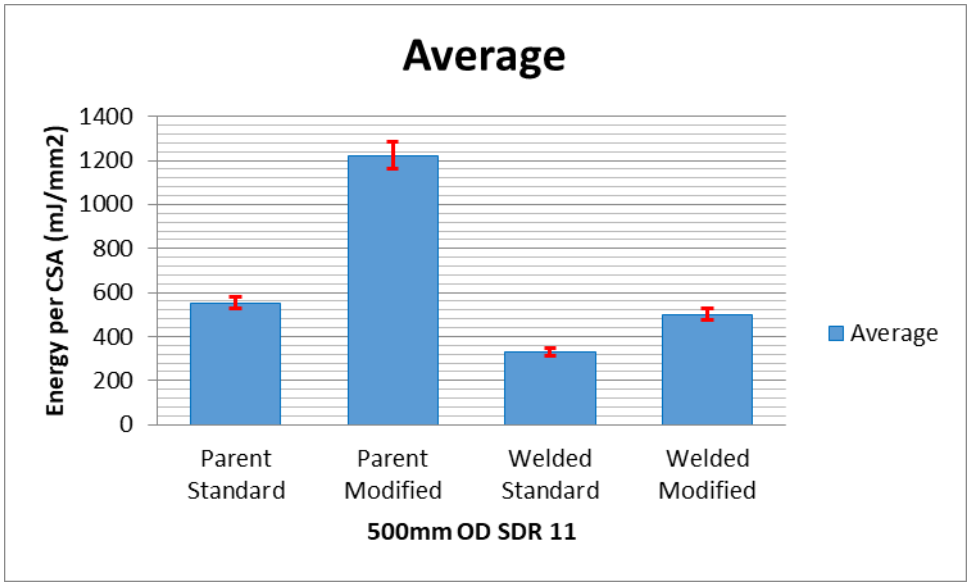

Figure 6-33, Total Energy per CSA (mJ/mm^2) for different cases on 500mm OD SDR 11 pipe

Energy per CSA for different conditions of 500mm OD SDR 11 is shown in Figure 6-33. Modified geometry in an unwelded situation provides the maximum energy per CSA on average. Modified geometry also provides more considerable energy per CSA compared to welded standard geometry, as expected.

Fracture surfaces of modified and standard geometry for unwelded 500mm OD SDR 11 pipe are shown in Figure 6-34 and Figure 6-35. The fracture surfaces for parent material using standard geometry shows that the specimen was failed due to void growth and had limited elongation before the specimen failed entirely. The fracture surface for the modified geometry on parent material indicates yielding and elongation, which has led to having more energy to break the specimen and indicates a ductile failure.

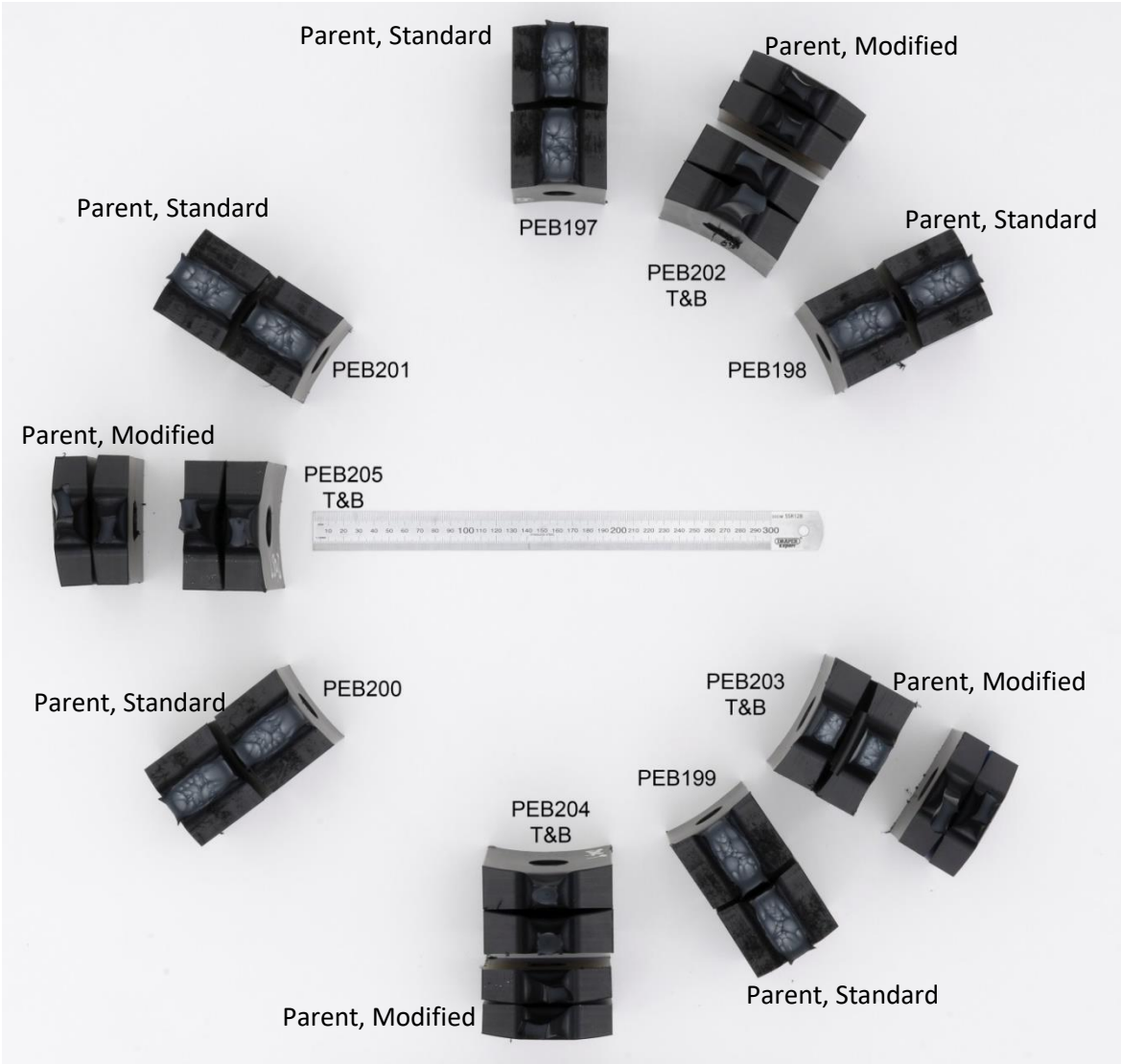

Figure 6-34, Fracture surface for parent 500mm OD SDR 11 pipe using standard and modified geometry

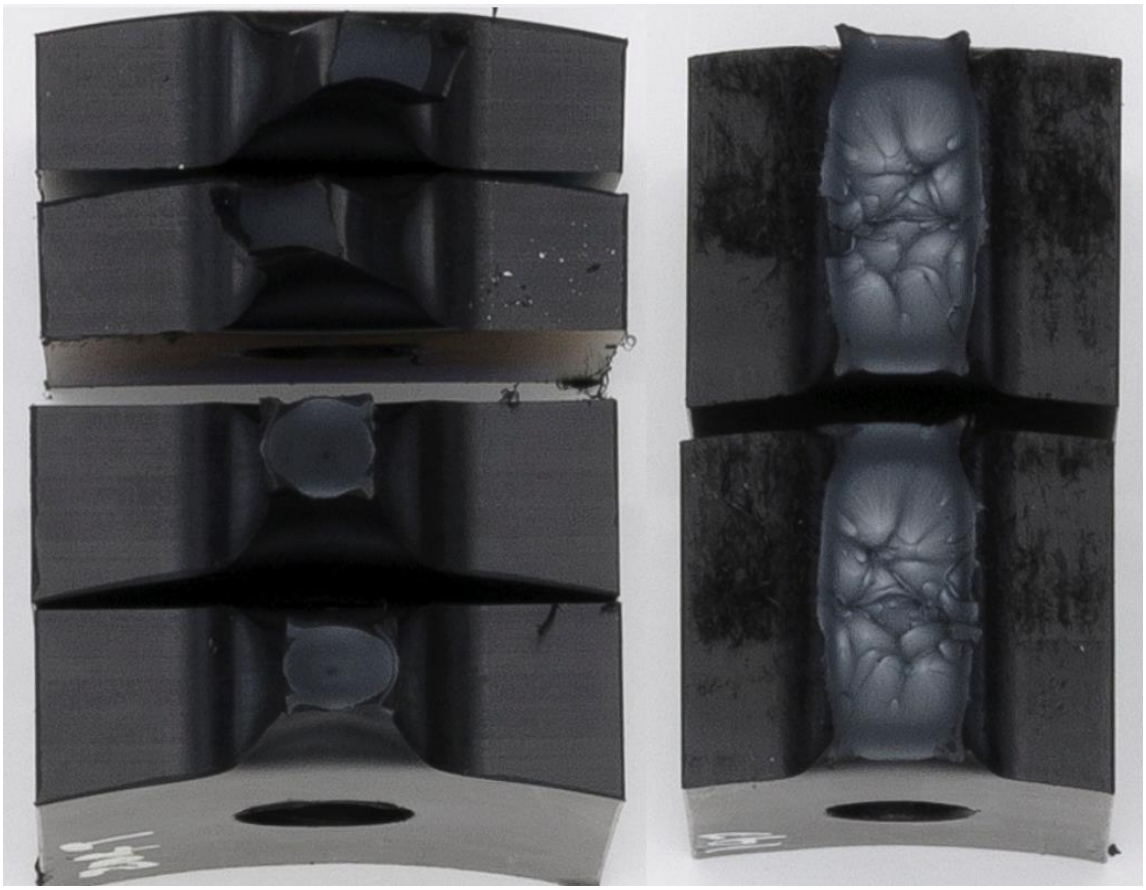

Figure 6-35, Fracture surface for parent modified specimen on the left (PEB204) and parent standard specimen on the right (PEB197) from 500mm OD pipe

Fracture surfaces of modified and standard geometry for welded 500mm OD SDR 11 pipe are shown in Figure 6-36 and Figure 6-37. It can be seen that on specimens where the standard geometry has been used, there is minimal deformation and specimen are broken off from the middle with an entirely flat surface which is undesirable. This study suggests the modified geometry experienced necessary elongations to provide useful, measurable data about the quality of the weld as opposed to the standard geometry, which provides little evidence for the quality of the welded joint.

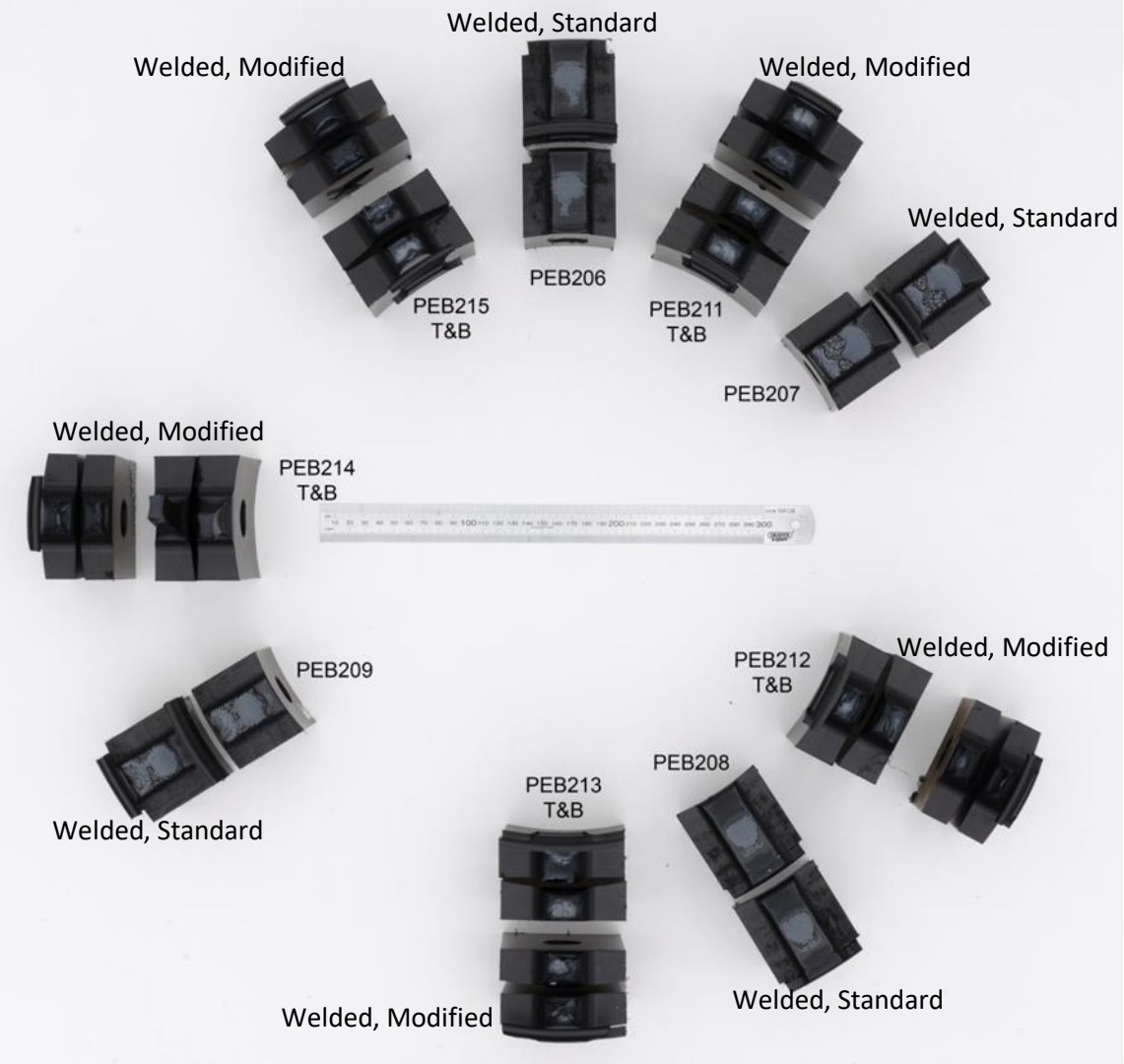

Figure 6-36, Fracture surface for welded 500mm OD pipe SDR 11 using standard and modified geometry

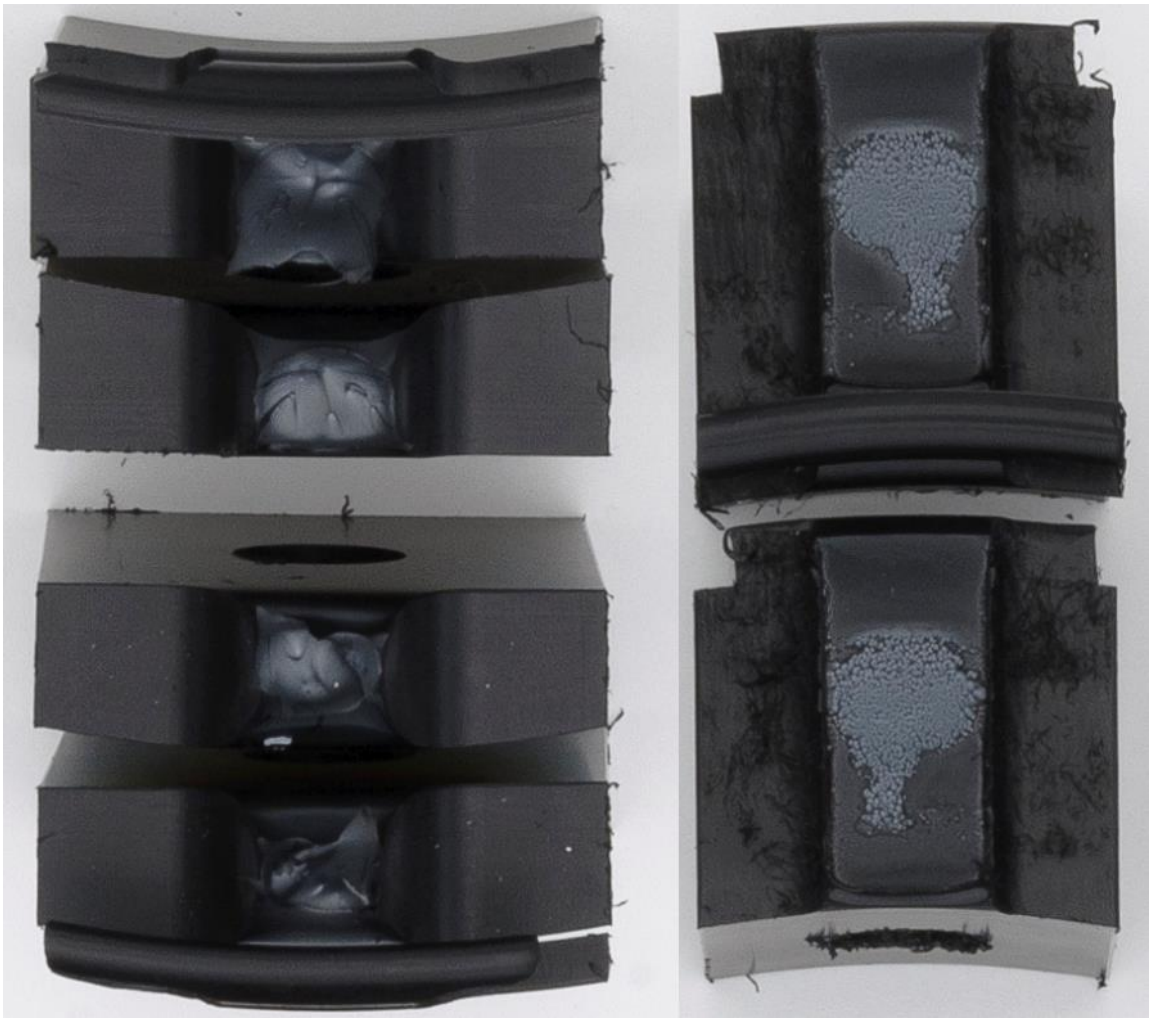

Figure 6-37, Fracture surface for welded modified specimen on the left (PEB213) and welded standard specimen on the right (PEB206) from 500mm OD pipe and from the same weld

6.11 Pipe with 630mm outer diameter

630mm OD SDR 11 pipe was the largest pipe size in diameter and thickness, which is experimented in this chapter. A similar welding machine as 500mm OD SDR 11 pipe (MC 1236 machine) is used for this pipe size diameter. The pipe was cut to half as the length of the pipes was 5 meters for each pipe size, which had to be welded. This was carried using a hand drill and jigsaw manually. The industrial saws available are not used as they are all used previously to cut metal pieces and are contaminated.

For unwelded parent pipe specimens, the standard specimen geometry is tested in full-thickness, and after being tensile tested, the specimens are failed with no elongation or ductility. Specimens with modified geometry are cut into half from the thickness, and after being tensile tested, they provided elongation in tensile tests which are shown in Figure 6-38.

The same geometry and procedure are used for the welded specimen. Specimens with standard geometry are failed with no elongation at the welded area of the specimen, and the specimen with modified geometry provided some elongations. The nominal stress-deformation graph for these specimens is shown in Figure 6-39.

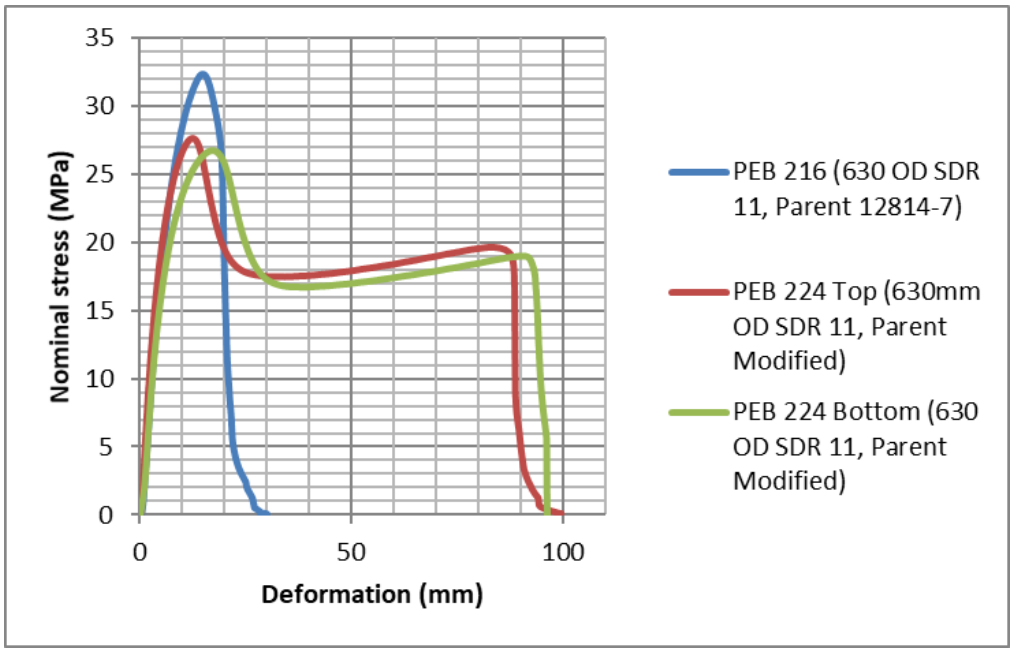

Figure 6-38, Nominal stress-Deformation graph for modified and standard geometry on parent 630mm OD SDR11 pipe

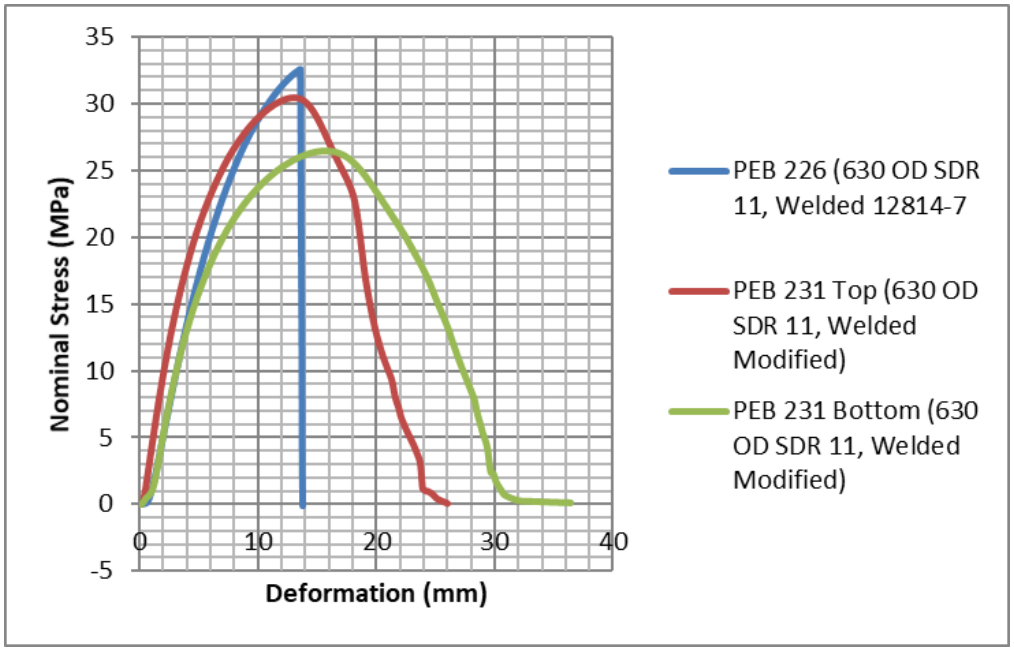

Figure 6-39, Nominal Stress-Deformation graph for modified and standard geometry on welded 630m OD SDR11 pipe

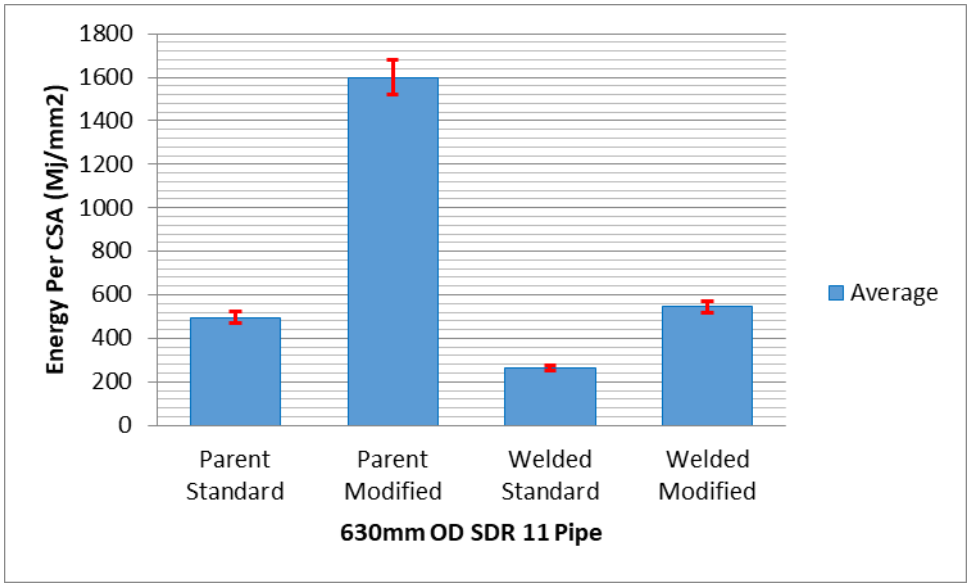

Figure 6-40, Total Energy per CSA (mJ/mm^2) for different cases on 630mm OD SDR 11 pipe

Energy per CSA for different conditions in 630mm OD SDR 11 pipe is shown in Figure 6-40. As expected, the largest average energy to break was for parent modified condition. For welded condition, the modified geometry also provided more sustainable energy to break value and from the specimen

geometry and fracture surface after the tensile test. It can be seen that most of the energy consumption for standard geometry are for areas throughout the specimen and not the welded area.

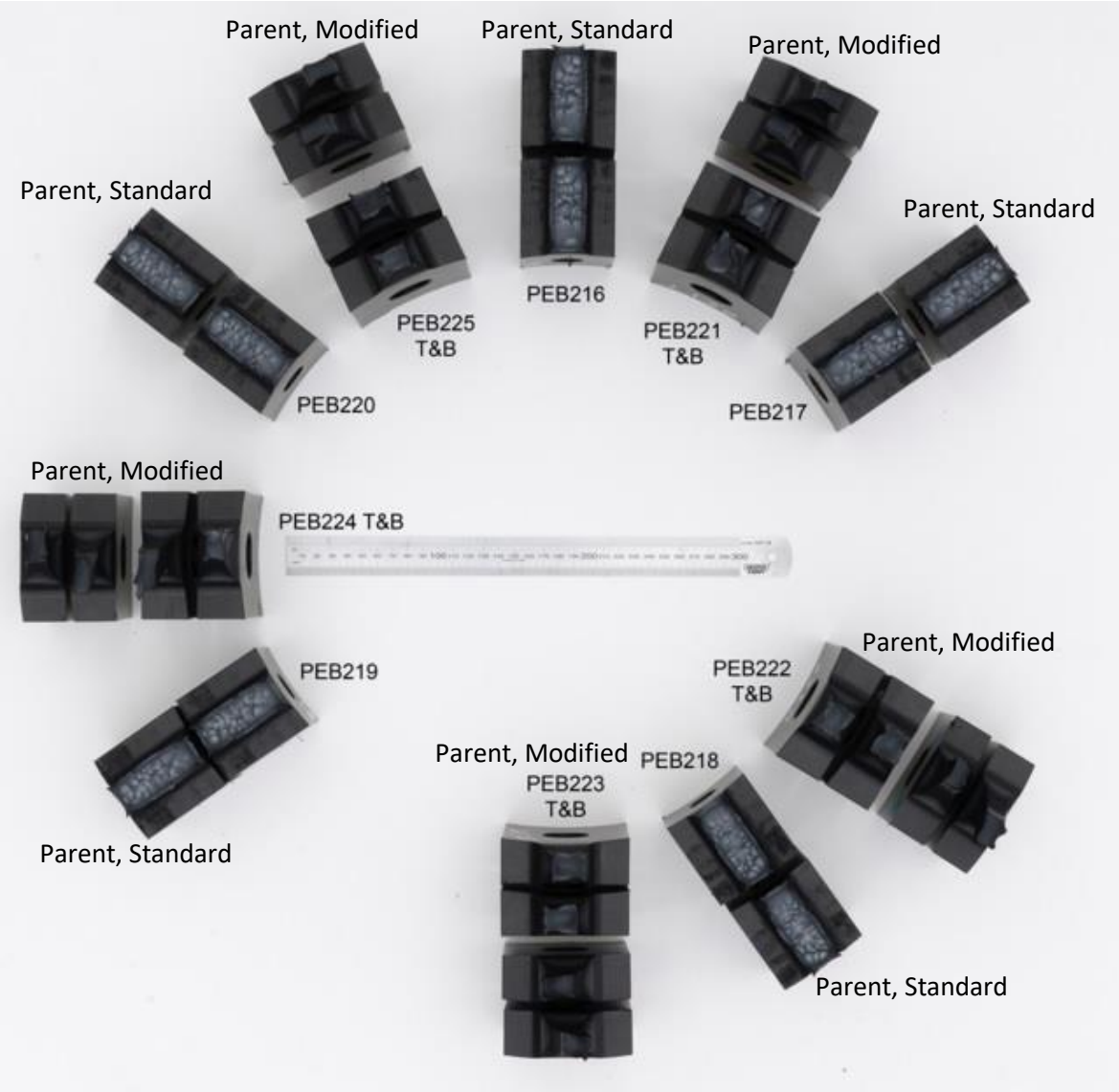

Figure 6-41, Fracture surface for parent 630mm OD pipe SDR11 using standard and modified geometry

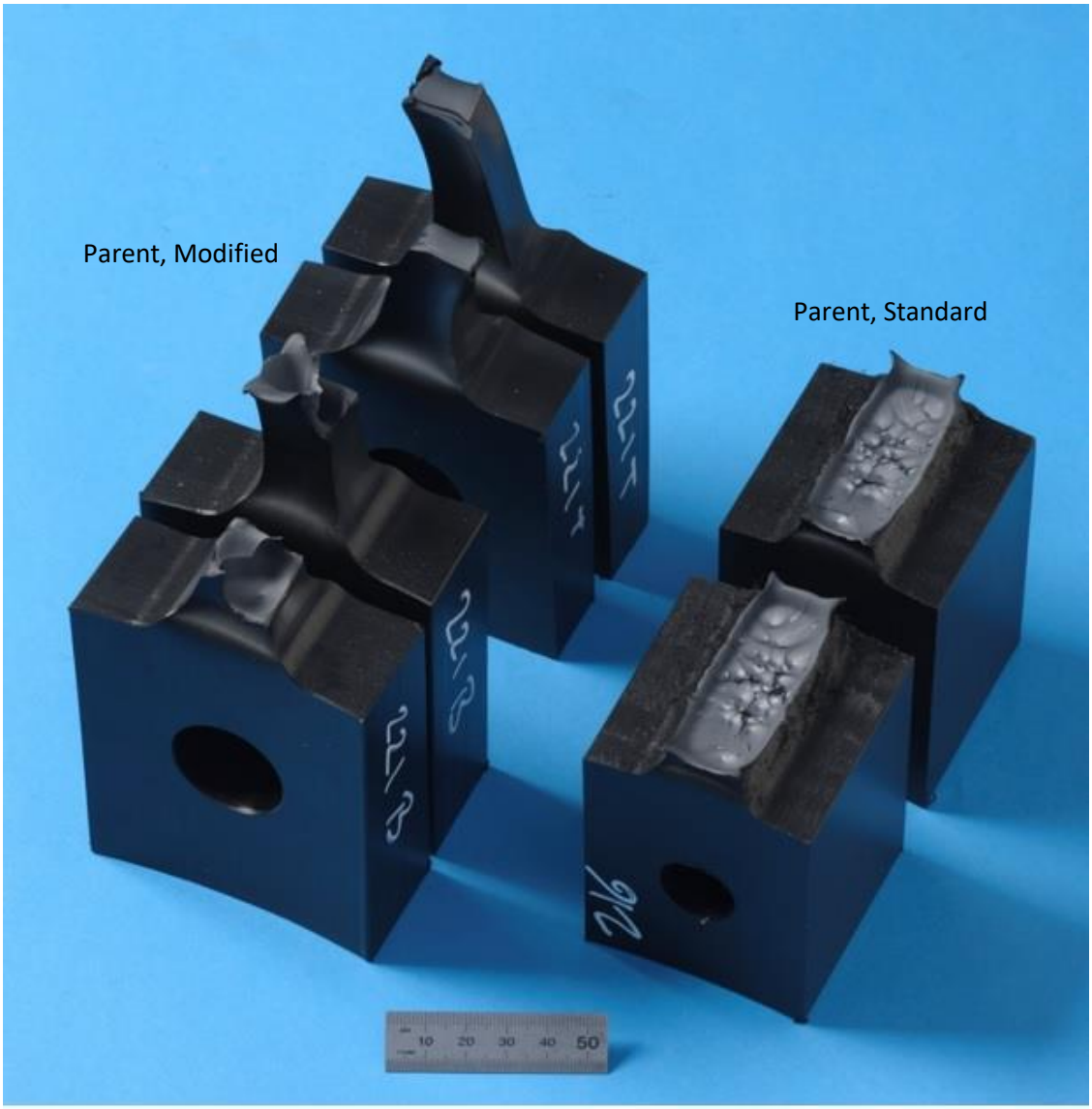

Figure 6-42, Fracture surface for parent 630mm OD pipe SDR 11 using standard on the right and modified geometry on the left

The fracture surfaces for parent 630mm OD pipes are shown in Figure 6-41. It is clear that the specimens with standard geometry are failed from micro void growth (PEB 220-219-218-217-216). Specimens with modified geometry experienced large elongations and failed from tearing (shear yielding) after complete elongation. Some of the specimens at the inner section of the pipe, despite tensile elongations, had single void growth (Figure 6-42), which might be due to the way the large-diameter pipes are cooled down in extruders.

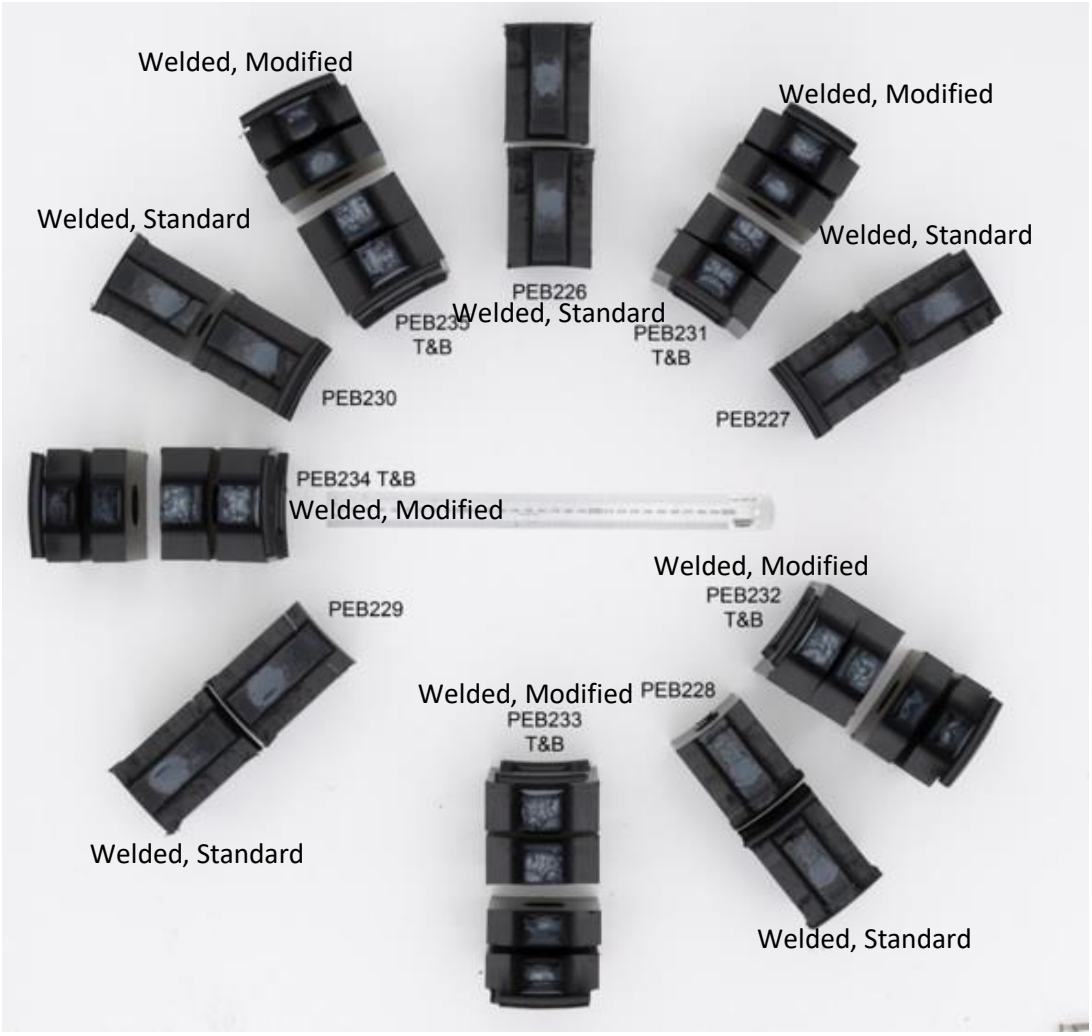

Figure 6-43, Fracture surface for welded 630mm OD pipe SDR 11 using standard and modified geometry

The fracture surfaces for welded 630mm OD pipe are shown in Figure 6-43. Welded specimen with standard geometry shows very little ductility, and as seen in 500mm OD pipe, the fracture surfaces are flat (PEB 230, 229, 228, 227, 226). The specimens with modified geometry provided some elongations, but as can be seen, the inner specimens provided less ductility both in the welded and unwelded situation (Figure 6-44).

Figure 6-44, Fracture surface for welded modified specimen on the left (PEB233) and welded standard specimen on the right (PEB226) from 630mm OD pipe and from the same weld

6.12 Comparison of Welding Factors

Welding factor, which is the ratio of total energy to break value of welded specimen against parent material, are calculated and compared for the modified and standard geometry. Figure 6-45 shows the welding factor for all pipe size diameters used in this experiment which are 140, 160, 250, 280, 500, 630mm OD.

Figure 6-45, Welding factors for different pipe sizes

In this chapter, modified geometries are proposed, which exhibited superior performance compared to the standard geometry (BS EN 12814-7) regarding elongation in parent pipe specimens. This improvement has led to a reduction in the value of the welding factor for modified geometry.

The reason for modified geometry to have a lower welding factor is having welded specimen using modified geometry to start necking at earlier stages of the test. This means although more considerable energy to break value for some welded specimen using standard geometry, the energy for the modified specimen is a better indication of the energy consumed to elongate the welded area.

6.13 Conclusion

In conclusion, in this chapter, three different modified geometries (thickness related) were proposed based on the findings of works carried out in chapters 3, 4 and 5. The reason behind the selection of different pipe sizes and welding machines used were explained in this chapter.

The main work carried out was to compare the performance of the modified geometry to the standard geometry (BS EN 12814-7) on different pipe sizes using parent and welded pipes.

It was shown that the modified geometry could differentiate the quality of the weld in all selected pipe sizes producing the right failure (ductile) and not allowing the test to fail from micro voids. The other advantage of the modified specimen is to have all failures occur in the welded area, which helps to have a more accurate reading for energy to break value of the specimen.

The failure comparison of specimens on modified and standard geometry in this chapter was carried from the same weld. The position of each modified and standard geometry was adjacent to each other in order to minimise uncertainties (weld quality, the position of the specimen on the pipe) which might affect the measurements. Despite all these conditions and having specimens (both standard and modified geometry) from one weld, it is seen on 280, 500 and 630mm OD pipe specimen using standard geometry have entirely flat fracture surface, where according to BS EN 12814-7 standard, this count as a cold weld. Assessing the weld using modified geometry provided elongation on the fracture surface, which proves the weld passes the criteria to be counted as a good weld.

Chapter 7. Conclusions and future works

7.1 Main findings of this thesis

The aim of this research was to investigate and improve the current standard geometry in quantifying the quality of welds in HDPE pipes. A comprehensive literature investigation, series of laboratory experiments (tensile tests, X-ray, DIC) were carried out to study the current standard geometry problems. The problem with the current standard is that the same waisted tensile test specimen geometry is used for all thicknesses. As stated in recent literature, when specimen thickness increases, ductility decreases and because of this change, the mode of failure in the specimen varies accordingly.

One of the geometry factors which was investigated in the literature and had an influence on the failure mode of specimens was the width of the waisted section. Chapter 3 of this thesis was fully based on four sets of experiments carried out to investigate the effect of the width of the waisted section on two thicknesses of 15 and 25mm. In two experiments, side plates were used to limit the movement in the waisted region of the specimen. In this chapter, the suggested total energy to break the value of a specimen was divided into different regions. Region 3, which was selected to be the cold drawing region, was proposed to be the most relevant parameter to indicate ductility. Specimen with 15mm thickness all failed in a fully ductile mode with maximum Region 3 energy taking place when the width of the waisted section is equal to the thickness. Specimen with 25mm thickness failed mostly due to void growth in a micro ductile manner. This specimen experienced little elongation, which could not be used entirely to investigate the effect of the width of the waisted section on this thickness due to its failure mode.

Specimens using 15mm thickness specimen all failed in ductile manner therefore, the next set of

experiments to investigate the effect of different geometry parameters, and to avoid changes in failure mode, 15mm thickness was used to carry out necessary tests. CCD optimisation technique was employed to investigate five different parameters of waisted geometry to understand their effects on responses. The parameters used in this investigation are width and radius of the waisted section, diameter, and distance between the loading holes. The responses used in this study are; total energy to break value, Region 3 to break value and elongation in loading holes of the specimen. Findings in this study suggest that, for total energy and Region 3 response, the radius of the waisted section and distance between the loading holes were two of the most influenced parameters which had the lowest P value. The width of the waisted section and width of the specimen were two of the most influential factors found in the elongation in the loading pin response. Based on desirability function, the best combination for waisted geometry on total energy, region 3, and elongation in the pin response is 15mm for width of the waisted section, 70mm for width of the specimen, 10mm for radius of the waisted section, 20mm for diameter of the loading holes, and 100mm for distance between the loading holes.

FEA technique was employed to model HDPE specimens. The use of FEA overcomes the challenges present in experiments such as machining and testing specimens with large thicknesses. Challenges of this modelling were producing necking in modelling as well as large deformation behaviour and failure mechanism. These challenges were tackled by using constitutive equations as well as using triaxiality as an indication of failure in this study. Using this technique, comparison against thickness, width and radius of the waisted section were carried out and compared with their triaxiality stress state. The study suggests that an increase in thickness would increase the triaxiality, and an increase in width and radius would reduce triaxiality, i.e. the limitation to increase the width is due to the increase in elongation around the loading hole. The limitation in increasing the radius of the waisted section could result in the specimen not failing from the welded area of interest.

As a result of the findings summarised above, three modified geometries were proposed (dimensions given in chapter 6). The proposed specimen geometry was then compared to standard geometry using welded and unwelded specimens on 140, 160, 250, 280, 500 and 630mm OD pipes. The thickness of 12.7 to 57.3mm was covered in these experiments, and for each condition (welded, unwelded, modified or standard geometry), around five specimens were tested. The results showed that modified specimen geometry has improved testing method in all range of thicknesses compared to traditional methods (BS-EN 12814-7). Despite having a ductile failure in all specimen, up to a thickness of 20mm (140, 160, 250mm), it could be seen that modified geometry using parent material provided the most extended elongation. On welded specimen with a thickness of lower than 20mm, the testing was improved by having necking take place at earlier stages of the test and have most of the yielding take place on the welded area. This would suggest that total energy data using a modified specimen would be a better indication of ductility in that specific test.

On specimens with thicknesses of over 20mm (280, 500, 640mm OD), welded and unwelded specimens using standard geometry failed rapidly just after reaching the necking in the test. In unwelded case standard geometry, the specimen failed in micro ductile mode from void growth and welded specimen barely any elongation, which an indication of the complete cold weld is. Specimen cut from the weld using modified geometry provided elongation, which is a pass criteria for the weld and specimen on unwelded modified geometry failed on fully ductile mode. The outcome of the research conducted in this thesis, which proposed a modified geometry for tensile tests, paves the way to enhance reliability in the examination of HDPE weld qualities.

7.2 Recommendations for future work

As mentioned in chapter 1, the quality examination of welds using the current standard geometry on specimens with thicknesses of over 20mm is challenging. The primary challenge is that all specimens fail in the same manner (brittle or micro ductile), which provides no useful information about the quality of welds. It is, therefore, necessary to run more tests in different applications to validate and inform the standard bodies regarding the improvement suggested in this thesis. Improvements have to be carried out on current standards for welding HDPE pipes. As one of the best methods of assessing the quality of welds (waisted tensile test using standard geometry) has failed to provide useful discrimination for larger thicknesses (e.g. 20mm) specimen, there is a question on how the welding procedure has been optimised prior. This research provided a test method to improve the quality of the weld by optimisation parameters involved in welding HDPE pipes.

Failure mechanisms of plastic using FEA is still a challenge in the field of material testing. Thus, more research is called regarding the failure mechanism of plastics, as in many cases, real experiments may not be feasible or practical. FEA has the potential to deliver valuable information on this research subject.

Bibliography

[1] D. Energy, “Use of PE Pipe in Non-Safety Related Service Water Piping at Catawba Nuclear Station,” 2006.

[2] N-755, *ASME Code N-755''Use of Polyethylene (PE) Plastic Pipe for Section 3, Devision1, Construction and section Xt Repair/Replacement Activiti3es'', Revision 6a, September 12, 2006.,* September 12, 2006.

[3] C. I. Brown and M. J. Troughton, “Qualifying long-term performance of butt fusion wleds in PE pipes from short-term test,” Baveno, Italy, 2004.

[4] F. A. Chipperfield and M. A. Troughton, “Comparision of short-term coupon tests for assessing the performance of butt fusion wleds in polyethyelne pipes,” New Orleans, 1999.

[5] M. G. Murch and M. J. Troughton, “A study of the applicability of the tensile weld test for thick walled polyethylene pipe,” 1995.

[6] M. G. Murch and . M. J. Troughton, “A study of applicability of the tensile weld test for thick walled polyethylene pipe,” 1995.

[7] K. A. Wilson, “Verification of butt fusion weld quality in large diamter PE100 water pipes,” Edinburgh, UK, 1995.

[8] P. J. Flory, “Principles of Polymer Chemistry,” 1953.

[9] L. H. Sperling, Introduction to Physical Polymer Science, New York: Wiley, 1986.

[10] J. W. Nicholson, The Chemistry of Polymers, Cambridge: Royal Society of Chemistry, 2006.

[11] S. L. Rosen, Fundamental Principles of Polymeric Materials, New York: Wiley, 1982.

[12] A. Ram, Fundamentals of Polymer Engineering, Plenum Press, 1997.

[13] A. Rudin, The Elements of Polymer Science and Engineering, San Diego: Academic Press, 1999.

[14] L. H. Sperling, Introduction to Physical Polymer Science, New York: Wiley, 1992.

[15] J. Brydson, Plastic Materials, Oxford: Butterworth-Heinemann, 1999.

[16] T. H. o. Plastics, “The History of Plastics,” 2005. [Online]. Available: www.americanplasticscouncil.org. [Accessed 11 January 2015].

[17] "RollePaaLinc," 1 2019. [Online]. Available: https://www.rollepaalinc.com/introduction.html. [Accessed 1 1 2019].

[18] c. Rauwendaal, "Polymer Extrusion," MacMillan Publishing Company, New York, 1986.

[19] P. W. Richard, Polymer Interfaces, Munich: Hnaser Publisher, 1994.

[20] W. V. Titow, "Solvent Welding of Plastics," 1977.

[21] G. Haim and H. P. Zade , "Welding of Thermoplastics," 1946.

[22] S. S. Voyutskii, Autohesion and adhesion of high polymers, 1963: John Wiley and Sons.

[23] P. G. De Gennes, "Reptation of a polymer chain in the presence of fixed obstacles," *Journal of chemical Physics,* pp. 552-572, 1971.

[24] P. Barber and J. R. Atkinson , "The use of tensile tests to determine the optimum consitions for butt fusion welding certain grades of polyethylene," *Journal of Material Science,* p. 1456, 1974.

[25] R. Parmar and J. Bowman, "Crack initiation and propagation paths for brittle failures in aligned and misaligned pipe butt fusion joints," *Polymer engineering and science,* vol. 29 (19), p. 1396, 1989.

[26] W. N. 4-32-08, *Specification for site fusion joining of MDPE pipe and fittings,* August 1988.

[27] A. J. Kinloch and R. J. Young , Fracture Behaviour of Polymers, London: Elesevier, 1983.

[28] X. Lu, X. Wang and N. Brown, "Slow fracture in homopolymer and copolymer of Polyethylene," *Journal of Material Science,* vol. 23, p. 643, 1988.

[29] J. R. Atkinson and D. R. Decourcy, "Assessment of Fusion Joint Quality and Some Evidence for hte presence of molecular orientations in Butt-Fusion Welds in Polyethyelene Pipes," *Plastics and Rubber processing and applications,* vol. 1, no. 4, 1981.

[30] J. R. Atkinson, "The use of tensile tests to determine the optimum conditions for butt welding polyethylene pipes of different melt flow index," *Journal of Material Science,* vol. 12, no. 8, pp. 1535-1551, 1977.

[31] P. Barber and J. R. Atkinson, "Some microstructural features of hte welds in butt welded polyethtylene and polybutene pipes," *Journal of Material Scince,* vol. 7, pp. 1131-1136, 1972.

[32] P. Braber and J. R. Atkinson, "The use of tensile tests to detemine the optimum conditions for butt fusion welding certain grades of polyethyelene,

polybutene-1 and polypropylene pipes," *Journal of material science ,* vol. 9, no. 9, pp. 1456-1466, 1974.

[33] S. C. Malguarnera and L. L. Earles, "The quality assurance of heat fused thermoplastic pipeline joints," Texas A&M University, San Francisco, 1982.

[34] G. Diedrich and E. Gaube, *Kunststoffe,* vol. 60, pp. 74-80, 1970.

[35] K. Kempe and G. Diedrich , *Kunstsoffe,* vol. 70, p. 8, 1980.

[36] J. M. Greig, *Pipes Pipelines International,* vol. 22, no. 1, pp. 16-24.

[37] P. John, *Kunststoffe,* vol. 72, pp. 713-715, 1982.

[38] I. K. Richard, B. Gaube and I. G. Diedrich, *Kunatatoffe,* vol. 50, no. 3, 1960.

[39] H. Potente and P. Tappe, *Material and Design,* vol. 5, no. 6, p. 273, 1985.

[40] H. Herforth, *Plastrevarbeiter,* vol. 33, no. 5, pp. 14-67, 1982.

[41] J. Hessel and P. John, *Kunststoffe,* vol. 74, 1984.

[42] Y. Mai and J. G. Williams, *Journal of Material Science,* vol. 14, 1973.

[43] G. Menges, "Arbeitsgemeinschaft Industrieller Forschungsvereiningungen Reserch Report".

[44] G. Menges, *DVS-Berichte,* pp. 62-65.

[45] M. J. Troughton and G. S. Booth, “Structural Integrity of butt fusion welded polyethyelene pipe-a review,” Abington Publishing, Cambridge, 2000.

[46] W. 4-32-08, *Fusion joining of polyethyelne pressure pipeline systems using PE80,* UK Water Industry, 2002.

[47] N. Wolters and B. Venema, “Mechanical quality of welds in polyethyelene pipe systems,” York University, 1982.

[48] H. J. Kwon, P. Y. B. Jar, “Toughness of High-Density Polyethylene in Plane-Strain Fracture,” *Polymer Engineering and science,* 2006.

[49] A. G. Atkins, Y. W. Mai, “Elastic and Plastic Fracture,” Chichester, England, 1985.

[50] K. B. Broberg, “Critical review of some theories in fracture mechanics,” *International Journal of Fracture Mechanic,* vol. 4, no. 11, 1968.

[51] X. H. Chen, Y. W. Mai, L. C. Zhang, Fracture of Polymers, Composies and Adhesives,, Amsterdam: Elsevier, 1999.

[52] T. Pardoen,F. Hachez, B. Marchioni, P.H. Blyth, J. Atkins, “Mode 1 fracture of sheet metal,” *J. Mech. Phys. Solids,,* pp. 52, 423, 2004.

[53] K. W. Neale,P. Tugcu, “Analysis of necking and neck propagation in polymeric materials,” *J. Mech. Phys. Solids,* vol. 33, pp. 323-337, 1985.

[54] J. W. Hancock and A. C. Mackenzie, “Mechanism of ductile failure in high-strength steels subjected to multi axial street states,” *J. mech. Phys. Solids,* vol. 24, pp. 147-169, 1976.

[55] A. C. A. O. H. A.S. Ognedal, “Behaviour of PVC and HDPE under highly triaxial stress state: An experimental and numerical study,” *Mehcnaics of Materials,* vol. 72, no. 0167-6636, pp. 94-108, 2014.

[56] A. C. O. H. S Olufsen, “Influence of stress triaxiality and strain rate on stress-strain behaviour and dilation of mineral-filled PVC,” *Polymer Testing,* vol. 75, pp. 350-357, 2019.

[57] K. Wilson, “Verification of butt fusion weld quality in large diameter PE100 water pipes,” in *Int. Conf on Plastic Pipes*, Edinburgh, 1995.

[58] ISO13586, “Plastics- Determination of fracture toughness (GIC and KIC). Linear elastic fracture mechanics (LEFM) approach.,” 2000.

[59] ASTMD5045, “Standard test methods for plane-strain fracture toughness and strain energy release rate of plastic materials,” 1993.

[60] T. Anderson, “Fracture Mechanics: Fundamentals and applications.,” *Boca Raton: CRC Press; 1995. p. 297-9.,* pp. 297-9, 1995.

[61] J. M. Hodgkinson, J. G. William, “J and Gc analysis of hte tearing of a high ductile polymer,” *J mater Sci,* pp. 16:50-6, 1981.

[62] R. Frassine, M. Rink, A. Pavan, “Size effects in the fracture of a pipe-grade high density polyethyelene,” *fatig Fract Engng Mate Struct,* pp. 20:1217-23, 1997.

[63] C. Grein, HH. Kausch, P. Beguelin, , “Characterisation of toughened polymers by LEFM using an experimental determination of plastic zone correction,” *Polym Test,* pp. 22:733-46, 2003.

[64] T. Vu-Khanh, FX. De Charentenay, “Mechanics and mechanisms of impact fracture in semi-ductile polymers,” *Polym engng Sci,* pp. 25:841-50, 1985.

[65] PM. Frontini, A. Fave , “Assessment of impact fracture toughness of PP-elastomeric poluolefin blends,” *J Macromol Sci,* pp. 30:2446-54, 2002.

[66] A. G. Atkins, Y. W. Mai, Elastic and plastic Fracture, Chichester, England: Ellis Horwood, 1985.

[67] K. W. Neal, P. Tugcu, “Analysis of necking and neck propagation in polymeric materials,” *J. Mech. Phys. Solids,* pp. 33: 323-337, 1985.

[68] H. J. Kwon, P. Y. B. Jar, “On the application of FEM to deformation of high denstiy polyethylene,” *Int. J. Solid Structures,* pp. 45:3521-3543, 2008.

[69] C. G'Sell, N. A. Aly-Helal, J.J. Jonas , “Effect of stress triaxility on neck propagation during tensile stretching of solid polymers,” *J. Mater. Sci.,* pp. 18:1731-1742, 1983.

[70] C. M. Buckley c, “Neck propagation in Polyethylene,” *J. Polym. Sci. Part : Polym. Phys,* pp. 42:2081-2091, 2004.

[71] F. A. Chipperfiled and M. J. Troughton, “Comparison of short-term coupon test for assessing the performance of butt fusion wleds in Polyethyelne pipes,” in *16th international plastic pipe fuel gas symposium*, New Orleans, 1999.

[72] K. Y. Benyounis, A. G. Olabi, M. S. J. Hashmi, “Effect of laser welding parameters on the heat input and weld bead profile,” *Journal of Materials Processing technology,* Vols. 164-165, pp. 978-985, 2005.

[73] M. J. Tsai, C. H. Li, “The use of grey relational analysis to determine laser cutting parametrs for QFN packages with multiple performance characteristics,” *Optics and Laser Technology,* vol. 41, no. 8, pp. 914-921, 2009.

[74] K. J. V. Charles RH, Fundamental concepts in the design of experiments, Oxford: University Press, 1999.

[75] K. Y. Benyounis, A. G. Olabi, “Optimisation of different welding process using statistical and numerical approaches- A reference guide,” *Journal of Advances in engineering software,* vol. 39, pp. 483-496, 2008.

[76] H. S. E. P. A. A. N. F. S. M. Barabadi H, “Optimization of myco-syntheized silver nanoparticles by respose surface methodology emplying Box-Behnken desgn,” *Inorganic and Nano-Metal Chemistry,* vol. 49, no. 2, pp. 33-43, 2019.

[77] E. M. M. H. F. G. John R. Wagner, “25 - Design of Experiments,” in *Extrusion (Second Edition)*, William Andrew Publishing, 2014, pp. 291-308.

[78] M. D. A.-C. C. Myers RH, Response Surface methodology: Process and Product Optimization Using Designed Experiments, New York: John Wiley & Sons, 2016.

[79] D. L. K.J. Kim, “Simultaneous optimization of mechanical properties of steel by maximizing exponential desirability functios,” *Journal of the Royak atatistical Society,* vol. Series C, no. 49 (3), pp. 311-325, 2000.

[80] A. C. Rudy, D. J. Deblieck, M. van Beek, K. Remerie, I. M. Ward, “Failure mechanisms in polyolefines: The role of crazing, shear yielding and the entanglement network,” *Polymer,* vol. 52, pp. 2979-2990, 2011.

[81] A. S. Ognedal, A. H. Clausen, M. Polanco-Loria, A. Benallal, B. Raka, O. S. Hopperstad,, “Experimental and numerical study on the behaviour of PVC and HDPE in biaxial tension,” *Mechanics of Material,* vol. 54, pp. 18-31, 2012.

[82] P. G. Higgs, R. J. Gaylord, “Slip-links, hoops and tubes: test of entanglement models of rubber elasticity,” *Polymer,* vol. 31, pp. 70-74, 1990.

[83] S. F. Edwards, T. H. Vilgris, “The effect of entaglement in rubber elasticity,” *Polymer,* vol. 27, pp. 483-492, 1986.

[84] M. G. Brereton and P. G. Klein, “Analysis of the rubber elasticity of polyethylene networks based on the slip link model of S.F. Edwards et al,” *Polymer,* vol. 27, pp. 970-974, 1988.

[85] P. Wu and E. V. D. Giessen, “On neck propagation in amorphous glassy polymers under plane starin tension,” *Int. J. Plast,* pp. 211-235, 1995.

[86] Q. Z. Fang, T. J. Wang and H. P. Z. H. G. Beom, “rate-dependent large deformation behaviour on PC/ABC,” *Polymer,* no. 50, pp. 296-304, 2009.

[87] C. G. Sell and J. J. Jonas, “Determination of the plastic behaviour of solid polymers at constant true strain rate,” *J, material Science ,* vol. 14, pp. 583-589, 1979.

[88] B. D. Coleman, “Neching and drawing in polymeric fibres under tension,” *Arch. Rat. mechanical,* vol. 83, no. 2, pp. 115-137, 1983.

[89] J. W. Hutchinson and K. W. Neale, “Neck Propagation,” *J. Mech. Phys. Solids,* vol. 31, no. 5, pp. 405-426, 1983.

[90] Y. Takahashi, T. Tomita, A. Shindo,, “Neck bulge propagation in polymeric clinders under internal pressure,” *Int. J. Mech. Sci,* vol. 32, no. 4, pp. 335-343, 1990.

[91] L. O. Fager and J. L. Bassani, “Plane strain neck propagation,” *Int. J. Solids Strut,* vol. 22, pp. 1243-1257, 1986.

[92] P. Tugcu and K. W. Neale, “Analysis of plain-starin neck propagation in viscoplastic polymeric fils,” *Int. J. Mech. Sci,* vol. 29, no. 12, pp. 793-805, 1987.

[93] P. Tugcu and K. W. Neale, “Analysis of neck propagation in polymeric fibres including the effect of viscoplasticity,” *ASME J. Eng. Mater. Tech,* vol. 100, pp. 395-400.

[94] P. Tugcu and K. W. Neale, “Necking and neck propagation in polymeric materials under pain-strain tension,” *Int. J. Solid Strut,* vol. 23, no. 7, pp. 1063-1085, 1987.

[95] S. Muhammad, P. Y. B and Jar, “Dtermining stress-strain relationship for necking in polymers based on macro deformatio nbehaviour,” *Journal of finite element analysis and design,* vol. 70, no. 71, pp. 36-43, 2013.

[96] H. H. Kausch, Polymer Fracture, Berlin: Springer Veralg, 1987.

[97] R. T. Moura, A. H. Clausen, E. Fagerholt, M. Alves and M. Langseth, “Impact on HDPE and PVC plates - experimental tests and numerical simulation,” *Int. J. Impact Eng,* vol. 37, pp. 580-598, 2010.

[98] ASTM D3100-8.03, *ASTM Annual Book of Standards,* West Conshohocken: American Society of Testing and Materials.

[99] X. H. Chen and L. C. Zhang, “Fracture of Polymers, Composites and Adhesives,” Amsterdam, 1999.

[100] A. S. Ognedal, A. H. Clausen, M. Polanco-Loria, A. Benallal, B. Raka, O. S. Hopperstad,, “Experimental and numerical study on the behaviour of PVC and HDPE in biaxial tension,” *Mechanics of Materials,* vol. 54, pp. 18-31, 2012.

[101] K. Broberg, “Critical review of some theories in fracture mechanics,” *Int. J. Fractt. Mech.,,* pp. 4,11, 1968.

[102] “Rollepaalinc,” 3 2019. [Online]. Available: https://www.rollepaalinc.com/introduction.html. [Accessed 3 2019].

Chapter 8. Appendix

8.1 Part A (Chapter 3)

Table 8-1, Data for Experiment 1 (15mm thickness unwelded flat sheet with side plates)

Specimen Number	Ligament	A/R	Region 1 mJ/mm²	Region 2 mJ/mm²	Region 3 mJ/mm²	Region 4 mJ/mm²	Energy per mJ/mm²
PEW1	25.15	1.676666667	146.3189	210.7829	186.7131	178.4177	722.232647
PEW2	15.2	1.013333333	98.55252	130.3081	445.7758	158.5483	833.184787
PEW3	10.3	0.686666667	61.15668	128.2256	454.1524	107.7772	751.3117809
PEW4	29.7	1.98	165.8866	281.6164	259.5868	277.2348	984.3246531
PEW5	35.15	2.343333333	214.7209	299.7811	295.3159	246.2795	1056.0973
PEW6	20.1	1.34	119.9251	197.3659	363.5994	201.1019	881.9923326
PEW7	11.95	0.796666667	73.5119	171.3825	436.0891	103.8492	784.8326534
PEW8	5.15	0.343333333	30.53173	83.73915	161.4517	85.06378	360.7863143
PEW9	15.05	1.003333333	99.85865	160.6913	481.9659	87.43594	829.951784
PEW10	2.75	0.183333333	18.47355	38.34407	99.05549	72.78805	228.661155
PEW11	8.15	0.543333333	54.3501	125.1737	113.4392	78.52077	371.4837801
PEW20	25	1.666666667	137.3628	212.5516	288.6015	91.86147	730.3773557

Table 8-2, Data for experiment 2 (25mm thickness, unwelded flat sheet with side plates)

Specimen Number	Ligament Length	Total E/ mJ/mm²	Region 1/ mJ/mm²	After yield / mJ/mm²	A/R
21	17.5	471.6191597	132.3915966	339.2275632	0.7
22	30	1093.876458	201.0629568	892.8135008	1.2
23	15	423.0128151	132.0820149	290.9308003	0.6
24	20	545.3362198	144.1109422	401.2252776	0.8
26	5	278.027867	45.61039305	232.417474	0.2

27	25	746.5236521	181.9856644	564.5379877	1
28	35	1132.223509	236.7374716	895.486037	1.4
29	40	1889.276635	301.9982003	1587.278435	1.6
30	10	336.6610294	80.3527229	256.3083065	0.4
31	45	1511.32523	330.5194758	1180.805754	1.8

Table 8-3, Data for Experiment 3 (15mm thickness, unwelded flat sheet)

Specimen Number	Ligament Length	A/R	Region 1 mJ/mm²	Region 2 mJ/mm²	Region 3 mJ/mm²	Region 4 Plain mJ/mm²	Energy per CSA mJ/mm²
PEW32	16.5	1.1	122.2556	196.9828	673.422	138.678231	1131.338624
PEW34	12.5	0.833333333	94.6313	183.4865	778.561	204.4157364	1261.09462
PEW35	15	1	108.9364	189.8866	926.858	139.7985832	1365.479327
PEW36	17.5	1.166666667	136.3021	195.9624	844.417	236.2082937	1412.889589
PEW37	20	1.333333333	165.1272	217.7314	728.929	139.0751114	1250.862878
PEW38	22.5	1.5	185.6129	208.1785	637.245	196.6742896	1227.710522
PEW39	25	1.666666667	307.5925	209.1136	910.897	236.7099753	1664.313252

8.2 Part B (Chapter 4)

Table 8-4, Data for DOE analysis (15mm flat sheet specimen)

std	The width of waisted section mm	The radius of the waisted section mm	The diameter of loading holes mm	The distance between loading holes mm	Width of Specimen mm	Energy to Break (J/mm^2)	Region3 (J/mm^2)	Elongation in Pin(mm)
PEW101	14.9	5.1	15.2	80	45.2	809.1961	364.3367	0.13
PEW102	24.9	5.1	15.2	80	45.2	1080.742	259.7089	1.24
PEW103	14.9	10.15	15.2	80	45.2	1132.874	616.336	0.12
PEW104	24.9	10.15	15.2	80	45.2	1834.252	1068.009	1
PEW105	14.9	5.1	15.2	80	65.2	835.1929	431.7355	0.12
PEW106	24.9	5.1	15.2	80	65.2	942.9599	258.1319	0.8
PEW107	14.9	10.15	15.2	80	65.2	1509.592	1013.874	0.12
PEW108	24.9	10.15	15.2	80	65.2	1304.365	648.2134	0.76
PEW109	14.9	5.1	25.2	80	55.2	688.7907	250.0623	1.2
PEW110	24.9	5.1	25.2	80	55.2	484.2177	376.8149	0.2
PEW111	14.9	10.15	25.2	80	55.2	1264.639	689.5782	0.2
PEW112	24.9	10.15	25.2	80	55.2	1757.6	919.177	1.2
PEW113	14.9	5.1	25.2	80	75.2	910.1076	486.4859	0.21
PEW114	24.9	5.1	25.2	80	75.2	1164.935	498.2933	0.7

PEW115	14.9	10.15	25.2	80	75.2	1649.092	1216.461	0.2
PEW116	24.9	10.15	25.2	80	75.2	986.8058	694.4145	0.5
PEW117	14.9	5.1	15.2	100	45.2	822.3246	378.4455	0.1
PEW118	24.9	5.1	15.2	100	45.2	1178.127	387.454	0.35
PEW119	14.9	10.15	15.2	100	45.2	1334.236	864.1671	0.15
PEW120	24.9	10.15	15.2	100	45.2	1999.388	1199.178	1.2
PEW121	14.9	5.1	15.2	100	65.2	1129.612	685.9159	0
PEW122	24.9	5.1	15.2	100	65.2	1032.216	384.0297	0.9
PEW123	14.9	10.15	15.2	100	65.2	2054.445	1649.253	0.2
PEW124	24.9	10.15	15.2	100	65.2	2526.694	1969.593	0.85
PEW125	14.9	5.1	25.2	100	55.2	1121.507	696.5928	0
PEW126	24.9	5.1	25.2	100	55.2	1388.922	708.0142	0.37
PEW127	14.9	10.15	25.2	100	55.2	2482.264	2121.505	0
PEW128	24.9	10.15	25.2	100	55.2	2703.693	2093.886	0.9
PEW129	14.9	5.1	25.2	100	75.2	1111.588	727.3299	0.2
PEW130	24.9	5.1	25.2	100	75.2	1104.976	487.3565	0.5
PEW131	14.9	10.15	25.2	100	75.2	1991.228	1567.873	0.6
PEW132	24.9	10.15	25.2	100	75.2	1645.587	933.4105	0.2
PEW133	8	7.65	20.2	90	60.2	1391.585	1112.596	0.15
PEW134	30.2	7.65	20.2	90	60.2	1252.616	771.1275	1.35
PEW135	20.2	3	20.2	90	60.2	752.8557	269.7414	0.2
PEW136	20.2	13.5	20.2	90	60.2	2757.398	2259.556	0.4
PEW137	20.2	7.65	20.2	90	36.2	1012.117	647.7364	fail
PEW138	20.2	7.65	20.2	90	84.2	1553.965	967.6948	0.35
PEW139	20.2	7.65	8	90	48	0	0	0
PEW140	20.2	7.65	32	90	72	0	0	0

PEW141	20.2	7.65	20.2	66	60.2	2034.212	1529.164	
PEW142	20.2	7.65	20.2	114	60.2	1886.057	1327.891	0.3
PEW143	20.2	7.65	20.2	90	60.2	1636.997	1065.347	0.35
PEW144	20.2	7.65	20.2	90	60.2	1669.388	1138.499	0
PEW145	20.2	7.65	20.2	90	60.2	1803.916	1317.454	0.35
PEW146	20.2	7.65	20.2	90	60.2	1729.729	1194.575	0.6
PEW147	20.2	7.65	20.2	90	60.2	1733.368	1188.844	0
PEW148	20.2	7.65	20.2	90	60.2	1713.618	1230.86	0.38
PEW149	20.2	7.65	20.2	90	60.2	1883.536	1393.809	0
PEW150	20.2	7.65	20.2	90	60.2	1486.788	938.9248	0.32

Table 8-5, ANOVA results for total energy response

Source	**SS**	**DF**	**MS**	**F**	**p-value**
Model	1.043E+007	12	8.694E+005	11.51	< 0.0001
A-Width of Waisted Section	*71422.35*	*1*	*71422.35*	*0.95*	*0.3377*
B-Radius of the Waisted Section	*6.727E+006*	*1*	*6.727E+006*	*89.07*	*< 0.0001*
C-Diameter of Loading Holes	*51454.19*	*1*	*51454.19*	*0.68*	*0.4149*
D-Distance between Loading Holes	*9.867E+005*	*1*	*9.867E+005*	*13.07*	*0.0010*
E-Width of Specimen	*865.66*	*1*	*865.66*	*0.011*	*0.9154*
AE	*4.752E+005*	*1*	*4.752E+005*	*6.29*	*0.0171*
BD	*3.410E+005*	*1*	*3.410E+005*	*4.52*	*0.0409*
CD	*1.270E+005*	*1*	*1.270E+005*	*1.68*	*0.2035*
A^2	*2.005E+005*	*1*	*2.005E+005*	*2.66*	*0.1124*
C^2	*4.690E+005*	*1*	*4.690E+005*	*6.21*	*0.0177*
D^2	*1.086E+005*	*1*	*1.086E+005*	*1.44*	*0.2388*

E^2	*1.509E+005*	*1*	*1.509E+005*	*2.00*	*0.1665*
Residual	2.568E+006	34	75519.09	N/A	N/A
Lack of Fit	*2.471E+006*	*27*	*91519.54*	*6.63*	*0.0075*
Pure Error	*96621.43*	*7*	*13803.06*	*N/A*	*N/A*
Total	1.300E+007	46	N/A	N/A	N/A

Table 8-6, ANOVA results for Region 3 energy

ANOVA for Response Surface Reduced Quadratic model					
Analysis of variance table [Partial sum of squares - Type III]					
Source	**Sum of Square**	**df**	**Mean Square**	**F Value**	**p-value Prob > F**
Model	1.014E+007	11	9.221E+005	13.14	< 0.0001
A-Width of Waisted Section	*74658.54*	*1*	*74658.54*	*1.06*	*0.3094*
B-Radius of the Waisted Section	*6.322E+006*	*1*	*6.322E+006*	*90.07*	*< 0.0001*

C-Diameter of Loading Holes	*1.472E+005*	*1*	*1.472E+005*	*2.10*	*0.1565*
D-Distance between Loading Holes	*9.078E+005*	*1*	*9.078E+005*	*12.93*	*0.0010*
E-Width of Specimen	*35187.82*	*1*	*35187.82*	*0.50*	*0.4836*
AE	*3.106E+005*	*1*	*3.106E+005*	*4.43*	*0.0427*
BD	*4.953E+005*	*1*	*4.953E+005*	*7.06*	*0.0118*
A^2	*1.003E+005*	*1*	*1.003E+005*	*1.43*	*0.2400*
C^2	*5.601E+005*	*1*	*5.601E+005*	*7.98*	*0.0078*
D^2	*94239.13*	*1*	*94239.13*	*1.34*	*0.2544*
E^2	*3.130E+005*	*1*	*3.130E+005*	*4.46*	*0.0419*
Residual	2.456E+006	35	70182.05	N/A	N/A
Lack of Fit	*2.316E+006*	*28*	*82714.35*	*4.12*	*0.0295*
Pure Error	*1.404E+005*	*7*	*20052.85*	*N/A*	*N/A*
Cor Total	1.260E+007	46	N/A	N/A	N/A

Table 8-7, ANOVA results for elongation in loading pin holes

ANOVA for Response Surface Linear model					
Analysis of variance table [Partial sum of squares - Type III]					
Source	**Sum of Squares**	**df**	**Mean Square**	**F Value**	**p-value Prob > F**
Model	4.56	5	0.91	10.62	< 0.0001
A-Width of Waisted Section	*3.69*	*1*	*3.69*	*43.02*	*< 0.0001*
B-Radius of the Waisted Section	*9.220E-004*	*1*	*9.220E-004*	*0.011*	*0.9180*
C-Diameter of Loading Holes	*0.10*	*1*	*0.10*	*1.21*	*0.2787*
D-Distance between Loading Holes	*0.11*	*1*	*0.11*	*1.32*	*0.2571*
E-Width of Specimen	*0.36*	*1*	*0.36*	*4.20*	*0.0469*

Residual	3.52	41	0.086	N/A	N/A
Lack of Fit	*3.24*	*34*	*0.095*	*2.35*	*0.1207*
Pure Error	*0.28*	*7*	*0.041*	N/A	N/A
Cor Total	8.08	46	N/A	N/A	N/A

8.3 Part C (Chapter 5)

Table 8-8, Constants used in constitutive equation

Crosshead speed (mm/min)	Strain Range	Parameters	Values
Linear Elastic part (a)	0-0.012	E	950
		υ	0.35
Non-linear deformation (b)	0.013-0.078	a	27
		b	0.02
		c	0.18
		d	-21
		e	14
Hollomon's equation for plastic deformation (c)	0.078-0.41	αk	30
		N	0.11
Work hardening deformation (d) Section 1	0.41-1.03	k	25.1
		M	0.31
		β	1.8
Section 2	1.03-1.34	k	21.1
		M	0.53
		β	1.8
Section 3	1.34-1.59	k	15.6
		M	0.79
		β	1.8
Section 4	1.59-1.99	k	20.7
		M	0.65
		β	1.75

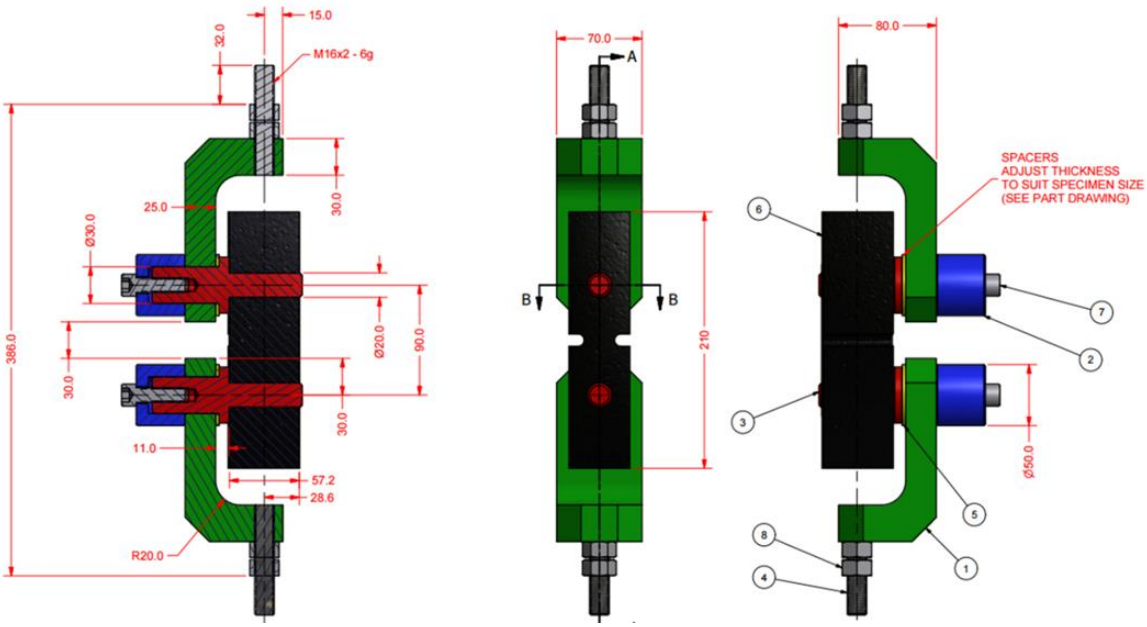

Figure 8-1, Tensile test engineering design for DIC purpose

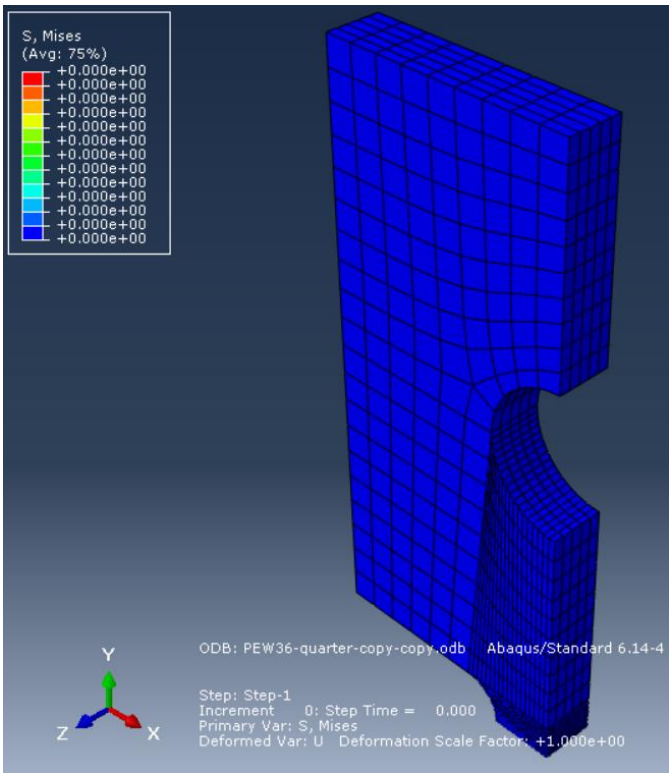

Figure 8-2, Initial increment and mesh for PEW36 specimen for FEA result Figure 5-3

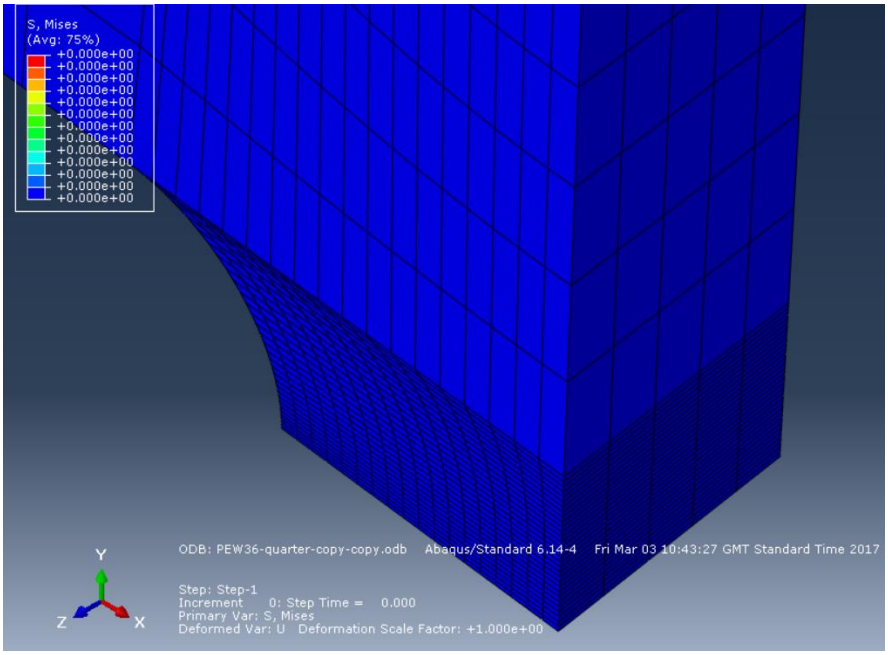

Figure 8-3, Mesh configuration for the wasited area of specimen PEW36 for FEA result Figure 5-3

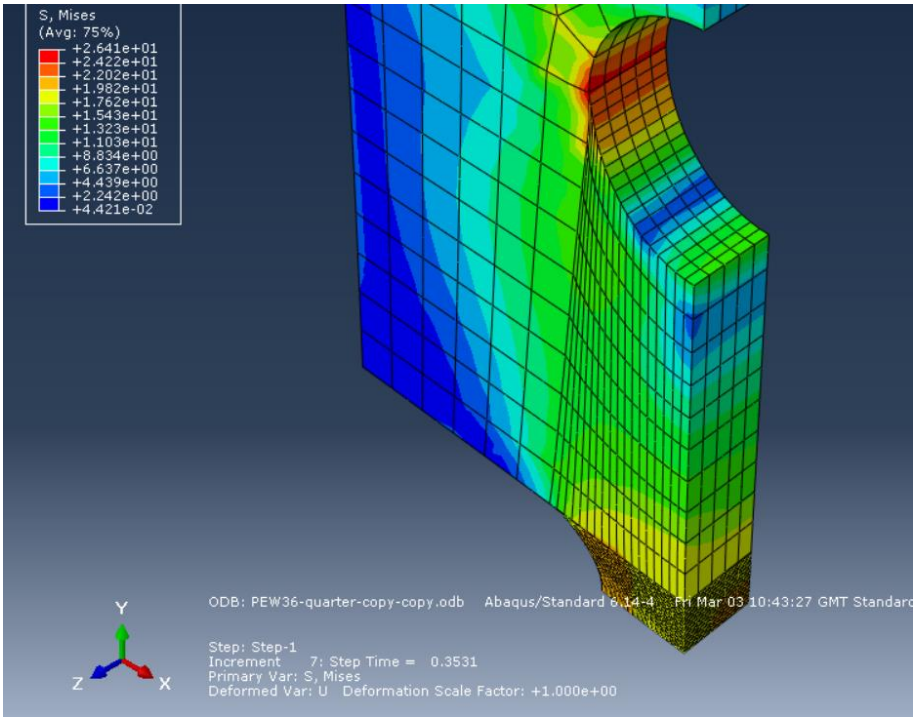

Figure 8-4, Increment 7 for PEW36 specimen for FEA result in Figure 5-3

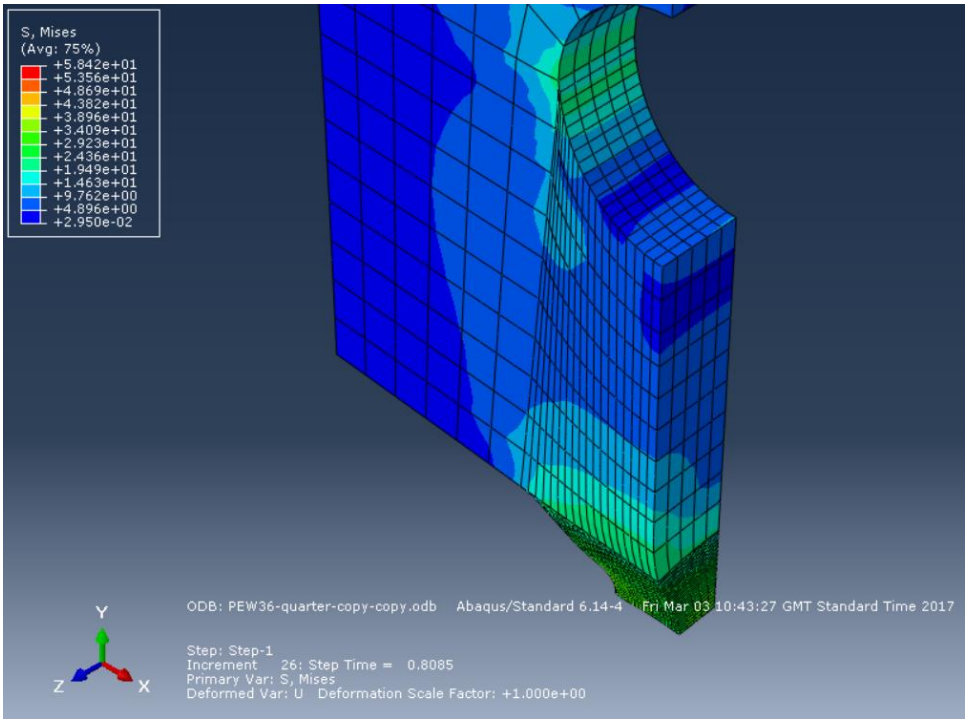

Figure 8-5, Increment 26 for PEW 36 specimen for FEA result in Figure 5-3

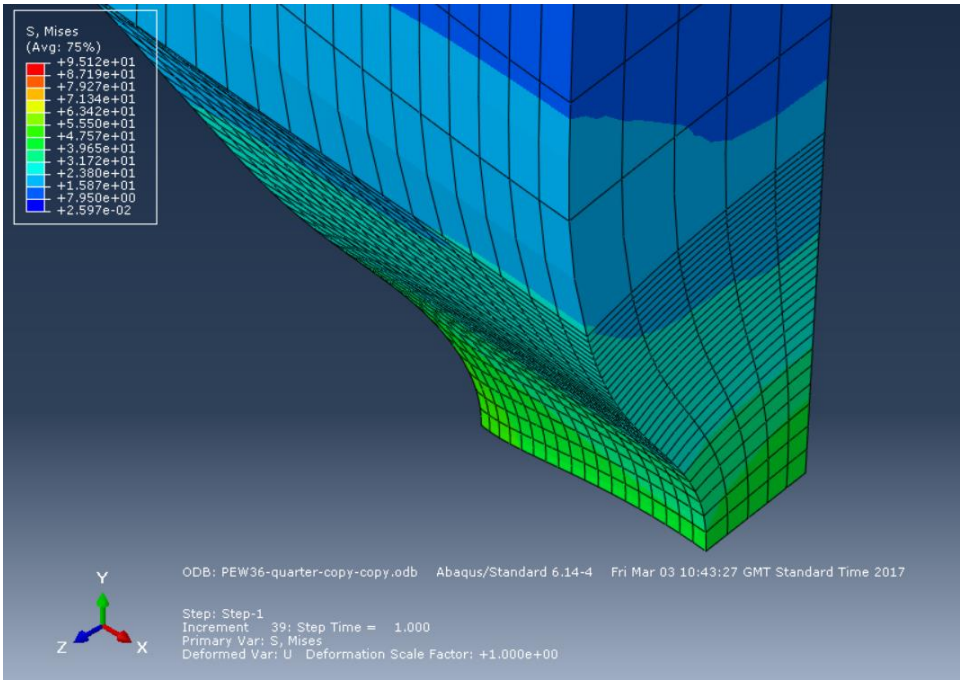

Figure 8-6, Increment 39 for PEW 36 for FEA result in Figure 5-3

8.4 Part D (Chapter 6)

Table 8-9, data for 140mm OD pipes

Specimen No	Parent/Weld	Geometry	Position	Pipe size	Pipe/weld no
PEB149	Parent	12814-7	2	140SDR11	140P01
PEB150	Parent	12814-7	8	140SDR11	140P01
PEB151	Parent	Modified	4	140SDR11	140P01
PEB152	Parent	Modified	10	140SDR11	140P01
PEB153	Parent	12814-7	2	140SDR11	140P02
PEB154	Parent	12814-7	8	140SDR11	140P02
PEB155	Parent	Modified	4	140SDR11	140P02
PEB156	Parent	Modified	10	140SDR11	140P02
PEB157	Parent	12814-7	2	140SDR11	140P03
PEB158	Parent	12814-7	8	140SDR11	140P03
PEB159	Parent	Modified	4	140SDR11	140P03
PEB160	Parent	Modified	10	140SDR11	140P03
PEB161	Weld	12814-7	2	140SDR11	140W01
PEB162	Weld	Modified	10	140SDR11	140W01
PEB163	Weld	12814-7	8	140SDR11	140W01
PEB164	Weld	Modified	4	140SDR11	140W01
PEB165	Weld	12814-7	2	140SDR11	140W02
PEB166	Weld	Modified	10	140SDR11	140W02
PEB167	Weld	12814-7	8	140SDR11	140W02
PEB168	Weld	Modified	4	140SDR11	140W02
PEB169	Weld	12814-7	2	140SDR11	140W03
PEB170	Weld	Modified	10	140SDR11	140W03
PEB171	Weld	12814-7	8	140SDR11	140W04

PEB172	Weld	Modified	4	140SDR11	140W04

Specimen No	Parent/Weld	Geometry	Position	Pipe size	Pipe/Weld no
PEB173	Weld-No Bead	12814-7	2	140SDR11	140W01-B
PEB174	Weld-No Bead	12814-7	8	140SDR11	140W01-B
PEB175	Weld-No Bead	Modified-1	4	140SDR11	140W01-B
PEB176	Weld-No Bead	Modified-1	10	140SDR11	140W01-B
PEB177	Weld-No Bead	12814-7	2	140SDR11	140W02-B
PEB178	Weld-No Bead	12814-7	8	140SDR11	140W02-B
PEB179	Weld-No bead	Modified-1	4	140SDR11	140W02-B
PEB180	Weld-No bead	Modified-1	10	140SDR11	140W02-B

Table 8-10, Data for 160mm OD pipe

Specimen No	Parent/Weld	Geometry	Position	Pipe size	Pipe/weld no
PEB101	Parent	12814-7	2	160SDR11	160P05
PEB102	Parent	12814-7	8	160SDR11	160P05
PEB103	Parent	Modified	4	160SDR11	160P05
PEB104	Parent	Modified	10	160SDR11	160P05
PEB105	Parent	12814-7	2	160SDR11	160P06
PEB106	Parent	12814-7	8	160SDR11	160P06
PEB107	Parent	Modified	4	160SDR11	160P06
PEB108	Parent	Modified	10	160SDR11	160P06

PEB109	Parent	12814-7	2	160SDR11	160P07
PEB110	Parent	12814-7	8	160SDR11	160P07
PEB111	Parent	Modified	4	160SDR11	160P07
PEB112	Parent	Modified	10	160SDR11	160P07
PEB113	Weld	12814-7	2	160SDR11	160W05
PEB114	Weld	Modified	10	160SDR11	160W05
PEB115	Weld	12814-7	8	160SDR11	160W05
PEB116	Weld	Modified	4	160SDR11	160W05
PEB117	Weld	12814-7	2	160SDR11	160W06
PEB118	Weld	Modified	10	160SDR11	160W06
PEB119	Weld	12814-7	8	160SDR11	160W06
PEB120	Weld	Modified	4	160SDR11	160W06
PEB121	Weld	12814-7	2	160SDR11	160W07
PEB122	Weld	modified	10	160SDR11	160W07
PEB123	Weld	12814-7	8	160SDR11	160W07
PEB124	Weld	modified	4	160SDR11	160W07

Table 8-11, Data for 250mm OD pipe

Specimen No	Parent/Weld	Geometry	Position	Pipe size	Pipe/weld no
PEB125	Parent	12814-7	12	250SDR17	250P013
PEB126	Parent	12814-7	4	250SDR17	250P013
PEB127	Parent	12814-7	8	250SDR17	250P013
PEB128	Parent	Modified	2	250SDR17	250P013
PEB129	Parent	Modified	10	250SDR17	250P013
PEB130	Parent	Modified	6	250SDR17	250P013

PEB131	Parent	12814-7	12	250SDR17	250P014
PEB132	Parent	12814-7	4	250SDR17	250P014
PEB133	Parent	12814-7	8	250SDR17	250P014
PEB134	Parent	Modified	2	250SDR17	250P014
PEB135	Parent	Modified	10	250SDR17	250P014
PEB136	Parent	Modified	6	250SDR17	250P014
PEB137	Weld	12814-7	12	250SDR17	250W013
PEB138	Weld	12814-7	4	250SDR17	250W013
PEB139	Weld	12814-7	8	250SDR17	250W013
PEB140	Weld	Modified	2	250SDR17	250W013
PEB141	Weld	Modified	10	250SDR17	250W013
PEB142	Weld	Modified	6	250SDR17	250W013
PEB143	Weld	12814-7	12	250SDR17	250W014
PEB144	Weld	12814-7	4	250SDR17	250W014
PEB145	Weld	12814-7	8	250SDR17	250W014
PEB146	Weld	Modified	2	250SDR17	250W014
PEB147	Weld	Modified	10	250SDR17	250W014
PEB148	Weld	Modified	6	250SDR17	250W014

Table 8-12, Data for 280mm OD pipe

PEB181	Parent	12814-7	1	280SDR11	280P15
PEB182	Parent	12714-7	4	280SDR11	280P15
PEB183	Parent	12814-7	7	280SDR11	280P15
PEB184	Parent	12814-7	10	280SDR11	280P15
PEB185	Parent	Modified-3	3	280SDR11	280P15
PEB186	Parent	Modified-3	6	280SDR11	280P15
PEB187	Parent	Modified-3	9	280SDR11	280P15

PEB188	Parent	Modified-3	11	280SDR11	280P15
PEB189	Welded	12814-7	1	280SDR11	280W15
PEB190	Welded	12814-7	4	280SDR11	280W15
PEB191	Welded	12814-7	7	280SDR11	280W15
PEB192	Welded	12814-7	10	280SDR11	280W15
PEB193	Welded	Modified-3	3	280SDR11	280W15
PEB194	Welded	Modified-3	6	280SDR11	280W15
PEB195	Welded	Modified-3	9	280SDR11	280W15
PEB196	welded	Modified-3	11	280SDR11	280W15

Table 8-13, Data for 500mm OD pipe

PEB197	Parent	12814-7	12	500SDR11	500P19
PEB198	Parent	12814-7	2	500SDR11	500P19
PEB199	Parent	12814-7	5	500SDR11	500P19
PEB200	Parent	12814-7	8	500SDR11	500P19
PEB201	Parent	12814-7	10	500SDR11	500P19
PEB202T	Parent-Cut/2	Modified	1	500SDR11	500P19
PEB202B	Parent-Cut/2	Modified	1	500SDR11	500P19
PEB203T	Parent-Cut/2	Modified	4	500SDR11	500P19
PEB203B	Parent-Cut/2	Modified	4	500SDR11	500P19
PEB204T	Parent-Cut/2	Modified	6	500SDR11	500P19
PEB204B	Parent-Cut/2	Modified	6	500SDR11	500P19
PEB205T	Parent-Cut/2	Modified	9	500SDR11	500P19
PEB205B	Parent-Cut/2	Modified	9	500SDR11	500P19
PEB205T	Parent-Cut/2	Modified	11	500SDR11	500P19
PEB205B	Parent-Cut/2	Modified	11	500SDR11	500P19
PEB206	Weld	12814-7	12	500SDR11	500W19
PEB207	Weld	12814-7	2	500SDR11	500W19

PEB208	Weld	12814-7	5	500SDR11	500W19
PEB209	Weld	12814-7	8	500SDR11	500W19
PEB210	Weld	12814-7	10	500SDR11	500W19
PEB211T	Weld-cut/2	Modified	1	500SDR11	500W19
PEB211B	Weld-cut/2	Modified	1	500SDR11	500W19
PEB212T	Weld-cut/2	Modified	4	500SDR11	500W19
PEB212B	Weld-cut/2	Modified	4	500SDR11	500W19
PEB213T	Weld-cut/2	Modified	6	500SDR11	500W19
PEB213B	Weld-cut/2	Modified	6	500SDR11	500W19
PEB214T	Weld-cut/2	Modified	9	500SDR11	500W19
PEB214B	Weld-cut/2	Modified	9	500SDR11	500W19
PEB215T	Weld-cut/2	Modified	11	500SDR11	500W19
PEB215B	Weld-cut/2	Modified	11	500SDR11	500W19

Table 8-14, Data for 630mm OD pipe

Specimen No	Parent/Weld	Geometry	Position	Pipe size	Pipe/weld no
PEB216	Parent	12814-7	12	630SDR11	630P21
PEB217	Parent	12814-7	2	630SDr11	630P21
PEB218	Parent	12814-7	5	630SDR11	630P21
PEB219	Parent	12814-7	8	630SDR11	630P21
PEB220	Parent	12814-7	10	630SDR11	630P21
PEB221T	Parent-Cut/2	Modified	1	630SDR11	630P21
PEB221B	Parent-Cut/2	Modified	1	630SDR11	630P21
PEB222T	Parent-Cut/2	Modified	4	630SDR11	630P21
PEB222B	Parent-Cut/2	Modified	4	630SDR11	630P21
PEB223T	Parent-Cut/2	Modified	6	630SDR11	630P21
PEB223B	Parent-Cut/2	Modified	6	630SDR11	630P21
PEB224T	Parent-Cut/2	Modified	9	630SDR11	630P21

PEB224B	Parent-Cut/2	Modified	9	630SDR11	630P21
PEB225T	Parent-Cut/2	Modified	11	630SDR11	630P21
PEB225B	Parent-Cut/2	Modified	11	630SDR11	630P21
PEB226	Weld	12814-7	12	630SDR11	630W21
PEB227	Weld	12814-7	2	630SDR11	630W21
PEB228	Weld	12814-7	5	630SDR11	630W21
PEB229	Weld	12814-7	8	630SDR11	630W21
PEB230	Weld	12814-7	10	630SDR11	630W21
PEB231T	Weld-cut/2	Modified	1	630SDR11	630W21
PEB231B	Weld-cut/2	Modified	1	630SDR11	630W21
PEB232T	Weld-cut/2	Modified	4	630SDR11	630W21
PEB232B	Weld-cut/2	Modified	4	630SDR11	630W21
PEB233T	Weld-cut/2	Modified	6	630SDR11	630W21
PEB233B	Weld-cut/2	Modified	6	630SDR11	630W21
PEB234T	Weld-cut/2	Modified	9	630SDR11	630W21
PEB234B	Weld-cut/2	Modified	9	630SDR11	630W21
PEB235T	Weld-cut/2	Modified	11	630SDR11	630W21
PEB235B	Weld-cut/2	Modified	11	630SDR11	630W21

Table 8-15, Data for all the weldings in this research

OD	SDR	Thickness	No of Welds	Temp(^{o}C)	Heating up time(s)	Changeover time (S)	Cooling Time (min)	Weld No	Welding Machine	Pressure(N/mm2)
140	11	12.7	2	211	127	8 to 10	16 to 24	140W01-02	BF315	0.15
140	11	12.7	2	211	127	8 to 10	16 to 24	140W03-04	BF315	0.15
160	11	14.5	2	209	145	8 to 10	16 to 24	160W05-06	BF315	0.15
160	11	14.5	2	209	145	8 to 10	16 to 24	160W07-08	BF315	0.15
200	11	18.2	2	206	182	8 to 10	16 to 24	200W09-10	BF315	0.15
200	11	18.2	2	206	182	8 to 10	16 to 24	200W11-12	BF315	0.15
250	17	14.7	1	209	147	8 to 10	16 to 24	250W13	BF315	0.15
250	17	14.7	1	209	147	8 to 10	16 to 24	250W14	BF315	0.15
280	11	25.5	1	202	255	10 to 12	24 to 32	280W15	BF315	0.15
280	11	25.5	1	202	255	10 to 12	24 to 32	280W16	BF315	0.15
500	11	45.5	1	200	455	16 to 20	45 to 60	500W19	Mc1236	0.15
500	11	45.5	1	200	455	16 to 20	46 to 60	500W20	Mc1236	0.15
630	11	57.3	1	200	573	20 to 25	60 to 80	630W21	Mc1236	0.15
630	11	57.3	1	200	573	20 to 25	60 to 80	630W22	Mc1236	0.15

Printed: 2017-05-02 14:35:01 UTC

DataLogger VAULT

McElroy Joint Report

Reference Number 553997

Job Details

Joint Number	500202
Joint Time	2017-05-02 13:56:33.0
Job	24458
Operator	MT/SMW

Fusion Machine

Machine Name	MegaMc 1236
Machine Model	*1236 AutoMegaMc-H
Piston Area	15.32 in²

Pipe Specifications

Pipe Material	PE100
Pipe Size	500 mm OD
Wall Thickness	DR 11

Pressures

Drag Pressure 35 psi

	Interfacial	Gauge
Bead Up	21.75 psi	178 psi
Heat Soak	0 psi	35 psi
Fuse	0 psi	0 psi
Cool	21.75 psi	178 psi

Fusion Specification

Fusion Type	Butt Fusion
Fusion Specification	DVS 2207-1 PE-HD:2005-09
Bead Time	0 seconds
Bead Size	3.6mm
Heat/Soak Time	454 seconds
Fuse Time	0 seconds
Open/Close Time	18 seconds
Cool Time	3240 seconds

	Minimum	Maximum
Bead Up	168 psi	187 psi
Heat Soak	0 psi	35 psi
Fuse	0 psi	0 psi
Cool	168 psi	187 psi

External Heater Temperatures

	Side A	Side B
One	200 C	201 C
Two	201 C	200 C
Three	200 C	202 C
Four	201 C	201 C

Logged Data Summary

Number of Data Points	152
Total Fusion Time	4109 seconds
Maximum Recorded Pressure	184 psi

Device Information

DataLogger Serial Number	MDL5-0613
Calibration Date	2016-05-12
Firmware Version	v5.1
Software Version	v1.1.2
Software Product Name	DL5m

Data Source

File Name \My Documents\Joint Reports\DL5 2017-05-02 13-56-33 Joint 500202 Job 24458 by MT_SMW.DL5

Upload Time 2017-05-02 14:01:34.0

Front-end Plot

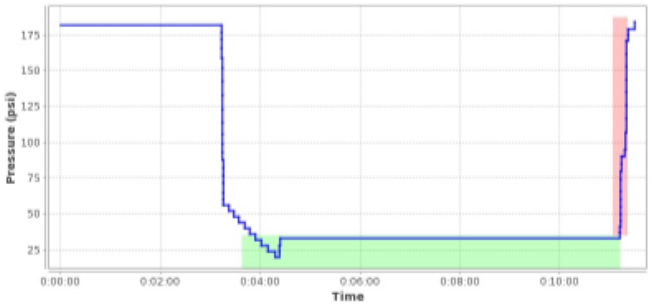

Heater Removal Plot

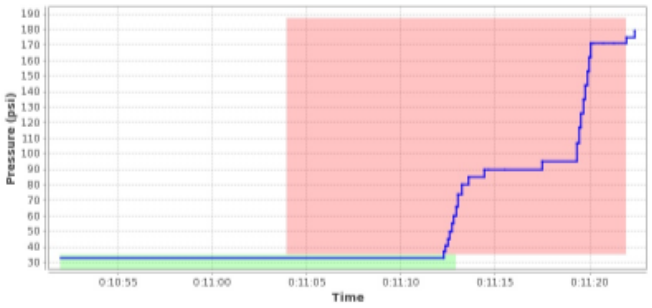

Summary Plot

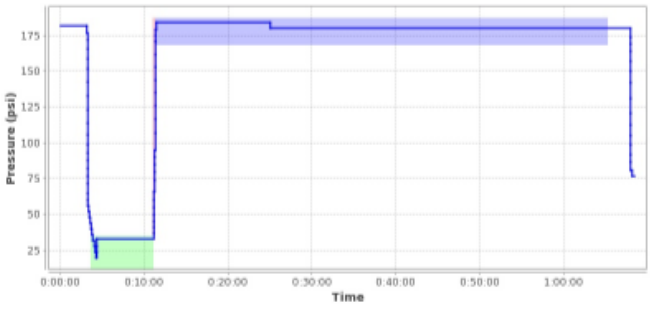

Notes

tuesday 2nd may

Figure 8-7, Weld report for the first 500mm OD pipe weld

Printed: 2017-05-02 14:39:34 UTC

DataLogger VAULT

McElroy Joint Report

Reference Number 500584

Job Details

Joint Number	71
Joint Time	2017-01-23 11:45:51.0
Job	24558
Operator	AK/MT

Fusion Machine

Machine Name	MegaMc 1236
Machine Model	*1236 MF
Piston Area	15.32 in²

Pipe Specifications

Pipe Material	PE100
Pipe Size	500 mm OD
Wall Thickness	DR 11

Pressures

Drag Pressure 40 psi

	Interfacial	Gauge
Bead Up	21.75 psi	183 psi
Heat Soak	0 psi	40 psi
Fuse	0 psi	0 psi
Cool	21.75 psi	183 psi

Fusion Specification

Fusion Type	Butt Fusion
Fusion Specification	DVS 2207-1 PE-HD:2005-09
Bead Time	0 seconds
Bead Size	3.5mm
Heat/Soak Time	454 seconds
Fuse Time	0 seconds
Open/Close Time	18 seconds
Cool Time	3240 seconds

	Minimum	Maximum
Bead Up	173 psi	192 psi
Heat Soak	0 psi	40 psi
Fuse	0 psi	0 psi
Cool	173 psi	192 psi

External Heater Temperatures

	Side A	Side B
One	204 C	205 C
Two	209 C	201 C
Three	209 C	203 C
Four	206 C	205 C

Logged Data Summary

Number of Data Points	248
Total Fusion Time	4029 seconds
Maximum Recorded Pressure	198 psi

Device Information

DataLogger Serial Number	MDL5-0613
Calibration Date	2016-05-12
Firmware Version	v5.1
Software Version	v1.1.2
Software Product Name	DL5m

Data Source

File Name \My Documents\Joint Reports\DL5 2017-01-23 11-45-51 Joint 71 Job 24558 by AK_MT.DL5

Upload Time 2017-02-23 16:17:08.0

Front-end Plot

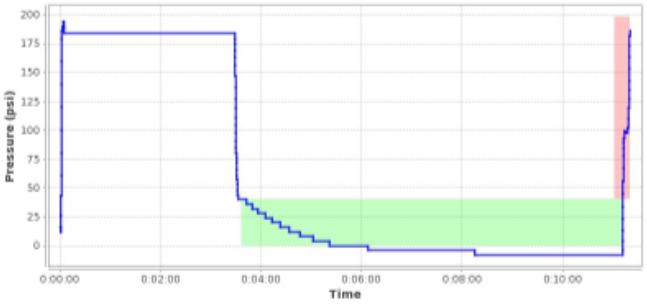

Heater Removal Plot

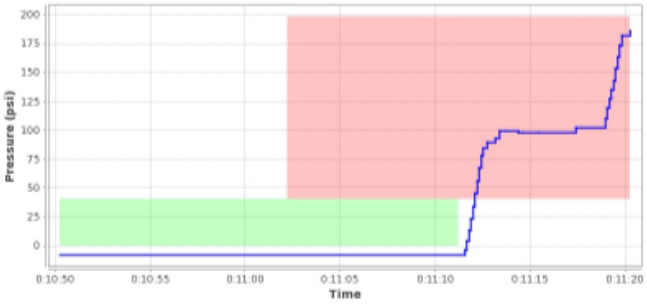

Summary Plot

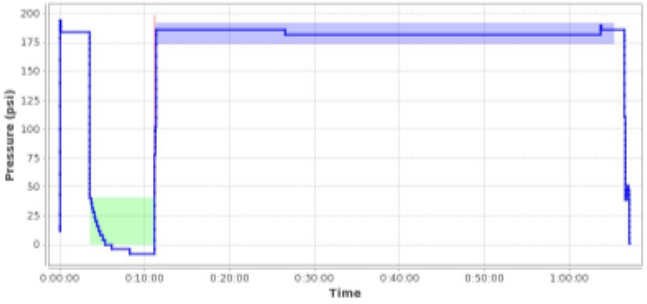

Notes

Standard DVS 500W20

Figure 8-8, Weld report for the second 500mm OD pipe

Printed: 2017-05-02 14:31:58 UTC

DataLogger VAULT

McElroy Joint Report

Reference Number 479211

Job Details

Joint Number	70
Joint Time	2017-01-17 14:24:09.0
Job	24558
Operator	AK/MT

Fusion Machine

Machine Name	MegaMc 1236
Machine Model	*1236 MF
Piston Area	15.32 in²

Pipe Specifications

Pipe Material	PE100
Pipe Size	630 mm OD
Wall Thickness	DR 11

Pressures

Drag Pressure 40 psi

	Interfacial	Gauge
Bead Up	21.75 psi	267 psi
Heat Soak	0 psi	40 psi
Fuse	0 psi	0 psi
Cool	21.75 psi	267 psi

Fusion Specification

Fusion Type	Butt Fusion
Fusion Specification	DVS 2207-1 PE-HD:2005-09
Bead Time	0 seconds
Bead Size	4.0mm
Heat/Soak Time	572 seconds
Fuse Time	0 seconds
Open/Close Time	21 seconds
Cool Time	4020 seconds

	Minimum	Maximum
Bead Up	251 psi	281 psi
Heat Soak	0 psi	40 psi
Fuse	0 psi	0 psi
Cool	251 psi	281 psi

External Heater Temperatures

	Side A	Side B
One	202 C	205 C
Two	203 C	201 C
Three	206 C	204 C
Four	205 C	205 C

Logged Data Summary

Number of Data Points	266
Total Fusion Time	5032 seconds
Maximum Recorded Pressure	305 psi

Device Information

DataLogger Serial Number	MDL5-0613
Calibration Date	2016-05-12
Firmware Version	v5.1
Software Version	v1.1.2
Software Product Name	DL5m

Data Source

File Name	\My Documents\Joint Reports\DL5 2017-01-17 14-24-09 Joint 70 Job 24558 by AK_MT.DL5
Upload Time	2017-01-17 15:04:04.0

Front-end Plot

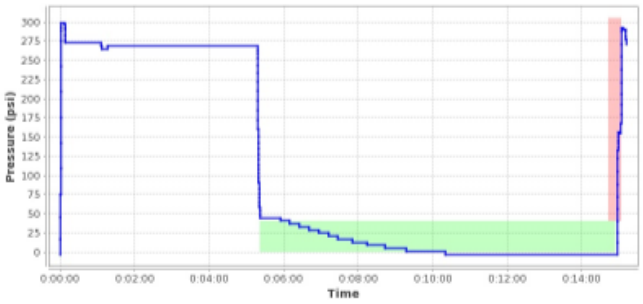

Heater Removal Plot

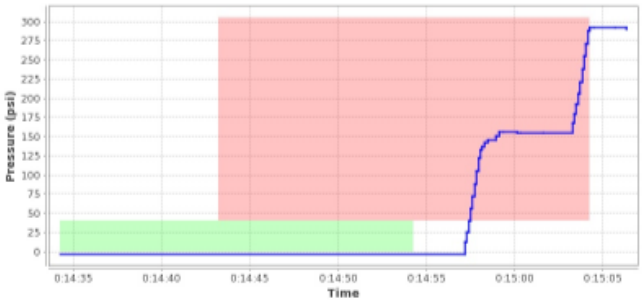

Summary Plot

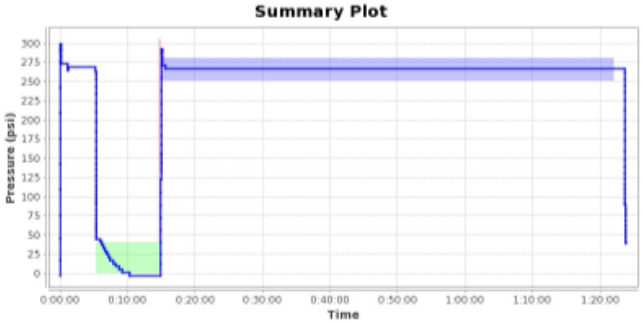

Notes

Standard DVS 630 W22

Figure 8-9, Weld report for first 630mm OD pipe weld

Printed: 2017-05-02 14:30:26 UTC

DataLogger VAULT

McElroy Joint Report

Reference Number 478196

Job Details

Joint Number	66
Joint Time	2017-01-13 14:07:12.0
Job	24558
Operator	AK

Fusion Machine

Machine Name	AK/MT
Machine Model	P1295 MF
Piston Area	15.32 in²

Pipe Specifications

Pipe Material	PE100
Pipe Size	630 " OD
Wall Thickness	DR 11

Pressures

Drag Pressure 50 psi

	Interfacial	Gauge
Bead Up	21.75 psi	0 psi
Heat Soak	0 psi	50 psi
Fuse	0 psi	0 psi
Cool	21.75 psi	0 psi

Fusion Specification

Fusion Type	Butt Fusion
Fusion Specification	DVS 2207-1 PE-HD:2005-09
Bead Time	0 seconds
Bead Size	
Heat/Soak Time	0 seconds
Fuse Time	0 seconds
Open/Close Time	0 seconds
Cool Time	0 seconds

	Minimum	Maximum
Bead Up	5,525 psi	25,032 psi
Heat Soak	0 psi	50 psi
Fuse	0 psi	0 psi
Cool	5,525 psi	25,032 psi

External Heater Temperatures

	Side A	Side B
One	200 C	203 C
Two	201 C	201 C
Three	204 C	202 C
Four	203 C	206 C

GPS Location

	Latitude	Longitude
2017-01-13 14:12:33 UTC	52°6'58.5"N	0°13'56.6"E

Logged Data Summary

Number of Data Points	360
Total Fusion Time	5155 seconds
Maximum Recorded Pressure	315 psi

Device Information

DataLogger Serial Number	MDL5-0613
Calibration Date	2016-05-12
Firmware Version	v5.1
Software Version	v1.1.2
Software Product Name	DL5m

Data Source

File Name	\My Documents\Joint Reports\DL5 2017-01-13 14-07-12 Joint 66 Job 24558 by AK.DL5
Upload Time	2017-01-16 16:23:57.0

Front-end Plot

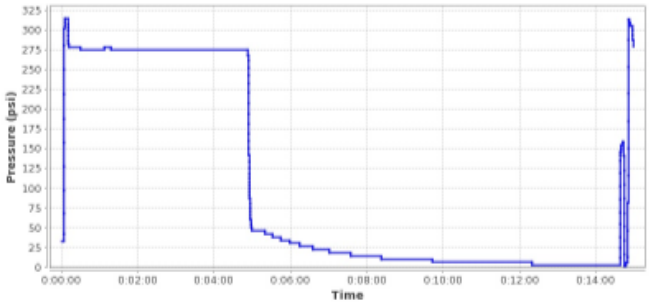

Heater Removal Plot

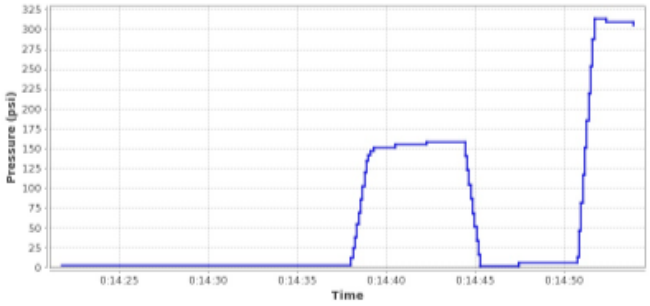

Summary Plot

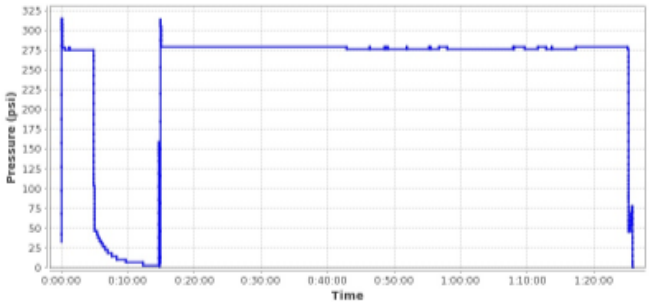

Notes

Standard DVS butt fusion - 630W21

Figure 8-10, Weld report for the second 630mm OD pipe weld

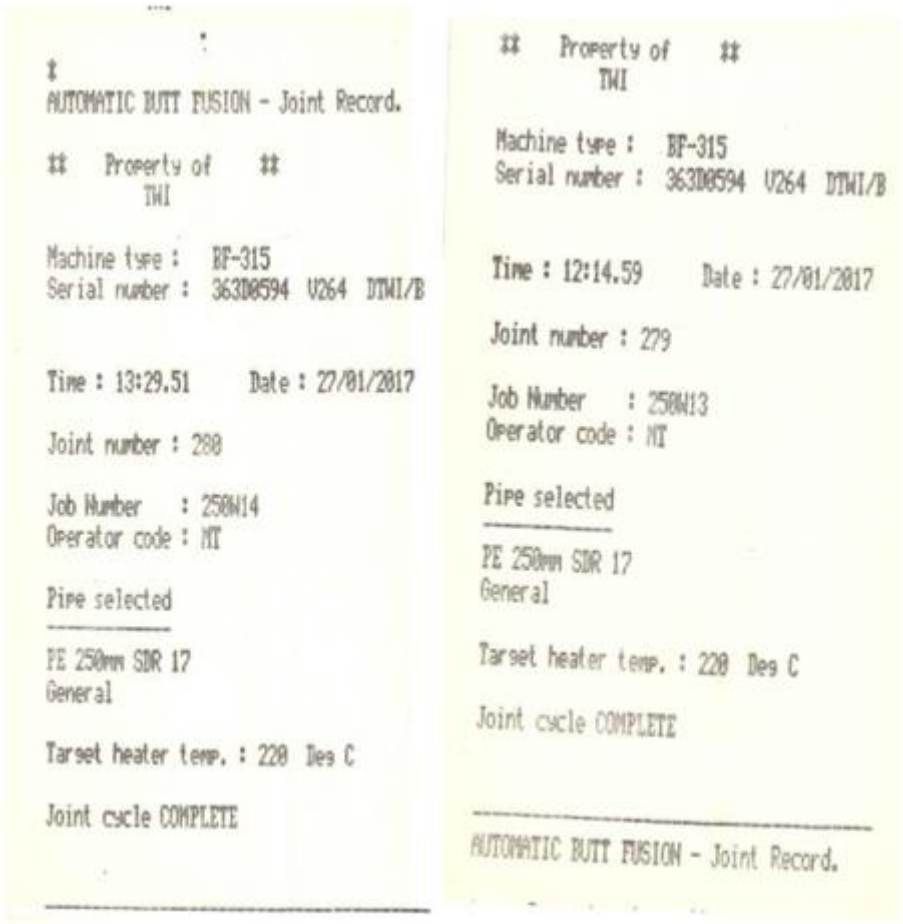

AUTOMATIC BUTT FUSION - Joint Record.

Property of TWI

Machine type : BF-315
Serial number : 363B0594 V264 DTWI/B

Time : 13:29.51 Date : 27/01/2017

Joint number : 280

Job Number : 250N14
Operator code : MT

Pipe selected

PE 250mm SDR 17
General

Target heater temp. : 220 Deg C

Joint cycle COMPLETE

Property of TWI

Machine type : BF-315
Serial number : 363B0594 V264 DTWI/B

Time : 12:14.59 Date : 27/01/2017

Joint number : 279

Job Number : 250N13
Operator code : MT

Pipe selected

PE 250mm SDR 17
General

Target heater temp. : 220 Deg C

Joint cycle COMPLETE

AUTOMATIC BUTT FUSION - Joint Record.

Figure 8-11, Weld reports for 250mm OD SDR17

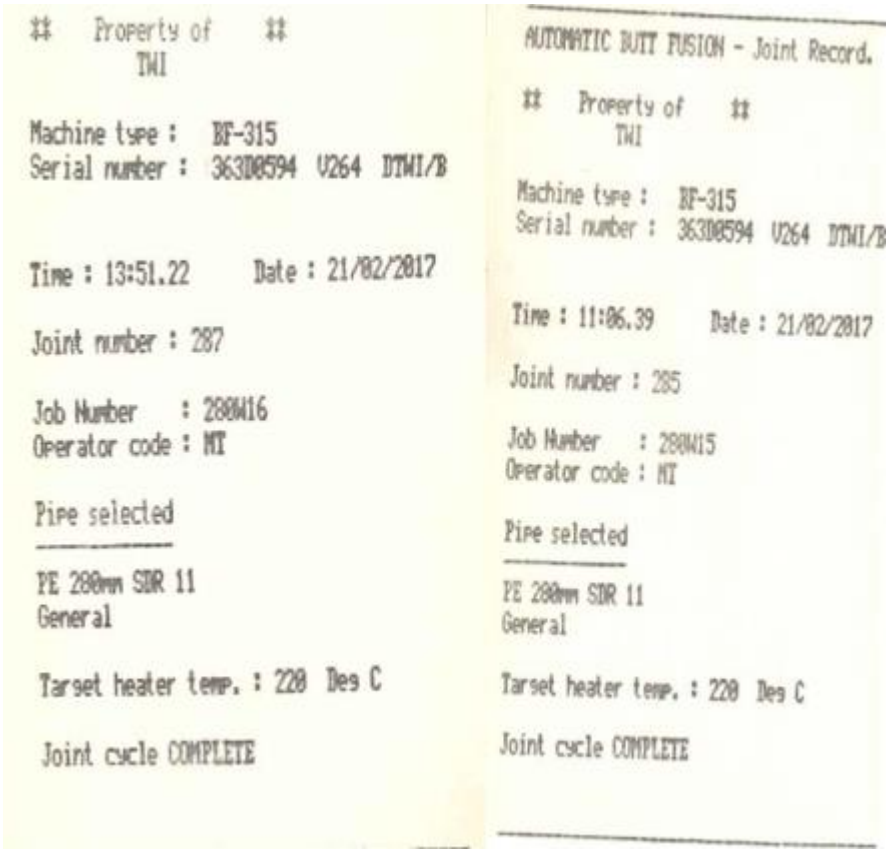

Property of TWI

Machine type : BF-315
Serial number : 363B0594 V264 DTWI/B

Time : 13:51.22 Date : 21/02/2017

Joint number : 287

Job Number : 280W16
Operator code : MI

Pipe selected

PE 280mm SDR 11
General

Tarset heater temp. : 220 Deg C

Joint cycle COMPLETE

AUTOMATIC BUTT FUSION - Joint Record.

Property of TWI

Machine type : BF-315
Serial number : 363B0594 V264 DTWI/B

Time : 11:06.39 Date : 21/02/2017

Joint number : 285

Job Number : 280W15
Operator code : MI

Pipe selected

PE 280mm SDR 11
General

Tarset heater temp. : 220 Deg C

Joint cycle COMPLETE

Figure 8-12, Weld reports for 280mm OD SDR11

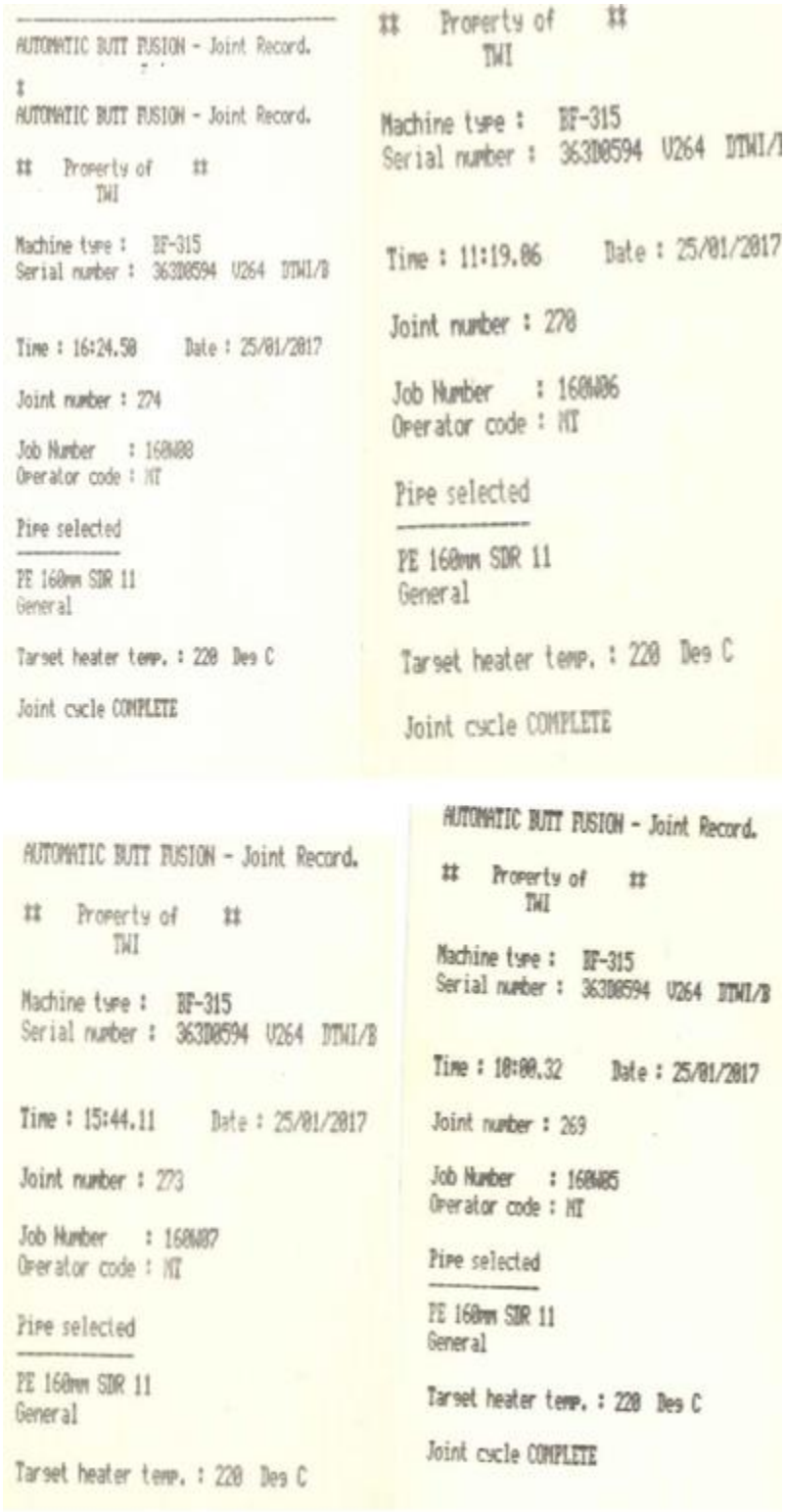

AUTOMATIC BUTT FUSION - Joint Record.

‡‡ Property of ‡‡
TWI

Machine type : BF-315
Serial number : 363D0594 U264 DTWI/B

Time : 16:24.58 Date : 25/01/2017

Joint number : 274

Job Number : 160A08
Operator code : MT

Pipe selected

PE 160mm SDR 11
General

Target heater temp. : 220 Deg C

Joint cycle COMPLETE

AUTOMATIC BUTT FUSION - Joint Record.

‡‡ Property of ‡‡
TWI

Machine type : BF-315
Serial number : 363D0594 U264 DTWI/B

Time : 11:19.06 Date : 25/01/2017

Joint number : 270

Job Number : 160A06
Operator code : MT

Pipe selected

PE 160mm SDR 11
General

Target heater temp. : 220 Deg C

Joint cycle COMPLETE

AUTOMATIC BUTT FUSION - Joint Record.

‡‡ Property of ‡‡
TWI

Machine type : BF-315
Serial number : 363D0594 U264 DTWI/B

Time : 15:44.11 Date : 25/01/2017

Joint number : 273

Job Number : 160A07
Operator code : MT

Pipe selected

PE 160mm SDR 11
General

Target heater temp. : 220 Deg C

AUTOMATIC BUTT FUSION - Joint Record.

‡‡ Property of ‡‡
TWI

Machine type : BF-315
Serial number : 363D0594 U264 DTWI/B

Time : 10:00.32 Date : 25/01/2017

Joint number : 269

Job Number : 160A05
Operator code : MT

Pipe selected

PE 160mm SDR 11
General

Target heater temp. : 220 Deg C

Joint cycle COMPLETE

Figure 8-13, Weld reports for 160mm OD SDR11